

TESIS DOCTORAL

ASPA COMO NUEVO REGULADOR DE LOS  
FIBROBLASTOS ASOCIADOS AL CÁNCER

PhD THESIS

ASPA AS A NEW REGULATOR OF CANCER-  
ASSOCIATED FIBROBLAST

AUTORA

CATALINA CAPÓ SERRA

DIRECTORES

DR FERNANDO CALVO GONZÁLEZ

DR JAVIER RODRÍGUEZ MARTÍNEZ

UNIVERSIDAD DE CANTABRIA

Escuela de Doctorado de la Universidad de Cantabria

Santander 2024



**UNIVERSIDAD DE CANTABRIA**

PROGRAMA DE DOCTORADO EN BIOLOGÍA MOLECULAR Y BIOMEDICINA



**TESIS DOCTORAL**

ASPA COMO NUEVO REGULADOR DE LOS FIBROBLASTOS  
ASOCIADOS AL CÁNCER

**PhD THESIS**

ASPA AS A NEW REGULATOR OF CANCER-ASSOCIATED  
FIBROBLASTS

**Realizada por:** Catalina Capó Serra  
**Dirigida por:** Fernando Calvo González y Javier Rodríguez Martínez

Escuela de Doctorado de la Universidad de Cantabria | Santander, 2024



El Dr. FERNANDO CALVO GONZÁLEZ, Profesor de Investigación del Consejo Superior de Investigaciones Científicas (CSIC) en el laboratorio de Microambiente Tumoral en el departamento de Señalización celular y molecular ubicado en el Instituto de Biomedicina y Biotecnología de Cantabria (IBBTEC), como Tutor/Director de esta Tesis y el Dr. JAVIER RODRÍGUEZ MARTÍNEZ, Investigador del Consejo Superior de Investigaciones Científicas (CISC) en el mismo instituto, como co-Director de esta Tesis

CERTIFICAN:

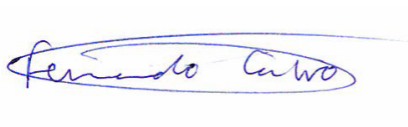
Que CATALINA CAPÓ SERRA ha realizado bajo su dirección el presente trabajo de Tesis Doctoral en el Instituto de Biomedicina y Biotecnología de Cantabria (IBBTEC) titulado:

*ASPA como nuevo regulador de los Fibroblastos Asociados al Cáncer*

Que consideran que dicho trabajo se encuentra terminado y reúne los requisitos necesarios para su presentación como Memoria de Doctorado al objeto de poder optar al grado de Doctor en Biología Molecular y Biomedicina por la Universidad de Cantabria.

Y para que conste y surta los efectos oportunos, expiden el presente certificado en Santander a 25 de marzo de 2024.

Fdo. Fernando Calvo González



Fdo. Javier Rodríguez Martínez





Esta Tesis ha sido realizada en el Instituto de Biomedicina y Biotecnología de Cantabria (IBBTEC) perteneciente a la Universidad de Cantabria (UC) y al Consejo Superior de Investigaciones Científicas (CSIC), en Santander (Cantabria, España).

La financiación para la realización de esta Tesis doctoral ha sido proporcionada por AECC (LABAE19044CALV y PRYCO211372RODR), MCIU/AEI/10.13039/501100011033 (RTI2018-096778-A-I00, PID2021-128107OB-I00); BBVA Leonardo Awards (IN[19]\_BBM\_BAS\_0076), y ERC (ERCCoG-101045756). La financiación para la realización de la estancia internacional en Beatson Institute ha sido proporcionada por EMBO (Embo scientific exchange grant) y FEBS (Summer internships).





*A es meus tres pilars:  
mon pare, ma mare,  
i tu, Pere Antoni.*



**SUMMARY/RESUMEN**



## SUMMARY

The crosstalk between cancer cells and the tumour microenvironment (TME) plays a critical role in the acquisition of molecular and cellular features underpinning tumour progression. Cancer Associated Fibroblasts (CAFs) are the major population within the TME and their contribution to most of the hallmarks of cancer is gradually emerging. CAFs present a pathologically activated phenotype driven by aberrant signalling pathways, which promotes extracellular matrix remodelling and pro-tumorigenic crosstalk to cancer and stromal cells. CAFs may also present metabolic adaptations that fuel cancer cell growth. However, how metabolic reprogramming assists in the pathological activation of fibroblasts, and its interplay with signaling and transcriptional rearrangements is not well defined. To identify new stromal modulators of cancer progression, gene expression datasets of cancerous and normal stroma from human breast, ovary, colon, prostate, and lung tissues were analysed. Consistent up or down-regulated genes were shortlisted based on their association with disease-free survival. These analyses revealed that the metabolic enzyme Aspartoacylase (ASPA) is consistently downregulated in CAFs of different tumour types and it is correlated with a poorer prognosis in human breast and prostate cancer. Molecular analyses informed that ASPA is downregulated by TGF $\beta$  and histone deacetylases (HDACs) signalling in fibroblasts. Further analyses using genetic manipulation in murine and human models, molecular characterization, and functional *in vitro* and *in vivo* assays revealed that ASPA expression in normal fibroblasts or CAFs affects their pro-tumour behaviour by regulating fibroblast activation, extracellular matrix remodelling capacity and crosstalk to cancer cells. This study provides new perspectives on the interplay between metabolic rearrangements and CAF emergence by describing a key role of the metabolic enzyme ASPA in regulating critical pro-tumour functions and phenotypes in CAFs.



## RESUMEN

La señalización entre las células cancerosas y el microambiente tumoral (TME) es crucial para entender los procesos subyacentes en la progresión tumoral. Los Fibroblastos Asociados al Cáncer (CAFs) constituyen un componente preponderante del TME y presentan un fenotipo patológicamente activado que promueve la remodelación de la matriz extracelular y el establecimiento de interacciones pro-tumorales con las células cancerosas y estromales. Los CAFs se caracterizan por presentar adaptaciones metabólicas y la activación aberrante de vías de señalización que promueven su activación y el crecimiento del tumor. Sin embargo, los mecanismos que subyacen a estos eventos no están completamente elucidados. Para identificar nuevos moduladores estromales de la progresión del cáncer, se analizaron bases de datos de expresión génica de estroma canceroso y normal de tejidos humanos de mama, ovario, colon, próstata y pulmón. Los genes consistentemente regulados al alza o a la baja se seleccionaron en base a su valor pronóstico. Estos análisis revelaron que el enzima metabólico Aspartoacilasa (ASPA) está consistentemente silenciado en CAFs de diferentes tipos de tumores y está correlacionado con un peor pronóstico en cáncer de mama y próstata humano. Nuestros análisis moleculares informaron que el silenciamiento de ASPA en CAFs es resultado de una activación de la cascada de señalización de TGF $\beta$  y es dependiente de histonas deacetilasas (HDACs). Análisis adicionales utilizando manipulación genética en modelos murinos y humanos, caracterización molecular y ensayos funcionales *in vitro* e *in vivo* revelaron que la expresión de ASPA en fibroblastos normales o CAFs afecta su comportamiento pro-tumoral al regular la activación de los fibroblastos, la capacidad de remodelación de la matriz extracelular y la interacción con células cancerosas. Este estudio proporciona nuevas perspectivas sobre la interacción entre reorganizaciones metabólicas y la generación de CAFs, al describir un papel clave de la enzima metabólica ASPA en la regulación de funciones y fenotipos pro-tumorales críticos en CAFs.



**ACKNOWLEDGEMENTS**  
**AGRADECIMIENTOS**  
**AGRAÏMENTS**



*Cuatro años y medio, se dice rápido.*

*Ha sido un proceso largo, y no siempre fácil. Sin embargo, las personas que han estado presentes en esta etapa de mi vida me han ayudado a allanar este camino. Tengo tanto a agradecer, que solo espero no dejarme a nadie.*

*Quiero agradecer en primer lugar a la persona que me dio la oportunidad de emprender este camino, Fernando. Gracias por confiar en mí y elegirme para formar parte de tu equipo. Ha sido un honor para mí, y he podido crecer tanto a nivel profesional, como personal. Espero que el lab siga creciendo y vayáis acumulando éxitos, como hasta ahora. Muchas gracias por enseñarme y guiarme estos años.*

*También quiero agradecer a Alberto Sánchez y José Luís por evaluarme y seguirme durante este tiempo. Gracias por vuestra implicación y por vuestros consejos.*

*On the other hand, I would like to thanks to Prof. Sara Zanivan and Dr. Emily Kay for their warm welcome to the Beatson Institute in Glasgow, and for all the help and mentoring during these three months. It has been a pleasure. Besides, I would like to acknowledge the EMBO scientific Exchange grant for the funding of the international internship.*

*Gracias también al personal del IBBTEC, especialmente a Charo, por lidiar con todos mis trámites burocráticos y siempre anteponer nuestros intereses. También a Pepi, por ir repartiendo alegría y bombones, que nos amenizaban las tardes.*

*Gracias a todos los otros laboratorios donde hemos ido a pedir/molestar. Al grupo de Ana Vi, a los Rada, a los Varela, y sobre todo a los Piero. Las tardes son más entretenidas escuchándoos dar voces o reír a carcajadas desde nuestro labo.*

*En especial, quiero agradecer a Laura, por ser tan buena y abrirte tan rápido con nosotras. ¡Como se nota que eres andaluza! Laura, espero que todo termine bien y ojalá poder volver para verlo. Y ya sabes, te espero en Mallorca (trae unas cuantas cookies de esas que tú sabes hacer). Un abrazo enorme.*

*También quiero agradecer a Ana toda su ayuda tanto profesional como personal. Por las charlas en el comedor, algunas más optimistas, otras que no tanto. Estoy muy contenta de haber estado presente en tus momentos de éxito este año, y los que quedan por llegar...Ánimo PI, la cima ya no está tan lejos.*

*A ti Berta, gracias por toda tu ayuda con los experimentos in ovo. Por tu paciencia y tu amabilidad.*

*Por supuesto, quiero agradecer a todo mi grupo por el tremendo apoyo en todo este tiempo. Desde el minuto uno que llegué, allá por el 2019, me sentí (casi) como en casa y la amistad surgió más rápido de lo que esperaba.*

*Bea, gracias por ser compañera de trabajo, piso, confinamiento, gorduras, y un largo etc. Hemos vivido muchas cosas en estos cuatro años y estás en muchos buenos recuerdos que me llevo a casa. Mucho ánimo para tu recta final, ¡que ya no queda nada! Nunca pierdas esa niña que llevas dentro, y que sale con los subidones de azúcar. Siempre tendrás casa en Mallorca.*

*Carmen, gracias por sacarnos unas risas con tus tremendos zascas, que sabemos que no van a malas, o eso dices tu... También te quiero dar las gracias por todo tu trabajazo haciendo bloques, cortando, y todo eso que tu tan bien sabes hacer. Mucho ánimo con todo y con la carrera!*

*Diane, thank you for all your help in these years. I have no doubt that your thesis will be amazing, as all the work that you have done until now. You will achieve whatever you want, and hopefully, next time, it will be closer to your family. We both know how hard it has been. Beaucoup d'encouragement, un énorme câlin!*

*Francesca, gracias por traer un poquito de Italia al lab. Espero que te vaya muy bien con tu proyecto y que disfrutes del proceso, estoy segura de que así será. ¡Aunque deberías ordenar tu escritorio! Mucha suerte con todo.*

*Javi, gracias infinitas por acogerme, así como lo has hecho. Has sido fundamental en esta etapa, tanto a nivel científico como personal. Gracias por toda la ayuda y sobre todo por las risas que nos hemos echado en no sé cuántas ocasiones. Eres un tío de p\*\*\* madre. Enzito tiene mucha suerte de tenerte a ti y a Ana. ¡Ánimo con todo y un abrazo enorme!*

*María, desde el minuto uno. Gracias. Estos años no hubieran sido lo mismo sin ti. Y como tu bien dices, si hubiera ido a otro lado no nos hubiéramos conocido, y la verdad que sería una gran pena. Aunque bien pensado, todos tus caminos llevan a sa Pobra, así que igual nos hubiéramos conocido en la plaza de mi pueblo. Gracias por el apoyo, por las risas, por alegrarnos el día a día, y por todos los momentos que hemos vivido juntas. Bihotzean eramaten zaitut. Te espero en Mallorca.*

*Miguel, que aunque estes en el zulo, nos acordamos de ti. Muchísimas gracias por toda tu ayuda bioinformática, que no ha sido poca. Por abrirnos las puertas de tu casa, y por tus historietas tan interesantes. ¡Un abrazo enorme!*

*Patri, la madrileña menos madrileña que he conocido. Muchísimas gracias por tu ayuda, especialmente en estos últimos meses, no sé qué hubiera hecho con los*

*ratoncillos de no ser por ti. Mucho ánimo con la tesis, pero viendo lo trabajadora que eres no tengo dudas de que todo te irá genial. Un abrazo enorme.*

*Silvia, mi arma. Gracias por estos años, compartiendo problemas, desesperación y alguna que otra alegría. Gracias también por dejarme formar parte de algo tan bonito como fue tu boda. Solo espero que en esta siguiente etapa te vaya todo muy bien y sigas tan feliz con Eduardo y tu Miyo. Gracias de corazón.*

*David, gracias por ser tan valiente y entrar en un labo lleno de chicas y caernos bien a todas. Me encantó conocerte y me llevo muchos recuerdos divertidos contigo. Por favor, ¡contrólate la glucosa!*

*Laurita, te tengo que agradecer tanto que no se ni por dónde empezar. Gracias, por estar allí siempre, con mis mil y una dudas sobre el doctorado, temas burocráticos, etc. Gracias por allanar el camino, y siempre tenderme la mano. Eres de las mejores personas que he conocido en esta etapa. No tengo dudas de que, a nivel profesional, vas a llegar a lo más alto, ya que a nivel personal no se puede ser mejor. Lo dicho, gracias por todo lo que tú ya sabes. Espero que nos veamos pronto, de corazón.*

*Sarita, poco fue el tiempo que compartimos en el IBBTEC, pero ya basto para ver que podíamos compartir tardes de cine y palomitas. Mil gracias, eres un encanto y espero que pronto puedas volver a Santander con tu Kai. ¡Un abrazo enorme, espero una visitilla!*

*Cris, gracias por estar en esta etapa de mi vida, y aunque solo compartimos piso año y pico, te fuiste siendo mi amiga. Gracias por tu apoyo, por hacerme runner durante una temporada, por abrirme las puertas de tu casa. Només esper poder tornar a visitar-te a la terreta, y tu en voler, a Mallorca. Moltes gràcies de tot cor.*

*Xisca, gràcies per dur un poquet de Mallorca a Santander. Només esper que te vagi tot bé i que puguis complir tots es teus somnis, tant professionals com personals. Tot sortirà bé. Mos veim per Mallorca!*

*Cati, gràcies infinites per es teu suport. Tot i que mos veim pics contats, sabem que sa nostra amistat sempre està allà. Gràcies per aquell viatge a Costa Brava, per ses rialles, que no son pagades. Per sempre esser-hi.*

*A ses nines, per tot es suport, per sempre creure en jo. Perquè quan torn, res pareix haver canviat. Només esper poder recuperar es moments perduts durant aquests quatre anys i disfrutar de sa vostre companyia. Vos estim.*

*A es padrins, per sempre preocupar-se i demanar-me “Com te va nina?” o de “I quan tornes Catalina?”. Aquesta tesi també va per ells.*

*A mon pare i ma mare, per recolzar-me incondicionalment en totes ses etapes de sa meva vida, tot i que impliqui que sa seva nina se'n va a viure a Barcelona, Santander o a Glasgow. Per sempre estar pendents de jo i ajudar-me en tot lo que faci falta, tant si es agafar un vol de 3 hores per acompanyar-me a Escòcia, com cuinar espinagades cada punt que torn. Sense voltros això no hagués estat possible. Aquesta tesi també es vostra. Vos estim molt.*

*I a tu, Pere Antoni. Fa quatre anys i mig que vivim a molts (massa) kilòmetres de distància, però sempre t'he notat a prop. Gràcies per recolzar-me en totes ses decisions de sa meva vida. Per deixar-me volar, sempre acompanyant-me i llevant-me pors que me sorgien per es camí. Gràcies per totes ses visites, tant a Santander com a Glasgow; Gràcies per descobrir món junts, per ses experiències viscudes i per créixer plegats, com sempre. No puc tenir millor company de vida. Ets incondicional i si he aguantat fins aquí, és gràcies a tu. Només esper poder recuperar tot aquest temps al teu costat, i seguir avançant de sa mà. T'estim.*

## **ABBREVIATIONS**



## ABBREVIATIONS

### ABBREVIATIONS

<b><math>\alpha</math>-HB:</b> $\alpha$ -hydroxybutyrate	<b>DEG:</b> Differentially expressed genes
<b><math>\alpha</math>-SMA:</b> smooth muscle actine protein	<b>DKK3:</b> Dickkopf WNT signalling pathway inhibitor 3
<b>2-HG:</b> 2-hydroxyglutarate	<b>DMEM:</b> High Glucose Dulbecco's Modified Eagle's Medium
<b>ACLY:</b> ATP-citrate Lyase	<b>DNA:</b> Deoxyribonucleic acid
<b>ACSS1/2:</b> Acyl-CoA Synthetase Short Chain Family Member 1/2	<b>ECL:</b> Enhanced chemiluminescence
<b>AKT:</b> Alpha Serine/Threonine-Protein Kinase	<b>ECM:</b> Extracellular matrix
<b>apCAF:</b> Antigen presenting Cancer-Associated Fibroblast	<b>EMT:</b> epithelial to mesenchymal
<b>ASNS:</b> Asparagine synthetase	<b>ERK:</b> extracellular signal-regulated kinases
<b>ASP-NAT:</b> aspartate N-acetyltransferase	<b>FAK:</b> focal adhesion kinase
<b>ASPA:</b> Aspartoacylase	<b>FAP:</b> Fibroblast activation protein
<b>ATF4:</b> Activating Transcription Factor 4	<b>FBS:</b> Fetal Bovine Serum
<b>ATP:</b> Adenosine triphosphate	<b>FOLH1:</b> folate hydrolase 1
<b>BSA:</b> Bovine serum albumin	<b>FRA2:</b> Fos-related antigen 2
<b>CAF:</b> Cancer associated fibroblast.	<b>GCP-II/III:</b> Glutamate carboxypeptidase II/II
<b>CAM:</b> chorioallantoic membrane	<b>GFP:</b> Green Fluorescent Protein
<b>CCL2:</b> monocyte chemoattractant protein-1, MCP-1	<b>GLS1:</b> Glutaminase 1
<b>CCM3:</b> Cerebral cavernous malformations	<b>GLUT1:</b> Glucose Transporter 1
<b>CD:</b> Canavan disease	<b>GO:</b> Gene Ontology
<b>CNS:</b> Central nervous system	<b>GRM3:</b> Glutamate Metabotropic Receptor 3
<b>COLL11A1:</b> Collagen Type XI Alpha 1 Chain	<b>GS:</b> Glutamine synthetase
<b>CTD:</b> Comparative Toxicogenomic Database	<b>HA:</b> Hyaluronan
<b>CX3CL:</b> Chemokine (C-X-C motif) ligand 3	<b>HDAC:</b> Histone deacetylases
<b>CXCL:</b> chemokine (C-X-C motif) ligand	<b>HGF:</b> Hepatocyte growth factor
<b>CXCR4:</b> C-X-C motif chemokine receptor 4	<b>HIF1<math>\alpha</math>:</b> Hypoxia Inducible Factor 1 Subunit $\alpha$
	<b>HLF:</b> Hepatic Leukaemia factor
	<b>hPC CAF:</b> human Prostate Cancer Cancer-associated fibroblast
	<b>HSF1:</b> Heat shock factor 1

## ABBREVIATIONS

**iCAF:** inflammatory Cancer-associated fibroblast

**IDH:** isocitrate dehydrogenase

**IFN $\gamma$ :** interferon  $\gamma$

**IGF-BP6:** Insulin-like growth factors binding protein-6

**IL1:** interleukin 1

**IL6:** interleukin 6

**JNK:** c-Jun amino N-terminal protein kinase

**KC:** Keratinocyte Chemoattractant

**KEGG:** Kyoto Encyclopaedia of Genes and Genomes

**KRAS:** Kirsten rat sarcoma virus

**LDH:** Lactate dehydrogenase enzyme

**LOXL2:** Lysyl oxidase like 2

**M-CSF1:** Macrophage Colony-Stimulating Factor-1

**MAPK:** Mitogen-activated protein kinases

**MCPI:** Monocyte Chemotactic protein-1

**MHC II:** Major Histocompatibility complex class II

**MIP1:** Macrophage inflammatory protein-1

**MMP:** matrix metalloproteases

**mTORC:** mammalian Target of rapamycin

**myCAF:** myofibroblast Cancer-Associated fibroblast

**NAA:** N-AcetylAspartate

**NAAG:** N-acetylaspartylglutamate

**NAALAD2:** N-Acetylated Alpha-Linked Acidic Dipeptidase 2)

**NAT8L:** N-acetyltransferase 8-like

**NDRG-3:** N-Myc downstream-regulated-3

**NF:** Normal Fibroblast

**NMDAR:** N-methyl-d-aspartate receptors

**OPN:** osteopontin

**OXPHOS:** oxidative phosphorylation

**PD106:** Diphenylamide 106

**PDGF:** Platelet derived growth factor

**PDGFR:** Platelet derived growth factor receptor

**PFA:** Paraformaldehyde

**PGC1 $\alpha$ :** Peroxisome proliferator-activated receptor-gamma coactivator (PGC)-1 $\alpha$

**PI3K:** phosphoinositide 3-kinase

**PPP:** Pentose phosphate pathway

**PRECOG:** PREdiction of Clinical Outcomes from Genomic Profiles

**PYCR1:** pyrroline-5-carboxylate reductase 1

**ROCK:** Rho Associated Coiled-Coil Containing Protein Kinase

**ROS:** Reactive oxygen species

**SDF1:** Stromal-Derived Factor 1

**SDH:** succinate dehydrogenase

**SDS-PAGE:** sodium dodecyl sulphate (SDS)-polyacrylamide gel electrophoresis (PAGE)

**SLC1A3:** Solute Carrier Family 1 Member 3

**SOX11:** SRY-related HMG-box

**SRF:** Serum response factor

**STC1:** stanniocalcin 1

**TAM:** Tumour associated macrophages

**TAZ:** Transcriptional coactivator with PDZ-binding motif

**TCA:** Tricarboxylic acid cycle

## ABBREVIATIONS

**TCGA:** The Cancer Genome Atlas

**TEAD:** Transcriptional enhanced  
associate domain

**TGF $\beta$ :** Transforming Growth Factor- $\beta$

**TIMP1:** Tissue inhibitor matrix  
metalloproteinase 1

**TME:** tumour microenvironment

**TNF $\alpha$ :** Tumour necrotic factor  $\alpha$

**TSA:** Trichostatin-A

**vCAFs:** vascular Cancer-Associated  
Fibroblasts

**VEGF:** Vascular endothelial growth  
factor

**WB:** Western Blot

**YAP:** yes-associated protein



**INDEX**



<b>1</b>	<b>INTRODUCTION</b>	<b>28</b>
<b>1.1</b>	<b>CANCER DISEASE</b>	<b>28</b>
1.1.1	CANCER EPIDEMIOLOGY	28
1.1.2	RISK FACTORS ASSOCIATED WITH CANCER	29
1.1.3	CANCER RECURRENCE	30
1.1.4	CHALLENGES AND FUTURE PERSPECTIVES	31
<b>1.2</b>	<b>TUMOUR MICROENVIRONMENT</b>	<b>32</b>
1.2.1	DEFINITION AND COMPOSITION	32
1.2.2	CANCER-ASSOCIATED FIBROBLASTS	35
<b>1.3</b>	<b>METABOLIC REPROGRAMMING IN TUMOURS</b>	<b>54</b>
1.3.1	METABOLIC REPROGRAMMING IN CANCER CELLS	54
1.3.2	METABOLIC REPROGRAMMING IN CAFs	57
1.3.3	METABOLITES AS SIGNALLING MOLECULES	59
<b>1.4</b>	<b>ASPARTOACYLASE ENZYME</b>	<b>60</b>
1.4.1	DEFINITION AND ACTION	60
1.4.2	NAA AND ASPA IN BRAIN	61
1.4.3	NAA AND ASPA OUTSIDE THE CNS	63
<b>2</b>	<b>HYPOTHESIS AND OBJECTIVES</b>	<b>68</b>
<b>3</b>	<b>MATERIALS AND METHODS</b>	<b>72</b>
<b>3.1</b>	<b>MATERIALS</b>	<b>72</b>
3.1.1	CELL LINES	72
3.1.2	ANIMALS	74
3.1.3	MEDIUMS, SOLUTIONS, KITS, AND REAGENTS	75
3.1.4	RECIPES	81
<b>3.2</b>	<b>EXPERIMENTAL PROCEDURES</b>	<b>83</b>
3.2.1	CELL BIOLOGY AND IN VIVO METHODS	83
3.2.2	MOLECULAR PROCEDURES	93
<b>3.3</b>	<b>COMPUTATIONAL ANALYSIS</b>	<b>103</b>
3.3.1	RNA-SEQUENCING (RNASEQ) PROCESSING AND ANALYSIS	103
3.3.2	GENE SET ENRICHMENT ANALYSIS (GSEA)	104
3.3.3	GENE EXPRESSION ANALYSIS OF CLINICAL DATASETS	105
3.3.4	ENRICHMENT ANALYSIS	105
3.3.5	SURVIVAL ANALYSIS	106
3.3.6	SINGLE CELL RNASEQ (SCRNASEQ) PROCESSING AND ANALYSIS	106
3.3.7	STATISTICAL ANALYSIS	110

<b>4</b>	<b>RESULTS</b>	<b>116</b>
<b>4.1</b>	<b>IDENTIFICATION OF ASPA AS A NEW TUMOUR STROMA GENE WITH PROGNOSTIC VALUE.</b>	<b>116</b>
4.1.1	GENE EXPRESSION ANALYSIS OF PUBLIC DATASETS FOR THE IDENTIFICATION OF CONSISTENTLY DYSREGULATED GENES IN THE TUMOUR STROMA.	116
4.1.2	ASPA IS CONSISTENTLY DOWNREGULATED IN CANCER STROMA, AND IT HAS PROGNOSTIC VALUE.	121
4.1.3	ASPA IS MAINLY EXPRESSED BY FIBROBLASTS.	124
4.1.4	ASPA NEGATIVELY CORRELATES WITH MYCAFs FEATURES.	127
<b>4.2</b>	<b>INVESTIGATING THE MECHANISM OF ASPA DOWNREGULATION IN CAFs.</b>	<b>134</b>
4.2.1	TGF $\beta$ SIGNALLING AS A POTENTIAL REPRESSOR OF ASPA IN CAFs.	134
4.2.2	TGF $\beta$ EXERT ITS EFFECT THROUGH TAZ IN MNFs.	136
4.2.3	HDAC AS POTENTIAL COMMON EFFECTORS OF ASPA REPRESSION IN FIBROBLASTS.	138
<b>4.3</b>	<b>TO INVESTIGATE ASPA FUNCTIONAL RELEVANCE IN FIBROBLASTS.</b>	<b>142</b>
4.3.1	ASPA DOWNREGULATION INDUCES FIBROBLAST ACTIVATION AND CONTRACTILITY.	142
4.3.2	ASPA DOWNREGULATION IN MNFs PROMOTES CANCER CELL PROLIFERATION <i>IN VITRO</i> .	146
4.3.3	ASPA LOSS IN NFs ACCELERATES TUMOUR EMERGENCE <i>IN VIVO</i> .	149
4.3.4	ASPA OVEREXPRESSION IN MCAFs DOES NOT AFFECT THEIR MYCAFs FEATURES.	151
4.3.5	ASPA OVEREXPRESSION IN HUMAN PCA CAFs HAS PROFOUND EFFECTS IN CAF BEHAVIOUR.	153
4.3.6	ASPA OVEREXPRESSION ATTENUATES HCAF CAPACITY TO PROMOTE TUMOUR GROWTH AND METASTASIS <i>IN VIVO</i> .	157
<b>4.4</b>	<b>TO INVESTIGATE THE MOLECULAR PROCESSES UNDERLYING ASPA FUNCTIONS IN FIBROBLASTS AND ITS IMPLICATION IN CANCER.</b>	<b>160</b>
4.4.1	ASPA SILENCING INDUCES A SPECIFIC GENE EXPRESSION PROGRAM IN NFs.	160
4.4.2	GENE ONTOLOGY ANALYSIS OF DIFFERENTIAL GENE EXPRESSION PROFILES INDUCED BY ASPA SILENCING IN NF.	161
4.4.3	GENE SET ENRICHMENT ANALYSIS OF DIFFERENTIAL GENE EXPRESSION INDUCED BY ASPA MODULATION IN NF.	163
<b>4.5</b>	<b>INVESTIGATING THE MECHANISM OF ACTION OF ASPA IN MODULATING CAF BEHAVIOUR.</b>	<b>170</b>
4.5.1	TGF $\beta$ -MEDIATED ACTIVATION OF FIBROBLASTS IS ENHANCED AFTER ASPA LOST.	170
4.5.2	ASPA MODULATION AFFECTS CANONICAL WNT SIGNALLING PATHWAY.	171

## INDEX

4.5.3	ASPA POTENTIALLY CONTRIBUTES TO EPIGENETIC REPROGRAMMING IN FIBROBLASTS.	174
4.5.4	INVESTIGATING PATHWAYS INTERCONNECTION.	177
4.5.5	ASPA MODULATION TRIGGERS METABOLIC REPROGRAMMING IN FIBROBLASTS.	179
<b>5</b>	<b><u>DISCUSSION</u></b>	<b><u>198</u></b>
<b>5.1</b>	<b>IDENTIFICATION OF ASPA AS A NEW TUMOUR STROMAL GENE WITH PROGNOSTIC VALUE.</b>	<b>198</b>
<b>5.2</b>	<b>TO INVESTIGATE THE MECHANISM OF ASPA DOWNREGULATION IN CAFs.</b>	<b>199</b>
<b>5.3</b>	<b>TO INVESTIGATE ASPA FUNCTIONAL RELEVANCE IN FIBROBLASTS.</b>	<b>201</b>
<b>5.4</b>	<b>INVESTIGATING THE MECHANISM OF ACTION OF ASPA IN MODULATING CAF BEHAVIOUR.</b>	<b>206</b>
5.4.1	STUDYING SIGNALLING PATHWAYS PERTURBATIONS AFTER ASPA MODULATION.	206
5.4.2	STUDYING METABOLIC REARRANGEMENTS AFTER ASPA MODULATION.	211
<b>6</b>	<b><u>CONCLUSIONS</u></b>	<b><u>216</u></b>

## FIGURES

### **Introduction/ Materials and Methods**

Figure 1. National Ranking of Cancer as a Cause of Death at Ages <70 Years in 2019. Figure taken from Sung H. et al (2021).

Figure 2. Schematic representation of the tumour microenvironment. Different cells represented: cancer cells, cancer associated fibroblasts, adipocytes, granulocytes, pericytes, macrophages and T-cells. Figure taken from Prajapati, P. et al (2016).

Figure 3. Contributions of activated/recruited stromal cells to the hallmarks of cancer. Figure taken from Hanahan, D. et al (2012).

Figure 4. Transforming Growth Factor beta canonical and non-canonical pathway. Source: BioRender.

Figure 5. Wnt signalling pathway. Source: BioRender.

Figure 6. Subtypes of CAFs depending on the stimuli received. Figure taken from Vaish, U. (2021)

Figure 7. CAF-directed therapies. Preclinical and clinical methods to target CAFs. Figure token from Gieniec, K.A (2019).

Figure 8. A comparison between cell metabolism of differentiated tissue vs proliferative or tumor. Figure taken from Heiden, V. et al (2009)

Figure 9. Schematic diagram showing the NAA metabolism and ASPA implication. Handmade.

Figure 10. Representation of NAA metabolism in brain. Figure taken from Long, Patrick M. et al (2013).

Figure 11. Schematic representation of cells inoculation into the chicken embryo.

Figure 12. Representation of Neubauer chamber.

Figure 13. Schematic representation of the workflow of tracing experiments.

Figure 14. Representative scheme of the Cytokines array protocol.

**Results**

Figure 1.1. Strategy followed to identify potential tumour stroma regulators.

Figure 1.2. Identification of consistently dysregulated genes in the tumor stroma vs normal tissue.

Figure 1.3. ASPA downregulation in stroma has prognostic value in breast cancer patients.

Figure 1.4. ASPA stromal downregulation is a consistent feature in cancer.

Figure 1.5. ASPA expression in stroma shows prognostic value in clinics.

Figure 1.6. ASPA is expressed by fibroblasts outside the CNS.

Figure 1.7. ASPA is downregulated in CAFs.

Figure 1.8. ASPA expression negatively correlates with CAFs and myCAF features (part 1).

Figure 1.9. ASPA expression negatively correlates with CAFs and myCAF features (part 2).

Figure 1.10. ASPA expression is downregulated in human and murine CAFs cell lines.

Figure 2.1. TGF $\beta$  downregulates ASPA expression.

Figure 2.2. TGF $\beta$  downregulates ASPA expression through TAZ signalling.

Figure 2.3. TGF $\beta$  downregulates ASPA expression through HDAC activity.

Figure 3.1. Aspa downregulation induces myCAF features and functions.

Figure 3.2. Aspa overexpression impairs TGF $\beta$ -mediated activation of fibroblasts.

Figure 3.3. Aspa downregulation in fibroblasts promotes cancer cell proliferation.

Figure 3.4. Aspa downregulation in fibroblasts promotes cancer cell proliferation in restrictive conditions.

Figure 3.5. Study of cytokines secreted after Aspa modulation in NFs.

Figure 3.6. Aspa downregulation in fibroblasts promotes cancer cell proliferation in vivo.

Figure 3.7. ASPA overexpression in fully CAFs does not exert an impairment in contractility or cancer cell proliferation.

Figure 3.8. ASPA overexpression in human PCa CAFs impairs myCAF features.

Figure 3.9. ASPA overexpression in human PCa CAFs attenuates their capacity to promote cancer cell growth.

## INDEX

Figure 3.10. Modulating ASPA expression in human PCa CAFs deters tumour growth and metastasis in vivo.

Figure 4.1. Aspa silencing induces a specific gene expression program in normal fibroblasts.

Figure 4.2. Transcriptomic changes induced by Aspa silencing in NFs are associated with CAF activation.

Figure 4.3. Transcriptomic changes induced by Aspa silencing in NFs are associated with CAF activation.

Figure 4.4. Transcriptomic changes induced by Aspa silencing in NFs are associated with CAF features.

Figure 4.5. Constitutive expression of ASPA represses TGF $\beta$ -induced fibroblast activation.

Figure 5.1. Aspa silencing enhances TGF $\beta$  signalling pathway in NFs.

Figure 5.2. Aspa expression impairs Wnt signalling.

Figure 5.3. Aspa as a potential regulator of acetyl-H3 levels.

Figure 5.4. Study of the pathway interconnection after the modulation of Aspa expression.

Figure 5.5. Transcriptomic study after Aspa modulation in mNFs.

Figure 5.6. Schematic representation metabolic pathways related to glycolysis, TCA and OXPHOS.

Figure 5.7. Aspa expression correlates with a higher glycolysis.

Figure 5.8. ASPA loss potentially correlates with higher OXPHOS activity.

Figure 5.9. Study of the energetic status of the cells after Aspa perturbation in mNFs and hCAFs.

Figure 5.10. Study of the TCA cycle activity after Aspa silencing.

Figure 5.11. Study of the TCA cycle activity after Aspa overexpression.

Figure 5.12. Study of the TCA cycle activity with exogenous NAA after Aspa modulation

Figure 5.13. Aspa expression triggers a glutamine dependency in hCAFs

Figure 5.14. Aspa silencing does not show a clear effect in glutamine dependency in NFs.

## **Discussion**

Figure 1. Discussion section. Representative scheme of the findings in this project.

## INDEX

### **TABLES**

Table 1. Table summarizing cell lines used in this project. Name, origin, source.

Table 2. Transfection reagent used in this project. Procedure and reagent specified.

Table 3. Table summarizing culture cell reagents used in this project. Company and reference number are specified.

Table 4. Table summarizing Western Blot reagents used in this project. Company and reference number are specified.

Table 5. Table of RNA extraction and purification reagents. Company and reference number are specified.

Table 6. Table summarizing DNA extraction from chicken embryo organs. Company and reference number are specified.

Table 7. Table summarizing RT and qPCR kits. Company and reference number are specified.

Table 8. Table of reagents used for bacterial culture and transformation. Company and reference number are specified.

Table 9. Kit used for plasmid extraction. Company and reference number are specified.

Table 10. Plasmid library of this project. Company and reference number are specified.

Table 11. Table summarizing factors and drugs used in this project. Company and reference number are specified.

Table 12. Table of luciferase assay reagents. Company and reference number are specified.

Table 13. Table of metabolomic reagents. Company and reference number are specified.

Table 14. Table of Seahorse assay reagents. Company and reference number are specified.

Table 15. Table for cytokine array study. Company and reference number are specified.

Table 16. Table summarizing laboratory solutions and buffers. Company and reference number are specified.

Table 17. Table summarizing fungible material used in this project. Company and reference number are specified.

Table 18. Software used in this project.

Table 19. Table summarizing siRNAs used in this thesis.

Table 20. Summary of the antibodies used in this thesis: protein, dilution, source, and reference number.

Table 21. Summary of oligonucleotides used in this thesis: protein, dilution, source, and reference number.



## **INTRODUCTION**



# 1 INTRODUCTION

## 1.1 CANCER DISEASE

### 1.1.1 Cancer epidemiology

Cancer is one of the main causes of death worldwide, with almost 20 million new cases and 10 million cancer-related deaths estimated in 2020 (Figure 1). This number is expected to increase to 29 million cases in 2040. In general, cancer incidence and overall mortality rates are increasing due to many socio-economic factors such as aging or changes in the risk factors associated to cancer. For example, breast cancer is the most diagnosed cancer, while lung cancer is presenting the highest number of deaths, which is tightly linked to the smoking habit of the population<sup>1,2</sup>. Despite of the increased incidence of the disease, tumour burden is being reduced as a result of primary prevention campaigns and better diagnosis, as well as with the development of improved personalized treatments.

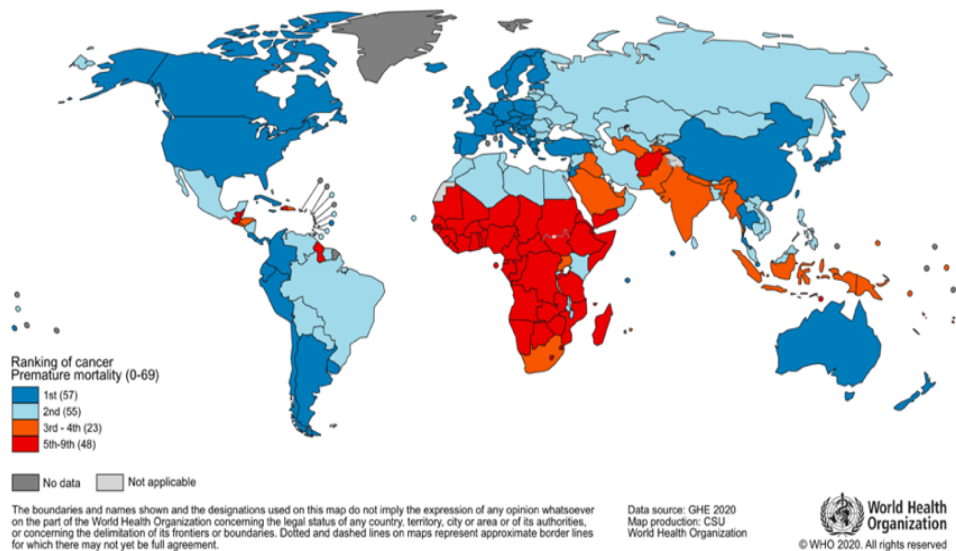


Figure 1. National ranking of cancer as a cause of death at ages over 70 Years in 2019. Figure taken from Sung H. et al (2021).

### **1.1.2 Risk factors associated with cancer**

Cancer is a disease with a multifaceted nature, encompassing intrinsic and extrinsic cues<sup>3</sup>. The onset of malignant cell growth can be influenced by external factors including the age of the patient, dietary habits, tobacco use, alcohol consumption, occupation exposures and environmental factors<sup>4</sup>. Notably, many of these risk factors are modifiable through lifestyle changes, which may reduce the susceptibility to develop cancer. Conversely, intrinsic factors are less modifiable and involve cell-intrinsic factors, as well as systemic or local changes at organism or tissue levels, such as alterations in metabolism, infections, inflammation and oxidative stress, among others<sup>3,4</sup>. While these intrinsic factors present greater challenges for direct intervention, ongoing research aims to develop therapies targeting specific genetic abnormalities and molecular/cellular dysregulations.

Therefore, understanding the interplay between these factors and their impact in cancer development is crucial for developing effective cancer prevention and treatment strategies. Lifestyle modifications, early detection and advancements in medical research and technology are critical components in the ongoing fight against cancer. All these elements require an improved understanding of the fundamental mechanisms underlying cancer emergence, development, dissemination and response to therapy.

### 1.1.3 Cancer recurrence

Metastasis represents the primary contributor to cancer recurrence and patient mortality. Consequently, individuals experiencing relapse often require the most aggressive treatments available, including chemotherapy, immunotherapy, targeted therapy and other advanced modalities. Nevertheless, these treatments are not always effective since patients with recurrent disease show a fast disease progression and higher tumour aggressiveness<sup>5</sup>. A key factor contributing to this challenge lies in the selective pressure exerted on the primary tumour during therapy, as only the most aggressive cancer cells can overcome the treatment, and will be the ones contributing to recurrence. Cells with metastatic potential in the primary tumour need to orchestrate a series of adaptations to proliferate, invade adjacent tissues, avoid immunosurveillance and colonize distal organs. Aggressive cancer cells can acquire different phenotypes and evolve to address all these different restrictions and requirements. Moreover, cancer cells can also manipulate their microenvironment generating nurturing niches required for the establishment of malignant phenotypes associated with tumour development and dissemination. These adaptations involve changes in the vasculature to provide the nutrients and oxygen required for fast uncontrolled growth; interfere with the host immune response; as well as the modulation of other stromal cells such as fibroblasts, that can become transformed into active pro-tumour entities<sup>6</sup>. Importantly, this intricate interplay is highly dynamic and both malignant cells and their surrounding environment co-evolve during cancer progression and therapy, underlying the paramount challenge in the understanding advanced cancer<sup>7</sup>.

### **1.1.4 Challenges and future perspectives**

Nowadays, numerous approaches are employed to delineate cancer risk and potential causes, with the foremost challenge being cancer prevention. Concurrently, studies have delved into understanding the molecular biology underlying the appearance of the disease, predominantly focusing on targeting intrinsic factors in cancer cells<sup>3,4</sup>. However, the emergent role of tumour stromal cells and their heightened genetic stability has positioned them as potential targets to impede tumour progression. Consequently, there is a significant growing interest in understanding the altered status of stromal cells within tumours and their contribution to distinct tumoral processes and characteristics<sup>6</sup>.

This scenario underscores the need for urgent development of novel approaches that integrate knowledge pertaining to the intrinsic effects of both cancer and stromal cells, coupled with external cues that trigger cancer development and dissemination.

### 1.2 TUMOUR MICROENVIRONMENT

#### 1.2.1 Definition and composition

In recent years, there has been a significant evolution in the understanding of cancer disease. Solid tumours are no longer solely perceived as a cluster of tumour cells. Instead, it is widely acknowledged that tumours encompass various cell types within the tumour stroma, which are both recruited and influenced by cancer cells. The dynamic interplay between malignant cells and stromal cells constitutes what is known as the Tumour Microenvironment (TME)<sup>8</sup>. The TME is a complex milieu comprising diverse cell types, including infiltrating immune cells, fibroblasts, endothelial cells forming blood and lymphatic vessels, pericytes and adipocytes, among other cell types. In addition, the TME contains non-cellular components shaping the extracellular matrix (ECM), which is a mixture of proteoglycans and glycoproteins such as collagens and laminins, that provides structural support for organs and tissues<sup>9</sup> (**Figure 2**). Typically, cell-specific markers allow the identification of various stromal cell types within this intricate milieu<sup>8,10</sup>. Furthermore, cancer cells exhibit the remarkable ability to modulate and assert dominance over the TME by orchestrating molecular and cellular events in their immediate surroundings. This manipulation corrupts various cell types within the TME, contributing ultimately to the establishment of a nurturing TME that is critical in tumour progression, dissemination and response to therapy<sup>10-</sup>

<sup>12</sup>.

## INTRODUCTION

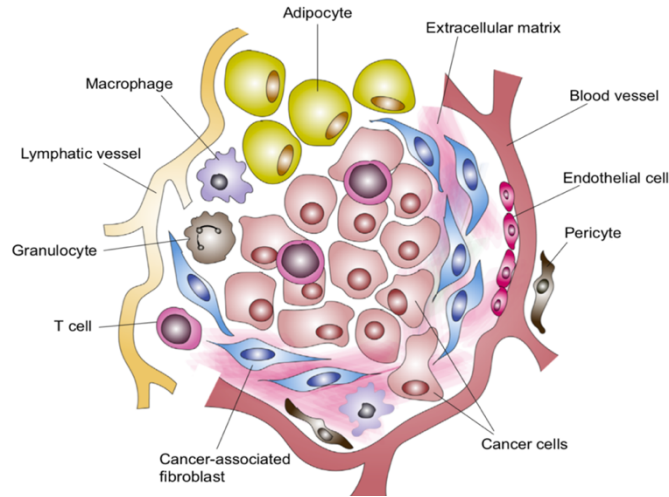


Figure 2. Schematic representation of the tumour microenvironment. Different cells represented: cancer cells, cancer associated fibroblasts, adipocytes, granulocytes, pericytes, macrophages and T-cells. Figure taken from Prajapati, P. et al (2016).

Comparisons between the function and structure of TMEs often draw parallels to wound healing or inflammatory processes. This analogy stems from the alterations observed in the tumour stroma during progression, mirroring features of pathological chronic inflammation. These modifications include the activation of common factors and the infiltration of inflammatory cells, among other shared characteristics<sup>10,11</sup>. This feature is associated with the acquisition of critical hallmarks in cancer, such as the promotion of tumour growth and invasion, enhanced formation of blood vessels (i.e. tumour-associated angiogenesis), the suppression of immunosurveillance and pathological ECM remodelling, among others. All these manipulations enable cancer cells to thrive, evade cell death, invade surrounding tissues and metastasize<sup>8,13</sup>. These pro-tumour properties and the reciprocal crosstalk between tumour cells and stromal cells are mainly driven by cytokines, chemokines, growth factors, inflammatory signals and matrix remodelling enzymes, which act against external and internal stimuli modulating cancer cell behaviour<sup>10</sup>. In addition, stromal cells can provide metabolites to sustain their altered phenotypes and

## INTRODUCTION

fuel cancer cell growth<sup>14</sup>. Thus, it has been described a well-established relationship between cancer cells and tumour stroma since tumours need to go through the reorganization of several biological processes in order to progress and disseminate. As a result, non-malignant cells in TME can show tumour-promoting functions at all stages of the tumorigenesis that are generally not observed in non-pathological conditions. Therefore, stromal cells can contribute to the acquisition of different hallmarks of cancer, promoting tumour initiation, growth and dissemination<sup>8,15</sup> (**Figure 3**). Consequently, targeting either tumour stromal cells or the mediators of their communication holds therapeutic potential across various tumour types and may complement established anti-cancer therapies<sup>10</sup>. This is well exemplified by the recent development of immunotherapies and anti-angiogenic therapies, targeting immune cells and abnormal tumour vasculature, respectively.

Among the different stromal cell types in tumours, Cancer-Associated Fibroblasts (CAFs) are of particular interest: they represent one of the most abundant components of the TME in many solid tumours and play an active role in most of the pro-tumoral processes associated with cancer progression, dissemination and resistance to therapy<sup>16</sup>.

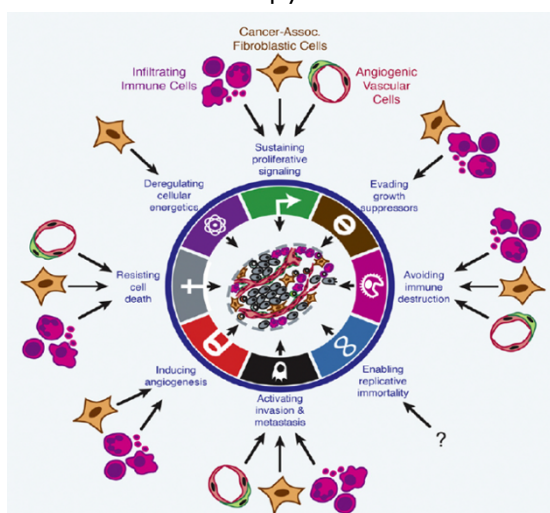


Figure 3. Contributions of activated/recruited stromal cells to the hallmarks of cancer. Figure taken from Hanahan, D. et al (2012).

### **1.2.2 Cancer-Associated Fibroblasts**

#### **1.2.2.1 Definition, origin and characteristics**

Normal fibroblasts (NFs) are cells of the connective tissue stroma that exhibit functions such as supporting tissue homeostasis, regulating ECM deposition, inflammation and epithelial cell proliferation and differentiation. Upon tissue damage or altered homeostasis, NFs can undergo a phenotypic change associated with an activated state<sup>16</sup>. This phenotype is characterized by secretion of Transforming Growth Factor- $\beta$  (TGF $\beta$ ) and a high expression of alpha-smooth muscle actin protein ( $\alpha$ SMA) which confers contractile properties to the fibroblasts for tissue remodelling, regeneration and repair. Given these characteristics, these activated fibroblasts are defined as myofibroblasts. In normal situations, activated fibroblasts either undergo apoptosis or revert to a quiescent state when their activity is no longer needed or the activating insult is removed<sup>17</sup>. The reversibility in these cells is a feature of fibroblasts in tissue remodelling processes and suggests a certain level of phenotypic plasticity in fibroblasts<sup>16,18,19</sup>. However, the scenario in cancer is completely different. Fibroblasts in cancer are continuously receiving activating stimuli, suffering a phenotypic transformation that results in a permanent pathological activation defined as Cancer-Associated Fibroblast (CAF)<sup>20</sup>.

It is widely acknowledged that CAFs form an heterogeneous population that likely emerges from the high level of plasticity inherent to fibroblasts as well as from the multiple cellular origins that contribute to them. A substantial proportion of the CAFs population arises from the normal resident fibroblasts of the tissue<sup>21</sup>. However, it has been described that mesenchymal stem cells<sup>22</sup>, adipocytes<sup>23</sup>, epithelial cells or endothelial cells<sup>24-26</sup>, among others, can be transformed into CAFs in certain settings or in response to specific signals or manipulations. In addition, CAFs present distinct features associated to their tissue of origin or the wide myriad of

## INTRODUCTION

signals that can alter their behaviour<sup>15,27</sup>, which will also influence CAF heterogeneity.

In general, CAFs are described as perpetually activated fibroblasts that undergo a phenotypic transformation which involves perturbations in key signalling pathways<sup>19</sup>, aberrant ECM deposition capacity<sup>28,29</sup>, increased cytoskeleton function associated with high levels of actomyosin contractility, a reprogrammed secretome and metabolic profile<sup>30-32</sup>, as well as an enhanced crosstalk with cancer cells to boost tumour proliferation, invasion and metastasis<sup>33-36</sup>. Additionally, CAFs can crosstalk to other stromal cells contributing to the creation of an immunosuppressive and inflammatory stroma<sup>16,37</sup>, which also contributes to the generation of a permissive microenvironment for the tumour progression.

### ***1.2.2.2 Mechanisms underlying the pathological activation of CAFs***

The signals governing the aberrant activation of CAFs are not completely understood. This activation is observed in other pathological conditions, such as tissue fibrosis or chronic inflammation, characterized by an abnormal ECM deposition<sup>38</sup>. It is known that TGF $\beta$  and other pro-inflammatory cytokines are the main mediators of fibroblast activation during wound healing and fibrotic processes<sup>39,40</sup>. Thus, since tumours present a persistent level of inflammation, it is expected that similar pathways may be implicated in the sustained activation of fibroblasts in cancer. Notably, it has been reported that growth factors, cytokines and other signals accumulated in the TME contribute to the transformation into CAFs, such as TGF $\beta$ , osteopontin (OPN), IL-6, IL-1 $\beta$  and many others<sup>41,42</sup>. Besides, several studies have described the mechanisms used by the cancer cells to pathologically activate the fibroblasts. For instance, cancer cells secrete TGF $\beta$  which can induce the pro-tumorigenic phenotype of the fibroblasts<sup>43,44</sup>. In addition, cancer cells and other stromal cells may also produce significant amounts of

## INTRODUCTION

Platelet Derived Growth Factor (PDGF) that accumulates in the tumour stroma. CAFs present Platelet-Derived Growth Factor Receptor- $\beta$  (PDGFR $\beta$ ) which is overexpressed in processes such as inflammation, wound healing, fibrosis or in tumours<sup>45</sup>. Therefore, PDGF has the capacity to recruit fibroblasts to the tumour stroma where they get activated<sup>46</sup>. Moreover, Wnt ligands can also promote the emergence of CAF phenotypes, as it has been reported that aggressive breast cancer cells secrete Wnt7a, which promotes fibroblast recruitment and activation. This ultimately promotes ECM remodelling and increased cancer cell migration and dissemination<sup>47</sup>. A similar mechanism has been reported for the secretion of LOXL2 factor by mammary cancer cells, which activates fibroblasts through FAK signalling<sup>48</sup>.

Furthermore, alterations in the matrix stiffness or contact signals, DNA damage, high reactive oxygen species (ROS) levels, metabolic reprogramming and changes in several signalling pathways can all influence the behaviour of resident fibroblasts, contributing to the emergence of the pro-tumorigenic CAFs phenotypes<sup>19,49</sup>.

### ***1.2.2.3 Disrupted signalling pathways in CAFs***

In the process of differentiation from a NF into a CAF, several signalling cascades have been shown to be perturbed. More importantly, an emerging myriad of pathways and biological processes have been shown to actively alter gene expression programs that will ultimately influence fibroblast behaviour and favour tumour progression.

#### **1.2.2.3.1 Transforming growth factor $\beta$ (TGF $\beta$ )**

As previously mentioned, TGF $\beta$  has been extensively studied in the field of CAFs due to its substantial contribution to the establishment of activated phenotypes<sup>50</sup>. TGF $\beta$  can act through both canonical and non-canonical mechanisms in CAFs. In the canonical pathway, TGF $\beta$  ligands initiate the phosphorylation and binding of TGF $\beta$  type II and type I receptors, leading

## INTRODUCTION

to the phosphorylation of Smad2/3. The Smad2/3 complex binds to Smad4 and translocates into the nucleus, enhancing the expression of TGF $\beta$  target genes, such as  $\alpha$ SMA, Fibroblast Activation Protein (FAP), as well as ECM- and immunomodulatory-related genes (**Figure 4**). This results in an increased contractile capacity, enhanced proliferation and ECM production, along with other pro-tumoral functions that trigger the pathological myofibroblastic activation<sup>51,52</sup>. Besides, it has been reported that YAP/TAZ factors (see 1.2.2.3.3) may also act as TGF $\beta$  effectors, regulating or even enhancing Smad translocation to the nucleus<sup>53,54</sup>.

On the other hand, the non-canonical TGF $\beta$  pathway activates several kinases such as Extracellular Signal-Regulated kinase (ERK), p38, Janus Kinase/STAT3, Phosphoinositide 3-Kinase (PI3K)/AKT or Rho (**Figure 4**), which are linked to CAF proliferation, metabolic reprogramming and apoptotic process<sup>19,55</sup>. For instance, after TGF $\beta$  stimulation, human skin fibroblasts presented a higher phosphorylation of ERK1/2, which upregulated FRA2 transcription factor that exerts a pro-fibrotic effect<sup>56</sup>. Another example of TGF $\beta$  non-canonical pathway is the reported activation of PI3K/AKT-p21 signalling under TGF $\beta$  signalling, which promotes fibroblasts' proliferation<sup>57</sup>. Besides, it has been observed that p38 suppresses an antagonist of the Wnt pathway, upregulating  $\beta$ -Catenin active form, which favoured fibrosis<sup>58</sup>.

Additionally, TGF $\beta$  has the capacity to activate NFs in several tumour types inducing a CAF phenotype and operates in an autocrine and paracrine manner between cancer cells and CAFs<sup>43,59,60</sup>.

## INTRODUCTION

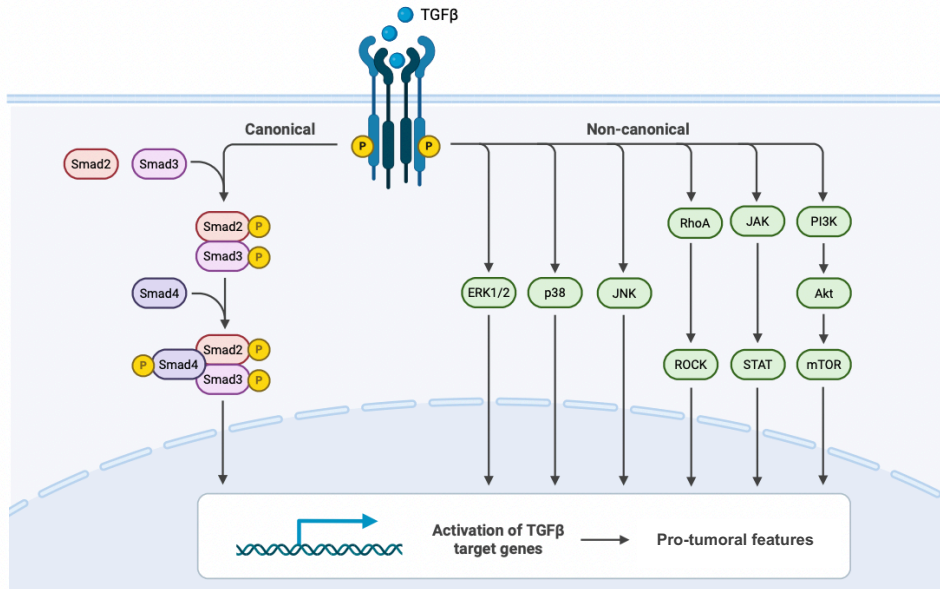


Figure 4. Transforming Growth Factor beta canonical and non-canonical pathway. Source: BioRender.

All these facts highlight the importance of the TGFβ pathway in the process of CAF activation and carcinogenesis, emphasizing its therapeutic potential to diminish fibroblast activation that is currently being explored in the clinic. For instance, enhanced TGFβ signalling has been observed in CAFs treated with cetuximab, leading to a decrease in treatment efficacy. The inhibition of SMAD3, however, restores the effectiveness of the treatment<sup>61</sup>. Additionally, in pancreatic cancer, the suppression of TGFβ pathway in CAFs resulted in the reversion of their aberrant activation and, ultimately, in tumour regression<sup>62</sup>.

## INTRODUCTION

### 1.2.2.3.2 Wnt Signalling

Perturbations in the Wnt signalling pathway are also observed in CAFs. In the canonical pathway, in the absence of Wnt ligands,  $\beta$ -catenin protein binds to the Axin complex and gets phosphorylated, leading to its degradation in the cytoplasm via ubiquitination<sup>19</sup>. In the presence of canonical Wnt ligands (Wnt1, 2 and 3a), the receptor gets phosphorylated, impeding  $\beta$ -catenin–Axin complex formation and blocking  $\beta$ -catenin degradation.  $\beta$ -catenin is then enabled to translocate into the nucleus, where it promotes the expression of its target genes. It has been described that Wnt/ $\beta$ -catenin signalling plays a key role in CAF activation, proliferation, ECM remodelling and cell plasticity<sup>19</sup> (**Figure 5**). For instance, in human melanoma, elevated levels of  $\beta$ -catenin were found in CAFs surrounding the tumour, conferring proliferative advantages and enhanced ECM remodelling capacity<sup>47,63</sup>. Additionally, it has been reported in breast cancer that Wnt3a can trigger the differentiation of adipocytes into CAFs, which exhibit an increased expression of ECM proteins collagen type I and fibronectin<sup>64</sup>. Importantly, CAFs may upregulate the production of Wnt ligands to promote Wnt/ $\beta$ -catenin signalling in a cell autonomous manner, or alter the expression of Wnt regulators<sup>65</sup>. DKK3, a HSF1 effector found to be consistently upregulated in CAFs, activates the canonical Wnt pathway and promotes  $\beta$ -catenin stabilization and signalling by potentiating the response to Wnt ligands<sup>65</sup>. Of interest, this mechanism also influences other canonical Wnt effectors such as YAP/TAZ factors, enhancing their signalling and function in CAFs<sup>66,67</sup>.

## INTRODUCTION

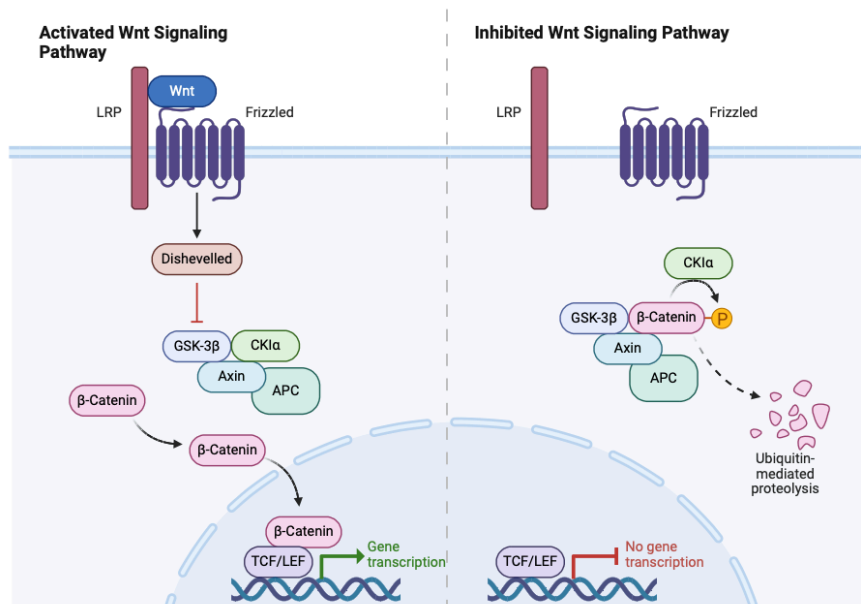


Figure 5. Wnt signalling pathway. On the right, inactivated Wnt signalling in the absence of Wnt ligands. On the left, pathway activation in response to Wnt ligand stimulation. Source: BioRender.

### 1.2.2.3.3 Mechanotransduction pathways: YAP/TAZ

The activation of the canonical Hippo pathway is initiated by signals associated primarily with cell polarity, cell-to-cell or cell-ECM adhesions, allowing for the regulation of tissue growth<sup>68</sup>. This pathway comprises a kinase cascade and the downstream effectors YAP1 and its paralog TAZ. YAP/TAZ are responsible for regulating the activity of TEAD family of transcription factors and TEAD-dependent target genes, mainly involved in cell proliferation, stemness, differentiation and other cellular processes. When the Hippo pathway is off, YAP/TAZ can translocate into the nucleus, binding TEAD and activating associated transcriptional programs. Conversely, when the Hippo pathway is on, it retains YAP/TAZ in the cytoplasm and prevents downstream signalling<sup>68</sup>.

Interestingly, it has been reported that in CAFs, physical and mechanical cues such as matrix stiffness, play a pivotal role in regulating

## INTRODUCTION

YAP/TAZ activity<sup>69</sup>. Through an Hippo-independent mechanotransduction process, YAP/TAZ serves as a sensor of extrinsic tension and forces, leading to its nuclear translocation. Besides, it has been observed that YAP-dependent matrix remodelling in response to mechanotransduction is necessary to generate and maintain CAFs' population in breast cancer<sup>70</sup>. Related to this finding, CCM3 has been reported to control the mechano-response of YAP in breast cancer CAFs<sup>71</sup>, and its dysregulation results in uncontrolled activation of YAP/TAZ, enhancing ECM remodelling and cancer cell dissemination. Of note, the enhanced actomyosin cytoskeleton and cellular contractility characteristic of CAFs have been shown to be critical in the activation of YAP/TAZ and other mechanotransduction pathways such as SRF/MAL<sup>72</sup>. In turn, YAP/TAZ activity in CAFs promotes the expression of key cytoskeletal genes and actomyosin contractility, which confers CAFs with critical pro-tumoral activities such as ECM remodelling, promotion of cancer cell invasion and angiogenesis<sup>65,70</sup>.

### 1.2.2.3.4 MAPK signalling pathway

CAFs' aggressive phenotype is further characterized by an enhanced activity of the major kinases comprising MAPK signalling, including ERK, c-Jun-N-terminal kinase (JNK) and p38, which are involved in responses to mitogens or stress<sup>55</sup>. These kinases will eventually activate transcription factors to promote the expression of genes related to the pro-tumorigenic behaviour of CAFs. Notably, it has been reported in ovarian cancer that TGF $\beta$  secreted by cancer cells activates p38 in CAFs, leading to the secretion of pro-tumorigenic cytokines which ultimately enhance the metabolic rearrangements favouring tumour progression<sup>73</sup>.

## INTRODUCTION

### 1.2.2.3.5 Heat Shock Factor 1

Heat Shock Factor 1 (HSF1) is involved in regulating protein stability and reduces stress caused by misfolding events due to the rapid proliferation in cancer<sup>19</sup>. Besides, in CAFs, HSF1 has been described to play a pivotal role in promoting the pro-tumorigenic phenotype of these cells. As mentioned before, HSF1 has been identified as a positive regulator of DKK3 in CAFs<sup>65</sup>. Moreover, it also promotes the expression of TGF $\beta$  and Stromal-Derived Factor 1 (SDF1), which contributes to CAFs' activation and cancer cell growth<sup>74,75</sup>. Furthermore, HSF1 in CAFs orchestrates changes in ECM composition and architecture, ultimately promoting cancer progression<sup>76</sup>.

### 1.2.2.3.6 Epigenetic adaptations

It is largely accepted that CAFs undergo an epigenetic reprogramming process to achieve their relatively stable pro-tumour phenotype. This process involves alterations in the epigenetic marks within the chromatin structure, leading to perturbations in gene expression. For instance, it has been described that several epigenetic modifications, such as methylation or acetylation, potentiate signalling pathways related to aggressive phenotypes or driving metabolic shifts to fuel cancer cells, among other perturbations<sup>34,77,78</sup>.

The chromatin architecture is regulated, in part, by enzymes known as histone deacetylases (HDACs). These enzymes participate in the removal of the acetyl group from the histones, fact that is associated with chromatin compaction and consequently, gene repression. Interestingly, their role in cancer has been the focus of many studies and there are HDAC inhibitors currently being tested in the clinic to treat cancer patients<sup>79</sup>. Besides, it has been described the potential link between TGF $\beta$  signalling and HDAC activity in fibroblasts. For instance, it has been reported that TGF $\beta$  blocks PGC1 $\alpha$  (an antifibrotic gene) via HDAC7 activity on its promoter, driving gene silencing

## INTRODUCTION

and achieving a pro-fibrotic fibroblast<sup>80</sup>. Moreover, blocking HDAC1/3/8 impeded TGF $\beta$ -mediated CAF transformation, reducing the ECM remodelling and contractile capacities of fibroblasts<sup>26</sup>. Taking these data together, the link of TGF $\beta$ -HDAC in CAFs shows a therapeutic potential to block CAFs differentiation and aggressive phenotypes, leading ultimately to the impairment of tumour growth and progression.

### **1.2.2.4 Implications in cancer**

The important role of CAFs in cancer is underlined by the significant correlation between the presence of CAFs and the development of highly aggressive tumours. In agreement, CAF content or CAF derived signatures are associated with a poorer prognosis or refractory tumours<sup>81,82</sup>.

It is now clear that activated fibroblasts or CAFs differ from the normal tissue fibroblasts in presenting tumour-promoting functions. Their crucial role in the TME is underscored by their versatile contributions to various tumoral processes. These include stimulating cancer cell proliferation through secreted factors or metabolites<sup>83,84</sup>; the aberrant formation of blood vessels by inducing angiogenesis<sup>85</sup>; promoting tumour progression, invasion and metastasis through ECM remodelling capacity<sup>36</sup>; enhancing the inflammatory state of the tumour and immunosuppression by secreted cytokines<sup>41,86</sup>; and even mediating the initiation of cancer through the alteration of cell-cell communications<sup>87</sup>. These processes can emerge from the expression and secretion of different factors that activate key pathways in the surrounding cells, including the malignant cells, establishing an intricate signalling network. Alternatively, CAFs can influence neighbouring cancer and stromal cells by actively modifying the ECM and altering the physical/chemical properties of the tumour. This wide range of pro-tumour functions already suggest a certain level of specialization within the CAF population and the presence of distinct CAF subtypes that may preferentially participate in specific functions (see 1.2.2.5).

## INTRODUCTION

### 1.2.2.4.1 Cancer cell and fibroblast crosstalk

CAFs secrete a wide variety of growth factors and inflammatory mediators that are accumulated in the TME and that influence tumour behaviour. For instance, in squamous cell carcinomas, it has been observed that CAFs enhance tumour cell proliferation through the secretion of Hepatocyte Growth Factor (HGF)<sup>88</sup>. In lung cancer, the secretion of interleukine-22 by CAFs has been reported to promote cancer cell proliferation and metastasis by activating critical signalling pathways, such as PIK3-AKT-mTOR<sup>83</sup>. Moreover, it has been described in prostate cancer that CAFs and cancer cells establish a crosstalk based on CX3CL1-CX3CR1 axis, that enhances migration and invasion of PC3 cancer cells<sup>89</sup>. In addition to growth and inflammatory factors, metabolites produced by CAFs have the capacity to fuel cancer cell metabolism, thereby promoting their survival and proliferation in a challenging microenvironment (see 1.3.2). Additionally, it is known that TMEs influence the epithelial state of cancer cells. It has been observed in breast cancer that the presence of CAFs is linked to a major mesenchymal phenotype of tumour cells. This feature is known as the Epithelial-to-Mesenchymal Transition (EMT) and is characterized by a heightened dissemination capacity and metastasis<sup>36</sup>. The mechanism underlying this phenomenon involves the activation of several signalling pathways (TGF $\beta$ , Erk, Jun and Rho) in cancer cells driven by CAFs<sup>36</sup>. TGF $\beta$  itself, which can be produced by CAFs, plays a crucial role in the EMT process, since Smad proteins induce the expression of E-Cadherin repressors, leading to EMT phenotypes<sup>90</sup>.

### 1.2.2.4.2 ECM generation and remodelling

Normal tissue homeostasis requires the generation of specific ECMs that serve as scaffold for different cells, maintaining tissue and organ architecture and modulating the adequate crosstalk between cell types required for their correct functioning. Of note, fibroblasts are the main

## INTRODUCTION

regulators of ECM generation and remodelling in most tissues and, therefore, play a critical role in tissue homeostasis<sup>9</sup>. Importantly, altered functions pertaining to ECM deposition and remodelling are exhibited by CAFs, producing a matrix of collagen fibers, hyaluronan, glycosaminoglycans and proteoglycans, leading to a significant modification in its composition. This phenomenon contributes to increased levels of desmoplasia and tissue stiffness in cancer contexts, which favours cancer cell proliferation, migration, invasion and metastasis<sup>9,91</sup>. For instance, it has been reported an enhanced expression of genes related to matrix deposition, such as type I and type III collagen, in breast cancer CAFs<sup>92</sup>. Besides, the aberrant capacity for matrix deposition involves the activation of several factors, including the Rho signalling pathway. This pathway leads to the formation of stable fibrillar adhesions that provide a physical scaffold for ECM deposition<sup>93,94</sup>. Moreover, high concentrations of fibronectin, another ECM component generated by CAFs, can attract cancer cells, enabling CAFs to enhance cancer cell invasion through matrix deposition<sup>95</sup>.

Furthermore, an augmented capacity for ECM remodelling is observed in CAFs, characterized by an increase in fiber crosslinking that promotes directed cancer cell migration and heightened stiffness<sup>96,97</sup>. This aberrant stiffness is achieved by the enzymes that mediate the crosslinking reaction of collagen into bundles, including the amine-oxidase lysyl oxidase (LOX) family<sup>96</sup>. The expression and secretion of these enzymes in the tumour stroma is due to cancer cells and fibroblasts. Specifically, LOXL2, secreted by tumour cells, has the ability to enhance the expression of  $\alpha$ SMA protein in CAFs as well as the contractile capacity through the activation of the FAK-integrin axis<sup>48,98</sup>. Additionally, the ECM can also promote tumour growth through type I collagen, which induces the expression of IL1, TNF $\alpha$ , or TGF $\beta$  in head and neck cancer cells<sup>99</sup>. The orchestration of matrix remodelling involves distinct processes mediated by different molecules and signalling pathways described below<sup>100</sup>.

## INTRODUCTION

### 1.2.2.4.2.1 ECM proteolysis

One mechanism implicated in the ECM remodelling is the proteolysis, which involves matrix metalloproteases (MMPs) that play a key role due to their capacity to degrade and remodel the ECM<sup>100</sup>. MMPs can be secreted by malignant cells, Tumour-Associated Macrophages (TAMs) and CAFs. In general, MMPs are accumulated in invadopodial structures in the cells, where they cleave different ECM components to facilitate the migration of cells through the ECM<sup>95</sup>. In CAFs, the expression of MMPs or other ECM degrading components can boost the proteolytic process to enhance cancer cell invasion<sup>101,102</sup>. For instance, in pancreatic cancer, the proteolytic function of CAFs can be driven by FAP protein, which can degrade gelatine and collagen I. It has been observed that FAP<sup>+</sup> CAFs produce fibronectin-rich ECMs with parallel collagen fibers. This collagen network allows cancer cell migration and invasion<sup>28</sup>.

In addition, MMP activity can promote the release of signalling factors into the tumour stroma and alter surrounding cells. It has been described that MMP2 and 9 can contribute to the differentiation of fibroblasts into contractile myofibroblasts by enhancing the release of secreted factors that are accumulated and embedded in the matrix<sup>101,102</sup>. Besides, it has been reported that latent form of TGF $\beta$  is released in the matrix derived from osteoclasts and endothelial cells, due to MMPs activity<sup>103,104</sup>.

### 1.2.2.4.2.2 Cellular contractility

Another mechanism involved in the matrix remodelling process of CAFs is associated with their contractile capacity, especially when the ECM proteolysis is somehow impaired.

The contractile capacity of CAFs can be modulated by different mechanisms including stimulation by secreted factors or by tissue stiffness. For example, the RhoA-ROCK pathway is activated by cytokines and TGF $\beta$  to induce myosin fiber phosphorylation and increase actomyosin contractility<sup>93</sup>.

## INTRODUCTION

Moreover, the transcription regulator YAP is also involved in the actomyosin contractility, as it promotes the expression of key cytoskeletal genes required to sustain the enhanced cytoskeleton characteristic of CAFs<sup>70</sup>. Related to this finding, it has been observed a correlation between nuclear YAP and  $\alpha$ SMA protein expression, since  $\alpha$ SMA can induce YAP nuclear translocation in myofibroblasts-like CAFs<sup>105</sup>.  $\alpha$ SMA is an actin isoform expressed in smooth muscle cells and myofibroblasts and its expression is positively correlated with a higher contractility of the matrix. It has been observed that TGF $\beta$  increases the levels of  $\alpha$ SMA expression, which is linked to the activated phenotype of the CAFs under this stimulus<sup>106,107</sup>. This contractile property confers a higher migratory capacity to CAFs in tumours and is directly linked to their ability to generate tracks within the ECM and boost cancer cell migration and invasion<sup>93</sup>.

### 1.2.2.4.2.3 Matrix stiffening

As a result of the increased matrix deposition, remodelling and cellular contractility, CAFs actively participate in the characteristic stiffening of the ECM observed in most solid tumours, directly impacting on the physical properties of tumours<sup>9,108</sup>. Changes in these physical properties can influence several tumour parameters, such as the activation of proliferative signalling for cancer cell growth and survival, induction of EMT and modulation of other stromal cells, mostly acting like a barrier for immune cell recruitment or compressing blood vessels (see 1.2.2.4.3 and 1.2.2.4.4). Notably, ECM stiffness plays a key role in impeding drug delivery in tumours, being a crucial physical barrier that must be overcome to enhance the efficacy of treatments<sup>108</sup>. For instance, it has been reported that a prior treatment targeting ECM molecules rescues drug efficacy in colorectal cancer liver metastasis<sup>109</sup>.

## INTRODUCTION

### 1.2.2.4.3 Immunomodulation by CAFs

Apart from cancer cells, CAFs are known to interact with other stromal cells to generate a TME that favours tumorigenesis. The capability of CAFs to drive tumour-promoting inflammation constitutes a pivotal event in the tumour progression, boosting immune suppression, cancer cell proliferation and malignant conversion<sup>10</sup>. Basically, CAFs promote the recruitment and activation of inflammatory immune cells, as well as suppressing anti-tumour immune cells. The mechanism underlying these processes involves the secretion of cytokines and chemokines that recruit and modulate the immune cells within the tumour milieu<sup>37</sup>. Tumour-Associated Macrophages (TAMs) is the major population of immune cells in CAF-rich areas, suggesting a potential interplay between both cell populations. Reports indicate that CAFs can recruit TAMs with M2-like phenotype by secreting Macrophage Colony-Stimulating Factor-1 (M-CSF1), IL6 or CCL2<sup>111,112</sup>. Besides, CAFs possess the capacity to influence T lymphocytes, generating a pro-inflammatory stroma rich in tumour-promoting T cells by secreting CXCL9/10/12<sup>37,113</sup>.

Additionally, the ECM derived from CAFs indirectly interfere in the immune infiltration of the tumour. It was observed that macrophages migrate towards hyaluronan (HA)-rich areas, and when disrupting HA synthase 2 in fibroblasts, an impairment in macrophage recruitment and angiogenesis was observed, indicating that the ECM derived from fibroblasts play a crucial role in modulating tumour inflammation<sup>114</sup>. Consequently, recent studies suggest that targeting CAFs could improve the efficacy of immunotherapies. For instance, the inhibition of IL6 is currently under preclinical and clinical trials<sup>115</sup>, while preventing fibroblast activation through TGF $\beta$  inhibition has demonstrated improvements in PD-L1 treatment in urothelial cancer<sup>116</sup>. Besides, in mouse pancreatic models, it has been described that the elimination of a particular CAF subpopulation resulted in a higher immune infiltration and tumour regression in response to PD-L1 treatment<sup>117</sup>.

## INTRODUCTION

### 1.2.2.4.4 Angiogenic properties of CAFs

CAFs can also interact and corrupt endothelial cells to boost angiogenesis to overcome the hypoxic conditions due to the fast proliferation of the tumour cells. In breast cancer, SDF-1 secreted from CAFs promote angiogenesis by recruiting endothelial progenitor cells into the tumour mass, leading to the growth of malignant cells by activating their CXCR4 receptor<sup>118</sup>. Besides, it has been reported that hypoxic human mammary CAFs promote endothelial cell sprouting via secretion of Vascular Endothelial Growth Factor (VEGF) and other pro-angiogenic factors, such as LOXL2 or staniocalcin 1 (STC1)<sup>85</sup>. In colon cancer, it has been demonstrated that WNT2 expression in CAFs enhanced the pro-angiogenic phenotype of these cells by activating signalling pathways to boost vessel formation and endothelial cell sprouting<sup>119</sup>.

Additionally, some modulatory events in the angiogenic process can be attributed to the ECM produced by CAFs. For instance, angiogenesis can be enhanced by the ECM stiffness, which induces signalling pathways in endothelial cells<sup>108</sup>. Besides, ECM degradation through MMPs can release angiogenic factors in the TME. For example, proteolytic cleavage of collagen type IV has been reported to expose a regulatory element of the protein that play a key role in angiogenesis<sup>120</sup>. On the other hand, the stiffness of the ECM may also negatively impact blood perfusion in tumours, as it appears to be a critical element contributing to abnormal angiogenesis. In this context, endothelial cells exhibit heightened outgrowth and branching, diminished cell-cell junctions and high permeability, which results in the formation of a leaky vasculature<sup>121</sup>.

Altogether, CAFs are considered one of the main contributors of critical features of aggressive TMEs. Giving the fact that they show a tight crosstalk with cancer cells and other stromal cells, it is critical to study how to disrupt these reciprocal interactions to impair tumour progression.

### 1.2.2.5 CAFs subpopulations

CAFs have been described originally as a uniform population of cells sharing morphology, location and the link to the pro-tumorigenic process. However, recent studies investigating CAFs in detail, leveraging in emerging technologies such as single-cell RNAseq (scRNAseq), have informed that CAFs present a high level of plasticity and heterogeneity, containing distinct subtypes. Currently, CAFs subpopulations can be classified in three main clusters based on molecular (i.e. gene expression) features: myCAFs (myofibroblast CAFs), with a strong ECM signature and high expression of  $\alpha$ SMA, which confers a high contractile phenotype; iCAFs (inflammatory CAFs) with an activated inflammatory secretome and high expression of IL-6 and low  $\alpha$ SMA; and apCAFs (antigen-presenting CAFs) with expression of Major Histocompatibility complex class II (MHC II)<sup>122</sup> (**Figure 6**). In addition, depending on the tissue of origin and pathological condition, other relatively rare CAF subtypes may also be found, such as vascular CAFs (vCAFs)<sup>123</sup> or lipo-CAFs<sup>124</sup>.

It has been reported that TGF $\beta$ /SMAD2,3 signalling promotes the generation of myCAFs, while IL1/JAK-STAT3 stimuli polarize CAFs into the inflammatory phenotype<sup>125</sup>. apCAFs are generated in response to IFN $\gamma$  stimuli<sup>126</sup>. Nevertheless, these phenotypic states are flexible and reversible along the tumorigenic process. Thus, the exact composition of CAFs can vary depending on the cancer type, the state of the tumour or the intratumor localization of these cells<sup>123,127</sup>. For example, it has been reported in pancreatic cancer that myCAFs are found in the proximity of the cancer cells, whereas iCAFs are localized in the surrounding areas<sup>127</sup>. Importantly, most of these subtypes present tumour promoting functions, although they may differ on the exact biological processes in which they participate. Thus, myCAFs are primarily associated with the exacerbated production of ECM and its remodelling, actively participating in the promotion of cancer cell growth and invasion. Besides, they may also produce additional secreted factors that

## INTRODUCTION

influence cancer and stromal cell behaviour<sup>127,128</sup>. On the other hand, iCAFs generally produce cytokines and chemokines that promote inflammation and modulate the immune cell compartment, although they may also promote malignant behaviours in cancer cells. Finally, apCAFs are less characterised and were initially associated with the group of atypical antigen-presenting cells that participate in T-cell stimulation. However, whether they can provide the requisite signals for complete activation of naïve T cells or potentially interfere with immune responses remains unclear<sup>122</sup>.

One of the main limitations in CAFs' research is that the established markers do not precisely differentiate these different subpopulations<sup>16,18</sup>. Therefore, it is necessary to decipher CAFs' complexity and identify markers to distinguish and target each subtype as a part of novel anti-cancer treatments.

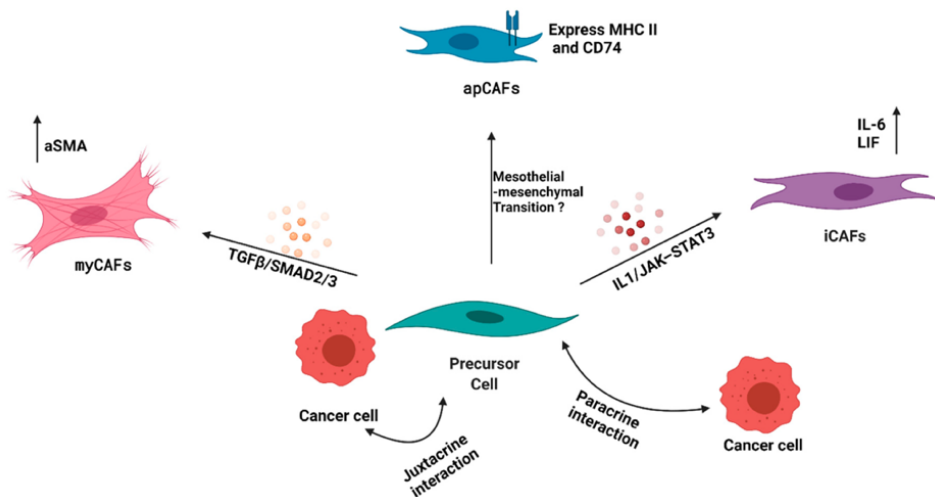


Figure 6. Subtypes of CAFs. Key molecular characteristics, regulatory signals and signalling cascades associated with the main CAF subpopulations are indicated. Figure taken from Vaish, U. (2021)

### 1.2.2.6 CAFs in therapy

CAFs have been reported to be present across all stages of tumour progression and due to their significant contribution, these cells are considered key players in the acquisition of malignant features. Furthermore, CAFs rarely present genomic aberrations and are considered to be genetically stable and therefore less prone to develop mechanisms of resistance. This characteristic makes them an attractive target for novel therapies attempting to impair the paracrine signalling between CAFs and cancer cells. Additionally, efforts to eliminate or normalize their phenotype are being explored as potential strategies to control tumour progression<sup>12,15,16</sup> (Figure 7).

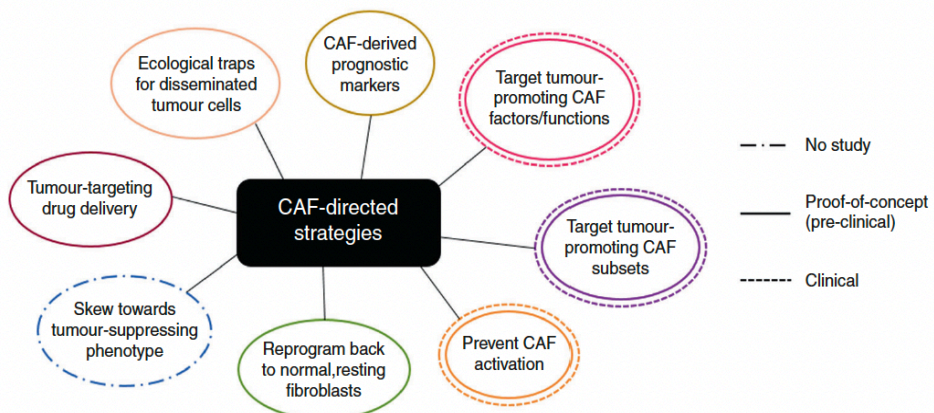


Figure 7. CAF-directed therapies. Preclinical and clinical methods to target CAFs. Figure taken from Gieniec, K.A (2019).

### 1.3 METABOLIC REPROGRAMMING IN TUMOURS

#### 1.3.1 Metabolic reprogramming in cancer cells

Under normal oxygen conditions (normoxia), glycolysis is enhanced in cells to obtain pyruvate, which subsequently enters the Tricarboxylic acid (TCA) cycle for catabolism and is directed towards the oxidative phosphorylation (OXPHOS) to generate energy and metabolites. However, under hypoxic conditions, anaerobic glycolysis is enhanced in normal cells, leading to the production of lactate from pyruvate and a reduction in OXPHOS activity<sup>129</sup> (**Figure 8**).

In the case of cancer cells, they go through a phenomenon that is known as metabolic reprogramming, which is a well-established hallmark of cancer and considered a potential target for therapy<sup>130–132</sup>. It is widely acknowledged that the metabolic activities in cancer cells differ from those in normal counterparts, as malignant cells exhibit an aberrant growth and proliferation driven by oncogenic signals in response to both cell-intrinsic and extrinsic stimuli. These signals lead the perturbation of several metabolic pathways in order to promote aerobic glycolysis, glutamine catabolism, macromolecular synthesis and redox homeostasis, among others processes<sup>133</sup>. Consequently, tumour cells can generate nutrients independently of extracellular growth factors to support their growth and proliferation. One widely known example of this metabolic reprogramming is the Warburg Effect, which consists of the activation of glycolysis and the secretion of lactate regardless of the presence of oxygen<sup>134–136</sup>. Thus, while normal cells obtain energy from mitochondrial OXPHOS, malignant cells promote aerobic glycolysis, which, although less efficient than mitochondrial respiration in ATP generation, facilitates the incorporation of nutrients for biomass production (**Figure 8**). Accordingly, it has been described that tumour cells exhibit an enhanced Pentose Phosphate Pathway and a robust up-regulation of Lactate dehydrogenase enzyme (LDH), correlating with

## INTRODUCTION

increased nucleotide synthesis and lactate production due to the Warburg effect<sup>137</sup>.

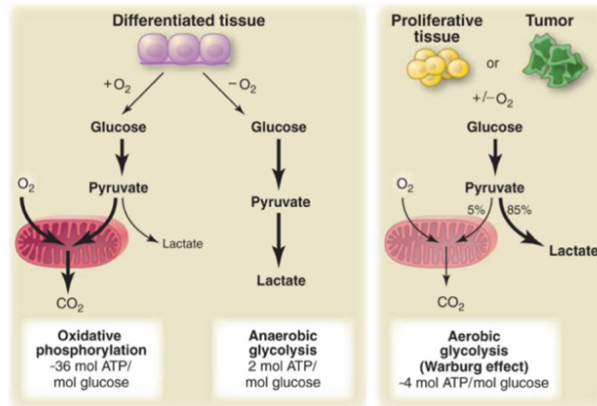


Figure 8. A comparison between cell metabolism of differentiated tissue vs proliferative or tumor. Figure taken from Heiden, V. et al (2009)

Several oncogenic mutations have been described to drive this proliferative metabolism. For instance, the activation of YAP/TAZ or MYC, has been shown to lead to a significant increase in glycolysis and the promotion of Warburg effect in tumour cells<sup>138,139</sup>. Aberrant activation of mTORC1, which drives anabolic processes such as protein and ribosome synthesis, lipogenesis or nucleotides generation, is commonly found in malignant cells<sup>140</sup>. In colorectal cancer, oncogenic KRAS promotes the expression of the glucose transporter GLUT1, enhancing glycolysis in cancer cells and providing a proliferative advantage in glucose-deprived scenarios<sup>141</sup>. Besides, highly vascularized tumours have been reported to present mutations in the enzyme succinate dehydrogenase (SDH), causing the accumulation of succinate and impairing the TCA cycle. In this setting, succinate stabilizes HIF- $\alpha$ , which, in turn, promotes angiogenesis<sup>142</sup>. Thus, it is noteworthy how cancer cells can reprogram their metabolism by modulating the expression of key metabolic genes, leading to rearrangements in several pathways favouring tumour progression.

## INTRODUCTION

Additionally, it is remarkable that cancer metabolism is a flexible network, with reported metabolic heterogeneity among patients and even at inter and intra-tumoral levels. This variability is attributed to the selective pressures from extrinsic factors such as the patient's own metabolism and changes in the TME, as well as intrinsic factors such as parental tissue characteristics and distinct oncogenic mutations<sup>133,137,138</sup>. In line with this, the same oncogene has been described to perturbate cancer cell metabolism differently depending on the cancer type. For example, MYC can enhance the consumption and catabolism of glutamine in liver cancer while promoting glutamine synthesis in lung cancer<sup>139</sup>. Moreover, metabolic pathways activated in disseminating cancer cells differ from those active in a localized tumour. Cancer cells from a primary tumour exhibit changes in their metabolism to favour migration, invasion and metastasis. For instance, breast cancer cells show an increase in asparagine synthesis, enhancing the expression of EMT proteins<sup>143</sup>. Moreover, in early stages of tumorigenesis MYC promotes the generation of alanine from pyruvate, while in advanced stages, it enhances the conversion of pyruvate to lactate<sup>144</sup>. Therefore, there is a considerable heterogeneity in the metabolic reprogramming of cancer cells both at tumour type and stage levels.

Importantly, metabolic changes are not restricted to cancer cells, as the TME metabolism can also adapt during tumour progression. Cancer cells must undergo these metabolic perturbations in order to overcome nutrient competition with stromal cells, environmental acidification, oxygen deprivation and other external factors. Additionally, cancer cells can secrete metabolites that modify the metabolism of neighbouring cells, leading to the acquisition of pro-tumorigenic phenotypes and promoting tumour progression<sup>145-147</sup>. Conversely, cancer cells can uptake metabolites secreted by the surrounding cells, establishing a metabolic symbiosis that can fuel tumour progression<sup>84</sup>. Therefore, the establishment of a metabolic crosstalk

## INTRODUCTION

with the TME is very important for malignant cells to proliferate and disseminate.

### 1.3.2 Metabolic reprogramming in CAFs

Non-malignant cells surrounding tumour cells must undergo metabolic reprogramming in response to signals emanating from the tumour or the altered TME. Moreover, these metabolic rearrangements are also a result of the fierce competition for nutrients and metabolites with highly proliferating cancer cells, hypoxia caused by compromised vasculature, and other limitations that cells need to overcome<sup>14</sup>. Focusing on CAFs, a lactate shuttle called “Reverse Warburg Effect” has been described, which consists of a metabolic crosstalk between CAFs and cancer cells. This process involves a reprogramming in the metabolism of CAFs characterized by the acquisition of a glycolytic phenotype. As a result, CAFs produce metabolites such as lactate or pyruvate, which are released into the tumour stroma and can be taken up by neighbouring cancer cells<sup>34,148,149</sup>. However, it is crucial to note that the reverse Warburg effect cannot be extended to all CAFs, as it varies depending on the cancer type. For instance, in colorectal and breast cancer, cancer cells exhibit an anaerobic glycolysis producing lactate that is taken up by CAFs<sup>30,150</sup>. Additionally, some studies have reported how cancer cells enhance OXPHOS in CAFs, while CAFs reciprocally boost glycolysis in cancer cells<sup>151</sup>. In oral squamous carcinoma, CAFs show high OXPHOS activity, favouring tumour progression<sup>152</sup>. Therefore, these findings challenge the largely established idea of CAFs undergoing a Reverse Warburg Effect, highlighting a variety of metabolic scenarios in CAFs that ultimately contribute to tumorigenesis.

Besides, substantial evidence supports the metabolic crosstalk between CAFs and cancer cells. For instance, CAFs can undergo autophagy and mitophagy, generating metabolites that cancer cells uptake and direct towards the Pentose Phosphate Pathway (PPP), acid nucleic synthesis or the mitochondrial TCA cycle to obtain energy. An example of this metabolic

## INTRODUCTION

crosstalk is observed in pancreatic stellate cells, which go through autophagic process to synthesize alanine that cancer cells subsequently consume<sup>153</sup>. Another evidence is the utilization of CAF-derived pyruvate in lymphoma tumours to fuel cancer cells' metabolism<sup>84</sup>. Additionally, CAFs play an important role in maintaining the redox homeostasis of cancer cells. In ovarian cancer, CAFs-derived glutathione balances redox stress in cancer cells<sup>154</sup>. In prostate cancer CAFs, p62 deficiency has been reported to favour tumour progression in glutamine-deprived scenarios by enhancing ATF4 stability, which targets Asparagine synthetase (ASNS) gene, therefore increasing asparagine synthesis and secretion into the TME<sup>155</sup>. Furthermore, evidence pointed out the mechanism whereby ECM properties modulate cell metabolism. In breast cancer CAFs, there is an enhanced expression of pyrroline-5-carboxylate reductase 1 (PYCR1) enzyme, which synthesizes proline, an abundant amino acid to generate collagen for the ECM deposition<sup>29</sup>. Moreover, mechanoactivation of YAP/TAZ through ECM stiffness promotes the expression of Glutaminase 1 (GLS1) and Aspartate/glutamine transporter SLC1A3 in both cancer cells and CAFs, establishing an exchange of CAF-derived aspartate and cancer cell-derived glutamine<sup>145</sup>.

Altogether, it is now evident that there is a critical relationship between the metabolism of both cancer cells and stromal cells. This interplay is considered a potential therapeutic target to deter tumour progression or to evade acquired resistance to treatments. However, the heterogeneity and flexibility of the processes leading to metabolic reprogramming poses a significant challenge. Notably, the metabolic phenotype of CAFs has been predominantly studied in the context of producing metabolites and other components for the cancer cells, with a limited focus on potential consequences in CAFs and its role in modulating their own characteristics and phenotype. Thus, studying changes in metabolic pathways in CAFs and exploring correlations with their behaviour could offer valuable insights in the field.

### 1.3.3 Metabolites as signalling molecules

It is worth noting that metabolites are not only intermediates of the metabolism since they can act as regulators of signalling pathways and perturb gene expression<sup>156</sup>. Thus, metabolic rearrangements can be potentially linked with more sustained changes in transcriptional programmes associated with cell fates and cellular states. The oncometabolite 2-hydroxyglutarate (2-HG), generated by the mutated enzymes isocitrate dehydrogenase 1 and 2 (IDH1/2), triggers the development of cancer by disrupting redox homeostasis of the cell, altering the methylation of DNA, and disrupting signalling pathways, among other functions<sup>157</sup>. Besides, the generation and accumulation of lactate, enhances the expression and stabilization of N-Myc downstream-regulated-3 (NDRG-3), which drives the activation of Raf-ERK1/2 pathway<sup>158</sup>. Another example of these links between metabolism and signalling perturbations was reported with Lactate Dehydrogenase A (LDHA), which is translocated to the nucleus under oxidative stress conditions. Nuclear LDHA generates a metabolite,  $\alpha$ -hydroxybutyrate ( $\alpha$ -HB), that activates Wnt signalling by epigenetic modifications<sup>159</sup>. Importantly, a tight link between metabolism and epigenetics is emerging. It has been described that acetate resulting from the acetyl-CoA metabolite, and the enzymes involved in the reaction (ACSS1/2) are key players in modulating the histone acetylation process, affecting in chromatin accessibility<sup>160,161</sup>. Thus, there is substantial evidence pointing out metabolites as signalling molecules, that can infer in signalling cascades and epigenetic reprogramming of cancer and stromal cells, leading to the tumour progression. However, whether metabolic rearrangements in CAFs contribute to the emergence or maintenance of their pathologically activated state or CAF subtypes through the modulation of distinct transcriptional programmes remains unsolved.

### 1.4 ASPARTOACYLASE ENZYME

#### 1.4.1 Definition and action

The Aspartoacylase enzyme, also known as ASPA, is implicated in the metabolism of N-Acetylaspartate (NAA) (**Figure 9**). This metabolite is generated in the mitochondria through the acetylation of aspartate by the enzyme aspartate N-acetyltransferase (Asp-NAT), which is encoded by the gene *NAT8L*. NAA is subsequently transported to the cytoplasm, where it can be catabolized by ASPA, yielding two products: aspartate and acetate<sup>162</sup>. The resulting acetate can be converted into acetyl-CoA by ACSS2 or by ACSS1. ACSS2, the nuclear-cytoplasmic form of the enzyme, is predominantly involved in providing Acetyl-CoA for lipogenesis and histone acetylation. In contrast, ACSS1, the mitochondrial form, directs Acetyl-CoA to the TCA cycle<sup>160,161</sup>. The fate of NAA-derived aspartate is not fully established; reports suggest it can be converted to oxaloacetate and enter the TCA cycle or used for protein synthesis<sup>162,163</sup>. Additionally, NAA can be transformed to N-acetylaspartylglutamate (NAAG) in the presence of glutamate through the enzyme NAAG synthase, encoded by the gene *RIMKLB*. This reaction can be reversed by GCP-II/III enzymes, encoded by the genes *FOLH1/NAALAD2*, respectively<sup>164</sup>.

Furthermore, ASPA has recently been observed to undergo cytosolic-nuclear shuttling in mouse glioma cells, rat brain and kidney cells. However, the nuclear function of ASPA is not yet established<sup>165,166</sup>. It has been observed that nuclear ASPA exhibits lower catalytic activity than cytosolic ASPA. This finding leads to the hypothesis that ASPA may have specific functions independent of NAA catalysis. For instance, it has been recently described that ASPA can directly bind and inhibit the LYN kinase, resulting in the impairment of tumour growth<sup>167</sup>. This discovery marks the first instance of a non-enzymatic role for ASPA, suggesting its potential significance in the regulation of tumorigenesis. Moreover, ASPA implications can be extended to transcriptional changes in

## INTRODUCTION

cells, as the NAA catabolism generates acetate that is destined to the histone acetylation process<sup>168</sup>.

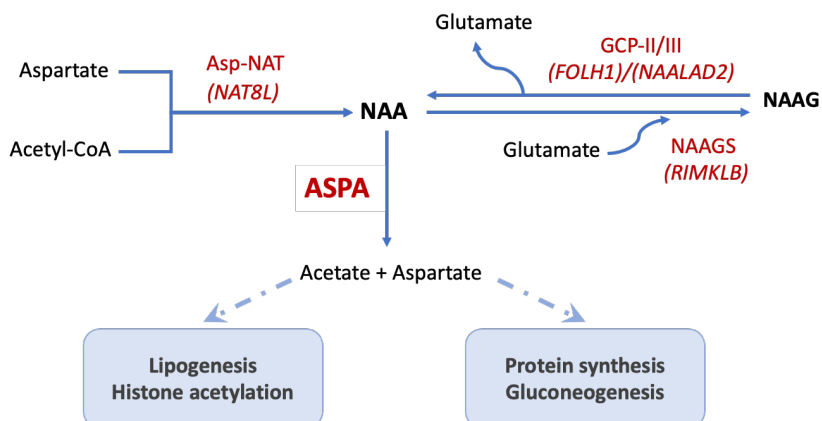


Figure 9. Schematic diagram showing the NAA metabolism and ASPA implication.

### 1.4.2 NAA and ASPA in brain

ASPA function has been primarily investigated in the central nervous system (CNS), where NAA is one of the main amino acid derivatives in the brain, serving as an important source of acetate. Acetate is directed towards myelin synthesis and other functions including neuronal osmoregulation and axon–glial signalling<sup>163</sup>. While NAA is produced in the mitochondria of the neurons, its primary catabolism occurs in oligodendrocytes, mediated by ASPA. However, specific transporters for NAA in oligodendrocytes have not been described yet<sup>163,166</sup>. The acetate resulting from ASPA-mediated NAA catabolism is converted into Acetyl-CoA by ACS1/2 with distinct implications such as histone acetylation, myelin lipid synthesis or TCA cycle. Additionally, NAA can also be transported to astrocytes by NAA dicarboxylate transporter (NaDC3/SLC13A3), facilitating its release into the circulatory system. Besides, NAA may undergo conversion to NAAG, activating GRM3 signalling for its uptake. NAAG can be restored to NAA by GCP-II/III enzymes expressed on the surface of the astrocytes. Glutamate, generated from NAAG catabolism or from peri-synaptic uptake, binds post-synaptic *N*-methyl-d-aspartate receptors (NMDAR) and is taken up by astrocytes, where it can be converted to glutamine and, subsequently, return to neurons for conversion

## INTRODUCTION

back to glutamate (**Figure 10**)<sup>166</sup>. Therefore, NAA and the products derived from its catabolism establish a tight paracellular network required for the correct function of the CNS. Importantly, the dysregulation of this network results in important defects in the system and are associated with neurological disorders (see 1.4.2.2).

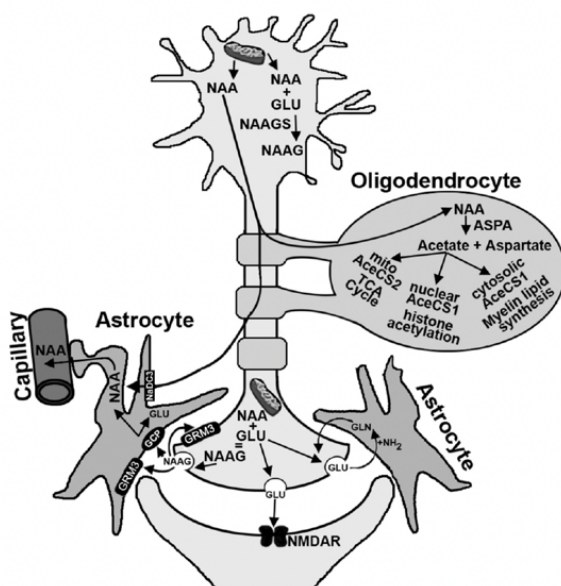


Figure 10. Representation of NAA metabolism in brain.  
Figure taken from Long, Patrick M. et al (2013).

### 1.4.2.1 Epigenetic changes in brain

Epigenetic rearrangements in the brain cells have been associated with the enzymatic activity of ASPA. Specifically, in oligodendrocytes, the catabolism of NAA has been shown to elevate the levels of  $\alpha$ -Ketoglutarate, a Krebs cycle intermediate. This increase has been linked to histone demethylase activity, leading to alterations in marks associated with cellular energetics (H3K4me3) and transcriptional repression (H3K9me3)<sup>169</sup>. Additionally, various sources of Acetyl-CoA are being suggested to contribute to the histone acetylation process. In the brain, ACSS2 is known to convert the acetate derived from ASPA activity to Acetyl-CoA, which plays a role in protein acetylation in this context<sup>166</sup>. These findings underscore the potential involvement of NAA catabolism in the epigenetic reprogramming of cells.

### **1.4.2.2 Canavan disease**

It has been reported a neuronal disease in the CNS related to NAA and ASPA, known as Canavan disease (CD). This disease consists of a neurometabolic disorder driven by the deficiency of ASPA in oligodendrocytes. Thus, NAA is accumulated in brain, reducing the source of acetate for myelination process of the neurons, which is essential for the correct function of the brain. Patients who suffer CD commonly show macrocephaly, seizures and hypomyelination, among other symptoms<sup>166,170,171</sup>. The genomic aberrations linked to this disease are associated with loss of function mutations in ASPA, which emerge as point mutations (Glu178Asp or Glu178Gln), reducing or blocking the catalytic activity, or big deletions that affect activity and protein folding<sup>172</sup>. Nowadays, gene replacement therapy is being explored to treat patients with CD. The optimal therapy approach consists of adeno-associated virus vectors carrying ASPA gene with oligodendrocyte type-specific tropism to cross the blood-brain barrier. So far, this option showed good outcomes in neonatal mouse brains<sup>171</sup>.

### **1.4.3 NAA and ASPA outside the CNS**

#### **1.4.3.1 Lipogenesis**

Over the past few years, studies on the role of NAA beyond the brain have emerged. It has been reported that *NAT8L* and *ASPA* are highly expressed in murine and human differentiated brown adipocytes, leading to the synthesis and catabolism of NAA. This fact leads to an increase of the lipid turnover and the expression of brown marker genes<sup>173</sup>. Additionally, in this study, it was demonstrated that silencing *NAT8L* in brown adipocytes triggers the upregulation of ATP-citrate Lyase (ACLY), which converts citrate to Acetyl-CoA. This suggests a compensatory effect to sustain the cytoplasmatic Acetyl-CoA pool for lipogenesis. Another study highlighted that *ASPA* knock-down in brown adipocytes leads to a reduction of lipid metabolism and the acetyl-CoA pool<sup>168</sup>. Furthermore, it has been reported

## INTRODUCTION

that the expression of genes associated with the NAA pathway is modulated by nutrient availability, as NAA is preferably produced from Acetyl-CoA and aspartate derived from glucose<sup>174</sup>. This finding indicates that NAA levels could act as a sensor for the energetic state of adipocytes. Besides, a decrease in H3 acetylation marks on lysine residues (H3K9 and H3K27) has been observed in brown adipocytes with *ASPA* knockdown, showing an impact on gene expression levels<sup>168</sup>. This last observation directly connects the NAA pathway to the epigenome, highlighting that perturbations in this pathway can impact on brown adipocyte phenotypes.

### **1.4.3.2 NAA and ASPA in cancer**

It has been reported that NAA or its catabolism is involved in many processes such as lipogenesis or histone acetylation, by converting the resulting acetate into acetyl-CoA. As previously mentioned, metabolic reprogramming is one hallmark of cancer and because of that, there have been studies focused on *ASPA* and NAA catabolism in cancer. NAA has been reported to be more abundant in tumours when compared to healthy tissues. Concomitantly, the expression of *NAT8L* is higher in cancer cells and, related to these results, *ASPA* is downregulated in tumour samples, suggesting that the role of NAA in tumorigenesis might not be only related to its catabolism, but because of NAA itself<sup>175,176</sup>. One example that corroborates these findings is that NAA promotes the M1 to M2 switch in TAMs of ovarian cancer by enhancing the expression of Glutamine synthetase (*GS*) gene, due to NAA competition with ligands of the N-methyl-D-Aspartate Receptor. Moreover, in this study they also revealed a positive correlation between *NAT8L* and *MKI67*, *GLS1* and *ACLY* genes, which links NAA synthesis to cell proliferation and glutamine and citrate metabolism<sup>170</sup>. Another study in ovarian cancer also pointed out that *NAT8L* is mediating an anti-apoptotic effect on cancer cells and, therefore, enhancing the proliferation of the malignant cells<sup>175</sup>. Besides, in lung carcinoma it has been observed that NAA itself improved cell survival in glucose-deprived conditions<sup>177</sup>. Of note, NAA has been proposed as a novel

## INTRODUCTION

circulating biomarker in lung carcinoma<sup>178</sup>. These findings confirm that NAA certainly has other metabolic-independent functions.

Nevertheless, the study of ASPA and its implication in cancer is still an emerging field. As previously mentioned, it has been reported in prostate cancer cells that ASPA is able to impair tumour progression by preventing LYN phosphorylation, therefore, blocking the activation of its down-stream targets, JNK1/2 and c-Jun<sup>167</sup>. Besides, in colon cancer it has been observed that ASPA was lost in CAFs, correlating with a poorer prognosis<sup>179</sup>. Considering these observations, ASPA emerges as a pivotal player in cellular energetic homeostasis, cell metabolism and epigenetic rearrangements, impacting on cell phenotype and potentially acting as a key regulatory factor.

## **OBJECTIVES**



## 2 HYPOTHESIS AND OBJECTIVES

In order to decipher new regulators of tumour stroma that drive cancer progression, our initial analyses identified *ASPA* as a gene consistently downregulated in CAFs and whose expression correlated with poor patient prognosis in several cancer types. Based on this, **we hypothesised that *ASPA* is a potential master regulator of CAFs phenotype**. Thus, our main goals were to determine the relevance of *ASPA* in modulating CAF behaviour and its implication in cancer progression and dissemination. To this end, the following objectives were proposed:

1. Confirm the altered status of *ASPA* in CAFs and investigate the mechanisms that regulate its expression in fibroblasts.
2. Delineate the role of *ASPA* in modulating pro-tumour functions in CAFs and its contribution to cancer progression.
3. Decipher the mechanism of action of *ASPA* in CAFs and how they influence CAF behaviour.



## **MATERIAL AND METHODS**



## 3 MATERIALS AND METHODS

### 3.1 MATERIALS

#### 3.1.1 Cell lines

In this project, the following cell lines were used (**Table 1**): murine NFs and CAFs derived from FVB/n mice. CAFs were isolated from murine mammary tumours generated through the expression of the polyoma middle T antigen oncogene under the mouse mammary tumour virus promoter (MMTV-PyMT). NFs were generated from normal tissue mammary glands. NF1, NF4, and CAF1, CAF2, CAF3 and CAF5 were isolated from these models, expanded and immortalized using hpv-E6 before passage 5<sup>70</sup>. Human prostate cancer fibroblasts were also used in this project: normal fibroblasts WPMY-1 (ATCC® CRL-2854™) from normal stroma of human prostate tissue, and CAF hTERT PF179T CAF (ATCC® CRL-3290™) cell line from prostate carcinoma were purchased from American Type Culture Collection. Primary cell lines of patient-derived CAFs (CAF 85-AD and 81-BI) and fibroblasts from adjacent pathologically normal tissue (NF 85-BI and 81-AI) were kindly provided by Dr. Francisco J. Vizoso (Fundación Hospital de Jove, Spain). Human colorectal NFs (NF hCRC) provided by Danijela Vignjevic (Institute Curie, France), and human breast primary NFs (NF hBC) provided by Clare Isacke (Institute of Cancer Research, UK). All human NF/CAFs were immortalized using hTERT.

In addition, the following cancer cell lines were used: D2A1 (RRID: CVCL\_OI90) are murine breast cancer cells from BALB/c mice, derived from spontaneous mammary tumours which were originated from a D2 hyperplastic alveolar nodule. These cells were a kind gift from Dr Sahai (Crick Institute, UK). TS1 murine breast cancer cells from MMTV-PyMT mice were also used in this project, kindly provided by Dr Johanna Joyce. PC3 cancer cells from bone metastasis of grade IV of prostate cancer, and DU145 cancer cells from brain metastasis of prostate cancer, were kindly provided by Dr Arkaitz Carracedo, originally obtained from Leibniz-Institute DSMZ-Deutsche

## MATERIALS AND METHODS

Sammlung von Mikroorganismen und Zellkulturen GmbH with the corresponding certificate of authenticity. 22Rv1 cancer cells from a human prostate carcinoma epithelial cell line derived from a xenograft that was serially propagated in mice, were kindly provided by Dr Arkaitz Carracedo, originally purchased from American Type Culture Collection.

All cancer cell lines were fluorescently labelled using pCII-GFP-Blasti vector. D2A1 were sorted by FACs to select the cells with higher GFP intensity. HEK293-FT (RRID: CVCL\_6911) from human embryonic kidney were used for virus generations.

All cells are adherent and were grown in a monolayer in polystyrene flasks or plates with complete media and maintained at 37 °C in a humidified atmosphere containing 5% CO<sub>2</sub>. All cells were routinely tested negative for mycoplasma infection with MycoAlert™ (Lonza).

Cell line	Origin	Cell type	Source
NF1, NF4	FVB/n normal mammary gland (immortalized with hpv-E6)	Fibroblast cell line	Established by Dr. Fernando Calvo
CAF1, CAF2 CAF3 CAF5	MMTV-PyMT mammary carcinoma (immortalized with hpv-E6)	Fibroblast cell line	Established by Dr. Fernando Calvo
NF1 TAZ <sup>mut</sup>	FVB/n normal mammary gland (immortalized with hpv-E6)	Fibroblast cell line	Patricia Carnicero (labmate)
WPMY-1	Human normal prostate tissue (immortalized with SV40)	Fibroblast cell line	Commercial
CAF PFT179	Human prostate carcinoma (immortalized with hTERT)	Fibroblast cell line	Commercial
CAF 85-AD	Human prostate carcinoma (immortalized with hTERT)	Fibroblast cell line	Dr. Francisco J. Vizoso (Hospital de Jove, Spain)
CAF 81-BI	Human prostate carcinoma (immortalized with hTERT)	Fibroblast cell line	Provided by Noemi (Hospital de Jove, Spain)
NF 85-BI	Human normal prostate tissue (immortalized with hTERT)	Fibroblast cell line	Provided by Noemi (Hospital de Jove, Spain)
NF 81-AI	Human normal prostate tissue (immortalized with hTERT)	Fibroblast cell line	Provided by Noemi (Hospital de Jove, Spain)
PC3	Human prostate carcinoma	Prostate cancer cell	Dr. Arkaitz Carracedo (CIC bioGUNE, Spain)

## MATERIALS AND METHODS

22RV1	Human prostate carcinoma	Prostate cancer cell	Dr. Arkaitz Carracedo (CIC bioGUNE, Spain)
DUI45	Human prostate carcinoma	Prostate cancer cell	Dr. Arkaitz Carracedo (CIC bioGUNE, Spain)
TS1	Murine mammary carcinoma	Breast cancer cell	Dr. Johanna Joyce (Agora Cancer Research Center)
D2A1	Murine mammary carcinoma	Breast cancer cell	Dr. Arkaitz Carracedo (CIC bioGUNE, Spain)
HEK293 FT	Human embryonic kidney	Epithelial cell line	Commercial

Table 1. Table summarizing cell lines used in this project. Name, origin, source.

### 3.1.2 Animals

#### 3.1.2.1 *Chicken embryo spontaneous metastasis model*

The chick embryo spontaneous metastasis model is an *in vivo* assay that presents many advantages and overcomes limitations in the study of the metastasis. The main reason for that is the accessibility of the chorioallantoic membrane (CAM) (**Figure 11**), a well-vascularized extraembryonic tissue located beneath the eggshell. Moreover, at this stage, the embryo is immunodeficient, therefore the CAM would not present rejection to the inoculated cells, allowing their growth. Thus, this model enables the study of tumour growth (weight and measurements), and the metastatic process including invasion, angiogenesis, and secondary tumour formation in different organs of the embryo such as brain, lungs, liver and distal CAM<sup>180</sup>. All experiments were performed according to the national guidelines for animal care in accordance with the European Union Directive. The eggs used for these experiments were facilitated by our collaborator Dr. Berta Casar.

#### 3.1.2.2 *Mice*

Wild-type FVB/n 6–8-week-old females (Charles River) were used as recipients for tumours. The *in vivo* experiment was approved by the relevant Authority and performed in accordance with the guidelines of the Committee of Animal Experimentation of the University of Cantabria (Project “Caracterización molecular y celular del papel del microambiente tumoral y los CAFs en la progresión tumoral, metástasis y resistencia a terapias

## MATERIALS AND METHODS

(antiCAFing)", References: PI/O5/19 and PI-O2-23). *In vivo* experiments were performed by qualified personnel with the required authorisations.

### **3.1.3 Mediums, solutions, kits, and reagents**

#### **3.1.3.1 Culture media for cells**

High Glucose Dulbecco's Modified Eagle's Medium (DMEM, Sigma Aldrich #D6429) supplemented with 10% Fetal Bovine Serum (FBS; Gibco #10270-106), and 1% of Penicillin/Streptomycin (Gibco #15140-122), and GlutaMAX-100x (Gibco #35050-061). This is referred as complete media in the text. Where indicated, specific drugs or factors were added at specific concentrations (**Table 11**). For certain experiments, FBS or glutamine concentration was reduced.

Where indicated, for 2D cocultures assays, Low Glucose Dulbecco's Modified Eagle's Medium (DMEM, Sigma Aldrich #D5546) supplemented with 1% of Penicillin/Streptomycin and variations of FBS and glutamine concentrations (see 3.2.1.12) was used.

For the Mitochondrial and glycolytic stress analysis, cells were cultured in Seahorse XF DMEM medium pH 7.4 (Agilent Technologies #103575-100) supplemented with 2 mM glutamine, 10 mM glucose and 1 mM sodium pyruvate.

For the metabolomic experiments with labelled glucose, cells were cultured in DMEM without glucose (Thermo fisher, 11966025), supplemented with Glucose- $^{13}\text{C}^6$  (CK isotopes, CLM-1396), 10% of FBS, 1% of Penicillin/Streptomycin and GlutaMAX. For the experiments with labelled glutamine, cells were cultured in complete DMEM supplemented with 10% of FBS, 1% of Penicillin/Streptomycin and Glutamine- $^{13}\text{C}^5$  (CK isotopes, CLM-1822).

### 3.1.3.2 Transfection reagents

Procedure	Reagent
siRNA transfection	Opti-MEM (1X) Reduced Serum Medium (Gibco #31985-070) and DharmaFECT® (Dharmacon™ #T-2001-03)
Plasmid transfection in HEK-293FT	ProFection Mammalian Transfection System-Calcium Phosphate kit (Promega #E1200)
Transient plasmid transfection	Lipofectamine 3000 (Invitrogen #L3000015)

Table 2. Transfection reagent used in this project. Procedure and reagent specified.

### 3.1.3.3 Conditioned media

Fibroblast-derived conditioned media were obtained by culturing the cells with DMEM supplemented with the desired concentration of FBS (2.5 or 0.2%), 1% of Penicillin/streptomycin and GlutaMax for 48 h. PC3-derived conditioned media were obtained by culturing the cells with complete DMEM at 2.5% of FBS for 48h. For the cytokine array experiment, fibroblasts were cultured in DMEM 0.2% FBS for 24 h.

All conditioned medias were then recovered and filtered through a 0.45µm filter to remove dead cells and stored at -80 °C for later use.

### 3.1.3.4 Cell culture reagents

Reagent	Company	Reference
Dulbecco's Phosphate Buffered Saline (PBS)	Sigma-Aldrich	D8537
0.05% Trypsin-EDTA (1X)	Gibco	25300-062
Dimethyl sulfoxide (DMSO)	Sigma-Aldrich	D8418
Collagen I, High concentration, rat tail	Corning	354249
ECM Gel from Engelbrecht-Holm-Swarm murine sarcoma	Sigma-Aldrich	E1270
Matrigel Matrix (Growth factor reduced)	Corning	354230
Fetal bovine serum (FBS)	Gibco	10270106
5x DMEM	Prepared in the institute facility	
PrestoBlue	Fisher	A13261

Table 3. Table summarizing culture cell reagents used in this project. Company and reference number are specified.

**3.1.3.5 Protein purification/extraction and Western Blot**

Reagent	Company	Reference
Laemmli Buffer 4x	BioRad	1610747
Dithiothreitol (DTT)	Fisher	R0861
Acrylamide 30%	Teknovas	1610158
Ammonium Persulfate (APS)	ThermoFisher	11816714
Tetramethylethylenediamine (TEMED)	Sigma-Aldrich	T9281
Protein weight marker	Bio-Rad	1610374
Tween 20	Sigma-Aldrich	P1379
Milk, Dry powder	NYZTech	MB26001
Methanol >98%	VWR	20847.307
Clarity Western ECL substrate	Bio-Rad	170-5061
Nitrocellulose Blotting Membrane	Amersham™	10600003
SDS 10%	Prepared in the institute facility	
Tris-HCL 1.0M pH 6.8		
Tris-HCl 1.5M pH 8.8		
Tris Buffered Saline solution 10x (TBS)		

Table 4. Table summarizing Western Blot reagents used in this project. Company and reference number are specified.

**3.1.3.6 RNA extraction and purification**

Reagent	Company	Reference
NZY Total RNA Isolation kit	NYZTech	MB13402
2-Mercaptoethanol	Aldrich	M6250
DNAse I	Roche	10104159001
Endonuclease-free water	Fisher	AM9937

Table 5. Table of RNA extraction and purification reagents. Company and reference number are specified.

**3.1.3.7 DNA extraction from chicken embryo model**

Reagent	Company	Reference
Puregene® Cell Lysis Solution	QIAGEN	158116
Puregene® Protein Precipitation Solution	QIAGEN	158126
Puregene® DNA Hydration Solution	QIAGEN	172048440

Table 6. Table summarizing DNA extraction from chicken embryo organs. Company and reference number are specified.

## MATERIALS AND METHODS

### 3.1.3.8 RT and qPCR

Reagent	Company	Reference
NZY First-Strand cDNA Synthesis Kit	NYZTech	MB12501
NZYSpeedy qPCR Green Master Mix (2x), ROX plus	NYZTech	MB22202

Table 7. Table summarizing RT and qPCR kits. Company and reference number are specified.

### 3.1.3.9 Bacterial culture and Transformation

Reagent	Company
Ampicillin	Prepared in the institute facility
Glycerol 87%	Prepared in the institute facility
LB Agar	Prepared in the institute facility

Table 8. Table of reagents used for bacterial culture and transformation. Company and reference number are specified.

### 3.1.3.10 Plasmid extraction kit and library

Kit	Company	Reference
E.Z.N.A. <sup>®</sup> Plasmid Mini Kit I (Q-Spin column)	VWR	D6942-02

Table 9. Kit used for plasmid extraction. Company and reference number are specified.

Plasmid name	Vector	Gene	Sequence
psPAX2		None	Addgene #12260
pMD2.G		VSV G	Addgene #12259
hTERT	pBABE-hygro-hTERT	hTERT	Addgene #1773
Scramble (shC)	Lenti-Tet-PLKO-Tet	SCR	
Sh3 ASPA	Lenti-Tet-PLKO-Tet	ASPA	CCGGGCTTCTGGTTTCT GTATTATTCTCGAGAATA ATACAGAAACCAGAAGC TTTTTG
Sh4 ASPA	Lenti-Tet-PLKO-Tet	ASPA	CCGGCCTTCACAACACC ACTTCTAACTCGAGTTAG AAGTGGTGTGTGAAGG TTTTTG
Empty vector (EV)	Lenti-TRIPZ Scramble	SCR	
ASPA overexpression (ASPA)	Lenti-TRIPZ ASPA	ASPA	
GFP	Lenti-pCSII-IRES2-GFP	GFP	
TEAD-Rerporter	8xGTIIIC-luciferase	TEAD	Addgene #34615
CMV-Renilla	pGL4.75[hRluc/CMV]	Renilla	Promega #E2261
NF1-TAZ <sup>mut</sup>	pLenti-EF-ires-blast	TAZ S89A	Addgene #52084

Table 10. Plasmid library of this project. Company and reference number are specified.

**3.1.3.11 Factors and drugs**

Factor/drug	Company	Reference	Concentration to use
Animal-Free Recombinant Human TGF- $\beta$ 1	Peprotech	AF-100-21C	5ng/mL
Interleukin 1- $\alpha$	Bio-Techne	400-ML-005/CF	1ng/mL
Interleukin 1- $\beta$	Fisher	PHC0814	3ng/mL
IFN $\gamma$	Inmunotools	11343536	100ng/mL
TNF $\alpha$	Fisher	PHC3015	10ng/mL
N-acetylaspartate	Sigma-Aldrich	00920	100 $\mu$ M
TGF- $\beta$ 1 receptor inhibitor type I	Sigma-Aldrich	SB 431542	5 $\mu$ M
XAV939	Sigma-Aldrich	X3004	1 $\mu$ M
p-p38 inhibitor	Sigma-Aldrich	SB 202190	10 $\mu$ M
Doxycycline	Sigma-Aldrich	D5207	2 $\mu$ M
Hygromycin	Merck	H3274	100ng/ $\mu$ l
Blasticidin	Corning	MDTC30-100-RB	10 $\mu$ g/ml
Pimelic Diphenylamide 106	Merck	SMLO313	25 $\mu$ M
Trichostatin A	Sigma	T8552	100 $\mu$ M
Oligomycin	Sigma	495455	1 $\mu$ M
FCCP	Sigma	C2920	0.5 $\mu$ M
Rotenone	Sigma	R8875	0.5 $\mu$ M
Antimycin	Sigma	A8674	0.5 $\mu$ M

Table 11. Table summarizing factors and drugs used in this project. Company and reference number are specified.

**3.1.3.12 Luciferase assay**

Reagent	Company	Reference
Dual-Luciferase Reporter Assay System	Promega	E1910
Dual-Glo <sup>®</sup> Luciferase Assay System	Promega	E2920
Lysis buffer	Promega	E2661

Table 12. Table of luciferase assay reagents. Company and reference number are specified.

**3.1.3.13 Metabolomics**

Reagent	Company	Reference
Extraction buffer	See section 3.1.4.7	
Glucose-13C <sup>6</sup>	CK isotopes	CLM-1396
Glutamine-13C <sup>5</sup>	CK isotopes	CLM-1822
Solution A	See section 3.1.4.7	
Solution B		
Solution C	Sigma-Aldrich	F9252

Table 13. Table of metabolomic reagents. Company and reference number are specified.

**3.1.3.14 Mitochondrial and glycolytic stress analysis**

Reagent	Company	Reference
XF Cell Mito Stress Kit	Aligent Technologies	103015-100
Glycolysis Stress Test Kit	Aligent Technologies	103020-100

Table 14. Table of Seahorse assay reagents. Company and reference number are specified.

**3.1.3.15 Cytokine array kit**

Reagent	Company	Reference
Mouse Cytokine Array C2000	Bionova	AAM-CYT-2000-8

Table 15. Table for cytokine array study. Company and reference number are specified.

**3.1.3.16 Laboratory solutions and buffers**

Reagent	Company	Reference
Absolute ethanol >99%	VWR	ALCHO310F5
Bovine serum albumin (BSA)	NZYtech	MBO4602
Paraformaldehyde solution 4% (PFA)	Thermo Scientific	J19943

Table 16. Table summarizing laboratory solutions and buffers. Company and reference number are specified.

**3.1.3.17 Fungible Material**

Material	Company	Reference
Cell culture dishes 60mm diameter	VWR	34-2318
Cell culture plates 100mm diameter	VWR	734-2321
Culture plates multiwell, 6-well	VWR	734-2323
Culture plates multiwell, 24-well	VWR	734-2325
Culture plates multiwell, 48-well	VWR	734-2326
Culture plates multiwell, 96-well	VWR	734-2327
Glass bottom plates, 24-well	MatTek	P24G-1.0-13-F
XF96 Cell Culture Microplates	Aligent Technologies	103794-100
F96 MicroWell™ White Polystyrene Plate	Thermo Scientific	136101
Flask T175	VWR	734-2315
Flask T75	VWR	734-2313
Cryovials	Sarstedt	72.379.002
Eppendorfs	Sarstedt	72.690.001
Eppendorfs RNase free	Eppendorf	O22431021
PCR Microplate	Axygen	PCR-96-LP-AB-C
Mr. Frosty™ freezing container	Nalgene	C1562

Table 17. Table summarizing fungible material used in this project. Company and reference number are specified.

### 3.1.3.18 Software

Software	Purpose
Fiji- Image J	Gel contraction
	2D, MOT
	Wound healing
StepOnePlus real-time PCR system	qPCR
Tracefinder	Metabolomics
Wave	Seahorse

Table 18. Software used in this project.

## 3.1.4 Recipes

### 3.1.4.1 Gel contraction mix.

Gel for the contraction assay was composed by a mixture of collagen-I and ECM gel mixture yielding a final collagen concentration of ~4.6 mg/mL and a final ECM gel mix concentration of ~2.2 mg/mL (Collagen-rich matrix hereafter). Gels also contained 10% FBS and were diluted in complete DMEM.

### 3.1.4.2 Lysis buffer for Western Blot

Lysis buffer was generated with Laemmli Sample Buffer 4x containing dithiothreitol (DTT) (0.07g in 1ml of Laemmli Sample buffer) diluted 1:1 with TRIS-HCL pH 6.8.

### 3.1.4.3 Polyacrylamide gels

Stacking gel: 4% acrylamide, 125 mM Tris-HCl pH 6.8, 0.4% SDS, 0.1% APS and 0.1% TEMED in H<sub>2</sub>O.

Resolving gel: acrylamide (percentage depends on the molecular weight of the analyzed protein), 375 mM Tris-HCl pH 8.8, 0.4% SDS, 0.1% APS and 0.1% TEMED in H<sub>2</sub>O.

### 3.1.4.4 Tris-Glycine 10x

To generate Tris-Glycine 10x, in a big beaker we added 30.3g of Trizma base (Sigma-Aldrich #T1503), 144g of Glycine (Sigma-Aldrich #G8898) and 500mL of hot Milli-Q water. Once the solids are diluted, we added up to 1L of Milli-Q water.

## MATERIALS AND METHODS

### **3.1.4.5 SDS-PAGE running and transfer buffer**

To generate the running buffer for the Western Blot, 880mL of Milli-Q water were mixed with 20mL of SDS 10% and 100mL of Tris-Glycine 10x. For the transfer buffer, 800mL of Milli-Q water was mixed with 100mL of Tris-Glycine 10x and 100mL methanol.

### **3.1.4.6 TTBS**

To generate the T-TBS to wash the membranes during WB, 900mL of Milli-Q water were mixed with 10mL of TBS 10x and 500 $\mu$ l of Tween 20 (Sigma-Aldrich #P1379).

### **3.1.4.7 Metabolomics**

Extraction buffer: prepared with methanol:ACN:water in ratio 5:3:2.

Solution A: consist of 5% Sodium Deoxycholate in H<sub>2</sub>O: NaOH 5N: H<sub>2</sub>O in ratio 1:2:7.

Solution B: prepared with 0.5g Sodium Copper EDTA, 40g Na<sub>2</sub>CO<sub>3</sub>, 8g NaOH in 2L of H<sub>2</sub>O.

## 3.2 EXPERIMENTAL PROCEDURES

### 3.2.1 Cell biology and in vivo methods

#### 3.2.1.1 *Chick embryo spontaneous metastasis model*

For this experiment, PC3 cancer cells were inoculated together with human prostate CAFs control and CAFs overexpressing *ASPA*. Fertilized chicken eggs were incubated in a rotatory incubator at 37 °C and 65 % humidity. On day 10 of incubation, a hole was drilled in the air sack with a 30-gauge syringe needle and another hole was drilled near the allantoid vein using a Dremel rotary tool, penetrating the shell membrane without damaging the CAM. To drop the CAM from the shell, a moderate vacuum was applied to the air sack hole using an automated pipette with a Tygon tube. Next, using a cutting disc (Dremel), a square window of approximately 1 cm<sup>2</sup> was made. After that, 5x10<sup>5</sup> PC3 tumour cells and 1x10<sup>6</sup> CAFs were suspended in 25µl of FBS-free DMEM and injected onto the CAM near the allantoid vein bifurcation (**Figure 11**). Windows on eggs were then sealed with tape and incubated for 5 days. Then, tumours were collected and weighed, and different organs were harvested, and processed for quantitative PCR to determine the number of human cells that intravasated to the CAM and spread to the other organs<sup>180,181</sup>.

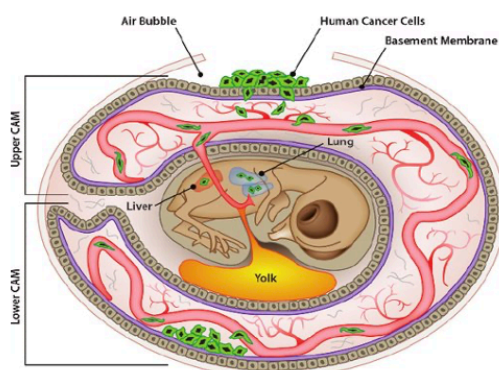


Figure 11. Schematic representation of inoculation of cells into the chicken embryo (chick embryo metastasis model).

### **3.2.1.2 *In vivo analysis of tumour growth using experimental murine models***

TS1 murine breast cancer cells were used to generate tumours in wild-type FVB/n. Briefly,  $5 \times 10^5$  TS1 cells and  $1.5 \times 10^6$  NF1-shC or NF1-sh4 ASPA were suspended in 100  $\mu$ L of PBS:Matrigel (50:50) and injected subcutaneously into 6–8 week old females the same day. Doxycycline was administered in water (1mg/mL), changed every two days to avoid degradation. Tumour size was measured every other day using callipers. To calculate tumour volume the formula  $V = (\text{MIN (width: length)} * (\text{MAX (width: length)})^2) / 2$  was used. All mice were culled once any of the growing tumours reached the maximum allowed size. To calculate tumour latency, mice with tumours reaching a minimum size of  $0.5 \text{mm}^3$  were considered as developing an observable tumour, and the day post-injection recorded and used for the disease-free survival calculation. Statistical analysis was performed using Long-Rank (Mantel-Cox) test.

### **3.2.1.3 *Cell culture and maintenance***

Cells were split between 2–3 days of culture to maintain cell confluence lower than 80% and not used after 10 passages. First, cells were washed with PBS and detached from the recipient with 0.05% trypsin-EDTA after 5 minutes of incubation at 37 °C. Then, trypsin was inactivated with DMEM at 10% of FBS and the media containing the cells was collected and 1:10 of the dilution was added into a new recipient to maintain the cells. The rest the cells were used for cell counting, to perform experiments or cryopreserved.

### **3.2.1.4 *Cell counting***

Cell counting was performed manually using a Neubauer chamber (Marienfeld). Briefly, 10  $\mu$ L of the cellular suspension was added in the chamber and cells on different squares were counted (**Figure 12**). Total cell number was calculated using the following formula:

## MATERIALS AND METHODS

$$\text{Cell concentration} \left( \frac{\text{Cells}}{\text{mL}} \right) = \frac{\text{number of cells per square}}{\text{number of squares}} \times 10^4$$

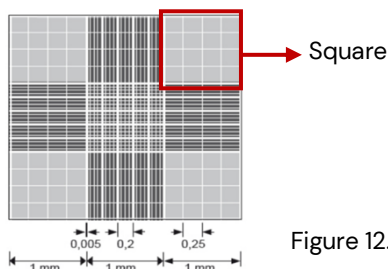


Figure 12. Representation of Neubauer chamber.

### 3.2.1.5 Cell Cryopreservation

For cryopreservation of cell lines, cell suspensions were centrifuged for 10 minutes at 1,000rpm. Then, the pellet was resuspended in FBS with 10% of DMSO. Cells were stored in cryovials that were immediately placed in  $-80^{\circ}\text{C}$  freezers using a Mr. Frosty™ freezing container for no longer than 2 months. For longer storage, cells were kept up to 6 months at  $-140^{\circ}\text{C}$  and then transferred into liquid nitrogen for permanent storage. For thawing cells, tubes were introduced in a water bath at  $37^{\circ}\text{C}$  and immediately diluted in complete DMEM. Cells were centrifuged to remove the DMSO and then resuspended in complete media and seeded in the flask.

### 3.2.1.6 Transient transfection

For transient RNAi-mediated gene silencing, fibroblasts were seeded at 60% confluency in a 6-well plate and transfected using DharmaFECT® transfection reagent and Opti-MEM cell culture media following manufacturer's instructions. Briefly, 5  $\mu\text{L}$  of siRNA solution (20  $\mu\text{M}$  stock) were diluted in 195  $\mu\text{L}$  of OptiMEM. In parallel, tubes containing 5  $\mu\text{L}$  of DharmaFECT diluted in 195  $\mu\text{L}$  of OptiMEM were prepared. Both tubes were vortexed and incubated for 5 minutes at room temperature (RT). Then, tubes were mixed and incubated for 20 min and finally, the mix were added to the cells dropwise and incubated for 5 h. After this time, 1 mL of complete DMEM was added to the plate. All siRNAs used in this thesis are summarized in **Table 19**. All-Star

## MATERIALS AND METHODS

siRNA was used as a negative control, as it has no homology to any known mammalian gene. When indicated, TGF $\beta$  was added 6 h after transfection.

Gene	Protein	Species	Reference
All-Star	All-Star	SCR	1027281
<i>Yap1</i>	YAP1	Mouse	D-046247-01
		Mouse	D-046247-02
		Mouse	D-046247-03
		Mouse	D-046247-04
<i>Wwrt1</i>	TAZ	Mouse	D-041057-01
		Mouse	D-041057-02
		Mouse	D-041057-03
		Mouse	D-041057-04
<i>Ctnnb1</i>	$\beta$ -Catenin	Mouse	D-040628-01
		Mouse	D-040628-02
		Mouse	D-040628-03
		Mouse	D-040628-04
<i>Srf</i>	SRF	Mouse	J-050116-09
<i>Hsf1</i>	HSF1	Mouse	D-040660-01
		Mouse	D-040660-02
		Mouse	D-040660-03
		Mouse	D-040660-04

Table 19. Table summarizing siRNAs used in this thesis.

For transient transfection of cDNA (i.e. luciferase),  $2 \times 10^4$  fibroblasts per well were seeded in 24-well plate. After 24 h, cells were transfected with  $2 \mu\text{g}$  of TEAD-reporter and 100ng of CMV-Renilla cDNA constructs (see 3.1.3.10) using lipofectamine 3000, according to the manufacturer's instructions. Briefly,  $1 \mu\text{L}$  of Lipofectamine 3000 reagent was diluted in  $25 \mu\text{L}$  of Opti-MEM, and master mix of DNA was prepared by diluting the required concentration of the plasmid in  $50 \mu\text{L}$  of Opti-MEM, plus  $2 \mu\text{L}$  of P3000 Reagent. Then, the diluted DNA was added in the tubes containing the Lipofectamine 3000 and the mix was incubated for 15 min. Then, the mix was added to cells.

### 3.2.1.7 Plasmid DNA purification from bacterial cultures

To generate stable cell lines, first *E. coli* DH5- $\alpha$  bacteria were transformed with the plasmid of interest (Table 10) following the heat-shock protocol. Finally, *E. coli* were inoculated into plates of LB-agar supplemented with the appropriate resistance antibiotic provided by the introduced

## MATERIALS AND METHODS

plasmid, in our case Ampicillin (50 $\mu$ g/mL). The next day, one single colony was collected and grown in liquid LB plus ampicillin in an incubator at 37 °C and shaking (140 rpm) overnight (O/N). Subsequently, plasmids were purified following EZNA Plasmid DNA Mini kit. The plasmids were diluted with 30 $\mu$ L of Elution buffer from the kit and DNA concentration was measured using the Nanodrop 2000 spectrophotometer (ThermoFisher Scientific).

### **3.2.1.8 Lentiviral infection of cells**

To generate cell lines stably expressing cDNA/shRNAs of interest, 3rd generation lentiviral infection was performed. For that, plasmids encoding for the factor of interest were purified, and lentiviral particles were generated by transfecting HEK-293FT cells with plasmids of interest and auxiliary plasmids (pdPAX2 and pMD2G) (**Table 10**), which are needed to generate the virus. HEK-293FT transfection was performed following Calcium Phosphate Transfection protocol using ProFection Mammalian Transfection System-Calcium Phosphate kit. First, HEK-293FT were seeded at 60% of confluency in p100 plates. The next day, HEK-293FT were transfected using 2 $\mu$ g of each plasmid diluted with 62 $\mu$ L of calcium phosphate and water until 500 $\mu$ L. In parallel, tubes containing 500 $\mu$ L of HEPES buffer (from the kit) were prepared. The content of the tubes containing the DNA was added into the buffer dropwise while generating bubbles inside. Once the mix was incubated for 30 min, it was added drop by drop to the HEK-293FT cells.

After 24 h of transfection, media containing transfection reagents was replaced by complete media. Next day, supernatants containing the lentiviral particles were collected in two rounds (48- and 72-h post-transfection). Supernatants were spun down to remove debris (1,500 rpm for 10 minutes) and filtered (using 45 $\mu$ m filters); the viral particles were then aliquoted and stored at -80 °C, ready to use for infection.

## MATERIALS AND METHODS

For cell infection,  $5 \times 10^4$  cells were seeded in 6-well plate with the collected media of the HEK-293FT diluted in fresh media in 1:1 ratio. In each well, polybrene (Millipore #TR-1003) was added at final concentration of  $5 \mu\text{g}/\text{mL}$  to boost the infection process. After 48 h of infection, medium was changed, and transfected cells were selected with the appropriate antibiotic for 3 days. This approach was employed to: (1) modulate *ASPA* expression (overexpression or shRNA-mediated silencing) in human and murine fibroblasts; (2) to immortalize human fibroblasts by overexpression of *hTERT*; (3) generate cell lines stably expressing *GFP*; (4) to potentiate TAZ activity in NFs by stably expressing a constitutive active mutant of TAZ (TAZ S89A).

(1) To silence *Aspa* in normal murine fibroblasts, a TET-PLKO-TET-on inducible doxycycline plasmid was used. Scramble shRNA and two individual shRNA targeting *Aspa* (Sh3-*ASPA* and Sh4-*ASPA*) were transfected in murine NF1, and selection was performed using Blasticidin at  $10 \mu\text{g}/\text{mL}$  final concentration. For *ASPA* ectopic expression, human prostate CAFs (PF179T and 85-AD), murine CAF1, and murine NF1 were transduced with a modified TRIPZ (Dharmacon) doxycycline inducible lentiviral construct in which the RFP and miR30 region was substituted by HA-*ASPA*, and puromycin resistance cassette was replaced by a hygromycin cassette. Cells were then selected with hygromycin at  $100 \mu\text{g}/\text{mL}$ . For the CAF1, two different clones (CAF 1.2 and CAF 1.3) were selected to perform the experiments.

(2) To immortalize primary human prostate fibroblasts NF85-BI and NF81-AI, and CAF85-AD and CAF81-BI, cells were infected by virus carrying *hTERT* plasmid. Then, cells were selected using hygromycin at  $100 \mu\text{g}/\text{ml}$ . Other immortalized human fibroblasts/CAFs were immortalized by the same procedure by other members of the lab.

(3) To generate PC3, 22RV1, DU145, TS1 and D2A1 GFP-labelled cells, cells were infected with virus generated with the Lenti-pCSII-IRES2-GFP system, and then selected with using Blasticidin at  $10 \mu\text{g}/\text{mL}$  final

## MATERIALS AND METHODS

concentration. D2A1 were then sorted by Flow cytometry to obtain cells that showed the most intense signal. Afterwards, cells were expanded and cryopreserved.

(4) To generate NF1 TAZ<sup>mut</sup>, NF1 was infected with virus generated with the pLenti-EF-FH-TAZ S89A-ires-blast system, which contains TAZ S89A mutation that impairs TAZ degradation. Cells were then selected with using Blasticidin at 10 $\mu$ g/mL final concentration.

For the cells transfected with inducible plasmids, the medium was supplemented with 2 $\mu$ M doxycycline for 5 days to induce cDNA/shRNA expression, and then confirmed by western blot.

### **3.2.1.9 ECM-remodelling assay**

To assess force-mediated matrix remodelling, the ECM-remodelling assay, also known as gel contraction assay, was performed. The day before the experiment, a 48-well multiwell plate was incubated O/N with 1% Bovine Serum Albumin (BSA) in plain DMEM at 37 °C in sterile conditions, to eliminate superficial tension of the plastic. The next day, the BSA was removed from the wells and 1x10<sup>5</sup> murine or human fibroblasts embedded in 100 $\mu$ L of gel contraction mixture (see 3.1.4.1) were added into the well. The mix was plated in triplicates and incubated 1 h at 37 °C to allow for gel solidification. Once the gel was set, cells were maintained in complete DMEM. Where indicated, TGF $\beta$  was added at 5 ng/mL final concentration; NAA was added at 100  $\mu$ M; SB431542 was added at 5 $\mu$ M; XAV939 was added at 1  $\mu$ M. Gel contraction was monitored daily by scanning the plates with a desktop scanner for later analysis.

To obtain the gel contraction value, the relative diameter of the well and the gel were measured using ImageJ software, and the percentage of contraction was calculated using the next formula:

## MATERIALS AND METHODS

$$\% \text{ Contraction} = \frac{(\text{Well area} - \text{Gel area})}{\text{Gel area}} \times 100$$

### **3.2.1.10 Matrigel On Top coculture**

24-well glass bottom plates were pre-coated with 100 $\mu$ L of Matrigel Growth Factor Reduced diluted 1:1 with PBS and incubated for 2 h. Next, 15x10<sup>3</sup> fibroblasts per well were seeded and once they were attached, 5x10<sup>3</sup> GFP-labelled cancer cells were seeded per well and allowed to adhere for 4 h. For MOT assay using conditioned media (CM) of fibroblasts, cancer cells were seeded directly onto the Matrigel.

Once cells were attached, medium was exchanged to complete DMEM at 2.5% FBS, or the CM of fibroblasts, and co-cultures were allowed to grow for 72 h. Cancer cell growth was monitored by acquiring the GFP signal in different areas of the well (up to five pictures) with a fluorescent microscope Nikon Eclipse TS100 (4X objective) every 24 h. Images were analysed using ImageJ and data analysed in GraphPad Prism. To calculate cancer cell growth index, area covered by cancer cells in each field of view was calculated.

### **3.2.1.11 Cultures with fibroblast-derived conditioned media**

Fibroblasts-derived CM at 0.2 or 2.5% of FBS was used for the proliferation experiments with D2A1-GFP labelled cancer cells. Briefly, 1x10<sup>3</sup> cancer cells per well were seeded and once the cells were attached, the media was changed for the fibroblasts-derived CM. The proliferation of cancer cells was monitored daily by acquiring the GFP signal in different areas of each well with a fluorescent microscope Nikon Eclipse TS100 (4X objective). Images were analysed as explained in the previous section.

### **3.2.1.12 2D Co-culture assay**

To study cancer cell proliferation in co-culture with fibroblasts, the 2D co-culture assay was performed. This experiment consists of seeding 2x10<sup>3</sup>

## MATERIALS AND METHODS

fibroblasts and  $1 \times 10^3$  GFP cancer cells in a 24-well plate with complete DMEM. When cells were attached, if needed, the media was changed for the media of desire: low glucose DMEM, variations in FBS (2–5%) and glutamine concentration (0–1%). Cancer cell proliferation was monitored during 7 days by acquiring the GFP signal in different areas of the well at 4X objective with the fluorescent microscope Nikon Eclipse TS100 every 24 h. Images were analysed as previously explained.

### **3.2.1.13 Wound healing**

To study the migratory capacity of the fibroblasts,  $4 \times 10^5$  cells were seeded per well in a 6-well plate to form a confluent monolayer. The next day, a straight scratch was performed in the center of the well mimicking a wound, using a 200 $\mu$ L pipette tip. Subsequently, wells were washed with 1 mL of PBS to remove debris and non-attached cells, and the well was replenished with DMEM at 2.5% FBS or CM of PC3 cancer cells at 2.5% of FBS. Then, migration of the cells was monitored by acquiring phase contrast images with the microscope Nikon Eclipse TS100 at 4X objective, every 2 h until the complete closure of the wound. Images were analysed using Fiji software and migration index was calculated by measuring the area of the wounded region lacking cells, and then normalize to TO images of each experiment.

### **3.2.1.14 Proliferation assay**

To study the proliferation rate of our cells, Prestoblue assay was performed with our hCAF-C and hCAF-ASPA with complete DMEM Glutamine-deprived, with the addition of NAA where indicated. For that,  $1 \times 10^3$  cells were plated in a 96-well plate in triplicates with 90  $\mu$ L of the media. Next day, 10 $\mu$ L of Prestoblue was added in each well. After 2 h of the addition of Prestoblue, the absorbance of the plate was read by a spectrophotometer at two wavelengths: 540 nm (reduced prestoblue) and 620 nm (oxidized prestoblue). After that, Prestoblue was aspirated and cells were washed with

## MATERIALS AND METHODS

PBS, and finally media was added into the wells. This process was daily repeated for 5 days.

The background (absorbance of the media only) was subtracted from both wavelengths and the correction factor and the % of difference in reduction was calculated using these formulas:

$$AOLW = \text{average Abs 540 media with Prestoblue} - \text{average Abs media only}$$

$$AOHW = \text{average Abs 620 media with Prestoblue} - \text{average Abs media only}$$

$$Ro = \frac{AOLW}{AOHW}$$

$$\% \text{ difference in reduction} = 100 - \left( \frac{\text{Abs540 dia X} - (\text{Abs620 dia X} \times Ro)}{\text{Abs540 dia 1} - (\text{Abs620 dia 1} \times Ro)} \right) \times 100$$

### 3.2.1.15 Factors and drug treatments

For all the experiments that involves gene/protein expression studies with drug treatments, cells were first plated in a 60mm dishes at 70% of confluency. Once the cells were attached, the drug was added into the media of the cells. In parallel, one plate was kept as a control, where instead of adding the drug, same volume of vehicle (DMSO, water or PBS) was added.

For the experiments using TGF- $\beta$ 1 receptor I inhibitor (SB431542), p38 inhibitor (SB202190), and Wnt inhibitor (XAV939), drugs were added at the indicated final concentration (**indicated in Table 11**) for 24 h. If needed, TGF $\beta$  stimulation was added 4 h after the addition of the drug.

For the experiments involving HDAC inhibitors, Trichostatin-A (TSA), a pan inhibitor of HDACs, was added at 100  $\mu$ M final concentration; Pimelic Diphenylamide 106 (PD106), a class I inhibitor, was used at 25  $\mu$ M final concentration. HDAC inhibitors were added for 24 h. Where indicated, TGF $\beta$  was added 4h after the addition of the drugs.

## 3.2.2 Molecular procedures

### 3.2.2.1 Western blot

To study protein expression by western blot (WB), cells after indicated perturbation were washed with PBS, and protein lysates were obtained by scrapping cells with Laemmli Sample Buffer 2x. Then, samples were sonicated (5 cycles of 30 seconds) and boiled at 95°C for 5 min. Proteins were resolved in sodium dodecyl sulphate (SDS)-polyacrylamide gel electrophoresis (PAGE) in running buffer. SDS-gels consisted of a stacking top and a resolving part composed of 15% acrylamide and were ran at 120 volts. Once the separation process was finished, proteins were transferred to nitrocellulose membranes at 400mA for 1 h in cold transfer buffer. Subsequently, the membrane was blocked with 5% of milk diluted in T-TBS for 1 h shaking at RT. Finally, the membranes were incubated O/N with primary antibodies at 1:1,000 dilution in a 5% milk T-TBS solution. The next day, membranes were washed with T-TBS (3 x 10 min) and incubated with anti-rabbit or anti-mouse immunoglobulin (Ig) peroxidase-conjugated secondary antibodies (1:10,000) prepared in a 5% milk T-TBS solution for 1 hr shaking at RT. After washing (3 x 10 min), Clarity Western ECL substrate kit was used at 1:1 ratio for protein detection using an Amersham ImageQuant 800 (Cytiva) imaging system. Antibodies used in this thesis are summarized in **Table 20**.

Analysis of Western Blots was performed using Fiji- Image J software. Protein amounts were normalized to the loading control protein.

Protein	Dilution	Source	Reference
GAPDH	1:5,000	Cell signalling	3683
ASPA	1:1,000	Abcam	ab223269
YAP/TAZ	1:1,000	Santa Cruz	sc-101199
β-Catenin active	1:1,000	Cell signalling	8814
αSMA	1:5,000	Sigma Aldrich	A5228
SMAD2/3	1:1,000	Cell signalling	8685S
pSMAD2/3	1:1,000	Cell signalling	8828S
HSF1	1:1,000	Cell signalling	4356
Ac-H3	1:1,000	Millipore	O6-599
H3	1:1,000	Cell signalling	3638

## MATERIALS AND METHODS

Beta-Tubulin I	1:1,000	Sigma Aldrich	T7816
P-PDHA1	1:1,000	Abcam	ab17761
PDHA1	1:1,000	Abcam	ab110334
Polyclonal Goat Anti Rabbit-HRP	1:10,000	Agilent Technologies	PO448
Polyclonal Goat Anti Mouse-HRP	1:10,000	Agilent Technologies	PO447
Cy3 SMA	1:1,000	Sigma	C6198
DAPI	1:1,000	Temecula California, Millipore	90229
Alexa Fluor® 488 Goat Anti- Rabbit IgG (H+L) Antibody	1:10,000	Invitrogen	A11008

Table 20. Summary of the antibodies used in this thesis: protein, dilution, source, and reference number.

### 3.2.2.2 Immunofluorescence

For immunofluorescence experiments,  $5 \times 10^3$  cells/well were seeded in sterilized cover glass slides placed into a 24-well plate. The next day, cells were fixed in 4% paraformaldehyde (PFA) for 10 min. Then, cells were permeabilized with 0.2% Triton X-100 for 7 min, followed by a blocking step of 3% BSA 0.1% Tween for 1 h. After that, cells were incubated with the corresponding primary antibody O/N at 4 °C in a humidified chamber. The following day, the primary antibody was washed with PBS (3 x 5 min washes) and cells were incubated with the corresponding secondary antibody for 1 h at RT. After washing the secondary antibody with PBS (3 x 5 min washes), glass covers were mounted in slides and imaged using a confocal microscope.

Immunofluorescence images were obtained using a TCS SP5 Confocal Microscope (Leica). For in vitro cell imaging, images were taken using the 4X/10X/20X objectives. Lasers of 405 Diode UV, Argon Helium-Neon (HeNe) 543 and HeNe 633 were used for the excitation of the corresponding fluorophores, and fluorescence was captured in the following wave lengths: blue fluorescence, between 420 nm and 480 nm; green fluorescence, between 500 nm and 540 nm; red fluorescence, between 606 nm and 656 nm.

### 3.2.2.3 RNA isolation

To obtain RNA, cells were plated at 70% of confluence in a 6-well plate and after 24 h, RNA was isolated using NZY Total Isolation Kit according to manufacturer's instructions. RNA quality and concentration were then measured using the Nanodrop. The RNA was diluted with Nuclease-Free Water and stored at -80 °C.

For RNA-sequencing,  $6 \times 10^5$  cells were plated in a p100 plate for 24 h. Where indicated, TGF $\beta$  was added at 5ng/mL final concentration. The next day, RNA extraction was performed using the same kit previously mentioned.

### 3.2.2.4 Real-Time Quantitative Reverse Transcription PCR (qRT-PCR)

For the qRT-PCR, 1 $\mu$ g of RNA was used to generate the cDNA following the NZY First-Strand cDNA Synthesis Kit. Finally, 50ng of cDNA were used for each reaction to perform the qPCR. It was performed in triplicates for each sample, using the NZYSpeedy qPCR Green Master Mix 2X ROX plus, according to the manufacturer's instructions in a StepOnePlus real-time PCR system. *Gapdh/GAPDH* was used as the housekeeping gene for the normalization of the data, and the quantification and comparison were obtained using the  $\Delta\Delta C_t$  method. Sequences of the oligonucleotides used for qRT-PCR are described in the table below:

Gene	Specie	Forward primer	Reverse primer
<i>Gapdh</i>	Murine	GTGCAGTGCCAGCCTCGTCC	GCCACTGCAAATGGCAGCCC
<i>Aspa</i>	Murine	ACATGGCTGCTGTTATTCATCC	GGGTACACGGTACAGTCTCCA
<i>ASPA</i>	Human	CCTGTGGGTATAGAAGTTGTCC	GGTTCCAGTCTTGATCCTGC
<i>ALU</i>	Human	ACGCCTGTAATCCCAGGACTT	TCGCCCAGGTGGCTGGGGCA

Table 21. Summary of oligonucleotides used in this thesis: protein, dilution, source, and reference number.

### **3.2.2.5 DNA extraction and quantification from chicken embryo**

For the extraction of genomic DNA from collected tissues from chicken embryo experiments, a DNA extraction kit was used. Following manufacturer's instructions, 600µL of lysis buffer containing 1µg/mL proteinase K (Sigma-Aldrich) were added to each tube, and subsequently homogenized using a Polytron and incubated O/N at 65 °C. Next day, 200µL of protein precipitation buffer were added and samples were vortexed and centrifuged at 13,000 rpm for 5 min. Supernatants were collected and transferred to another tube containing 800µL of cold isopropanol for DNA precipitation. Then, samples were centrifuged at 13,000 rpm for 5 min, pellets were rinsed with 200µL of 70 % ethanol, and centrifuged. Pellets containing genomic DNA were then dried O/N and resuspended in 200µL of hydration buffer. Finally, DNA was quantified in each sample using Nanodrop, and purified DNA was preserved at -20 °C for qPCR analysis. Briefly, the genomic DNA obtained in the previous step was prepared at final concentration of 30ng/µL and 1µL was added in each reaction. *ALU* sequences are primate-specific transposable elements, which conform around 10% of the human genome and are not present in chickens. Thus, to detect the presence of human tumour in the different tissues, a PCR for *ALU* was performed. qPCR was performed as usual, and murine *Gapdh* was used as a housekeeping gene since it presents high homology with the chicken *Gapdh*, and the quantification and comparison were obtained using the  $\Delta\Delta C_t$  method.

### **3.2.2.6 Gene expression analysis of isolated cell types from murine mammary tumours**

To analyse *Aspa* expression in different cell types from murine mammary tumours, we employed RNA generated from a previous study<sup>65</sup>. Briefly, MMTV-PyMT tumours were minced and digested with a mixture of DNase and Liberase (Roche Diagnostics). On enzymatic digestion, samples

## MATERIALS AND METHODS

were passed through a 100- $\mu$ m filter. Cells were incubated for 5 min at RT in 2 mL NH<sub>4</sub>Cl solution (0.8% in H<sub>2</sub>O) to eliminate red blood cells. Cells were then directly used for FACS staining and sorted with a FACSAria flow cytometer (BD Biosciences). Single cell suspensions of tumour cells were labelled with FITC Rat Anti-Mouse CD45 Clone 30-F11 (BD Pharmingen™, 553079), APC Rat Anti-Mouse CD31 Clone MEC 13.3 (BD Pharmingen™, 561814), PE/Cy7 anti-mouse CD326 (Ep-CAM) (BioLegend, 118215) and PE anti-mouse CD140a (PDGFRa) (BioLegend, 135905). For cell sorting, four populations (CD45+ for immune cells, CD31+ for endothelial, EPCAM+ for epithelial and PDGFRA+ for CAFs) were collected and processed for RNA extraction and qRT-PCR.

### **3.2.2.7 Luciferase reporter assay**

For the luciferase assay, TEAD-reporter construct (8xGT1IC-luciferase) and CMV-Renilla plasmid were used. TEAD is a transcription factor that binds to YAP/TAZ factors; therefore, it is used to measure TAZ activity. On the other hand, Renilla activity is used as a housekeeping activity, since Renilla luciferase reaction provides a stabilized luminescent signal that decays slowly over the course of the measurement. For the experiment,  $2 \times 10^4$  fibroblasts per well were seeded in 24-wells plate. After 24 h, cells were transiently transfected with 2 $\mu$ g of TEAD-reporter and 100ng of CMV-Renilla cDNA constructs using the Lipofectamine 3000 protocol. Following the Dual-Luciferase Reporter Assay System manufacturer's instructions, cells were lysed 48 h after transfection in 100 $\mu$ L of Passive Lysis Buffer (PLB). 20 $\mu$ L of the cell lysates were added in a F96 MicroWell™ White Polystyrene Plate, plus the other reagents for the luciferase emission detection using Dual-Glo® Luciferase Assay System. Dual-reporter assays are performed as follows: (i) inject Luciferase Assay Reagent II; (ii) measure firefly luciferase activity; (iii) inject Stop & GloR Reagent and (iv) measure Renilla luciferase activity. The acquisition of luminescence is done by using the luminometer GloMax®-Multi+ Detection System (Promega).

## MATERIALS AND METHODS

To analyse luciferase assay results, we extracted the baseline of every sample in order to obtain the real quantification of our reporter following the equation above. With this equation we obtain the activity of our reporter gene.

$$\text{Firefly Fold} = \frac{\text{firefly read}}{\text{Renilla read}}$$

### 3.2.2.8 Tracing experiments

Metabolomic studies were performed with murine NF-shC, NF-sh3-*ASPA* and NF-sh4-*ASPA*, and with human CAFs and CAF overexpressing *ASPA* (CAF-*ASPA*) to check which metabolic pathways were perturbed by the modulation of *ASPA*. These metabolomic studies consisted of tracing experiments with labelled glucose or glutamine that allowed us to follow the labelled carbons through all the cell metabolism and decipher which pathways were altered in our cell lines due to *ASPA* modulation.

For this experiment, the following protocol was performed (**Figure 13**). First, cells were plated in a 6-well plate at 50% of confluence with complete media for 24 h. Next, plates were washed with PBS and media was changed for media containing the labelled metabolite of choice, in our case it was Glucose-<sup>13</sup>C<sup>6</sup> or Glutamine-<sup>13</sup>C<sup>5</sup>. In this way, we were able to follow the labelled carbons destination throughout the cell metabolism. After 24 h, the metabolite extraction protocol for the intracellular metabolites was performed. Briefly, cells were washed with ice cold PBS and the ice-cold extraction buffer was added into the wells and incubated at 4 °C for 5-10 min. After that, the extraction buffer was collected into ice-cold eppendorfs tubes and centrifuged for 5 min at 16,000 x g at 4 °C. Then, 200µL of the supernatant was transferred into the mass spectrometer vials or stored at -80 °C until samples were processed. Plates were kept at 4 °C for the posterior protein quantification of each well.

For the extracellular metabolites, after 24 h incubation with the labelled metabolite, 10µL of the medium was added into tubes containing

## MATERIALS AND METHODS

500 $\mu$ L of the ice-cold extraction buffer. The tubes were shaken for 10 min at 4 °C. Subsequently, samples were centrifuged for 5 min at 16,000 x g at 4 °C and finally, 200 $\mu$ L of the supernatant was added into the mass spectrometer vials and stored at -80 °C. Plates were kept at 4 °C for the posterior protein quantification of each well.

Samples were processed using a Q-Exactive Orbitrap mass spectrometer (Thermo Scientific) in combination with a Thermo Ultimate 3000 HPLC system. Briefly, 5 $\mu$ L of cell extract was injected and the metabolites were separated over a 15 min mobile phase gradient, from an initial ACN content of 80%, ACN with 20% ammonium bicarbonate (pH 9.2), decreasing to 20% CAN, with a flow rate of 200  $\mu$ L min<sup>-1</sup>. Metabolites were detected over a period of 25 min using the Q-Exactive mass spectrometer across a mass range of 75–1,000 *m/z* and at a resolution of 35,000 (at 200 *m/z*). Peak identification and area quantification of the metabolites were performed using TraceFinder software by comparison of the retention time and exact ion mass to an authenticated standard.

In order to normalize the data obtained from Tracefinder software, the 6-well plates were processed using the modified lowry method to quantify the protein after metabolite extraction. First, a standard curve of BSA plate (0–500 $\mu$ g) was prepared into a 6-well plate. Using in parallel the standard plate and sample plates, next step was to air dry the wells. Then, 300 $\mu$ L of solution A (**Table 13**) was added in each well and shook at RT for 40 min. After that, 10 volumes/well of solution B (**Table 13**) was added and shook for 10 minutes at RT. Then, 300 $\mu$ L of solution C (**Table 13**) was added in each well and shook slowly for 40 min at RT. Finally, the absorbance was read at 750nm with the spectrophotometer. The protein amount in each well is calculated with the formula generated using the linear standard curve. Following this procedure, we normalized the peak area of the metabolites obtained by the Tracefinder with the protein amount of the respective sample. In order to

## MATERIALS AND METHODS

reduce experimental noise emerging from metabolite analyses of different biological replicates, we normalize data with the total sum method (as no internal standards were employed)<sup>182</sup>. The total sum method scales each sample so that the sum of squares of all abundances in that sample equals 1. We employed this normalization method for all metabolites included in the initial analyses, obtaining a relative abundance for all metabolites within a sample, that were employed for further analyses and representation.

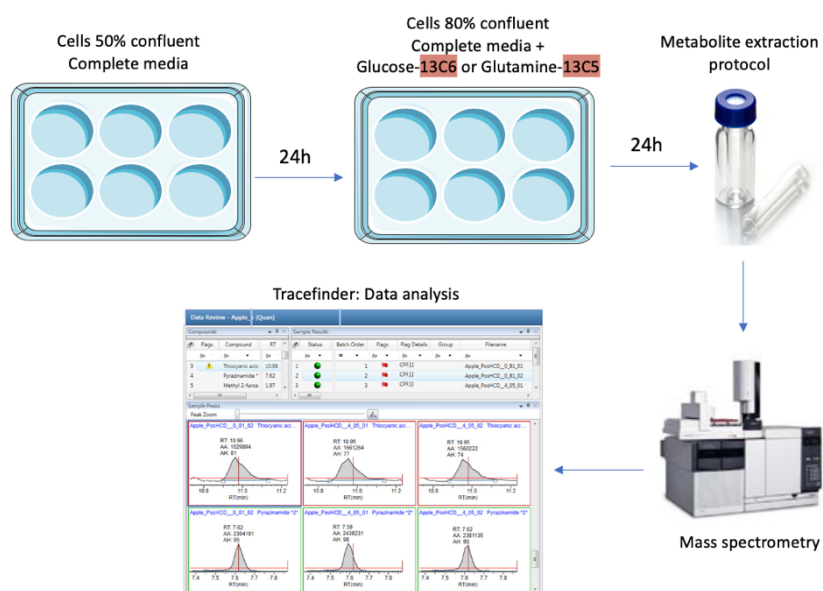


Figure 13. Schematic representation of the workflow of tracing experiments.

### 3.2.2.9 Mitochondrial and glycolytic stress analysis

To assess the energetic state of the fibroblasts, seahorse analysis was kindly performed by PhD student Peio Azcoaga in Dra. Maria Muñoz Caffarel lab. The first day, cells were plated in XF96 Cell Culture Microplates at a cellular density of 30,000 cells/well. Next day, for the Oxygen Consumption Rate (OCR) determination, the media was changed for Seahorse XF DMEM medium pH 7.4 supplemented with 2 mM glutamine, 10 mM glucose and 1 mM sodium pyruvate for 1h, prior to the measurements using the XF Cell Mito Stress Kit. For this experiment, oligomycin (ATP synthase inhibitor) was used at 1 $\mu$ M;

## MATERIALS AND METHODS

FCCP (uncoupler, mimics physiological “energy demand”) at 0.5 $\mu$ M; Rotenone and antimycin (block complex I and complex III, respectively) at 0.5 $\mu$ M.

For glycolytic metabolism measurements, cells were incubated in normal complete DMEM for 1 h prior to injections using the Glycolysis Stress Test Kit.

Experiments were run in a XF96 analyser, and raw data were normalised to cellular content calculated by crystal violet method. The following measurements were performed in this experiment: Basal glycolysis (GlycoPER) refers to Proton Efflux Rate derived from glycolysis; Basal Proton Efflux Rate (PER) refers to the number of protons exported by cells into the assay medium over time, expressed as pmol/min; MitoOCR/GlycoPER refers to the ratio between mitochondrial oxygen consumption and glycolytic activity; Basal respiration refers to the oxygen consumption used to meet cellular ATP demand resulting from mitochondrial proton leak. Shows energetic demand of the cell under baseline conditions; ATP production refers to the decrease in oxygen consumption rate upon injection of the ATP synthase inhibitor oligomycin and represents the portion of basal respiration that was being used to drive ATP production; Spare respiratory capacity refers to the capability of the cell to respond to an energetic demand as well as how closely the cell is to respire to its theoretical maximum. The ability of the cells to respond to demand can be an indicator of cell fitness or flexibility.

To analyse the data from these experiments, background values were extracted, and all parameters were normalized to the control sample.

### **3.2.2.10 Cytokine array**

For the cytokine profile study, the RayBio® C-Series Mouse Cytokine Antibody Array kit was used (protocol represented in **Figure 14**). This kit allows the detection of 62 cytokines using the CM of the cells of interest, in our case, CM from NF-shC and NF-sh4 ASPA were obtained after 24 h in culture at 0.2%

## MATERIALS AND METHODS

of FBS, according to the protocol. First, antibody membrane arrays were placed into the incubation Tray and blocked for 30 min at RT. Then, 1mL of conditioned media was added into each well (containing the arrays) and incubated O/N at 4 °C. The next day, media was removed, and wells were washed as the protocol indicates. Then, the biotinylated antibody cocktail was added into each well and incubated O/N at 4 °C. Subsequently, membranes were washed, and HRP–Streptavidin was incubated O/N at 4 °C. Finally, the membranes were washed and transferred onto a plastic sheet where the detection buffer was added to proceed to the chemiluminescence detection using Amersham ImageQuant 800 (Cytiva) imaging system.

To analyse the results, background parameter was subtracted, and each result was normalized with the median of the positive controls of the array.

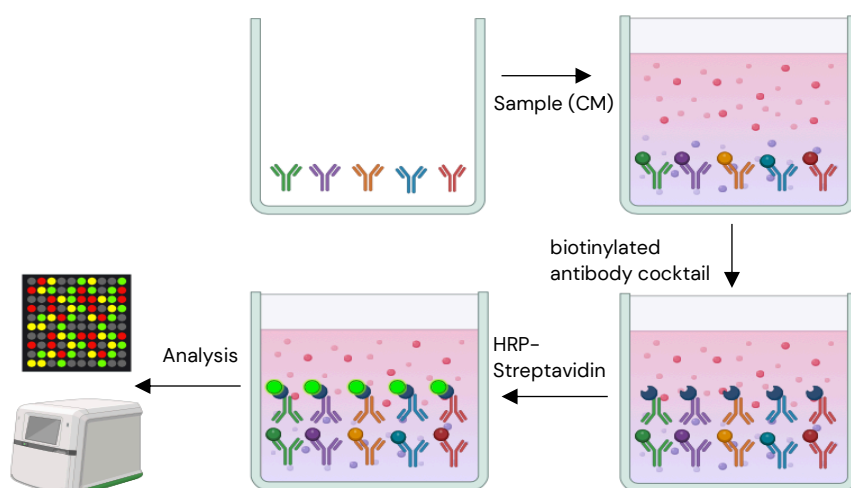


Figure 14. Representative scheme of the Cytokines array protocol.

### 3.2.2.11 Immunohistochemistry analysis of human tumours

Representative immunohistochemistry images of ASPA expression in colon and prostate cancer tissues were retrieved from the online platform ProteinAtlas (<https://www.proteinatlas.org/humanproteome/pathology>).

### 3.3 COMPUTATIONAL ANALYSIS

#### 3.3.1 RNA-sequencing (RNAseq) processing and analysis

RNA-seq analysis was performed to investigate the transcriptional responses in fibroblasts after *ASPA* modulation. RNA quality was checked by RNA ScreenTape analysis in an Agilent TapeStation system. Samples were then sent to the Centro Nacional de Analisis Genómico (CNAG) for RNA sequencing.

After Quality control and library preparation (TruSeq Stranded mRNA Reference Guide #10000000040498 v00), stranded RNAseq was sequenced at 40 million reads per sample (2x150bp) using an Illumina NovaSeq 6000 S4.

RNAseq data was pre-processed by the bioinformatician in our group to perform quality check, removal of contaminants, alignment (Genome Reference: GRCm38) and quantification. Subsequent analyses were performed using either 'count' or 'tpm' (Transcript Per Million) matrix datasets. Principal Component Analysis (PCA) and hierarchical clustering were performed using pre-filtered datasets (removing rows with no counts, or with only a single count across all samples) after 'regularized logarithm' (rlog) transformation.

DESeq2 software was used to identify the Differentially Expressed Genes (DEGs, cut-off:  $P_{adj} < 0.05$ ) and fold changes between experimental conditions, following the program guidelines. This dataset was also employed to derive gene signatures (genesets) associated with *Aspa* modulation in fibroblasts. Unless stated otherwise, expression values for each gene represented in the figures or tables were z-score normalized from the 'tpm' matrix dataset.

### 3.3.2 Gene Set Enrichment Analysis (GSEA)

Transcriptomics data were processed and analysed using the Gene-set enrichment analysis (GSEA) software, developed by the Broad Institute of MIT and Harvard (USA) and available at [www.broadinstitute.org](http://www.broadinstitute.org). For transcriptomic analyses by GSEA, gene count RNA-seq data was first pre-processed using the Voom Normalization from the GenePattern platform, following the program guidelines (expression value filter threshold=1). This module pre-processes RNA-Seq data into a form suitable for use downstream in analyses such as GSEA. Pre-processed data was then run through GSEA software following the programme guidelines. The specific settings applied in all analyses were: Number of Permutations (1000), Permutation Type (Gene set), Enrichment statistic (Weighted), and Metric for ranking genes (*t* Test). Analysed gene sets were retrieved from the Molecular Signatures Database (MSigDB) from the Broad Institute of MIT and Harvard (USA). In addition, in-house manually curated gene sets or gene sets from specific publications were employed. Results were represented using an in-house adapted script from GSEA Multi-sample Running Enrichment plots.

To calculate the gene-signature score in each sample, we used single sample Gene Set Enrichment Analysis (ssGSEA) Projection Software from the GenePattern platform, following the programs guidelines. This analysis calculates separate enrichment scores for each pairing of sample and gene set. Each ssGSEA enrichment score represents the degree to which the genes in a particular gene set are commonly up or downregulated within a sample. ssGSEA scores were z-score normalised.

Similar approaches (GSEA and ssGSEA) were employed to investigate the enrichment and/or expression of particular gene signatures in stromal datasets.

### 3.3.3 Gene expression analysis of clinical datasets

Gene expression analyses of human tumour stroma were retrieved from NCBI Gene Expression Omnibus (GEO). Datasets include: Finak (GSE9014, Breast), Karnoub (GSE8977, Breast), Yeoung (GSE40595, Ovary), Nishida (GSE35602, Colon), Navab (GSE22863, Lung) and Planche (GSE26910, Prostate). Additional datasets include: GSE20086 (human breast NF and CAFs), GSE70468 (human colon NF and CAFs), GSE35350 (human ovarian NF and CAFs), GSE22862 (human lung NF and CAFs), and GSE68164 (human prostate NF and CAFs). For microarray-based datasets, probe-to-gene was performed using the highest variance probe. These datasets were employed in other bioinformatics approaches including DESeq2, GSEA and ssGSEA.

To identify consistent differentially expressed genes (DEGs) in cancer stroma vs normal stroma, we studied the up and down-regulated DEGs in the Finak (GSE9014, Breast), Yeoung (GSE40595, Ovary) and Nishida (GSE35602, Colon) datasets (cutoff  $P_{adj} < 0.05$ ) and identified common up and downregulated genes, that were employed in subsequent analyses. This analysis was represented using the difference on mean z-score between cancer and normal stroma gene expression.

### 3.3.4 Enrichment analysis

DEGs and other gene signatures obtained from previous differential analyses were also processed for enrichment analyses using the “Enrichr” platform or online platforms such as “DAVID” and “g:Profiler”. Briefly, “Enrichr” and “DAVID” were employed to perform functional enrichment analysis (over-representation analysis) of candidate gene lists over Gene Ontology datasets such as KEGG, GOTERM\_BP and GOTERM\_MF. “g:Profiler” was employed to perform functional enrichment analysis of candidate gene list over manually curated-user provided datasets, provided as “.gmt” files.

### 3.3.5 Survival analysis

Analysis of combined hazard ratios in all cancer types was performed using the PRECOG platform (<https://precog.stanford.edu/>). The MetaZ (“Matrix of Z-scores in PRECOG”) and TCGA (“Z-score matrix for TCGA RNA-seq datasets ordered by gene the same as the main PRECOG matrix”) files were downloaded (version July 2020). The metric “Unweighted\_meta-Z\_of\_all\_cancers” for consistent up and downregulated genes in cancer stroma was employed to represent hazard ratios in both PRECOG and TCGA datasets.

The analysis of clinical relevance of specific genes or gene set expression was assessed using publicly available data from the CANCERTOOL<sup>183</sup> platform for breast (Lu and Metrabric dataset), lung (Okayama dataset) and prostate cancer (TCGA dataset). For lung cancer, we also employed the dataset from the KM-plotter platform ([www.kmplot.com](http://www.kmplot.com))<sup>184–186</sup>. For colorectal cancer, the GSE17538 dataset was employed<sup>187</sup>. In all cases, Disease-Specific Survival was analysed. In all cases, mean expression was used to dichotomise the different tumours into high and low groups. In addition, survival analysis based on gene expression on breast cancer stroma was performed using the Finak Dataset (GSE9014)<sup>188</sup>. Consistent up and downregulated genes were represented based on the Hazard Ratio associated to their expression and the p-value. Survival curves were estimated based on the Kaplan–Meier method and compared using a log-rank test.

### 3.3.6 Single cell RNAseq (scRNAseq) processing and analysis

For initial scRNAseq analysis in normal tissues, the ProteinAtlas platform was used<sup>189</sup> and tables describing *ASPA* expression in different cell clusters (colour-coded by cell type) for breast, colon, lung, ovary, and prostate were retrieved. In addition, scRNAseq analysis was performed from public datasets of breast and bladder human cancers by the bioinformatician in our

## MATERIALS AND METHODS

lab. Breast scRNAseq data was obtained from the European Genome-Phenome Archive, reference E-MTAB-1060<sup>190</sup> and consists of 14 fresh human breast tumour tissue samples dissociated into single cells and viably frozen, 7 exhausted and 7 non-exhausted, without prior cell type enrichment. Bladder scRNAseq data was obtained from the China National Center for Bioinformation, reference GSA-Human HRA000212<sup>191</sup> and consists of tumour and 3 normal mucosae samples processed immediately after being obtained from bladder cancer patients of the study. Our analyses included only the ones with publicly uploaded metadata, remaining 5 tumour samples and 2 mucosae: ("BC1", "BC2", "BC4", "BC5", "BC7", "Mucosa1", "Mucosa3").

Each sample was pre-processed individually following the same methodology of their original publication, with some changes in software versions in R.

For Breast cancer from Cords 2023: This dataset was generated using the 10x Genomics platform, and the raw data pre-processing, quality control steps, and main cell type annotation have been described. Briefly, gene-by-cell matrices were generated from the raw sequencing data using CellRanger (10x Genomics, v3.0.1) and subsequently transformed into Seurat objects (Seurat v3.0.2). After removing high-confidence doublets using the DoubletFinder Package, all Seurat objects were merged, and single cells with >7500 or <200 genes, with >75000 read counts, or with >20% of reads mapping to mitochondrial RNA were excluded. Highly variable genes were identified by the `sctransform` wrapper in Seurat and used to construct principal components. The principal components covering the highest variance in the dataset were used as input for graph-based clustering. Differential gene expression analysis was performed for the resulting clusters, and main cell types were annotated based on the cluster expression of established marker genes (EPCAM and CDH1 for epithelial cells, PECAM1 and VWF for endothelial cells, PDGFRB and FAP for fibroblasts, CD3, CD4, CD8, and

## MATERIALS AND METHODS

NCRI for the T and NK cell fraction, CD14, ITGAX and HLA-DRA for myeloid cells, MS4A2 for mast cells and basophils, MS4A1 for B cells, and immunoglobulin-encoding genes for plasma cells). For the present study, all clusters annotated as “fibroblasts” in the original dataset were used for downstream analysis. All scRNA-seq analyses were done using R. We used the Seurat package (5.0.1) function `sctransform` to normalise and scale the data, using the variables “percent.mt” (mitochondrial genes), “percent.krt”, and “percent.MGP” for regression (KRT and MGP were detected across all cell types in some samples due to contamination originating from apoptotic tumour cells). After running PCA, the first 25 components were used for both graph-based clustering using the Seurat functions `Find Neighbours` and `Find Clusters` as well as dimension reduction analysis such as UMAP.

Bladder samples from Chen 2020: Cell Ranger (version 2.2.0) was used to process the raw data, demultiplex cellular barcodes, map reads to the transcriptome, and down-sample reads (as required to generate normalized aggregate data across samples). These processes produced a raw unique molecular identifier (UMI) count matrix, which was converted into a Seurat object by the R 4.2.2 package Seurat (version 5.0.1). Cells with UMI numbers <1000 or with over 10% mitochondrial-derived UMI counts were considered low-quality cells and were removed. In order to eliminate potential doublets, single cells with over 6000 genes detected were also filtered out. Finally, 52721 single cells remained, and they were applied in downstream analyses. After quality control, the UMI count matrix was log normalized. Since sample from eight patients were processed and sequenced in batches, patient number was used to remove potential batch effect. Then, for each tumour type, all samples were merged. We used `Select Integration Features` to find 2000 most variable genes to perform the integration and minimise batch effect and `Find Integration Anchors` to perform the integration of the samples. `Integrate Data` function was used to integrate data and create a new matrix, in which potential batch effect was regressed out. Integrated datasets

## MATERIALS AND METHODS

were again scaled, linear (PCA) and non-linear (UMAP) dimensional reductions calculated, and clusters discovered with Find Neighbours and Find Clusters at 0.5 resolution using the Louvain algorithm. Single R 2.2.0 was used in conjunction with celldex's Human Primary Cell Atlas Data to assign cell type to each individual cell. The fibroblasts populations were extracted from the merged datasets at this point filtering the cells assigned as "fibroblasts". These new datasets were again scaled, dimensionally reduced, and clustered as the previous ones.

Once all these processes were performed and individual cells were assigned to specific clusters/cell types, we could assign the expression of normalized gene counts to each cell. Individual cell gene signature expression of indicated gene signatures was calculated with Seurat's Add Module Score function. Either target gene or gene signature were projected on the UMAP graphs to obtain a visualization of gene expression per cluster. In addition, matrices of gene/gene signature expression per cell were further processed for additional analyses. Briefly, for correlation analyses, the Pearson coefficient between the expression of particular genes/gene signatures was calculated for each identified cell type. For analyses of expression in each cell cluster, the average expression per cell type was calculated and then scaled within a 1 to 0 range (1 high expression, 0 no expression). For genes, where the lowest value was always 0, average values were scaled by dividing by the highest average value. For gene signatures, where certain cell types might contain negative values, average values were scaled by subtracting the minimum average value and dividing by the total range (maximum average value minus minimum average value). For certain analyses, cell types were further stratified depending on the tissue of origin (mucosal or tumour in the BLCA dataset).

### 3.3.7 Statistical analysis

Statistical analyses were performed using GraphPad Prism (GraphPad Software, Inc.). When n permitted, values were tested for Gaussian distribution using the D'Agostino–Pearson normality test. For Gaussian distributions, paired or unpaired two-tailed Student's t-test and one-way ANOVA with Tukey post-test (for multiple comparisons) were performed. P-values of less than 0.05 were considered statistically significant. Unless stated otherwise, error bars represent Standard Deviation (SD). Where indicated, individual p-values are shown; alternatively, the following symbols were used to describe statistical significance: \*P < 0.05; \*\*P < 0.01; \*\*\*P < 0.001; \*\*\*\*P < 0.0001; n.s, non-significant. GraphPad Prism was also used to generate graphs and heatmaps.



**RESULTS**



**IDENTIFICATION OF *ASPA* AS A NEW TUMOUR  
STROMA GENE WITH PROGNOSTIC VALUE.**

---



## 4 RESULTS

### 4.1 IDENTIFICATION OF *ASPA* AS A NEW TUMOUR STROMA GENE WITH PROGNOSTIC VALUE.

#### 4.1.1 Gene expression analysis of public datasets for the identification of consistently dysregulated genes in the tumour stroma.

There is a growing need to decipher the molecular intricacies that shape the TME. This interest aims to improve our understanding of cancer disease and discover potential targets for novel therapeutic strategies. Over the recent years, numerous investigations employed clinical specimens to perform in-depth molecular characterization of the stromal compartment across various types of tumours, contrasting them with their normal tissue counterparts. These studies present an opportunity to explore relevant differences between tumour stroma and healthy stroma, aiming to identify consistent expression patterns that could play a significant role in the generation of pathological TMEs. In a previous study from the host lab, a consistent analysis of this type of datasets identified *DKK3* as a gene consistently upregulated in tumour stroma. Further analyses indicated that *DKK3* was potentiating the aggressive phenotype of CAFs through the activation of Wnt/ $\beta$ -Catenin and YAP/TAZ signalling, ultimately boosting cancer cell progression<sup>65</sup>.

Focused on the identification of new potential TME regulators, we employed a similar strategy leveraging on existing gene expression datasets for the identification of genes consistently dysregulated in tumour stroma across different tumour types. Next, candidate genes were shortlisted based on their clinical relevance assessing the association between their expression levels and prognosis, both in whole tumour and in stromal datasets (**Figure 1.1**).

## RESULTS

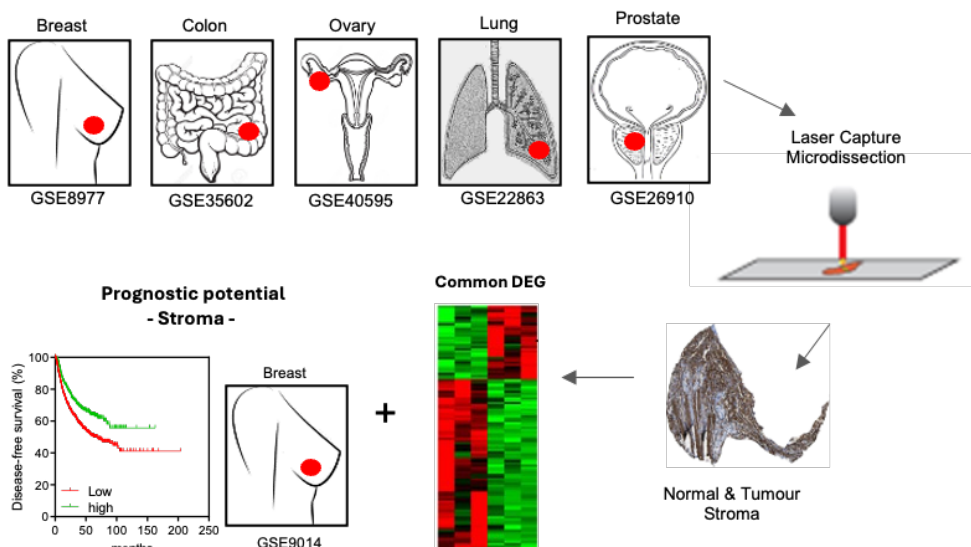


**Figure 1.1. Strategy followed to identify potential tumour stroma regulators.** Diagram showing the procedure behind the transcriptional analysis of normal and cancerous stroma from multiple tumour types. Stromal areas were isolated using laser capture microdissection and subjected to gene expression analysis. Gene Expression Omnibus reference numbers of datasets included in our analysis are provided for each study.

In line with this idea, we first performed a gene expression analysis on publicly available stroma datasets from normal and cancerous tissues. In general, these datasets were generated after the stromal and epithelial regions of a tissue (normal/cancer) were separated by laser capture microdissection and then processed through gene expression analyses. For this study, we used datasets of 5 different tumour types where the stroma has been reported to be critical in tumour progression: breast (GSE8977), colon (GSE35602), ovary (GSE40595), lung (GSE22863), and prostate (GSE26910) cancer. Then, gene expression analysis was performed to decipher the differentially expressed genes (DEGs) in the cancerous stroma (vs normal stroma) in the indicated datasets (**Figure 1.2.A**). Subsequently, overlapping analysis was conducted to identify consistently common up/downregulated DEGs across all datasets. A total of 13 common upregulated genes and 19 downregulated genes were identified (**Figure 1.2.B**).

## RESULTS

Finally, prognosis associations for the expression of each gene in bulk tumours were performed based on TCGA and PRECOG (<https://precog.stanford.edu/>). This analysis consists of an overall metric of prognostic value for individual genes taking into account its relevance in 36 different types of tumours. The analysis revealed several upregulated genes associated with bad prognosis, such as *KIF14*, *COL11A1* or *SOX11*, which have been linked to poor outcomes in cholangiocarcinoma, breast and gastric cancer, respectively<sup>192-194</sup> (**Figure 1.2.C**). Thus, this reinforces the validity of our approximations. On the other hand, the Hazard Ratio analysis also identified genes whose downregulation was associated with a shorter patient survival. For instance, *HLF* downregulation has been reported to show poorer prognosis in glioma patients<sup>195</sup>, and *ASPA* has been described to block prostate cancer progression<sup>167</sup> (**Figure 1.2.C**).

## RESULTS

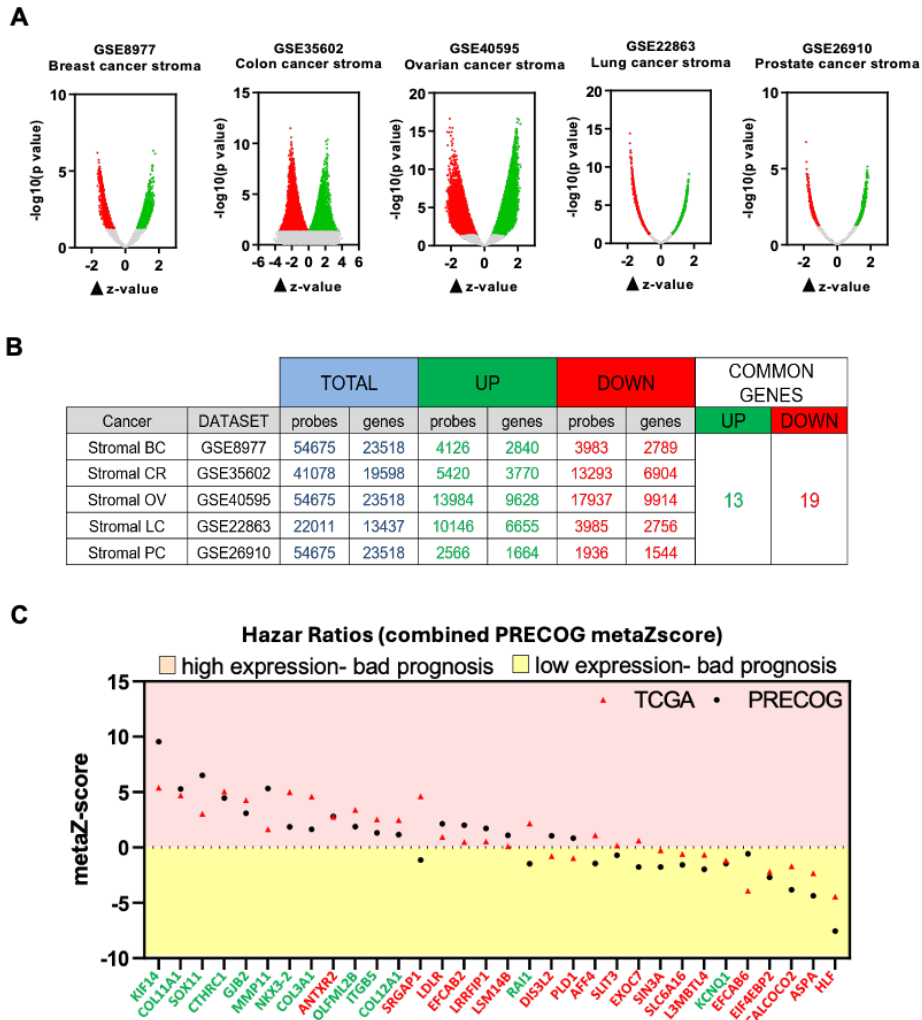


**Figure 1.2. Identification of consistently dysregulated genes in tumor stroma vs normal stroma (A)** Scatter plots showing the differentially expressed genes (UP, green; DOWN, red; non-significant, grey) in the cancerous stroma (vs normal stroma) in the indicated datasets. **(B)** Table summarising the overlapping analysis to identify consistently common up/downregulated genes in all datasets. **(C)** Analysis of global Hazard Ratios scores (multi-tumour) for indicated genes based on TCGA and PRECOG metaZscores. Genes consistently upregulated and downregulated in cancer stroma are shown in green and red font, respectively.

## RESULTS

To further investigate the relationship of these DEGs with prognosis value, a similar approach was employed based on their expression in breast cancer stroma<sup>188</sup>. Several genes were highlighted as a key prognosis factor in this context. For example, high expression of *SLC6A16* and *COL3A1* in breast cancer stroma were associated with poor prognosis, whereas patients with high expression of *ASPA* and *ITGB5* presented a longer survival (**Figure 1.3**). Intriguingly, *ITGB5* was found to be upregulated in cancer stroma in our previous analysis, but low levels of expression were associated with poorer survival. Reciprocal findings were observed for *SLC6A16*. Given these discrepancies, we decided to discard these genes, leaving two genes as potential candidates for further investigation: *COL3A1* and *ASPA*. Since the role of collagens in cancer stroma is relatively well-defined, we decided to focus in *ASPA* for further studies, given (i) its dysregulation in cancer stroma, (ii) its prognostic value in whole tumour and stromal datasets, and (iii) the limited knowledge of their role in cancer stroma and tumour progression.

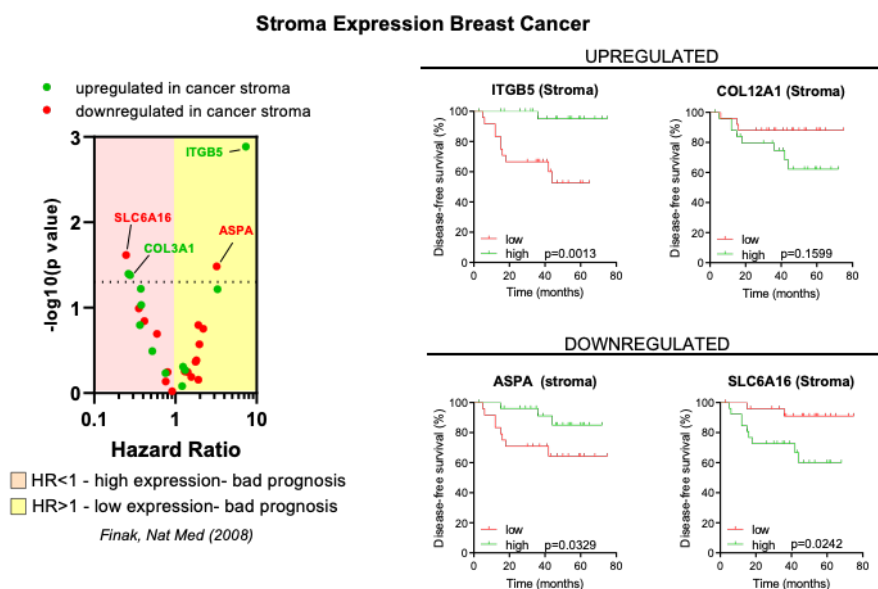


**Figure 1.3. ASPA downregulation in stroma has prognostic value in breast cancer patients.** Analysis of the prognostic value of the identified genes based on the expression in breast cancer stroma. Graph on the left shows the hazard ratio for each upregulated (green) or downregulated (red) gene against the p-value. Graphs on the right show the disease-free survival of breast cancer patients stratified on stromal gene expression of indicated genes. Statistical analysis was performed using Gehan-Breslow-Wilcoxon test.

## RESULTS

### 4.1.2 ASPA is consistently downregulated in cancer stroma, and it has prognostic value.

In order to decipher the implication of ASPA in cancer stroma, its expression was further analysed in normal stroma vs tumour stroma in the datasets coming from **Figure 1.2.A**. ASPA showed a reduced expression in tumour stroma across several types of cancers including breast, colon, ovary, lung, and prostate (**Figure 1.4.A**).

Next, we investigated the pattern of expression of the ASPA protein in tissue samples of colon and prostate cancer from the ProteinAtlas database<sup>196</sup>. This analysis informed that ASPA stains preferentially the stroma and not the epithelial compartment (**Figure 1.4.B**). In addition, ASPA expression was restricted to elongated cells that resembled fibroblasts.

Since ASPA is implicated in the catabolism of NAA<sup>163</sup> (**Figure 1.4.C**), the expression of NAA metabolism-related genes were checked in same datasets. For instance, *FOLH1*, *ACLY*, *PDHB* or *PDHX* were up regulated in tumour stroma. *FOLH1* has been described in NAA metabolism, reverting NAAG into NAA<sup>164</sup>, whereas *ACLY*, *PDHB* and *PDHX* are related to the acetyl-CoA synthesis. Specifically, *ACLY* generates cytosolic acetyl-CoA from citrate, and it has been related to ovarian cancer progression<sup>170</sup>. *PDHB/X* are implicated in the conversion of pyruvate to acetyl-CoA in the mitochondria, and its inhibition resulted in the impairment of esophageal squamous cell carcinoma proliferation<sup>197</sup> (**Figure 1.4.D&E**). However, none of these NAA-related genes (apart from ASPA) showed consistent and significant dysregulation in cancer stroma. Thus, *FOLH1* and *ACLY* appeared to be upregulated in cancer stroma in most tissues except for breast and lung, where no significant variation was observed.

## RESULTS

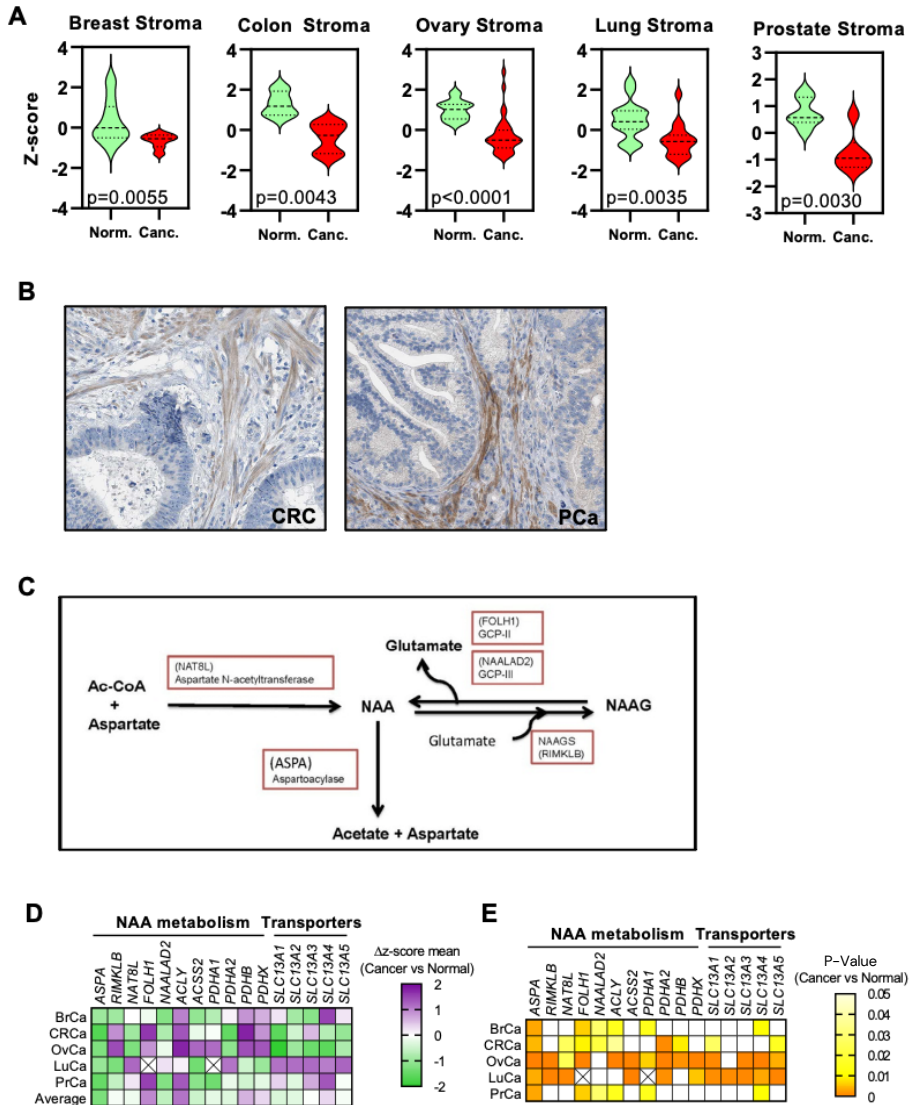


**Figure 1.4. ASPA stromal downregulation is a consistent feature in cancer. (A)** Violin plots showing ASPA expression (z-score) in normal and cancer stroma from breast, colon, ovarian, lung and prostate tissues. **(B)** ASPA staining in colorectal (CRC) and pancreatic (PCa) tissues. **(C)** Diagram showing the main molecular function described for ASPA. **(D)** Heatmap showing the average z-score of genes related to NAA metabolisms in normal and cancer stroma from breast, colon, ovarian, lung and prostate tissues. **(E)** Heatmap showing the difference in p-values for genes related to NAA metabolisms between cancer and normal stroma from breast, colon, ovarian, lung and prostate tissues.

## RESULTS

Based on our findings, which indicate that *ASPA* expression is lost in tumour stroma, we decided to assess the prognosis value of this event in several cancer types. Overall, low *ASPA* expression in bulk tumour datasets was correlated with a poorer disease-free survival in breast, colon, lung, and prostate cancers (**Figure 1.5**). Giving the relevance of *ASPA* expression in the stroma and its correlation with clinical outcomes, we decided to study this gene in more detail.

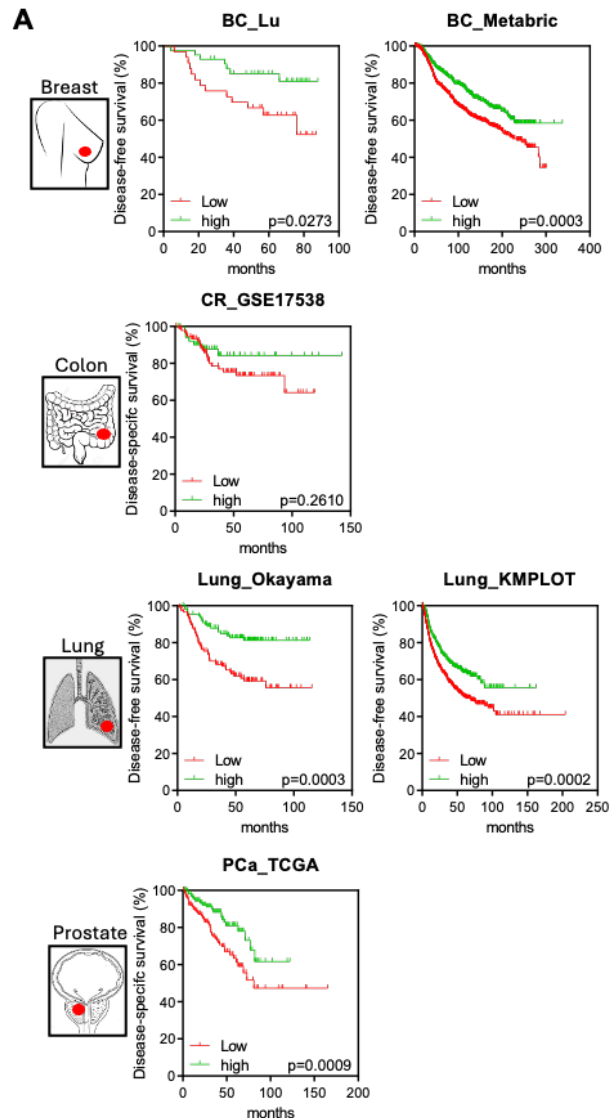


**Figure 1.5. *ASPA* expression in stroma shows prognostic value in bulk tumour clinical datasets.** Kaplan-Meier plots of disease-free survival patients stratified on levels of *ASPA* expression in stroma of breast, colon, lung, and prostate cancers. Statistical analysis was performed using Mantel-Cox test.

### 4.1.3 *ASPA* is mainly expressed by fibroblasts.

So far, our data indicated that *ASPA* is expressed in normal stroma and is drastically lost in tumour stroma from several cancer types. Nevertheless, *ASPA* expression has been fully described in CNS, specifically in oligodendrocytes. Thus, next we aimed to investigate which cellular component was expressing *ASPA* in the stroma. For that, the average expression of *ASPA* (nTPMs) in different cell clusters in normal human breast, colon, ovary, lung and prostate tissues was checked in scRNAseq data from ProteinAtlas. *ASPA* expression in breast, lung and prostate was mainly expressed by fibroblasts (in green) and other cell types such as smooth muscle cells (**Figure 1.6**). In ovary, *ASPA* was primarily expressed by undefined stromal cells whereas in colon expression values were very low for all cell clusters. In these two datasets, no fibroblasts were identified within the different cell clusters (not shown in **Figure 1.6**).

Next, to further corroborate that *ASPA* is mainly expressed by fibroblasts, scRNAseq data from breast<sup>190</sup> and bladder cancer<sup>198</sup> (**Figure 1.7.A&C**) was used to study *ASPA* and NAA-related genes expression in the different cell populations. Results indicated that *ASPA* is expressed by fibroblasts in both systems (**Figure 1.7.B&D**). Of note, in bladder cancer, neurons showed the highest *ASPA* expression, followed by the fibroblasts. This outcome was anticipated given the extensively documented role of *ASPA* in the brain<sup>164</sup>. To further analyse *ASPA* and NAA-related genes in stroma, an analysis with the stratified data based on their origin (normal stroma or tumour stroma) was performed in bladder cancer. *ASPA* was highly expressed by fibroblasts of the normal mucosae, when compared to the tumour mucosae (**Figure 1.7.E**), corroborating our findings in **Figure 1.4.A**. Overall, these data indicate that *ASPA* is preferentially expressed in fibroblasts in human tissues outside the CNS, and it is lost during CAF transformation. Finally, we checked *ASPA* expression in different cellular compartments in breast cancer derived

## RESULTS

from PyMT mice model (Figure 1.7.F). Similar to human specimens, *Aspa* was highly expressed in fibroblasts from normal mammary glands, and its expression was drastically reduced in fibroblasts associated to tumours (Figure 1.7.G).



**Figure 1.6. ASPA is expressed by fibroblasts outside the CNS.** Bar plots showing the average expression of ASPA (nTPMs) in different cell clusters associated with particular cell types in normal human breast, lung and prostate tissues. scRNAseq data extracted from ProteinAtlas.

RESULTS

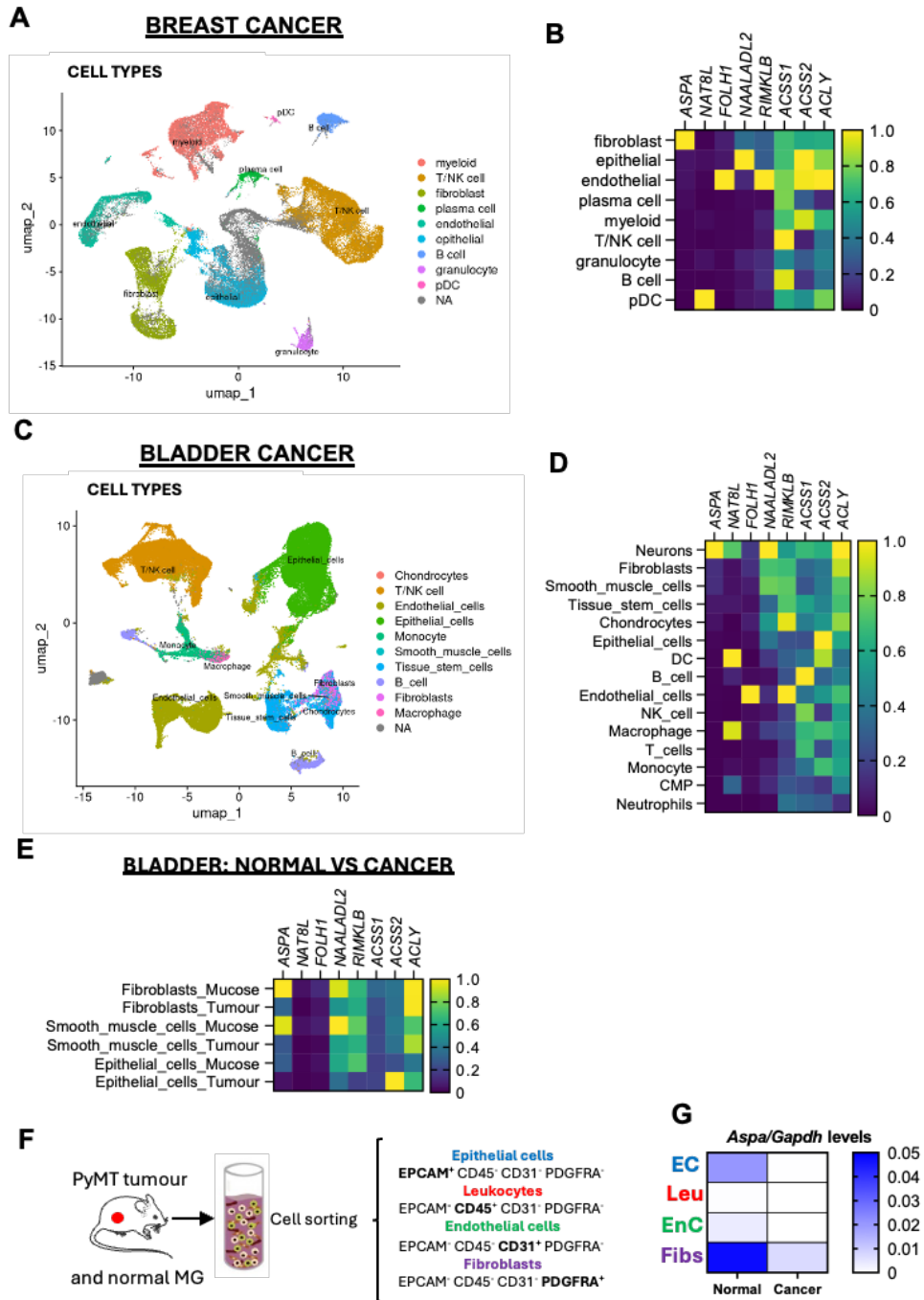


**Figure 1.7. ASPA is downregulated in CAFs.** (A) UMAP graph of scRNAseq data from human breast cancer tissues showing the cell clusters and cell type classification. Each dot represents a single cell; colours represent the assigned cell types. (B) Heatmap showing the scaled expression of NAA-related genes in the indicated cell types from (B). (C) UMAP graph of scRNAseq data from human bladder normal and cancer tissues showing the cell clusters and cell type classification. Each dot represents a single cell;

## RESULTS

colours represent the assigned cell types. **(D)** Heatmap showing the scaled expression of NAA-related genes in the indicated cell types from (D). **(E)** Heatmap showing the scaled expression of NAA associated genes in the indicated cell types from human bladder, stratified on their tissue of origin (normal mucosae or cancer). **(F)** Diagram showing the procedure for gene expression analysis of different cellular compartments in breast cancer derived from PyMT mice model. **(G)** Colour coded table showing the expression of *Aspa* in the different cellular compartments in tumour vs normal stroma.

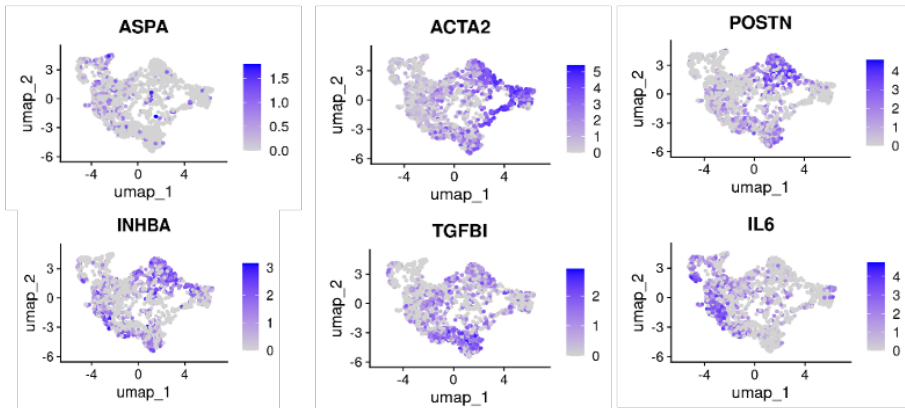
### 4.1.4 *ASPA* negatively correlates with myCAFs features.

Our prior data indicates that *ASPA* is mainly expressed by NFs and its expression is lost in CAFs. Thus, next we aimed to study if *ASPA* loss is correlated with any specific subtype of CAF. First, we leveraged on the scRNAseq analyses focusing on fibroblast clusters. Initial UMAP analysis of fibroblast clusters in the bladder cancer dataset suggested a negative correlation between *ASPA* expression and the expression of myCAF markers and TGF $\beta$ -target genes<sup>127</sup> (**Figure 1.8.A**). Thus, fibroblast clusters expressing *ASPA* presented very low levels of *ACTA2*, *POSTN* and *TGFBI* expression and vice versa. On the other hand, *ASPA* expression presented a minimal overlap with *IL6* expression, a marker of iCAF subtypes<sup>123</sup>. Further analysis on both bladder and breast scRNAseq datasets confirmed these observations. Stratification of fibroblasts into no *ASPA* expression (null), low *ASPA* expression (below the average of expressing fibroblasts) and high *ASPA* expression (above average) showed a strong negative correlation with myCAF markers (i.e. *LRRC15*, *POSTN*) and no relevant correlation with iCAF markers (i.e. *IL1A*, *CXCL12*, *IL6*) (**Figure 1.8.B**). Overall, these results suggested that *ASPA* loss may be a global characteristic of CAF/myCAF conversion.

## RESULTS

### A

#### BLADDER FIBROBLAST CLUSTERS



### B

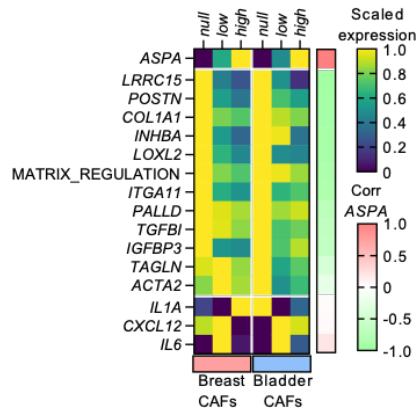


**Figure 1.8. ASPA expression negatively correlates with CAFs and myCAF features in fibroblasts from clinical samples. (A)** UMAP graphs of scRNAseq fibroblasts clusters from human bladder. Each dot in the graph represents a single cell; colour indicates the level of expression of indicated genes as indicated by the bar on the right. **(B)** Heatmap showing the scaled average expression and correlation to ASPA expression (bar on the right) of genes associated to CAF subtypes in breast and bladder CAFs extracted from scRNAseq datasets. CAFs from each dataset were stratified based on their ASPA expression (null, no expression; low, expression below the average; high, expression above the average).

Next, we decided to study this in detail investigating ASPA gene expression in isolated primary NFs and CAFs from human breast, colon, ovary, lung and prostate tissues. A significant loss of ASPA was observed in CAFs when compared to NFs in all tumour types, indicating that this characteristic was maintained *in vitro* (Figure 1.9.A). In these settings, ASPA expression was also negatively correlated with CAFs and myCAF markers (Figure 1.9.B).

## RESULTS

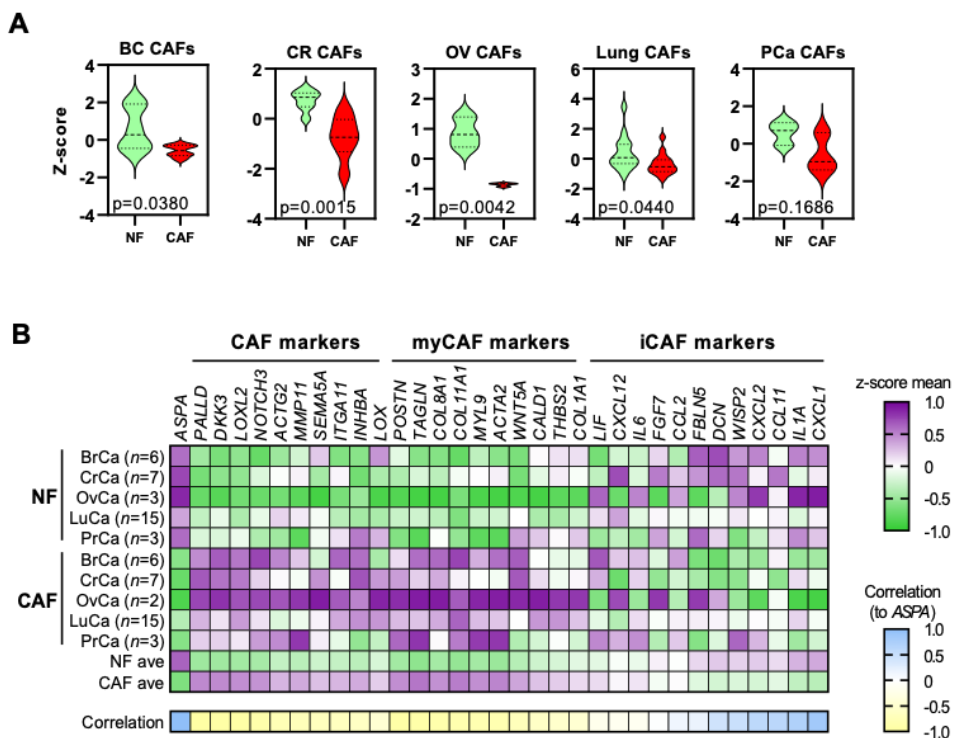


**Figure 1.9. ASPA expression negatively correlates with CAFs and myCAF features in isolated fibroblasts in vitro. (A)** Graphs showing the z-score expression for ASPA in NF and CAFs from human breast (BC), colon (CR), ovarian (OV), lung and prostate (PCa) tissues. **(B)** Heatmap showing average gene expression (z-score) of ASPA, and genes associated with general CAFs, myCAF features and iCAF features in NFs and CAFs of breast (BrCa), colorectal (CrCa), ovary (OvCa), lung (LuCa) and prostate (PrCa) human tissues. Gene expression is represented as the mean z-score. At the bottom, correlation coefficient between ASPA and each individual gene.

Subsequent analysis of ASPA expression by WB in isolated immortalized and primary human prostate CAFs cell lines confirmed the downregulation at both protein and gene levels compared to NFs (**Figure 1.10.A&B**). Of note, ASPA protein negatively correlated with  $\alpha$ SMA (ACTA2), a myCAF marker (**Figure 1.10.A**). We also investigated *Aspa* expression in immortalized murine NFs (NF1, 4) and CAFs (CAF1, 2, 5) cell lines generated from the PyMT breast cancer model. WB analysis confirmed the downregulation of *Aspa* in all CAFs, with qPCR and immunostaining providing additional confirmation and revealing a negative correlation between  $\alpha$ SMA and ASPA (**Figure 1.10.C-E**).

RESULTS

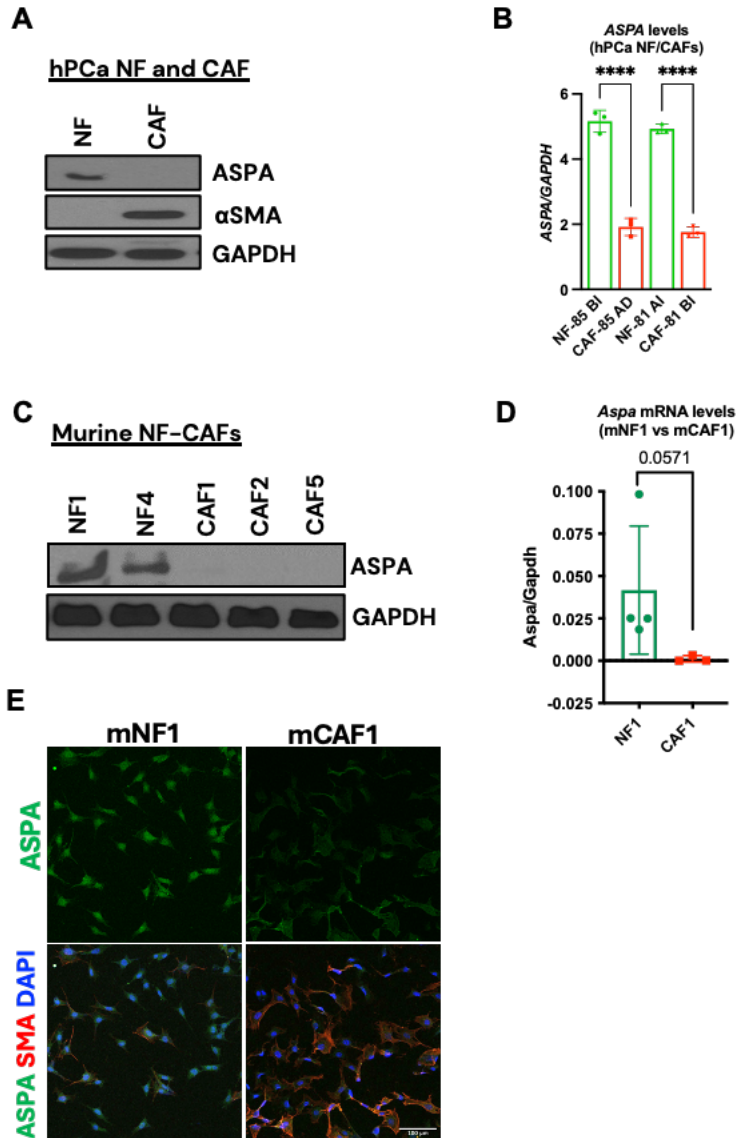


**Figure 1.10. ASPA expression is downregulated in human and murine CAF cell lines.** (A) Representative WB show the expression of ASPA,  $\alpha$ SMA and GAPDH in immortalized NFs and CAFs from prostate cancer (hPC). (B) Graph showing ASPA mRNA levels in two additional primary NF and CAFs from human prostate cancer (hPCa), relative to *GAPDH*. (C) Western blot show the expression of *Aspa* and *Gapdh* in our murine NFs and CAFs. (D) *Aspa* gene quantification in murine NF1 and CAF1 relative to *Gapdh* gene expression (n=3-4; each "n" is the average of triplicates). (E) Images show ASPA (green),  $\alpha$ SMA (red) and DAPI (blue) immunostaining in murine NF1 and CAF1. Statistical significance: \*P < 0.05; \*\*P < 0.01; \*\*\*P < 0.001; \*\*\*\*P < 0.0001.



**INVESTIGATING THE MECHANISM OF ASPA  
DOWNREGULATION IN CAFs.**

---



## 4.2 INVESTIGATING THE MECHANISM OF ASPA DOWNREGULATION IN CAFs.

### 4.2.1 TGF $\beta$ signalling as a potential repressor of ASPA in CAFs.

Given the fact that *ASPA* expression is lost in human and murine CAFs, we aimed to investigate the mechanism by which *ASPA* is repressed in these cells. As outlined in the introduction, several factors alter the behaviour of CAFs inducing different phenotypes that participate in tumour progression, such as TGF $\beta$ <sup>19,52</sup>, IL1 $\alpha$ / $\beta$ <sup>125</sup>, TNF $\alpha$ <sup>99</sup> or IFN $\gamma$ <sup>126</sup>, among others. Consequently, murine normal fibroblasts (mNF1) were exposed to those stimuli for 24 hours to assess the impact on *Aspa* expression.

Results indicated a significant repression of *Aspa* gene expression with TGF $\beta$  and IL1 $\alpha$  stimuli compared to the control (Vh) condition (**Figure 2.1.A**). TGF $\beta$  and IL1 $\alpha$  effects were also investigated by WB in mNF1 and mNF4. In both cell lines, only TGF $\beta$  exhibited a substantial impact on *Aspa* protein expression (**Figure 2.1.B**). To further corroborate this effect, human normal fibroblasts from prostate (NF hPCa), colorectal (NF hCRC), and breast (NF hBC) cancer were exposed to TGF $\beta$  stimulation. WB analysis demonstrated a downregulation of ASPA protein expression in all the systems, implying that TGF $\beta$  acts as the main negative regulator of *ASPA* gene expression (**Figure 2.1.C**). This result is in line with previous analyses where we observed a negative correlation between *ASPA* expression and the expression of myCAF markers, most of them TGF $\beta$ -responsive genes.

In light of these findings, inhibitors of TGF $\beta$  receptor I (SB431542), and P38 (SB202190) were tested to investigate whether disrupting TGF $\beta$  upstream signalling (receptor), or the non-canonical pathway (P38) could rescue *ASPA* expression during TGF $\beta$  stimulation. Results revealed that in TGF $\beta$ -stimulated mNF1, *ASPA* expression was restored with SB431542 but not with SB202190, suggesting that TGF $\beta$ -mediated *Aspa* silencing is driven by the canonical pathway. Conversely, the same approach in mCAF1 showed no recovery of

## RESULTS

ASPA expression in any condition, indicating that in this cell line, *Aspa* might be silenced by alternative mechanisms (Figure 2.1.D).

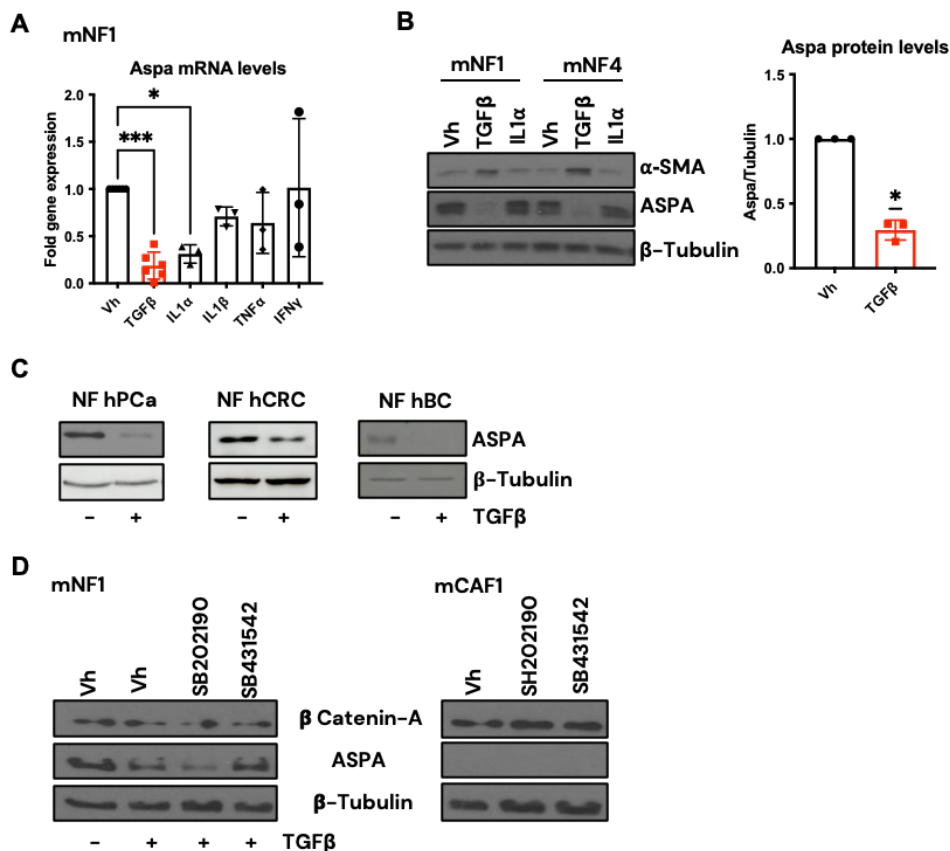


**Figure 2.1. TGFβ downregulates ASPA expression. (A)** *Aspa* mRNA levels in murine NF1 after exposure to TGFβ (5 ng/mL), IL1α (1 ng/mL), IL1β (3 ng/mL), TNFα (10 ng/mL) and IFNγ (100 ng/mL) for 24h (n=3-6; each "n" is the average of the triplicates). **(B)** Representative WB showing expression of ASPA, αSMA and β-Tubulin proteins in murine NF1 and NF4 after activation with TGFβ or IL1α as in (A). Graph shows normalized protein expression values for ASPA (n=3; each "n" is the average of the triplicates). **(C)** Representative WB showing expression of ASPA in NFs from human PCa, CRC and BC after stimulation with TGFβ (5 ng/mL) for 24 h. **(D)** Western blot showing non-phospho (active) β-Catenin (Ser33/37/Thr41) (β-Catenin-A), ASPA and β-tubulin expression in mNF1 and mCAF1 after TGFβ receptor I (SB431542) and p38 (SB202190) inhibition, at 5 μM and 10 μM respectively. Where indicated, TGFβ (5 ng/mL) was added 4 h after the inhibitors. Statistical significance: \*P < 0.05; \*\*P < 0.01; \*\*\*P < 0.001; \*\*\*\*P < 0.0001.

## RESULTS

### 4.2.2 TGF $\beta$ exert its effect through TAZ in mNFs.

In order to elucidate which factor downstream of TGF $\beta$  was responsible for repressing *ASPA* expression, several pathways interconnected with TGF $\beta$  were disrupted by transient RNAi-mediated gene silencing<sup>54,66,199-201</sup>. YAP/TAZ,  $\beta$ -catenin and SRF were silenced in mNF1 under TGF $\beta$  stimulation. WB showed that only the silencing of TAZ led to the recovery of *ASPA* expression (**Figure 2.2.A**). Of note, TAZ has been described to regulate the nuclear-cytoplasmic shuttling of Smad2/3-4 proteins<sup>53</sup>. Thus, to further confirm the link between TGF $\beta$  and TAZ factor, TAZ protein expression and activity was studied in TGF $\beta$ -stimulated mNF1, revealing an increase of both (**Figure 2.2.B&C**). Additionally, a constitutive active TAZ (TAZ<sup>mut</sup>) when expressed in unstimulated mNF1 exhibited decreased *ASPA* expression compared to mNF1 control, further indicating TAZ as the downstream effector of TGF $\beta$ -mediated repression of *ASPA* expression (**Figure 2.2.D**). Moreover, perturbation in TGF $\beta$ -related pathways were performed in mCAF1. However, no *ASPA* recovery was achieved in this cell line, emphasizing that *Aspa* expression might be regulated by other mechanisms in fully activated CAFs (**Figure 2.2.E**). Of note, TAZ silencing did not show *ASPA* recovery in human prostate CAFs, but inhibition of TGF $\beta$  receptor I (SB431542) blocked TGF $\beta$ -induced effect on *ASPA* protein expression (**Figure 2.2.F**). This result suggests that TGF $\beta$ -mediated repression of *ASPA* in hPC CAFs is mediated by other effectors rather than TAZ. Our results also suggested the presence of different regulatory regions at the *ASPA* locus between mouse and human cell lines; Thus, the murine genome may present TAZ-regulatory regions upstream the *Aspa* locus not present in humans.

## RESULTS

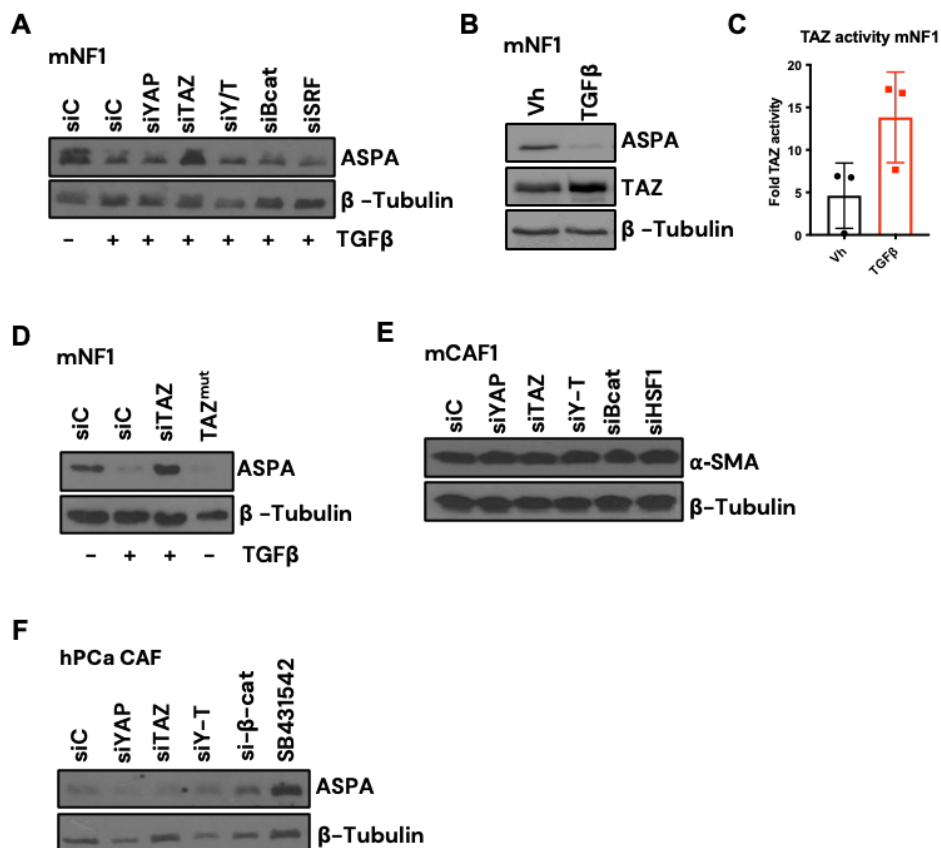


**Figure 2.2. TGFβ downregulates ASPA expression through TAZ signalling.** (A) Representative WB showing ASPA and β-Tubulin expression in mNF1 in response to TGFβ (5 ng/mL) for 24 h. As indicated, mNF1 were transfected with RNAi control (siC), or targeting YAP (siYAP), TAZ (siTAZ), YAP/TAZ (siY/T), β-catenin (siBcat) or SRF (siSRF). (B) Representative WB showing ASPA, TAZ and β-Tubulin protein expression in mNF1 after stimulation with TGFβ (5 ng/mL) for 24 h. (C) Graph showing fold TAZ activity measure with specific luciferase reporter in mNF1 after stimulation with TGFβ (n=3; each “n” is the average of the triplicates). (D) Representative WB showing ASPA and β-Tubulin levels in mNF1 after transfection with control (siC) or TAZ (siTAZ) RNAi. Alternatively, TAZ activity was enhanced by constitutive expression of a constitutive active mutant (TAZ<sup>MUT</sup>). Where indicated, cells were stimulated with 5 ng/mL of TGFβ for 24 h. (E-F) Representative WB showing ASPA, αSMA and β-tubulin in mCAF1 and hPca-CAF after modulation of specific signalling cascades associated with CAFs and TGFβ. In (E), no ASPA expression was detected. As indicated, cells were transfected with RNAi control (siC), or targeting YAP (siYAP), TAZ (siTAZ), YAP/TAZ (siY-T), β-catenin (siBcat) or HSF1 (siHSF1). hPca-CAFs were also incubated with 5 μM of SB431542.

## RESULTS

### 4.2.3 HDACs as potential common effectors of ASPA repression in fibroblasts.

To explore the potential common mechanism underlying *ASPA* repression across all cell lines, encompassing both murine and human CAFs, other gene repression processes were investigated, such as epigenetic changes in chromatin. A previously described association between TGF $\beta$  signalling and HDAC activity suggested that the TGF $\beta$  pathway requires HDACs to silence the expression of particular genes<sup>80,202</sup>. HDACs promote the removal of acetyl groups from histones, which favours chromatin compaction and consequently, gene repression. Importantly, this particular epigenetic reprogramming process can contribute to the acquisition of CAFs phenotype<sup>26,80</sup>. Taking this under consideration, HDAC inhibitors (TSA and PD106) were tested in our TGF $\beta$ -stimulated cell lines to examine the potential recovery of *ASPA* expression. TSA treatment induced upregulation of histone acetylation, as expected. Interestingly, in certain systems we could observe that TGF $\beta$  stimulation induced a reduction on Ach3 levels that was recovered by HDAC inhibitor treatment, and that was negatively correlated with the expression of myCAF marker SMA (**Figure 2.3.A**). Besides, in mNF1, TSA demonstrated a rescue of *ASPA* protein expression when compared to the TGF $\beta$ -stimulated control (**Figure 2.3.A&B**). This result was further confirmed with PD106, which also led to a recovery of *ASPA* expression at both protein and gene level (**Figure 2.3.C&D**). Both inhibitors exhibited same effect on *ASPA* expression in unstimulated mCAF1 and mCAF3 (**Figure 2.3.E&F**), and a similar trend was observed using TSA in hPCa CAFs (**Figure 2.3.G**). These findings suggested a critical role of acetylation in the regulation of *ASPA* repression and suggest a model whereby myCAF conversion promotes the loss of *ASPA* in fibroblasts.

## RESULTS

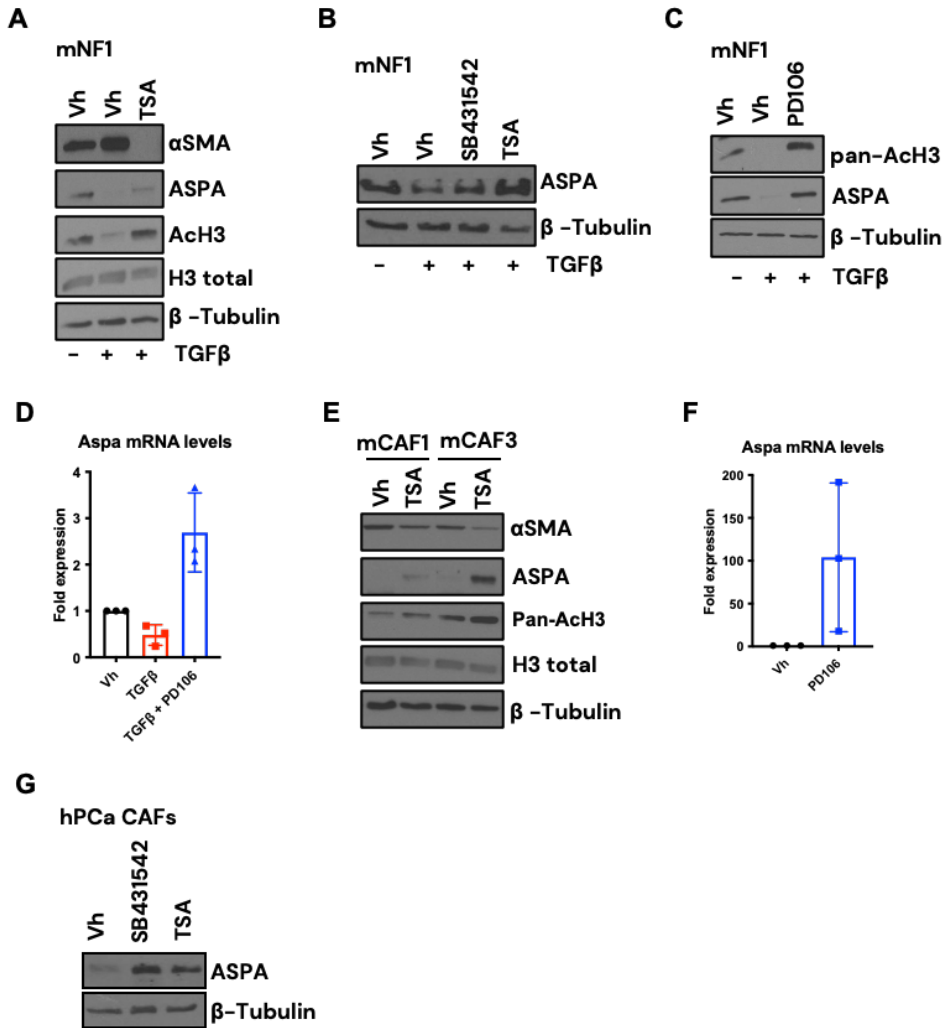


**Figure 2.3. TGFβ downregulates ASPA expression through HDAC activity. (A-B)** Representative WB showing ASPA, αSMA, acetylated-H3 (ac-H3), total H3 and β-Tubulin in mNF1 exposed to Vehicle (Vh), TGFβ (5 ng/mL), or TGFβ plus TSA (Pan inhibitor, 100 μM) for 24 h. **(C)** Representative WB showing pan-acetyl-H3 (pan-ach3), ASPA and β-tubulin levels in mNF1 control or exposed to TGFβ (5 ng/mL) plus PD106 (class I inhibitor, 25 μM) for 24 h. **(D)** Graph shows fold expression of *Aspa* mRNA in mNF1 exposed to Vehicle (Vh), TGFβ (5 ng/mL), or TGFβ plus PD106 (class I inhibitor, 25 μM) for 24 h (n=3; each “n” is the average of the triplicates). **(E)** Representative WB show ASPA, αSMA, pan-acetylated-H3 (Pan-ach3), total H3 and β-Tubulin in mCAF1 and mCAF3 exposed to Vehicle (Vh) or TSA (Pan inhibitor, 100 μM) for 24 h. **(F)** Graph shows fold expression of *Aspa* mRNA in mCAF1 exposed to Vehicle (Vh) or PD106 (class I inhibitor, 25 μM) (n=3; each “n” is the average of the triplicates). **(G)** Representative WB showing ASPA and β-Tubulin expression in hPCa CAFs after addition of SB431542 (5 μM) and TSA (100 μM) for 24h.

**TO INVESTIGATE ASPA FUNCTIONAL  
RELEVANCE IN FIBROBLASTS.**

---



## RESULTS

### 4.3 TO INVESTIGATE ASPA FUNCTIONAL RELEVANCE IN FIBROBLASTS.

#### 4.3.1 *Aspa* downregulation induces fibroblast activation and contractility.

Our previous results revealed a negative correlation between *Aspa* and myCAF markers, suggesting that *Aspa* loss in fibroblasts is a critical event in their differentiation into CAF/myCAFs (**Figure 1.8 and 1.9**). Consequently, we aimed to study the functional and phenotypic characteristics of myCAF subtypes *in vitro* after genetic modulation of *Aspa*. To do so, mNF1 were transfected with two individual doxycycline-inducible shRNA targeting *Aspa* (NF-sh3 and NF-sh4), and the negative control was transfected with an empty vector (NF-shC). Then, expression of gene markers ascribed to the three main CAF subtypes (myCAFs, iCAFs and apCAFs) was studied after *Aspa* silencing. Our analysis revealed a significant correlation between *Aspa* loss and the upregulation of myCAF markers (**Figure 3.1.A**). For instance, we observed a marked increase in the expression of *Postn*, *Acta2*, *Palld*, *Myl9* or *Col1a1*, in NF-sh3/4 when compared to NF-shC. Genes associated with increased TGF $\beta$  signalling in fibroblasts and myCAF subtypes were also upregulated, such as *Tgfb1*, *Lrcc15*, *Ctgf*. On the other hand, markers for iCAF subtypes did not present consistent changes: *Il6* and *Cxcl12* levels increased whereas *Ccl2* and *Lif* decreased after *Aspa* silencing. When apCAF markers were analysed, we observed that most of them were downregulated after *Aspa* depletion in mNFs (*Saa3*, *Ly6c1*, *H2-T3*) but the canonical apCAF marker *Cd74* was upregulated.

These findings were further supported by WB, where the silencing of *Aspa* led to increased  $\alpha$ Sma expression, supporting the importance of *Aspa* as a key regulator of myCAF conversion (**Figure 3.1.B**). Notably, no protein changes in  $\alpha$ Sma were observed upon addition of the *Aspa* substrate (i.e. NAA) in either cell line, indicating that NAA accumulation upon *Aspa* silencing does

## RESULTS

not influence myCAF phenotypes (**Figure 3.1.C**). Additionally, NAA accumulation was measured by HPLC system as a readout of *Aspa* perturbations in our cell lines. NAA presented an accumulation in NF1-sh3/4 compared to NF1-shC, which was further evidenced by the addition of external NAA in the culture media (**Figure 3.1.D**).

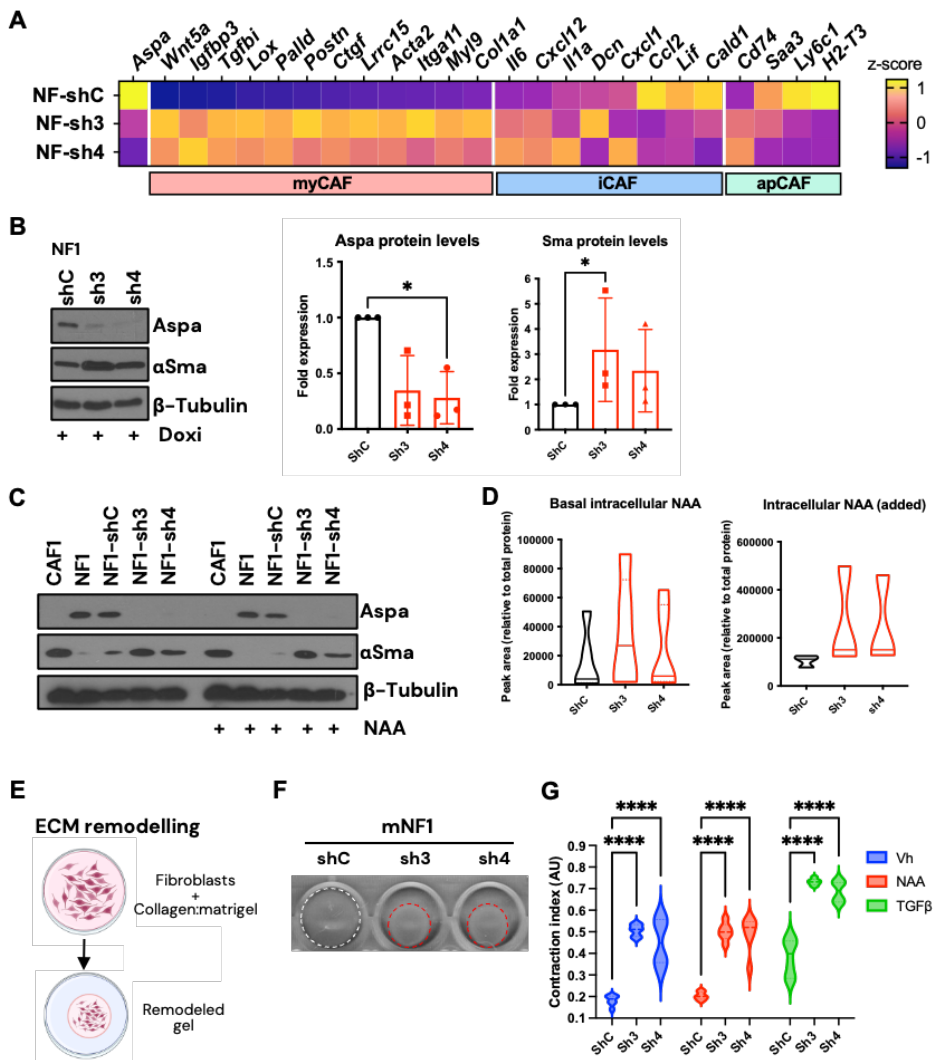


**Figure 3.1. *Aspa* downregulation induces myCAF features and functions. (A)** Heatmap of myCAF, iCAF and apCAF marker gene expression in mNF1 after *Aspa* silencing with two individual shRNA (Sh3 and Sh4). Control was transfected with and empty vector (ShC). Mean z-score values are represented. Data extracted from RNAseq experiments (triplicates). **(B)** Representative WB showing *Aspa*,  $\alpha$ Sma and  $\beta$ -tubulin expression in mNF1 after silencing of *Aspa* with two independent shRNA (sh3 and sh4) and with an shControl (shC). Graphs on right show quantification of fold

## RESULTS

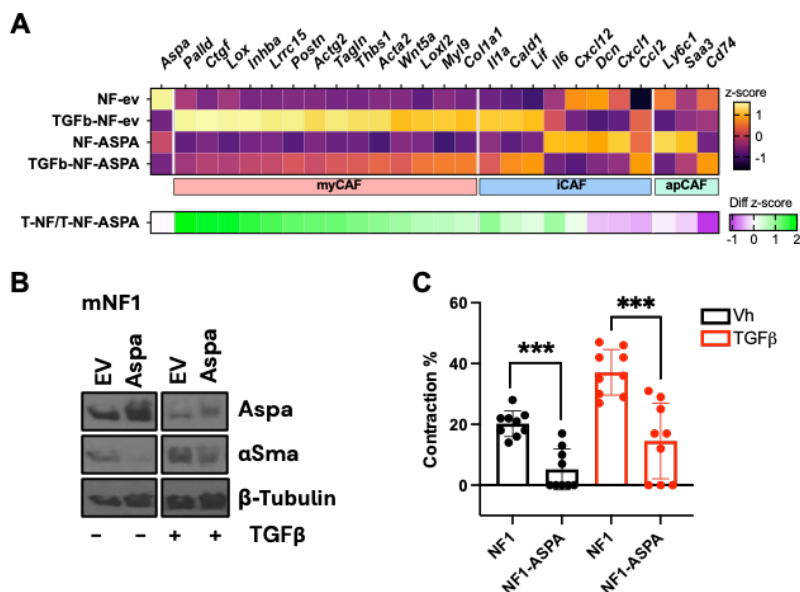
expression of *Aspa* and  $\alpha$ Sma levels (n=3). **(C)** Representative WB showing *Aspa*,  $\alpha$ Sma and  $\beta$ -tubulin expression in control mCAF1 and mNF1, and in mNF1 after silencing of *Aspa* (sh3 and sh4). Where indicated, cells were treated with NAA at 100 $\mu$ M for 24 h. **(D)** Graph showing peak area of basal intracellular NAA (left) and intracellular NAA after the addition of exogenous NAA in the media (at 100 $\mu$ M for 24h) (right) in NF1-shC and NF1-sh3/4. Peak area normalized to total protein, (n=3–5, each “n” is the average of triplicates). **(E)** Diagram showing the setup of the gel contraction assay to assess the ECM remodelling activity of fibroblasts. **(F)** Images show representative gel contraction assay of mNF1 after silencing *Aspa* with two independent shRNAs or with shControl (shC). **(G)** Graphs show quantification of gel remodelling capacity of mNF1-shC, mNF1-sh3 and mNF1-sh4 after incubation with vehicle (Vh), TGF $\beta$  (5ng/mL) and NAA (100 $\mu$ M) for 24 h (n=3; each “n” is the average of triplicates). In all cases, cell lines were induced with 5-day doxycycline treatment (2 $\mu$ M). Statistical significance: \*P < 0.05; \*\*P < 0.01; \*\*\*P < 0.001; \*\*\*\*P < 0.0001.

As mentioned in the introduction, myCAF subtypes are characterized by their enhanced cellular contractility and capacity to remodel the ECM. Consequently, we explored these features in mNF1 after *Aspa* perturbation using the ECM contraction assay (**Figure 3.1.E**). This assay revealed a significant increase in the contractile capacity of NFs upon *Aspa* silencing compared to NF-shC (**Figure 3.1.F**). Besides, exogenous NAA did not affect their contractile capacity (**Figure 3.1.G**), correlating with the results of  $\alpha$ Sma expression. TGF $\beta$  is a key inducer of myCAFs phenotype and their contractile capacity<sup>51,88</sup>. Notably, we observed that *Aspa* silencing potentiated the effect of TGF $\beta$  in this context (**Figure 3.1.G**).

Considering that the effect of TGF $\beta$  is enhanced after *Aspa* silencing, suggesting a potential negative effect in TGF $\beta$ -induced responses, and since *Aspa* is lost during TGF $\beta$  stimulation (previous chapter), we tested the effect of constitutive expression of *Aspa* in TGF $\beta$ -induced fibroblast activation. For that, a stable cell line of mNF1 overexpressing human *ASPA* under a constitutive promoter was generated (NF1-*ASPA*), and the negative control was transfected with an empty vector (NF1-EV). Then, gene marker expression of the three CAF subtypes (myCAFs, iCAFs and apCAFs) was studied in NF1-EV and NF1-*ASPA* in basal conditions and after TGF $\beta$  stimulation. Our analysis revealed a significant correlation between *Aspa* loss and the upregulation of

## RESULTS

most of myCAF markers when comparing EV vs TGF $\beta$ -EV, while no clear correlation was observed with iCAF and apCAF markers (**Figure 3.2.A**). Notably, the constitutive expression of *Aspa* attenuated the effect of TGF $\beta$  in NF1 transformation to myCAF phenotypes, as most of the myCAF genes presented reduced expression when comparing TGF $\beta$ -NF-ASPA vs TGF $\beta$ -EV. These results corroborate that *Aspa* may act as a negative regulator of TGF $\beta$  signals in fibroblasts. These findings were further confirmed by WB, where the constitutive expression of *Aspa* resulted in a decrease of  $\alpha$ Sma protein expression both in basal conditions and after TGF $\beta$  stimulation (**Figure 3.2.B**). In agreement, ECM remodelling analysis confirmed that ASPA overexpression in mNFs results in decreased contractile activities under basal conditions and after TGF $\beta$ -induced activation (**Figure 3.2.C**). These findings suggest that *Aspa* expression impairs TGF $\beta$ -induced activation of fibroblasts and modulates myCAF phenotypes and functions. Since the remodelling of the ECM is highly implicated in cell migration, invasion and metastasis, our results suggest that *Aspa* potentially impacts on these critical pro-tumour functions of CAFs. Notably, NAA does not appear to modulate NFs or NFs after *Aspa* depletion, suggesting a potential role of *Aspa* independent of its metabolic function.



## RESULTS

### Figure 3.2. *Aspa* overexpression impairs TGF $\beta$ -mediated activation of fibroblasts.

(A) Heatmap of myCAFs, iCAFs and apCAFs marker gene expression in control mNF1 (NF-EV) and mNF1 with *ASPA* overexpression (NF-*ASPA*). Where indicated, cells were stimulated with TGF $\beta$  (5ng/mL) for 24 h. Mean z-score values are represented. Data extracted from RNAseq experiments (triplicates). Purple to green heatmap at the bottom represents z-score differences between NF-EV stimulated with TGF $\beta$  (T-NF) and NF-*ASPA* stimulated with TGF $\beta$  (T-NF-*ASPA*). (B) Representative WB showing *Aspa*,  $\alpha$ Sma and  $\beta$ -tubulin expression in control mNF1 (NF-EV) and mNF1 with *Aspa* overexpression (NF-*ASPA*). Where indicated, cells were stimulated with TGF $\beta$  (5ng/mL) for 24 h. (C) Graph showing gel contraction activities at 24h of control mNF1 (NF-EV) and mNF1 with *ASPA* overexpression (NF-*ASPA*). Where indicated, cells were stimulated with TGF $\beta$  (5ng/mL) (n=9, from 3 biological replicates). In all cases, NF-EV and NF-*ASPA* were subjected to a 5-day doxycycline treatment (2 $\mu$ M). Statistical significance: \*P < 0.05; \*\*P < 0.01; \*\*\*P < 0.001; \*\*\*\*P < 0.0001.

### 4.3.2 *Aspa* downregulation in mNFs promotes cancer cell proliferation *in vitro*.

It has been reported that CAFs significantly contribute to cancer cell proliferation by secreting growth factors, cytokines, metabolites, or by modulating the ECM<sup>83,84,88</sup>. Consequently, our next objective was to study the functional impact of *Aspa* silencing in NF behaviour by assessing the fibroblast capacity to promote cancer cell growth in co-cultures systems. To investigate this, stable cell lines with *Aspa* silenced (mNF1-sh3 and -sh4) and the control (mNF1-shC) were co-cultured in DMEM at 5% of FBS with murine D2A1 breast cancer cells, which were labelled with GFP (Figure 3.3.A). The experiment was monitored daily, and the GFP-positive area was quantified to calculate D2A1 proliferation. Results revealed a significant increase in D2A1 proliferation when co-cultured with NF1-sh3 and NF1-sh4 at 48 h (Figure 3.3.B). Additionally, the same approach was employed using murine TS1 breast cancer cells, which exhibited a similar trend to the D2A1 proliferation.

## RESULTS

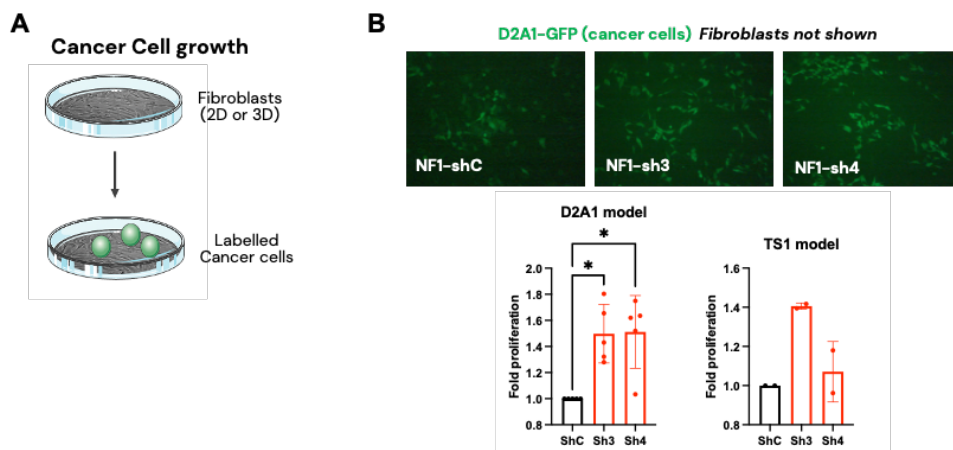


**Figure 3.3. *Aspa* downregulation in fibroblasts promotes cancer cell proliferation.** (A) Diagram showing methodology to assess fibroblast crosstalk to cancer cells in 2D/3D co-culture assays. (B) Representative images show D2A1 murine BC cancer cell (GFP, green) when co-cultured with the indicated mNF1 (not shown) in 2D assays. Graphs showing normalized cancer cell number after 2 days for assays employing D2A1 (left graph) ( $n=4$ ; each “ $n$ ” is the average of two wells, 5 pictures/well), or with alternative murine BC model TS1 (right graph) after 24 h for assays ( $n=2$ ; each “ $n$ ” is the average of two wells, 5 pictures/well). Both experiments were performed with DMEM at 5% of FBS. Statistical significance: \* $P < 0.05$ ; \*\* $P < 0.01$ ; \*\*\* $P < 0.001$ ; \*\*\*\* $P < 0.0001$ .

In addition to the previous results, further assays were performed to explore the potential mechanism whereby *Aspa* downregulation in fibroblasts promotes cancer cell proliferation. The same coculture experiment of **Figure 3.3.B** was performed with the D2A1 model but adding the substrate of *Aspa*, NAA (**Figure 3.4.A**). The experiment revealed a similar trend, where mNF1-sh3/4 increased cancer cell proliferation compared to mNF1-shC. Importantly, NAA addition did not appear to affect the fold growth induction promoted by *Aspa* deletion in NFs. Besides, cancer cell proliferation was studied in culture with the CM from fibroblasts at 0.2% of FBS in order to study cell proliferation in a restrictive environment. Results revealed a higher D2A1 proliferation when cultured with CM of mNF1-sh3/4 (**Figure 3.4.B**), suggesting that the effect on cancer cell proliferation might be due to secreted factors. Finally, we performed an additional experiment on 3D co-culture conditions, where both cancer cells and fibroblasts were cultured on the top of Matrigel (Matrigel On Top, MOT) in DMEM with 2.5% of FBS. This assay mimics a restrictive environment due to the stiffness of the Matrigel and the nutrient deprivation

## RESULTS

and showed a trend to increased D2A1 proliferation when cocultured with NF1-sh3/4 in basal conditions (Vh), that was further increased with the addition of NAA (**Figure 3.4.C**).

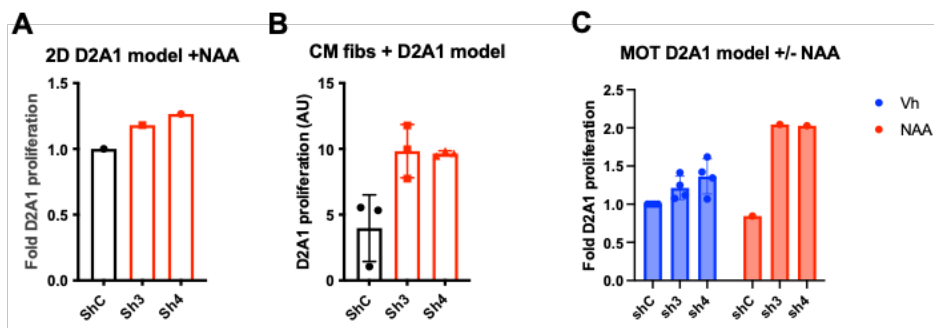


**Figure 3.4. *Aspa* downregulation in fibroblasts promotes cancer cell proliferation in restrictive conditions.** (A) Graph shows fold D2A1 proliferation after 48 h when cocultured with mNF1-shC and mNF1-sh3/4 in DMEM at 5% of FBS, with the addition of 100 $\mu$ M NAA (n=1; each “n” is the average of two wells, 5 pictures/well). (B) Graph shows D2A1 proliferation cultured in CM at 0.2% of FBS of mNF1-shC and mNF1-sh3/4 after 72 h of assay (n=3; each “n” is the average of 2 wells, 5 pictures/well). (C) Graph showing fold D2A1 proliferation in coculture with mNF1-shC and mNF1-sh3/4 in DMEM at 2.5% of FBS on MOT at 48 h. Where indicated, Vh or 100 $\mu$ M NAA was added (for Vh, n=4 each, “n” is the average of 2 wells, 5 pictures/well; for NAA n=1, each “n” is the average of 2 wells, 5 pictures/well).

Given these evidences suggesting that *Aspa* loss in NFs triggers the aggressive activation of the fibroblasts, which shows an enhanced promotion of cancer cell proliferation, we decided to study if these crosstalk towards cancer cells was driven by changes in key cytokines after *Aspa* modulation. To do so, a cytokine assay was performed with mNF1-shC and mNF1-sh4 cultured with complete DMEM at 0.2% of FBS (same conditions as the CM used in **Figure 3.4.B**). Results presented several cytokines that were upregulated upon *Aspa* silencing (**Figure 3.5**), such as Fractalkine (CX3CL1), which has been reported to stimulate breast and prostate cancer cell proliferation<sup>203,204</sup>; Insulin Growth Factor Binding Protein-6 (IGF-BP6), which has been described to be involved in the aberrant collagen deposition of fibroblasts through TGF $\beta$  signalling<sup>205</sup>; Keratinocyte Chemoattractant (KC), which has been linked to tumour inflammation and cancer cell proliferation<sup>206</sup>; Monocyte Chemotactic protein-1 (MCP1), which has been observed to

## RESULTS

promote tumour invasion and metastasis, angiogenesis, among others<sup>207</sup>; MIP-1 $\gamma$ , which has been reported to enhance tumour cell survival and metastasis upon TGF $\beta$  signalling<sup>208</sup>; Tissue inhibitor of matrix metalloproteinase-1 (TIMP-1), which has been proposed as a prognosis marker of colon cancer metastasis<sup>209</sup>, and its upregulation enhances CAFs recruitment into the TME<sup>210</sup>; Osteopontin (OPN), which has been linked to the activation of CAFs and cancer progression<sup>41</sup>; and finally, Pentraxin 3, which has been proposed as a prognosis marker in ovarian cancer<sup>211</sup>. Thus, these data indicate a change of the secretory phenotype in the mNFs after *Aspa* silencing, being more prone to enhance tumour progression.

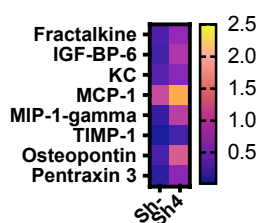


**Figure 3.5. Analysis of cytokines secreted after *Aspa* silencing in mNFs.** Heatmap showing signal intensity of cytokines secreted by NF1-shC and NF1-sh4. Signals were normalized to the positive controls of the kit (n=1; each "n" is the average of duplicates).

### 4.3.3 *Aspa* loss in NFs accelerates tumour emergence *in vivo*.

To further corroborate the impact of *Aspa* loss in NFs on tumour growth, both mNF1-shC and mNF-sh4 cells were co-injected with TS1 cancer cells subcutaneously in syngeneic FVB/n mice (**Figure 3.6.A**). This experiment revealed that *Aspa* silencing in NFs accelerated tumour growth in the early phases (**Figure 3.6.B&C**). On the other hand, differences on tumour growth were lost at later stages (**Figure 3.6.C**). In agreement, mice injected with TS1 + mNF1-sh4 had a reduced tumour latency (i.e. tumours required less time to become observable) (**Figure 3.6.D**). Therefore, these results suggest that the expression of *Aspa* in fibroblasts could attenuate cancer cell proliferation, whereas the silencing of *Aspa* in NFs accelerates TS1 proliferation, particularly during early stages of tumour progression. Of note, it is likely that mNF-shC

## RESULTS

eventually lost *Aspa* expression as a result of the interaction with cancer cells or a corrupting tumour stroma, leading to less evident differences in later stages of the disease. Further studies need to be done in order to overcome this experimental limitation.

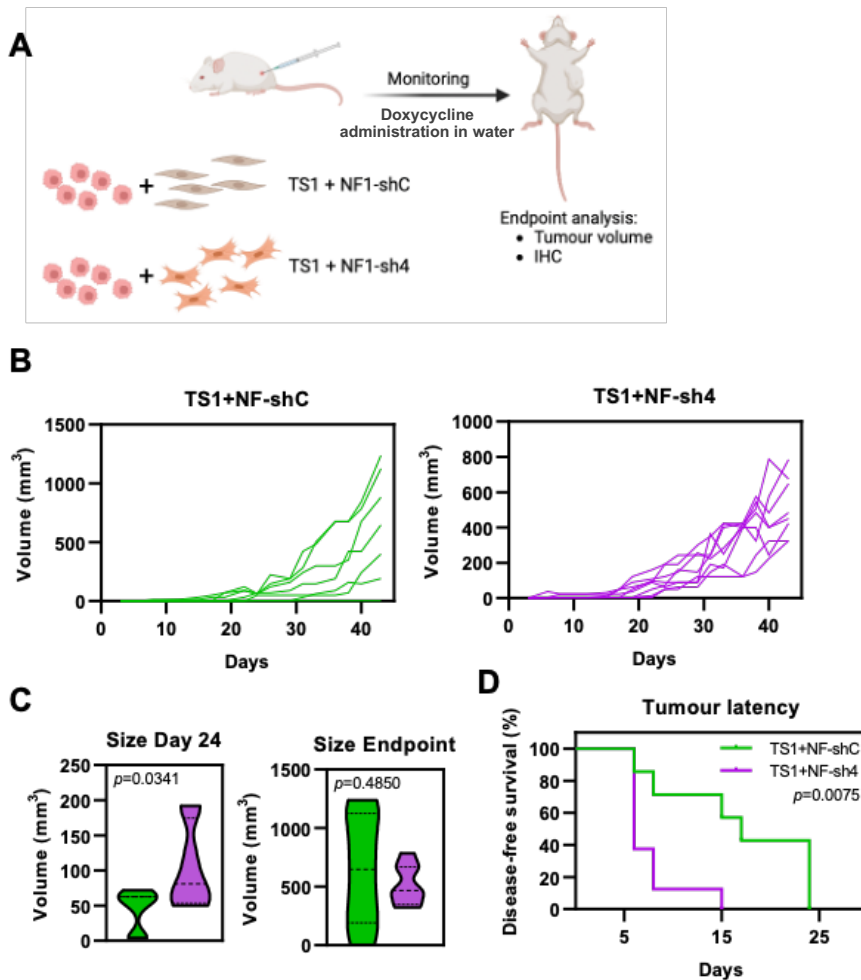


**Figure 3.6. *Aspa* downregulation in fibroblasts accelerated tumour progression *in vivo*.** (A) Schematic representation of the *in vivo* mice experiment. Done using BioRender. (B) Graphs showing tumour volume (mm<sup>3</sup>) for 43 days in mice co-injected with TS1+mNF1-shC (left) and TS1+mNF1-sh4 (right). N=7 (mNF-shC) and 8 (mNF-sh4). (C) Graph showing tumour volume (mm<sup>3</sup>) in mice co-injected with TS1+mNF1-shC (green) and TS1+mNF1-sh4 (purple) at day 24 and at endpoint (day 43). (D) Graph showing disease-free survival ratios of mice carrying tumours generated by TS1 cancer cells co-injected mNF1-shC (green) and mNF1-sh4 (purple). Statistical analysis was done using Long-Rank (Mantel-Cox) test.

#### 4.3.4 *Aspa* overexpression in mCAFs does not affect their myCAFs features.

Based on previous evidence indicating that *Aspa* modulates NF phenotypes, our objective was to extend functional assays to a fully CAF phenotype and investigate whether *Aspa* overexpression attenuates their aggressive behaviour. To achieve this, mCAF1 were transfected with an inducible plasmid to overexpress human *ASPA*. Two clones were chosen to perform the experiments: mCAF 1.2 and mCAF 1.3. CAF-EV was transfected with an empty vector and was used as a control. First, *ASPA* overexpression was confirmed by WB upon doxycycline addition. Of note,  $\alpha$ Sma protein levels were not changed despite of *ASPA* expression in CAFs (**Figure 3.7.A**). Subsequently, ECM remodelling assay was conducted, revealing no consistent differences between CAFs overexpressing *ASPA* (1.2 and 1.3) and the control (EV). Additionally, exogenous NAA did not affect their contractile capacity (**Figure 3.7.B**). Finally, co-cultures assays with D2A1-GFP cancer cells were performed in DMEM at 5% of FBS. This experiment showed no significant difference in cancer cell proliferation when co-cultured with the CAF control (EV) compared to the combined data of CAFs overexpressing *Aspa* (CAF-*ASPA*) (**Figure 3.7.C**). To further study the potential implication of *ASPA* expression in CAFs in relation to cancer cell proliferation, we explored this crosstalk in more restrictive conditions such as the MOT assay. MOT assays with the D2A1 model showed a decrease of cancer cell proliferation when cocultured with mCAF overexpressing *ASPA* compared to EV (**Figure 3.7.D**). Nevertheless, with TS1 model no significant difference in cancer cell proliferation was achieved when co-cultured with the CAF control (EV) compared to the combined data of CAFs overexpressing *ASPA* (CAF-*ASPA*) (**Figure 3.7.E**). Finally, the MOT with the CM of mCAF1-*ASPA* showed a trend to decreased D2A1 proliferation when compared to CM from mCAF1-EV (**Figure 3.7.F**).

## RESULTS

These results suggest that *ASPA* overexpression in a fully transformed CAF is not sufficient to induce any observable phenotypic shift, although some trend can be observed in more restrictive proliferative conditions.

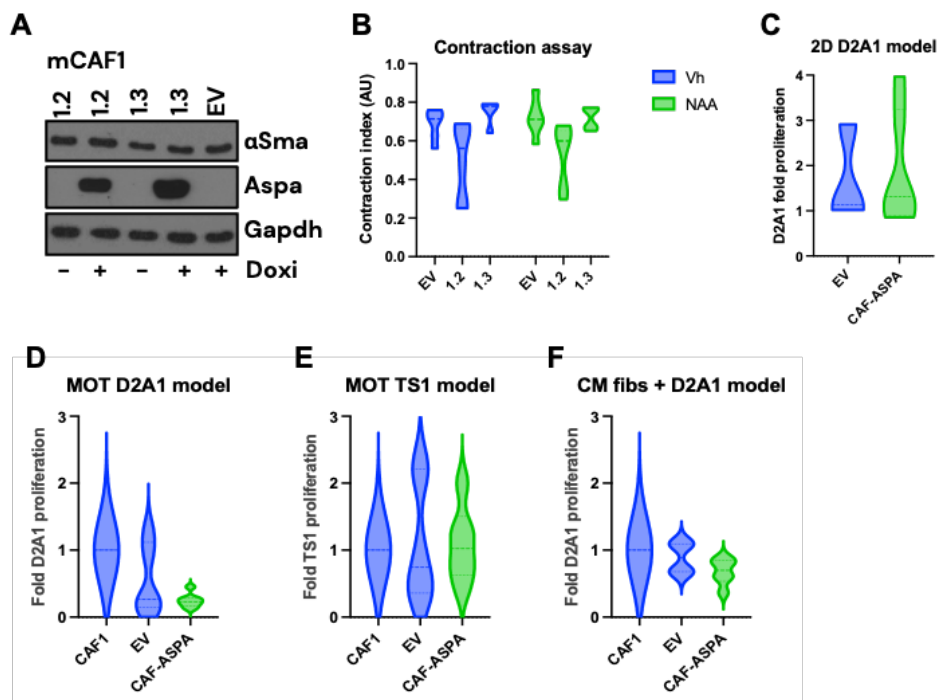


**Figure 3.7. ASPA overexpression in mCAF1 does not affect contractility or cancer cell proliferation.** (A) Representative WB showing  $\alpha$ Sma, Aspa, and Gapdh expression in stable cell lines of mCAF1 overexpressing ASPA upon Vh (Doxi -) or 2  $\mu$ M doxycycline addition (Doxi +) for 5 days (CAF 1.2 and CAF 1.3). CAF-EV was transfected with an empty vector and was used as a control. (B) Graph showing the quantification of ECM remodelling assay of mCAF1 overexpressing ASPA (1.2 and 1.3). CAF-EV was used as a control. Where indicated NAA was added at 100  $\mu$ M for 24 h (n=6, from 2 biological replicates). All cells received 2  $\mu$ M doxycycline induction for 5 days. (C) Graph showing the quantification of fold D2A1 cancer cell proliferation in coculture with mCAF1 EV or the combined data of mCAF1 overexpressing ASPA (1.2 and 1.3) in DMEM at 5% of FBS (n=3-6; from 2 biological replicates). (D) Graph showing D2A1 fold proliferation when cocultured with mCAF1, mCAF1 EV or the combined data of mCAF1 overexpressing ASPA (1.2 and 1.3) after 72 h of MOT assay in DMEM at 2.5% of FBS. Data normalized to mCAF1 (n=5-7, from 2 biological replicates). (E) Graph showing TS1 fold proliferation when cocultured with mCAF1, mCAF1 EV or the combined data of mCAF1 overexpressing ASPA (1.2 and 1.3) after 72 h of MOT assay in DMEM at 2.5% of FBS. Data normalized to mCAF1 (n=6, from 2 biological replicates). (F) Graph showing D2A1 proliferation when cultured in CM (DMEM at 2.5% of FBS) from mCAF1, mCAF1 EV or mCAF1 overexpressing ASPA (1.2 and 1.3) after 72 h of MOT assay. Data normalized to mCAF1 CM (n=4-6, from 2 biological replicates). In all graphs, CAF-EV and CAF-ASPA were previously induced using 2  $\mu$ M doxycycline for 5 days.

## RESULTS

### 4.3.5 *ASPA* overexpression in human PCa CAFs has profound effects in CAF behaviour.

Considering that murine CAFs showed no modulation by *ASPA* expression, and might be regulated by different mechanisms, we decided to move to the human PCa fibroblasts system. Consequently, we aimed to replicate the same approaches with our human prostate cancer NFs and CAFs. However, hNFs failed to silence *ASPA* using an inducible plasmid (not shown). Therefore, we focused on the hCAF<sub>s</sub> overexpressing *ASPA* (hCAF-*ASPA*) after doxycycline induction, as confirmed by WB (**Figure 3.8.A**). Remarkably, the overexpression of *ASPA* triggered the loss of  $\alpha$ SMA expression, when compared to hCAF<sub>s</sub> control. These findings were further supported by immunostaining, where *ASPA* overexpression reduced the number of  $\alpha$ SMA<sup>+</sup> CAFs (**Figure 3.8.B**). Additionally, NAA metabolite levels were studied by HPLC. Our data revealed a clear NAA accumulation in hCAF-C, while the overexpression of *ASPA* triggered the catabolism of this metabolite. The addition of exogenous NAA presented the same trend (**Figure 3.8.C**).

Subsequently, ECM remodelling assays were conducted in this system, revealing a reduction in the contractile capacity of hCAF<sub>s</sub> with *ASPA* overexpression (hCAF-*ASPA*), compared to control CAFs (hCAF-C) (**Figure 3.8.D**). Furthermore, the migratory capacity of these cells was investigated following *ASPA* overexpression. To do so, a scratch was performed on a monolayer of fibroblasts, mimicking a wound. Then, media was changed by CM from PC3 cancer cells to stimulate migration. Results demonstrated a decrease in hCAF<sub>s</sub> migration with *ASPA* overexpression (hCAF-*ASPA*) compared to hCAF-Control (**Figure 3.8.E**).

Additionally, the ability of CAFs to promote cancer cell growth was investigated. PC3-GFP cancer cells were co-cultured with hCAF-C and hCAF-*ASPA* in DMEM at 5% of FBS. The results revealed that *ASPA* overexpression in

## RESULTS

hCAFs attenuates their capacity to promote cancer cell growth compared to hCAF-C (**Figure 3.8.F**).

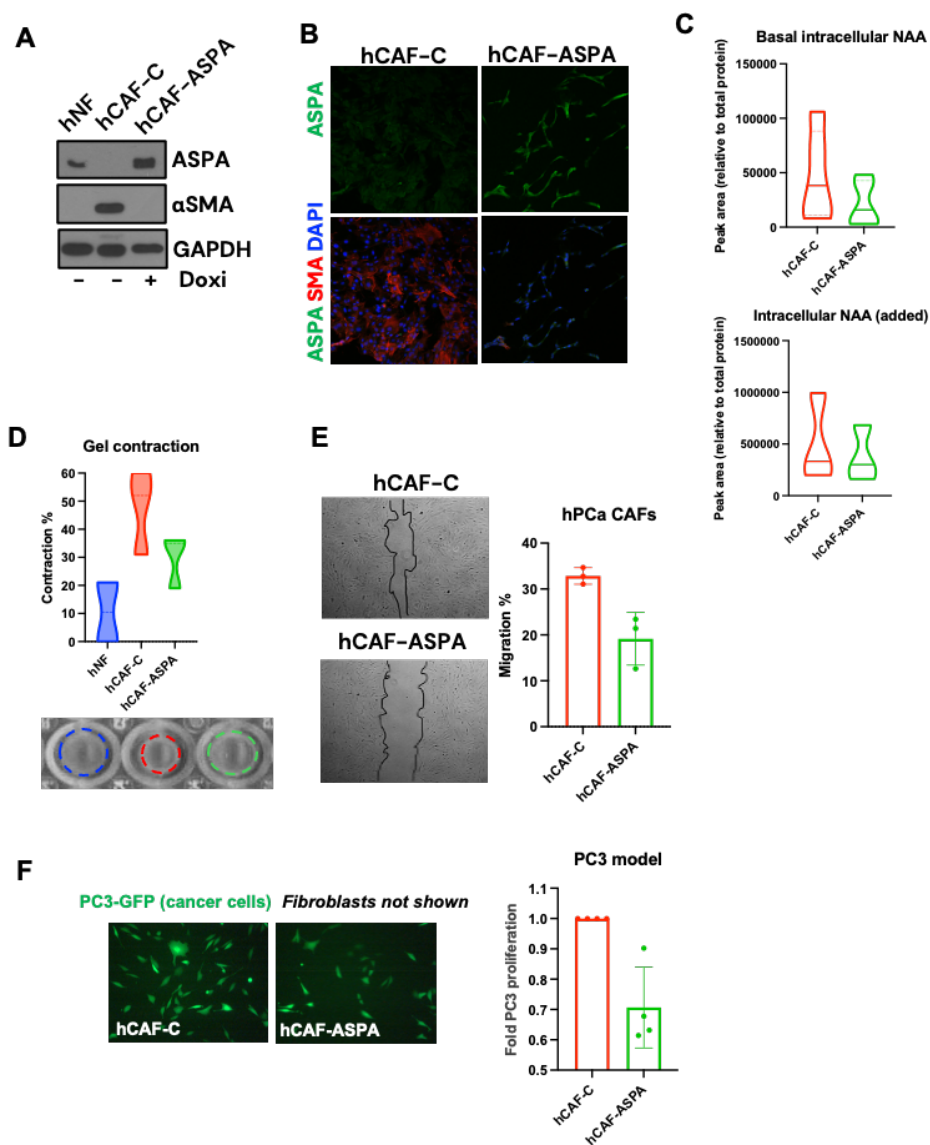


**Figure 3.8. ASPA overexpression in human PCa CAFs impairs myCAF features.** (A) Representative WB showing ASPA,  $\alpha$ SMA and GAPDH expression in NF and CAFs from human PCa. Where indicated, ASPA was overexpressed in CAFs using doxycycline-inducible systems for 5 days ( $2 \mu\text{M}$ ). (B) Representative images showing ASPA (green),  $\alpha$ SMA (red) and DAPI (blue) immunostaining in hCAF-control (hCAF-C) or hCAF overexpressing ASPA (hCAF-ASPA). (C) Graph showing normalised peak area of basal intracellular NAA (top graph) and intracellular NAA after the addition of exogenous NAA in the media (at  $100 \mu\text{M}$  for 24 h) (bottom graph) in hCAF-C and hCAF-ASPA. Peak area normalized to total protein, ( $n=3-5$ , each “n” is the average of triplicates). (D) Representative images (bottom) and graph (top) showing gel remodelling capacity of

## RESULTS

prostate hNF, hCAF control and hCAF-ASPA (n=3; each "n" is the average of triplicates). **(E)** Representative images showing endpoint wound-healing assays for prostate hCAF control (hCAF-C) or hCAF-ASPA (hCAF-ASPA) stimulated with PC3 conditioned media at 8 h. Graph on the right shows quantification of cell migration (n=3). **(F)** Representative images show PC3 cancer cells (GFP, green) when co-cultured with hCAF-C and hCAF-ASPA (not shown) in 2D assays with DMEM at 5% of FBS. Graph shows normalized cancer cell number after 48h (n=4; each "n" is the average of 2 wells, 5 pictures/well).

Further studies were performed to unravel *ASPA* implication in the crosstalk to cancer cells in the human PCa system. First, the coculture PC3 cancer cells with the addition of NAA showed similar results (**Figure 3.9.A**) as the basal coculture (**Figure 3.8.F**). Besides, cocultures with other human PCa cells, 22RV1 and DU145, were performed. In the case of 22RV1, cocultures presented a trend to decrease cancer cell proliferation with hCAF-ASPA, compared to hCAF-C in both conditions, Vh and NAA (**Figure 3.9.B**). On the other hand, DU145 did not show any difference in basal conditions (Vh), while the addition of NAA presented an increase of cancer cell proliferation in hCAF-ASPA (**Figure 3.9.C**). Of note, this last experiment was performed once, thus we consider it still preliminary data.

To further study the capacity of CAFs to boost cancer cell proliferation after *ASPA* modulation, cocultures in nutrient restrictive conditions were performed. In order to do that, PC3-GFP cancer cells were cocultured with hCAF-C and hCAF-ASPA in low glucose media at 2 or 5% of FBS, and experiments were monitored daily until day 5. In both assays, a higher cancer cell proliferation was observed when PC3 were cocultured with hCAF-C, (PC3+hCAF), while coculture of PC3 with hCAF-ASPA (PC3+hCAF-ASPA) and PC3 cultured alone showed reduced proliferation (**Figure 3.9.D-E**). Finally, MOT assays with DMEM at 2.5% of FBS was performed with PC3 and DU145 cancer cells. PC3 showed a slight trend to decreased proliferation in coculture with hCAF-ASPA, which was more evident by the addition of NAA (**Figure 3.9.F**). On the other hand, DU145 showed reduced proliferation when

## RESULTS

cocultured with hCAF-ASPAs compared to hCAF-C in both conditions, Vh and NAA (Figure 3.9.G).

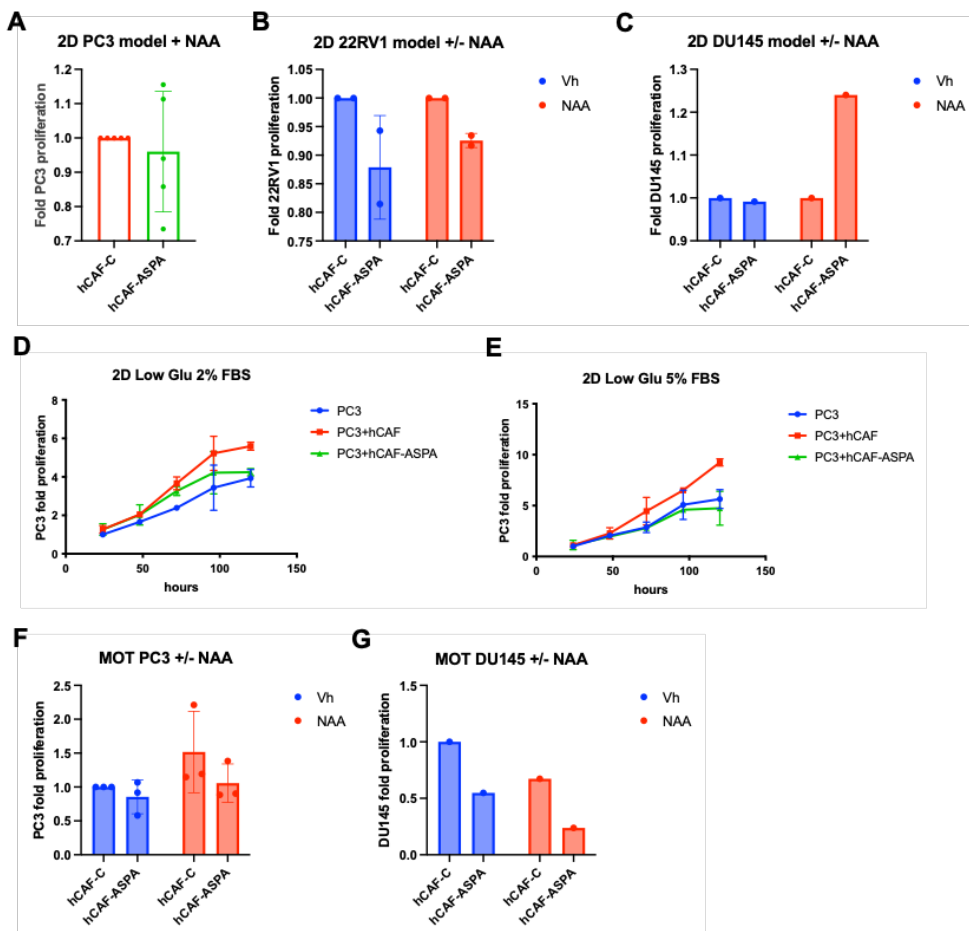


**Figure 3.9. ASPA overexpression in human PCa CAFs attenuates their capacity to promote cancer cell growth. (A)** Graph shows fold PC3 proliferation after 48 h of assay, in coculture with hCAF-C and hCAF-ASPAs with DMEM at 5% of FBS, with the addition of 100 $\mu$ M NAA (n=5; each "n" is the average of 2 wells, 5 pictures/well). **(B)** Graph showing fold 22RV1 proliferation in coculture with hCAF-C and hCAF-ASPAs, with DMEM at 5% of FBS, with Vh or 100 $\mu$ M NAA at 48 h of assay (n=2 each each "n" is the average of 2 wells, 5 pictures/well). **(C)** Graph showing fold DU145 fold proliferation in coculture with hCAF-C and hCAF-ASPAs, with DMEM at 5% of FBS, with Vh or 100 $\mu$ M NAA, at 48 h of assay (n=1; each "n" is the average of 2 wells, 5 pictures/well). **(D-E)** Graphs showing PC3 fold proliferation cultured alone, or with hCAF-C and hCAF-ASPAs, in low glucose DMEM at 2% and 5% of FBS for 5 days (n=2; each "n" is the average of 2 wells, 5 pictures/well). **(F)** Graph showing PC3 fold proliferation in coculture with hCAF-C and hCAF-ASPAs on MOT assays after 48 h, with Vh or 100 $\mu$ M NAA (n=3; each "n" is the average of 2 wells, 5 pictures/well). **(G)** Graph showing DU145 fold proliferation in coculture with hCAF-C and hCAF-ASPAs on MOT assays after 48 h, with Vh or 100 $\mu$ M NAA (n=1; each "n" is the average of 2 wells, 5 pictures/well).

## RESULTS

### 4.3.6 ASPA overexpression attenuates hCAF capacity to promote tumour growth and metastasis *in vivo*.

Our previous results indicated that ASPA overexpression in a human PCa CAFs attenuates their contractile capacity, cell migration, and interaction with cancer cells. Consequently, we aimed to investigate the biological impact of these alterations *in vivo*. Thus, the chicken embryo model was used to inject PC3-GFP cancer cells along with either hCAF-Control or hCAF-ASPA (**Figure 3.10.A**). Tumour growth was assessed at endpoint (day 5 post-inoculation) by measuring tumour weight, while metastasis was evaluated through PCR analysis using human-specific primers. Our data indicated that tumours formed by PC3 co-inoculated with hCAF-ASPA were significantly smaller when compared to those formed by PC3 co-inoculated with hCAF-C (**Figure 3.10.B**). Besides, brain metastases were only detected in embryos co-inoculated with PC3 and hCAF-Control (**Figure 3.10.C**). Consequently, these results suggest that ASPA expression in hCAFs *in vivo* attenuates the capacity of CAFs to promote tumour growth and metastasis.

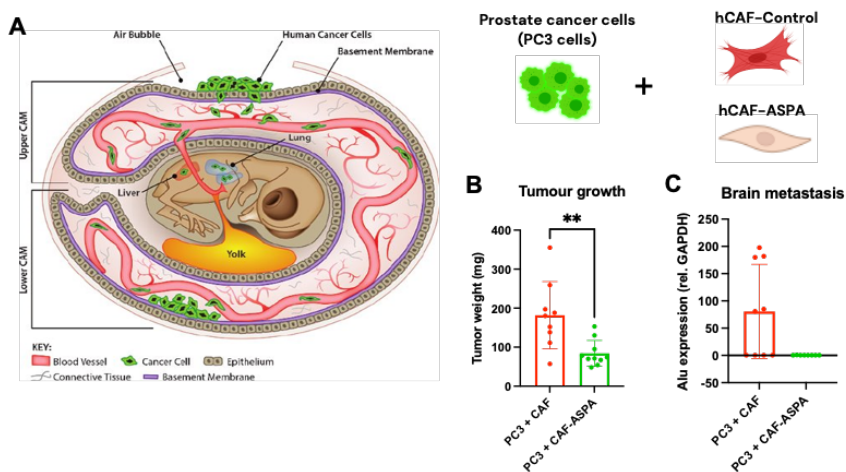


**Figure 3.10. Modulating ASPA expression in human PCa CAFs deters tumour growth and metastasis *in vivo*.** (A) Diagram showing methodology to assess tumour promoting functions in hCAF using the chicken embryo model. Human CAFs (control or overexpressing ASPA) were co-inoculated with PC3, and tumour growth was assessed after 5 days. (B) Graph shows endpoint tumour weight of PC3 tumours engrafted in the embryo with human PCa CAFs control (CAF) or CAFs overexpressing ASPA (CAF-ASPA) (n=9-10). (C) Brain metastasis score (*ALU* expression relative to *Gapdh*) of experiments from (B) (n= 9). Statistical significance: \*P < 0.05; \*\*P < 0.01; \*\*\*P < 0.001; \*\*\*\*P < 0.0001.

**TO INVESTIGATE THE MOLECULAR PROCESSES  
UNDERLYING ASPA FUNCTIONS IN  
FIBROBLASTS AND ITS IMPLICATION IN  
CANCER.**

---



#### 4.4 TO INVESTIGATE THE MOLECULAR PROCESSES UNDERLYING *Aspa* FUNCTIONS IN FIBROBLASTS AND ITS IMPLICATION IN CANCER.

The *in vitro* functional experiments of mNF1 with stable silencing of *Aspa* demonstrated a role of this protein in shaping the pro-tumoral phenotype of these cells. Nevertheless, the functional analysis did not unravel the molecular mechanisms underlying *Aspa* mechanism of action. Thus, to further decipher how *Aspa* operates in fibroblasts, in-depth molecular characterization was performed in mNF1 after modulation of *Aspa* expression.

##### 4.4.1 *Aspa* silencing induces a specific gene expression program in NFs.

RNAseq analysis of mNFs after stable silencing of *Aspa* with two independent shRNAs was performed to study consistent changes in gene expression modulated by *Aspa*. Principal component analysis (PCA) of transcriptomics data showed that NF1 with *Aspa* silenced (“sh\_*Aspa*\_3/4”) clustered more closely in comparison with the NF1 control (“sh\_control”), which clustered separated from these other groups (**Figure 4.1.A**). Additionally, analysis revealed differentially expressed genes (DEGs) when comparing both Sh3 and Sh4 to ShC. For instance, *Tgfb1* was commonly upregulated when *Aspa* was silenced. This gene has been linked to ovarian cancer progression<sup>212</sup> (**Figure 4.1.B**). Besides, a representation of the DEGs in the heatmap clearly showed that the silencing of *Aspa* induces a drastic change in the transcriptomic program of NFs (**Figure 4.1.C**).

## RESULTS

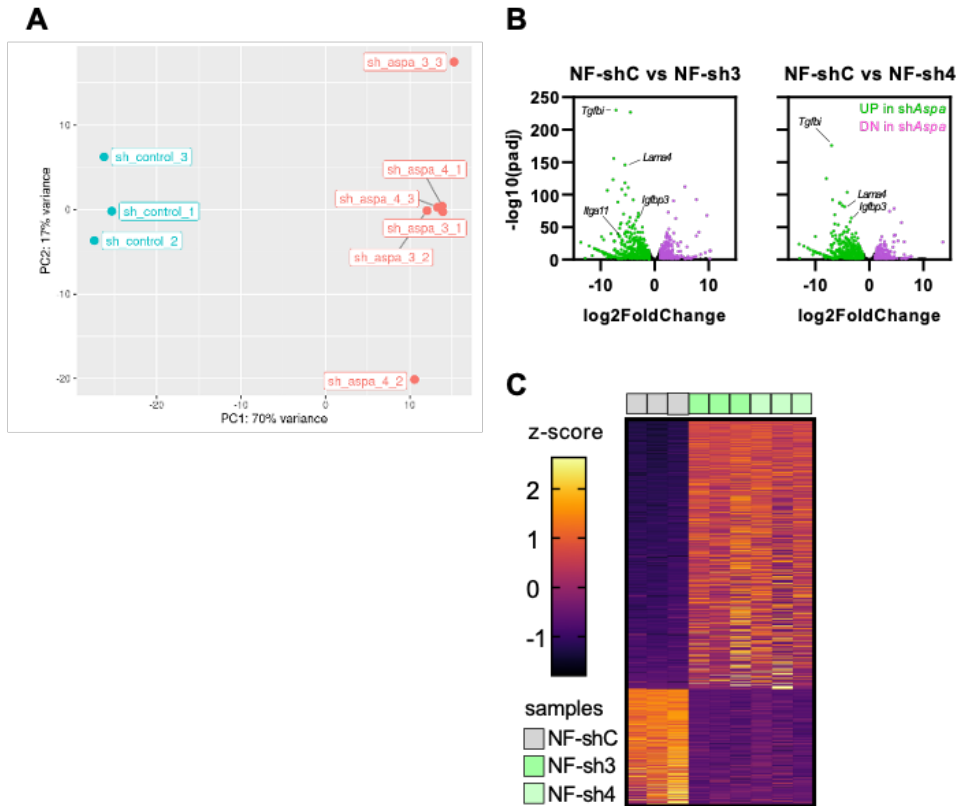


**Figure 4.1. *Aspa* silencing induces a specific gene expression program in normal fibroblasts.** (A) Graph showing the PCA of NF1 control (ShC) and NF1 shAspa (sh3 and Sh4) (n=3). (B) Graph showing the differentially expressed genes (DEGs) in murine NF1 after silencing *Aspa* expression with two independent shRNAs. Some relevant genes are indicated. (C) Heat map showing the z-score values of consistently up and downregulated genes with  $\text{Padj} < 0.05$  after silencing *Aspa*.

### 4.4.2 Gene ontology analysis of differential gene expression profiles induced by *Aspa* silencing in NF.

To gain insights into the biological and molecular processes altered by *Aspa* loss in NFs, we proceeded to perform a gene ontology (GO) enrichment analysis of common and specific DEGs, both up- and downregulated in NF1-sh3 and NF1-sh4.

## RESULTS

First, a global enrichment analysis was performed using the Comparative Toxicogenomic Database (CTD) gene set, which provides information about interactions between chemicals, genes and diseases. This database includes the Kyoto Encyclopaedia of Genes and Genomes (KEGG) dataset, which is a collection of biological information compiled from published material, and the REACTOME database (REACT), which is an open access pathway database. The enrichment analysis of the common upregulated DEGs found in both NF1-sh3 and NF1-sh4 compared to the NF1-shC showed several enrichments of biological processes normally present in activated fibroblasts, such as ECM organization, collagen biosynthesis and formation, and Wnt signalling, among others (**Figure 4.2**). These results suggest that perturbing *Aspa* potentially alters the expression of genes associated with pro-tumoral functions of CAFs.

Besides, the same approach was employed using a list of curated gene sets which include a collection of genes that have been manually selected and organized based on specific criteria, such as involvement in a biological pathway, association with a disease, or participation in a particular cellular process. In our case, "Curated genesets" included relevant molecular and biological processes related to the CAF phenotype. This analysis revealed that the most significant enriched signatures in upregulated DEGs were those related to HSF1 signalling and CAFs signatures, among other signalling pathways related to the aggressive behaviour of CAFs (i.e. TGF $\beta$ , integrins, FAK) (**Figure 4.2**). This result suggested that the silencing of *Aspa* in NFs triggers a transcriptomic change, leading to signalling rearrangements to induce aggressive phenotypes.

## RESULTS

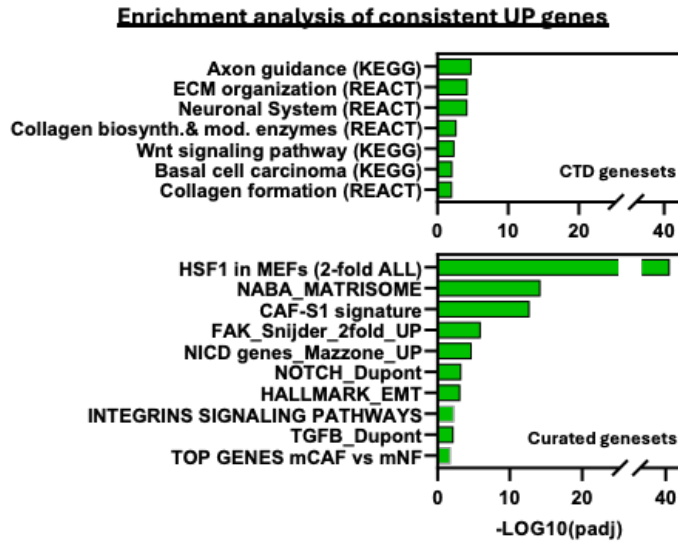


**Figure 4.2. Transcriptomic changes induced by *Aspa* silencing in NFs are associated with CAF activation.** Enrichment analysis of DEGs upregulated after silencing *Aspa* in NFs using CTD and Curated geneset lists.

### 4.4.3 Gene set enrichment analysis of differential gene expression induced by *Aspa* modulation in NF.

To further understand the molecular mechanism whereby *Aspa* exerts its function in NFs, the same RNAseq dataset obtained from the stable silencing of *Aspa* in both NF1-sh3 and NF1-sh4 was interrogated using Gene Set Enrichment Analysis (GSEA). For this analysis, we used signatures from MSigDB Hallmarks and CTD, as well as our Curated dataset. This analysis revealed an enrichment in hallmarks of fatty acid metabolism, OXPHOS and mTORC1 signalling in NF1-shC (in green), when compared to both NF1-sh3 and NF1-sh4. Besides, CTD dataset indicated an enrichment of arginine and amino acid biosynthesis (and related pathways) in NF1-shC compared to both NF1-sh3/sh4 (**Figure 4.3**). This result suggests that the loss of *Aspa* in NFs may induce relevant changes in metabolism.

## RESULTS

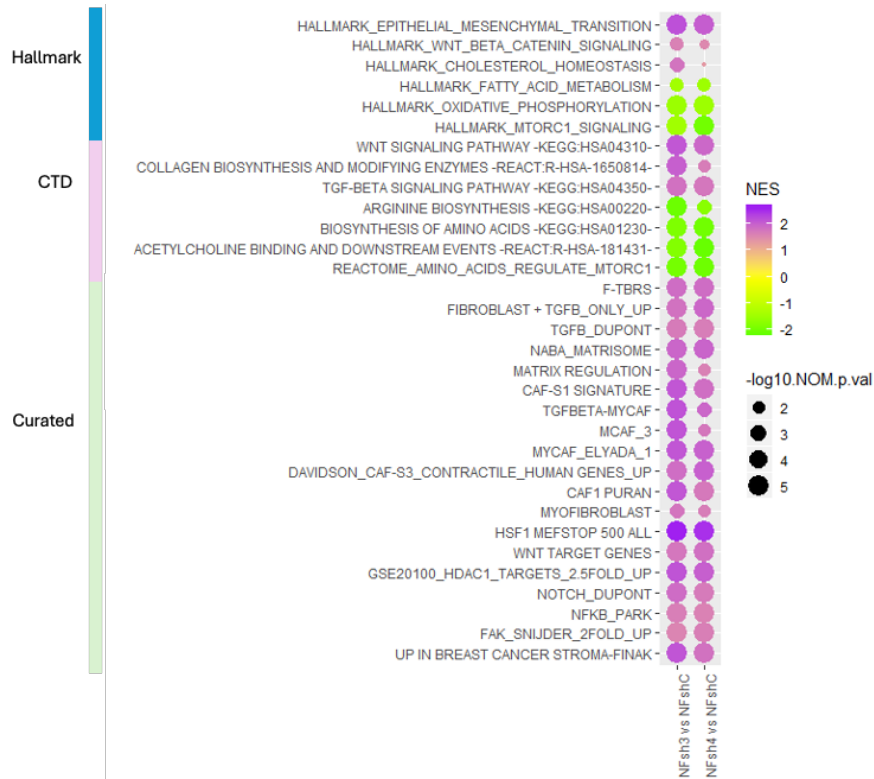
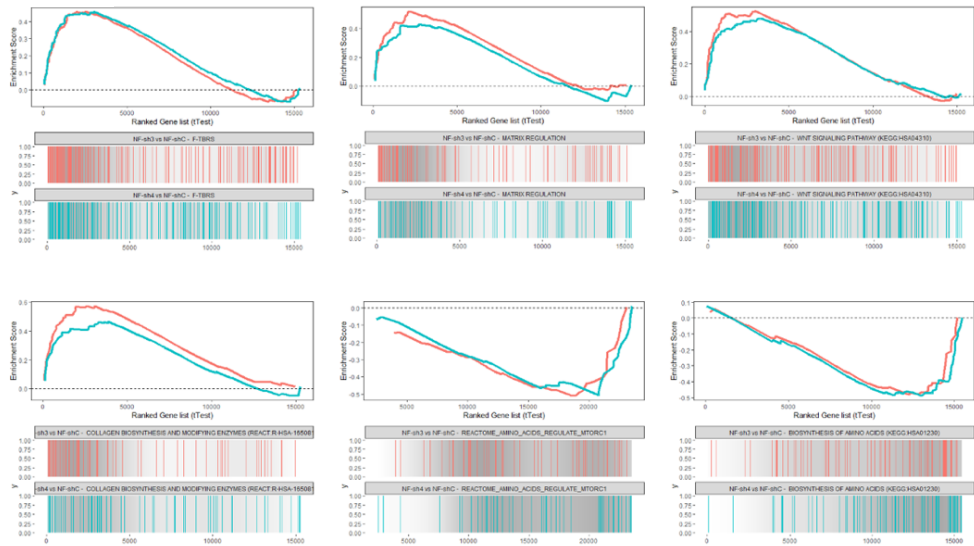


**Figure 4.3. Transcriptomic changes induced by *Aspa* silencing in NFs are associated with CAF activation.** Bubble plot showing GSEA Normalized Enrichment Score (NES, heatmap purple to green) and False Discovery Rate (FDR, size of the bubbles) of representative genesets up- or downregulated in NFs after *Aspa* silencing with two independent shRNAs (NF-sh3 vs NF-shC and NF-sh4 vs NF-shC). *F-TBRs*: fibroblast specific *TGFβ* response signature.

On the other hand, Hallmark, CTD and curated gene set revealed that in both NF1-sh3 and NF1-sh4 there was an enrichment of signatures related to CAFs pathways (i.e. EMT, Wnt or  $TGF\beta$  signalling), collagen-related processes, myCAF phenotypes, HDAC target genes, and stromal signatures of breast cancer associated with poor prognosis (Finak) among others (**Figure 4.3 and Figure 4.4.A**). Besides, genes related to these perturbed pathways were studied in more detail. For example, we observed an upregulation of *WNT2* or *NOX4*, related to breast cancer stromal signatures; *POSTN*, *MMP9* and *LYN*, related to matrix regulation and contractility; *THBS2* and *TGFB2* related to  $TGF\beta$  activity; and several target genes of Wnt signalling, HSF1 and HDAC1 (**Figure 4.4.B**).

## RESULTS

**A**



**B**

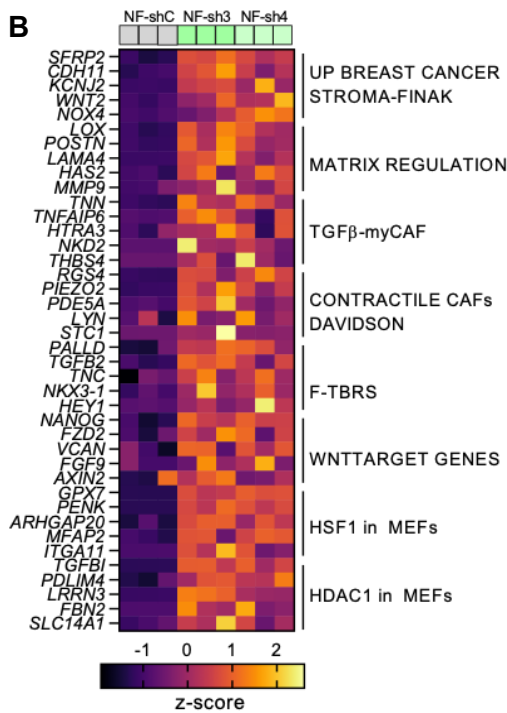


**Figure 4.4. Transcriptional changes induced by *Aspa* silencing in NFs are associated with CAF features. (A)** GSEA blots showing Pan TGF $\beta$  response signalling, matrix regulation, Wnt signalling, collagen biosynthesis and amino acid related signatures in NF1-sh3 and -sh4 compared to NF1-shC. **(B)** Heat map showing z-score values of indicated genes associated with indicated gene sets in mNF1-shC, mNF1-sh3 and mNF1-sh4 (in triplicates).

## RESULTS

Taken all these results together, the gene expression analyses suggest that *Aspa* loss in NFs induces transcriptional programs associated with the aberrant activation of these cells, favouring the differentiation into a CAF phenotype.

Moreover, RNAseq analysis was also performed in the murine NF1 overexpressing *ASPA* (NF1-*ASPA*) and the control NF1-EV, upon TGF $\beta$  stimulation. PCA analysis of transcriptomics data showed that NF1-*ASPA* ("oe") and NF1-EV ("ev") formed a cluster away from samples stimulated with TGF $\beta$ : NF1-*ASPA* ("oe\_TGF") and NF1-EV ("ev\_TGF"). When exploring the PCA of TGF $\beta$ -stimulated NFs, we observed that constitutive *ASPA* expression induced a different transcriptional state, as "oe\_TGF" samples clustered separately from "ev\_TGF" samples (**Figure 4.5.A**). These results are in line with our previous functional observations.

RNAseq data was interrogated by GSEA, using the signatures from Hallmarks and curated dataset. This analysis revealed a series of signatures that were modulated upon *ASPA* constitutive expression in NFs. Thus, signatures related to fibroblast activation, such as TGF $\beta$  signalling, contractile genes, EMT, IL2 and STAT5 signalling, and Wnt/ $\beta$ -catenin pathway were significantly upregulated upon TGF $\beta$  stimulation in NF1-EV ("T-NF-ev vs NF-ev"), but also significantly altered upon constitutive expression of *ASPA* during TGF $\beta$  stimulation ("T-NF-ev vs T-NF-*ASPA*") (**Figure 4.5.B**). Some of those signatures were also altered in basal conditions upon constitutive expression of *ASPA* (i.e. "EMT", "F-TBRS", "Contractile CAFs", "Beta-catenin", "Wnt") (**Figure 4.5.C**). This result indicates that the overexpression of *ASPA* impairs the TGF $\beta$ -induced shift in the transcriptomic profile to drive fibroblast activation.

## RESULTS

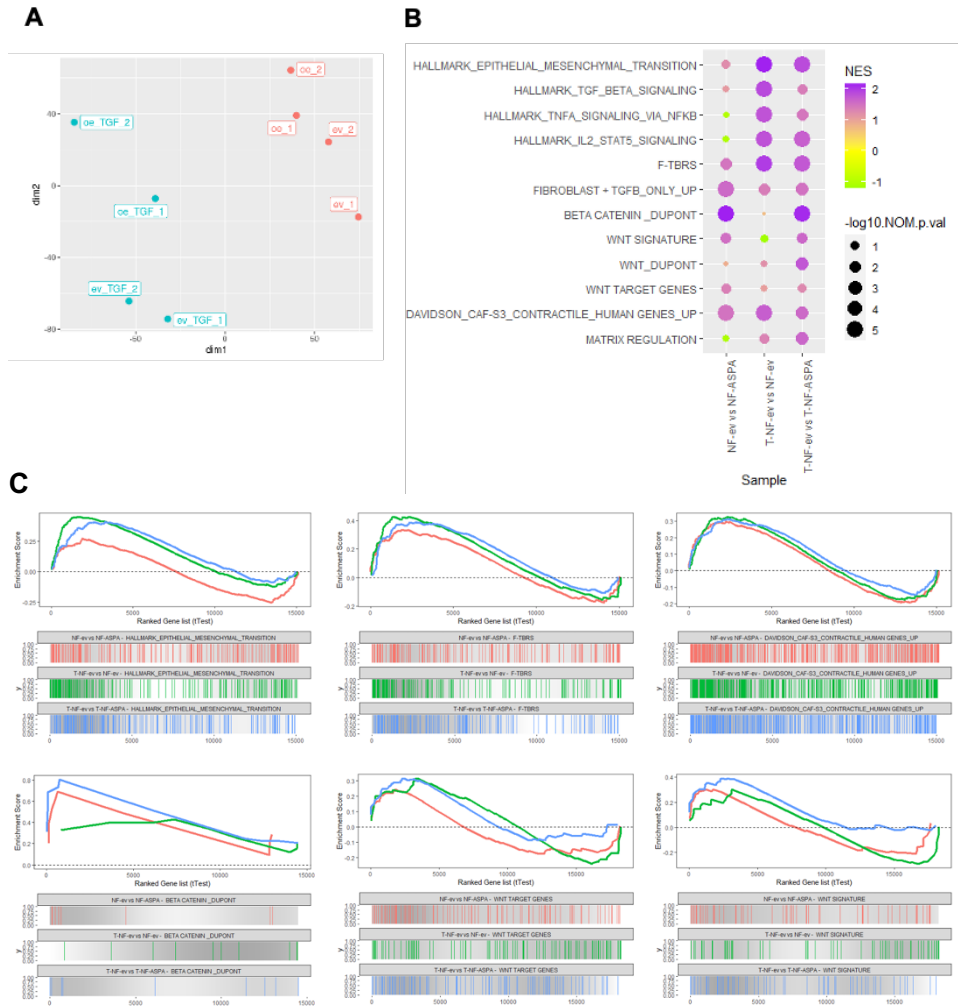


**Figure 4.5. Constitutive expression of ASPA represses TGF $\beta$ -induced fibroblast activation.** (A) Graph showing the PCA of mNF1 after ASPA overexpression (OE and EV) in basal conditions and after TGF $\beta$  stimulation (OE-TGF $\beta$  and EV-TGF $\beta$ ). (B) Bubble plot showing GSEA Normalized Enrichment Score (NES, heatmap purple to green) and False Discovery Rate (FDR, size of the bubbles) of representative gene sets up or downregulated in mNF1 after ASPA overexpression (NF-ev vs NF-ASPA), after TGF $\beta$  stimulation (T-NF-ev vs NF-ev) or differences in TGF $\beta$ -induced responses upon constitutive ASPA expression (T-NF-ev vs T-NF-ASPA). Specific comparisons are indicated at the bottom. (C) GSEA blots showing ETM, Pan TGF $\beta$  response signalling (F-TBRS), contractile,  $\beta$ -catenin, Wnt signalling signatures in NF1-EV vs NF1-ASPA (red), NF1-EV + TGF $\beta$  vs NF1-EV (green), and NF1-EV + TGF $\beta$  vs NF1-ASPA + TGF $\beta$  (blue).

**INVESTIGATING THE MECHANISM OF ACTION  
OF ASPA IN MODULATING CAFs' BEHAVIOUR.**

---



## RESULTS

### 4.5 INVESTIGATING THE MECHANISM OF ACTION OF ASPA IN MODULATING CAFs' BEHAVIOUR.

#### 4.5.1 TGF $\beta$ -mediated activation of fibroblasts is enhanced after *Aspa* lost.

Our transcriptomic studies revealed a strong upregulation of TGF $\beta$  after *Aspa* loss in mNFs, while the constitutive expression of *ASPA* attenuated TGF $\beta$ -mediated effects in these cells. Thus, since the cytokine array analysis did not include TGF $\beta$ -related secreted factors, the genes associated with TGF $\beta$  receptors and ligands were further studied using our transcriptomic dataset. Results showed a strong upregulation of TGF $\beta$  ligands, such as *Tgfb2* and *Tgfb3*<sup>213</sup>, and TGF $\beta$ -related factors such as *Tgfa*<sup>214</sup> and *Tgfb1*<sup>215</sup> in NF1-sh3/sh4 when compared to NF1-shC. Besides, all TGF $\beta$  canonical Smad genes presented an upregulation upon *Aspa* silencing (**Figure 5.1.A**). These results suggest that silencing *Aspa* in fibroblasts induces the autocrine activation of TGF $\beta$  signalling via the production and secretion of TGF $\beta$  ligands.

Taking into account these observations, we studied TGF $\beta$  downstream effectors, Smad proteins, and target genes such as  $\alpha$ Sma in TGF $\beta$ -stimulated NF1-ShC and NF1-sh4. Results showed that the activation of NF1-shC with TGF $\beta$  stimulus decreased *Aspa* expression (as previously shown) and increases the phosphorylated Smad 2/3 (pSmad2/3) and  $\alpha$ Sma protein expression, which was reverted by the inhibition of TGF $\beta$  receptor I (SB431542) (**Figure 5.1.B**). Besides, NF1-sh4, which already showed an aberrant activation upon *Aspa* silencing, presented a decrease of  $\alpha$ Sma expression by inhibiting TGF $\beta$  receptor (SB431542) (**Figure 5.1.C**). Considering that TGF $\beta$  signalling relates to a higher capacity to remodel the ECM, we decided to perform an ECM remodelling assay using the inhibitor of TGF $\beta$  receptor I (SB431542), in order to study if by blocking this autocrine pathway activation, we would be able to revert fibroblast activation after *Aspa* silencing. Results indicated that SB431542 attenuated the contractile capacity elicited by *Aspa* silencing in NF1-sh4, while NF1-shC did not show a clear effect with SB431542. This result

## RESULTS

indicates that the TGF $\beta$  pathway is more active after *Aspa* silencing and that it participates in the increased contractile phenotype induced by *Aspa* loss (Figure 5.1.D).

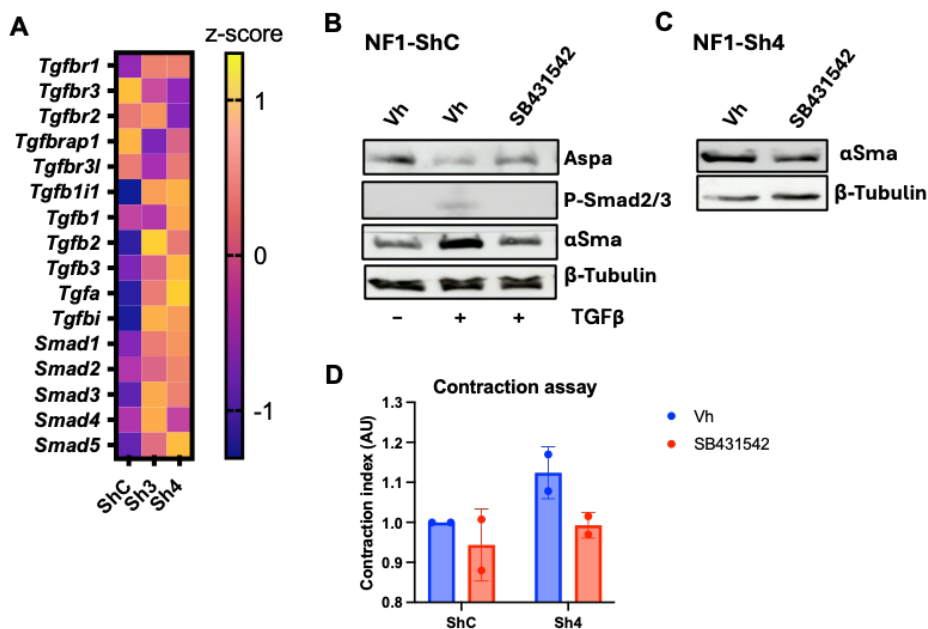


**Figure 5.1. *Aspa* silencing enhances TGF $\beta$  signalling pathway in NFs.** (A) Heatmap showing mean z-score values of gene expression of TGF $\beta$  receptors, ligands and TGF $\beta$ -signalling related factors in murine mNF1-shC and mNF1-sh3/4 (average of 3 biological replicates from RNAseq data). (B) Representative WB showing *Aspa*, phospho-Smad2(Ser465/467)/Smad3 (Ser423/425),  $\alpha$ Sma and  $\beta$ -Tubulin expression in mNF1-shC using the inhibitor of TGF $\beta$  receptor with 5  $\mu$ M SB431542 for 24 h. Where indicated, TGF $\beta$  (5ng/mL) was added 4 h after the addition of the drug. (C) Representative WB showing  $\alpha$ Sma and  $\beta$ -tubulin expression in mNF1-sh4 after addition of 5  $\mu$ M of TGF $\beta$  receptor inhibitor SB431542 for 24 h. (D) Graph showing contraction index in mNF1-shC and mNF1-sh4 with Vh or after inhibiting TGF $\beta$  receptor I with 5  $\mu$ M of SB431542 for 48 h (n=2, each "n" is the average of triplicates). In all cases, shC and shAspa expression was induced with 5-day doxycycline treatment (2 $\mu$ M).

### 4.5.2 ASPA modulation affects canonical Wnt signalling pathway.

It has been reported a role for Wnt signalling in promoting pro-tumour features in CAFs, such as enhancing the ECM remodelling capacity and tumour cell proliferation and progression<sup>63,64</sup>. The RNAseq analysis highlighted an enrichment in Wnt signalling pathway in mNF1 with stable silencing of *Aspa*. Again, the cytokine array did not include Wnt secreted factors, so we

## RESULTS

leveraged on the transcriptomic dataset to further study the expression of genes associated with this pathway. Genes related to the canonical Wnt pathway, such as *Wnt2* or *Wnt6*, and the non-canonical *Wnt2b*, *Wnt4*, *Wnt5b*, *Wnt10a/b* and *Wnt11*<sup>216–218</sup> presented a clear upregulation upon *Aspa* silencing. Besides,  $\beta$ -Catenin coding gene, *Ctnnb1*, showed a slight increase on expression after *Aspa* knock-down. Moreover, *Lrp5*, which encodes a co-receptor that activates canonical Wnt pathway<sup>219</sup>, presented a clear upregulation in NF1-sh3/4 (**Figure 5.2.A**).

Considering these data, our aim was to validate this finding *in vitro*. To do so, the active form of  $\beta$ -Catenin ( $\beta$ -Catenin Active) was checked by WB in mNF1-sh3/4 compared to the control (shC). Results revealed a negative correlation between *Aspa* and activated  $\beta$ -Catenin levels (**Figure 5.2.B**). Additionally, mNF1 overexpressing *Aspa* (NF1-ASPAs) showed a slight decrease of  $\beta$ -Catenin active levels at basal conditions, and further difference was observed under TGF $\beta$  stimulation (**Figure 5.2.C**). This last result suggests that *Aspa* could act as a potential repressor of TGF $\beta$ -mediated  $\beta$ -Catenin activation<sup>58</sup>. In addition, it suggests that the differences in  $\beta$ -catenin activation after *Aspa* silencing may be connected to TGF $\beta$  ligands modulation, i.e. that the observed effects in  $\beta$ -catenin activation are a result of increased TGF $\beta$  signalling after *Aspa* loss. Besides,  $\beta$ -Catenin active levels were also reduced when overexpressing ASPAs in the hPCa CAFs (hCAF-ASPAs) compared to the control (hCAF-C) (**Figure 5.2.D**).

Then, ECM remodelling capacity was investigated using a canonical Wnt inhibitor that increases  $\beta$ -catenin degradation, XAV939. For that, mNF1-shC and mNF1-sh4 were used in gel contraction assays in basal conditions (Vh) or with XAV939. Results showed that the enhanced gel contraction activity resulting from *Aspa* silencing in mNF1-sh4 was abrogated by XAV939 treatment. Of note, inhibiting Wnt signalling in mNF1-shC did not affect their ECM remodelling activities (**Figure 5.2.E**). These findings suggest that the

## RESULTS

activation of Wnt pathway triggered by *Aspa* silencing is also mediating the enhanced contractile capacity of these cells.

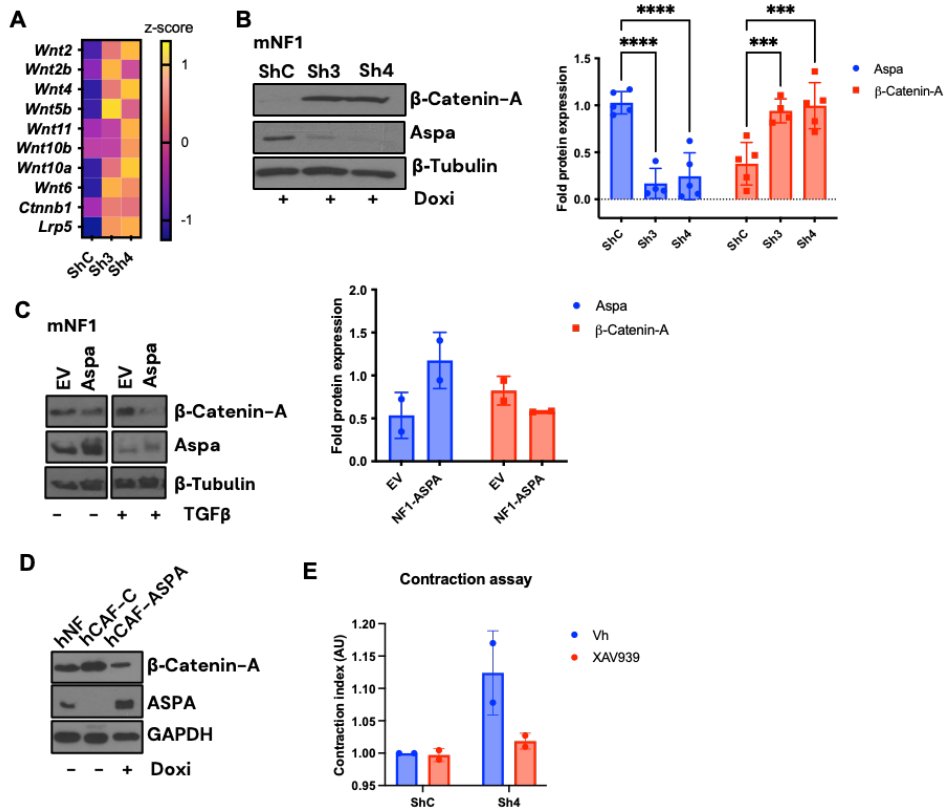


**Figure 5.2. *Aspa* expression impairs Wnt signalling.** (A) Heatmap showing mean z-score values of gene expression of Wnt ligands and Wnt-related factors in mNF1-shC and mNF1-sh3/4 (average of 3 biological replicates from RNAseq data). (B) Representative WB showing non-phospho (active) β-Catenin (Ser33/37/Thr41) (β-Catenin-A), *Aspa* and β-tubulin protein levels in mNF1 after inducible silencing of *Aspa* with two independent shRNA (sh3 and sh4) and with an shControl (shC). Graphs on the right show quantification of fold activated β-catenin levels and *Aspa* expression, relative to β-tubulin (n=5). (C) Representative WB showing activated non-phospho (active) β-Catenin (Ser33/37/Thr41) (β-Catenin-A), *Aspa*, and β-tubulin levels in mNF1 with constitutive expression of *ASPA* (*Aspa*) or empty vector (EV) with or without stimulation with TGFβ (5ng/mL) for 24 h. Graph on the right shows quantification of fold activated β-catenin levels and *ASPA* expression (n=2). (D) Representative WB showing non-phospho (active) β-Catenin (Ser33/37/Thr41) (β-Catenin-A), *ASPA* and GAPDH protein levels in human PCa normal fibroblast (hNF), CAF control (hCAF-C) and CAF overexpressing *ASPA* (hCAF-*ASPA*). (E) Graph showing the quantification of the ECM remodelling assay with mNF1-shC and mNF1-sh4 under basal conditions (Vh) and with canonical Wnt signalling inhibitor XAV939 at 1 μM (n=2; each "n" is the average of triplicates). In all cases, cells were subjected to 2 μM doxycycline treatment for 5 days except for hNF and hCAF-C that were not treated. Statistical significance: \*P < 0.05; \*\*P < 0.01; \*\*\*P < 0.001; \*\*\*\*P < 0.0001.

## RESULTS

### 4.5.3 *Aspa* potentially contributes to epigenetic reprogramming in fibroblasts.

Our transcriptomic data revealed an enrichment of HDAC-dependent signatures in mNF1 with *Aspa* silenced, suggesting *Aspa* as a potential negative regulator of HDAC activity. In that sense, several studies have suggested that HDACs are key effectors of transcriptional changes associated with CAF/myCAF emergence, including TGF $\beta$ -induced transcriptional programs<sup>80,167,220,221</sup>. Additionally, it has been demonstrated the role of ASPA in histone acetylation processes in brain by generating acetate, which can be converted to Acetyl-CoA and directed to the nucleus to modulate histone acetylation<sup>166</sup>. To address if *Aspa* was a negative regulator of HDAC, first, the expression of genes related to the histone acetylation process were investigated. Our results showed an upregulation of *Hdac3* (class I), and *Hdac6/9* (class II)<sup>222</sup> upon *Aspa* silencing in mNF1. On the other hand, class I *Hdac1/2* presented variability in their expression between mNF1-sh3 and mNF1-sh4. Besides, *Hat1*, which is in charge of acetylating the histones, presented a trend to decrease upon *Aspa* silencing (**Figure 5.3.A**). These results suggest that the loss of *Aspa* in NFs enhances the deacetylation process of the histones, potentially impacting on chromatin compaction.

Next, we aimed to study the correlation between *Aspa* modulation and histone 3 acetylation (Ac-H3) levels. In the experiment testing several factors implicated in the activation of fibroblasts (TGF $\beta$  and IL1 $\alpha/\beta$  stimuli), a significant decrease of Ac-H3 levels was observed in correlation with the loss of *Aspa* expression under TGF $\beta$  signalling (**Figure 5.3.B**). To discern if Ac-H3 levels were decreased due to a direct effect of TGF $\beta$  or due to decreased *Aspa* expression, the same approach was investigated with the mNF1 overexpressing ASPA (NF1-ASPA). Results indicated that with the constitutive expression of ASPA, Ac-H3 levels were maintained even under TGF $\beta$  stimulation, compared to the control (EV) in the same condition. These findings suggest that the expression of *Aspa* could modulate Ac-H3 levels in

## RESULTS

fibroblasts. Besides, the addition of NAA led to an increase in Ac-H3 levels in NF-EV, while the addition of TGF $\beta$  (and the subsequent loss of *Aspa* expression) reverted this effect (**Figure 5.3.C**). In addition, the role of ASPA in histone acetylation was also investigated in human cell lines. Thus, when generating hPCa CAFs overexpressing *ASPA* (CAF-*ASPA*) in two different models, an increase in Ac-H3 levels was observed compared to the control (CAF) (**Figure 5.3.D**)

Overall, our results suggest that *Aspa* could contribute to histone acetylation by its enzymatic activity, as the addition of its substrate, NAA, potentially increases the resulting acetate from its catabolism. Conversely, when adding TGF $\beta$ , *Aspa* expression is lost, and NAA cannot be catabolized. Thus, there is no increase of the acetate intracellular pool and a subsequent reduction in Ac-H3 is observed. However, we cannot rule out that *Aspa* contribution to histone acetylation could be an indirect effect of its potential effect on TGF $\beta$  signalling. In this scenario *Aspa* silencing may be potentiating TGF $\beta$  signalling leading to an increased effect over histone acetylation, due to a higher HDAC activity; on the other hand, *Aspa* expression may reduce TGF $\beta$  signalling and its downstream effect on ac-H3 levels.

## RESULTS

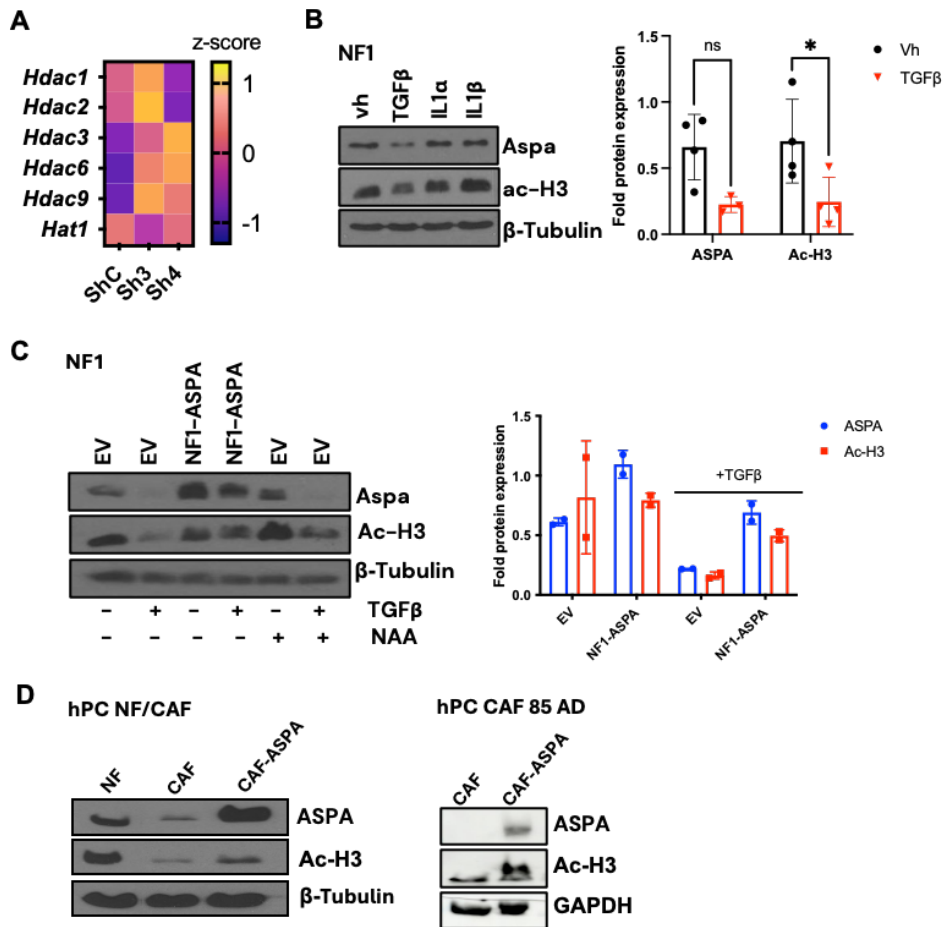


**Figure 5.3. *Aspa* as a potential regulator of acetyl-H3 levels.** (A) Heatmap showing mean z-score values of gene expression of *Hdac* and *Hat* genes in mNF1-shC and mNF1-sh3/4 (average of 3 biological replicates from RNAseq data). (B) Representative WB showing Aspa, Acetyl-H3 (ac-H3) and  $\beta$ -tubulin protein levels in mNF1 under TGF $\beta$  (5 ng/mL), IL1 $\alpha$  (1 ng/mL) and IL1 $\beta$  (3 ng/mL) stimulation for 24 h. On the right, graph showing the quantification of fold protein expression (n=3-4). (C) Representative WB showing Aspa, Ac-H3 and  $\beta$ -tubulin levels in mNF1 control (EV) and mNF1 with a doxycycline-inducible ASPA expression (NFI-ASPAs). Where indicated, TGF $\beta$  (5 ng/mL) and/or NAA (100  $\mu$ M) was added for 24 h. In all cases, cells were subjected to 2  $\mu$ M doxycycline treatment for 5 days. On the right, graph showing quantification of fold protein levels of indicated experimental points (n=2). (D) Representative WB of ASPA, Ac-H3 and  $\beta$ -tubulin/GAPDH levels in human prostate NFs and two CAF models on control conditions or after induced expression of ASPA expression (CAF-ASPAs). CAF-ASPAs cells were subjected to 2 $\mu$ M doxycycline treatment for 5 days, whereas hNF and hCAF were not treated. Statistical significance: \*P < 0.05; \*\*P < 0.01; \*\*\*P < 0.001; \*\*\*\*P < 0.0001.

#### 4.5.4 Investigating pathways interconnection.

In order to study the interconnection of these perturbed pathways upon *Aspa* modulation, mNF1-shC and mNF1-sh4 were employed to investigate how the inhibition of TGF $\beta$  pathway (SB431542), Wnt pathway (XAV939) or HDAC activity (PD106) affected each other. First, our preliminary data indicated that SB431542 in TGF $\beta$ -stimulated mNF1-shC inhibited the activation of downstream effectors Smad2/3, target genes such as  $\alpha$ Sma, HSF1 expression levels and  $\beta$ -Catenin activation (**Figure 5.4.A**). Similar findings were observed with HDAC inhibitor PD106, where TGF $\beta$ -induced *Aspa* downregulation was also diminished. On the other hand, Wnt signalling inhibition with XAV939 did not affect any of those markers, apart from the decrease of active  $\beta$ -Catenin active levels as expected. Importantly, mNF1-sh4 which already presented higher levels of all these proteins mentioned above in basal conditions, showed similar trend upon the addition of the inhibitors (**Figure 5.4.B**).

These data suggests that TGF $\beta$  is the main effector of all these pathway perturbations, triggering enhanced Smad/ $\beta$ -catenin/HDAC/HSF1 activities, increasing  $\alpha$ SMA, potentiating the functional activation of fibroblasts. At least, at the level of cellular contractility/gel contraction, both TGF $\beta$  and Wnt signalling appear to be necessary for functional changes downstream of *Aspa* loss. In addition to that, we have observed that TGF $\beta$  effects are, at least, partially driven by HDAC activity, since the inhibitor PD106 reduces the TGF $\beta$ -mediated activation of these cells.

RESULTS

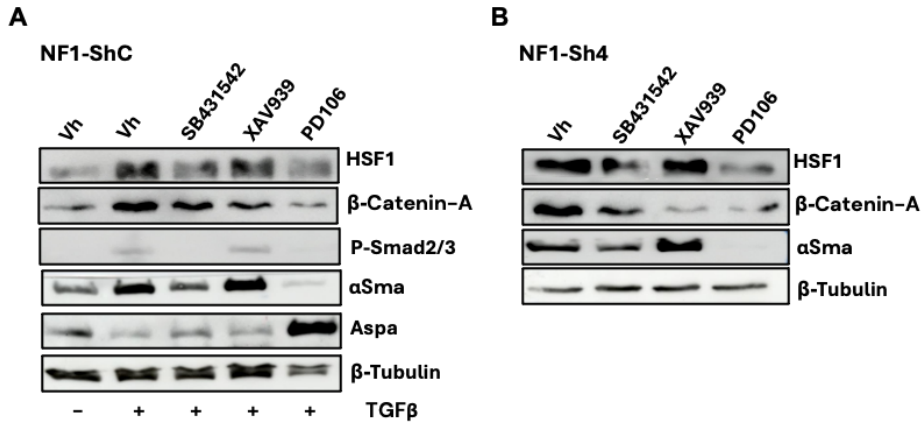


**Figure 5.4. Study of the pathway interconnection after the modulation of *Aspa* expression.** (A) Representative WB showing the expression of HSF1, non-phospho (active)  $\beta$ -Catenin (Ser33/37/Thr41) ( $\beta$ -Catenin-A), phospho-Smad2(Ser465/467)/Smad3 (Ser423/425) (P-Smad2/3),  $\alpha$ Sma, Aspa and  $\beta$ -Tubulin expression in mNF1-shC after the addition of SB431542 (5  $\mu$ M), XAV939 (1  $\mu$ M) and PD106 (25  $\mu$ M) for 24 h. Where indicated, TGF $\beta$  (5 ng/mL) was added 4 h after the addition of the drugs. (B) Representative WB showing the expression of HSF1, non-phospho (active)  $\beta$ -Catenin (Ser33/37/Thr41) ( $\beta$ -Catenin-A),  $\alpha$ Sma and  $\beta$ -Tubulin in mNF1-sh4 after the addition of SB431542 (5  $\mu$ M), XAV939 (1  $\mu$ M) and PD106 (25  $\mu$ M) for 24 h. All cells were subjected to 2 mM doxycycline treatment for 5 days.

## RESULTS

### 4.5.5 *Aspa* modulation triggers metabolic reprogramming in fibroblasts.

#### 4.5.5.1 *Aspa* silencing drives transcriptomic changes in metabolic pathways in fibroblasts.

As described in the previous chapter, transcriptomic analyses informed of significant enrichment of signatures associated to aggressive CAF phenotypes (Wnt and TGF $\beta$  pathway, elastic fiber and collagen formation, HSF1 signalling, HDAC1/2 and myofibroblasts signatures) after *Aspa* depletion in NFs. Notably, when analyses focused in signatures downregulated in NF-sh3/4 vs NF-shC, the analysis pointed out to changes in metabolic pathways such as signatures associated to PPP, arginine and proline metabolism, glycolysis, mTORC1 and gluconeogenesis processes (**Figure 5.5**). Based on these results we decided to investigate metabolic rearrangements in NF/CAFs resulting from *ASPA* modulation.

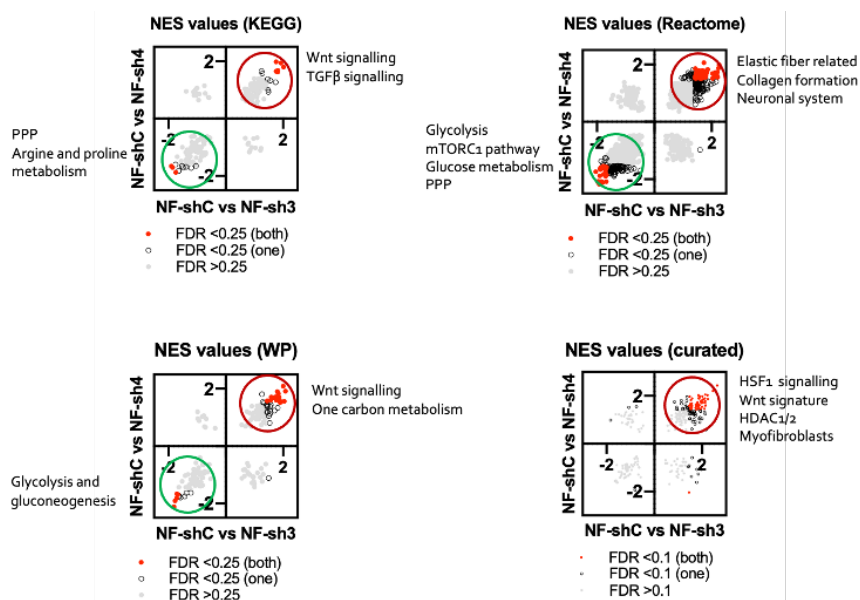


**Figure 5.5. Transcriptomic study after *Aspa* modulation in mNFs.** Graphs showing GSEA Normalized Enrichment Scores (NES) for signatures from KEGG, Reactome, WP and curated databases, when either mNF1-sh3 or mNF1-sh4 were compared with mNF1-shC. A negative NES indicates signatures enriched in mNF1-shC and a positive NES indicates signatures enriched in mNF1-sh3/4. Each dot represents an individual gene set/signature. Red dots represent signatures with FDR<0.25 for both comparisons, black empty dots represent signatures with FDR<0.25 for only one comparison, and grey dots represent signatures with FDR>0.25.

## RESULTS

### 4.5.5.2 *Aspa* expression correlates with enhanced glycolysis.

First, we aimed to study the expression of the genes associated to key metabolic processes such as glycolysis, TCA cycle and OXPHOS (Figure 5.6) after *Aspa* modulation in our cell lines.

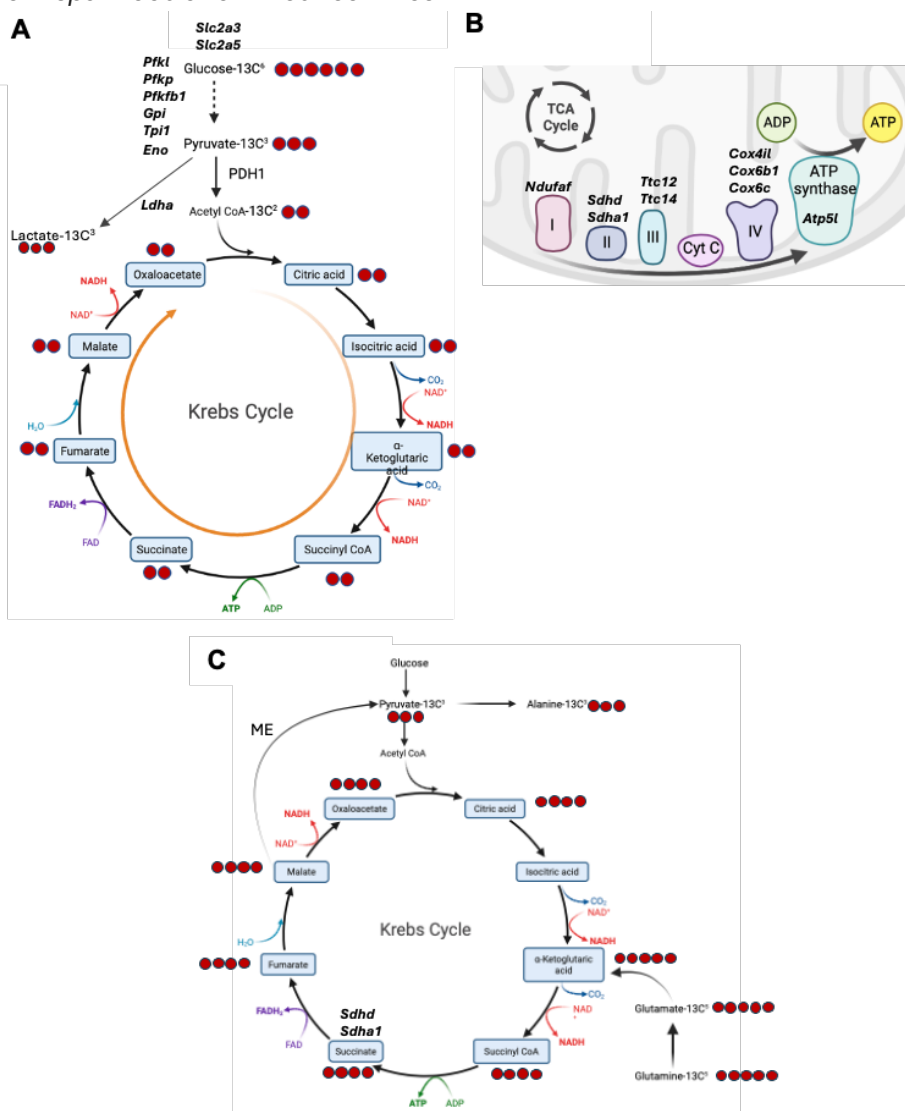


**Figure 5.6. Schematic representation metabolic pathways related to glycolysis, TCA and OXPHOS. (A)** Diagram showing the main steps of of glucose metabolism, key metabolites, and enzymes. The diagram focuses on TCA intermediates generated from Glucose-13C<sup>6</sup>. **(B)** Respiratory chain complexes of the mitochondria. **(C)** Diagram showing key steps of glucose and glutamine metabolism within the TCA, including key metabolites and enzymes. The diagram focused on TCA intermediates generated from Glutamine-13C<sup>5</sup>. Malic enzyme (ME) catalyses the conversion of Malate into pyruvate. In all schemes, labelled carbons indicated as red circles. Relevant genes are represented in the schemes. Done using BioRender.

## RESULTS

Transcriptomic analysis revealed a strong upregulation of glycolytic genes in mNF1-shC compared to the mNF1-sh3/4 (**Figure 5.7.A**). Notably, a relevant proportion of those genes were also affected by constitutive expression of ASPA in TGF $\beta$ -stimulated NFs. Amongst them, there were *Slc2a3* and *Slc2a5*, which are glucose transporters; and subunits of the Pfk kinase complex (*Pfkl*, *Pfkp* and *Pfkfb1*), the key enzyme that positively regulates glycolysis<sup>223</sup> (**Figure 5.7.A,B and Figure 5.6.A**). Other genes related to glycolysis presented similar trends, including *Gpi1*, *Tpi1* and *Eno2*. These findings suggest that ASPA expression is highly related to an enhanced glycolytic flow, while its downregulation triggers an attenuation of this process. In order to decipher if the glycolysis is oxidative or non-oxidative, expression levels of *Ldha* gene, responsible for the conversion of pyruvate to lactate were studied. Results showed a trend to increased *Ldha* expression in mNF1-shC, even though the differences did not reach significance (**Figure 5.7.C and Figure 5.6.A**). Related to that, lactate accumulation in the media was studied in order to corroborate our findings of *Ldha*. We performed Glucose-<sup>13</sup>C<sup>6</sup> tracing and monitored the generation of lactate from glucose. Results showed a trend to increased extracellular lactate-<sup>13</sup>C<sup>3</sup> in mNF1-shC compared to mNF1-sh4, while no clear differences were observed with mNF1-sh3 (**Figure 5.7.D**). This analysis was repeated in the human PCa CAF systems; however, no differences were observed when comparing hCAF-C with hCAF-ASPA (**Figure 5.7.D**).

## RESULTS

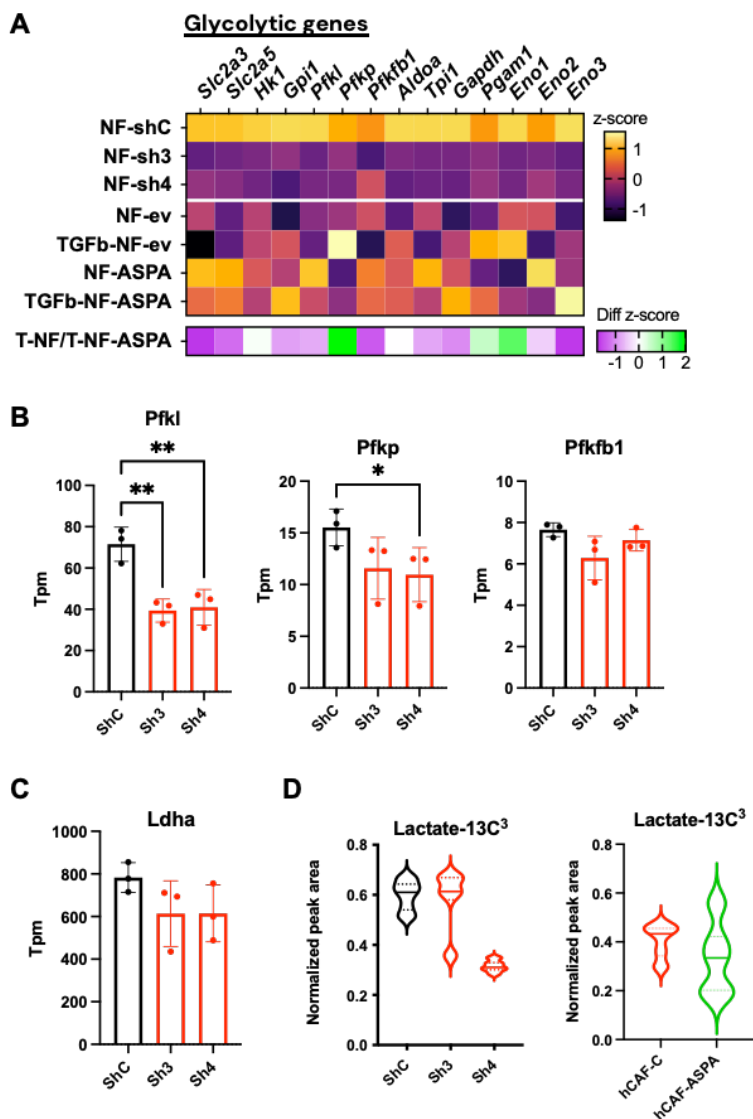


**Figure 5.7. *Aspa* expression correlates with a higher glycolysis.** (A) Heatmap showing average z-score values of glycolytic gene expression in mNF1-shC, mNF1-sh3/4 and mNF1-EV, mNF1-EV + TGF $\beta$ , mNF1-ASPAs, and mNF1-ASPAs + TGF $\beta$  (triplicates). Difference in mean z-score between mNF1-EV + TGF $\beta$  (T-NF) vs mNF1-ASPAs + TGF $\beta$  (T-NF-ASPAs) is represented at the bottom. Where indicated, cells were stimulated with 5 ng/mL of TGF $\beta$  for 24 h. (B) Graphs showing gene expression (in TPMs) of *Pfkfb1*, *Pfkfb1* and *Pfkfb1* in mNF1-shC, and mNF1-sh3/4 (n=3). (C) Graph showing gene expression (in TPMs) of *Ldha* in mNF1-shC, and mNF1-sh3/4 (n=3). (D) Graph showing peak area of extracellular lactate-13C<sup>3</sup> coming from Glucose-13C<sup>6</sup> in mNF1-shC and mNF1-sh3/4 (left), and hCAF-C and hCAF-ASPAs (right). Peak area normalized to total metabolites (n=15, from 5 biological replicates). In all cases, cells were treated with 2  $\mu$ M doxycycline for 5 days except for hCAF-C. Statistical significance: \*P < 0.05; \*\*P < 0.01; \*\*\*P < 0.001; \*\*\*\*P < 0.0001.

## RESULTS

To further investigate changes associated to cell metabolism, genes related to OXPHOS process were investigated. This analysis informed of the upregulation of relevant genes after *Aspa* silencing in NFs. For instance, *Ttc12* and *Ttc14*, related to the complex III of the mitochondrial respiratory chain were increased upon *Aspa* silencing. Besides, *Cox4i1*, *Cox6b1* and *Cox6c*, which are involved in complex IV, and *Atp5l*, related to ATP synthesis, showed the same pattern (**Figure 5.8.A and Figure 5.6.B**). On the other hand, there were also genes that behaved in opposite direction, such as *Ndutfaf6/7* genes of the complex I, or *Atp5b/d* of the ATP synthase complex. Additionally, when comparing mNF1-EV vs mNF1-ASPA, we could observe a downregulation upon ASPA overexpression of genes conforming complex IV of the respiratory chain, such as *Cox4i1*, *Cox6b1*, *Cox6c* and *Cmc2*. Besides, TGF $\beta$  stimulation triggered a downregulation of Complex IV genes in mNF1-EV, that was more drastic when overexpressing ASPA. Thus, these results indicate that *Aspa* expression might be associated with an impaired OXPHOS activity in the mitochondria (**Figure 5.8**).

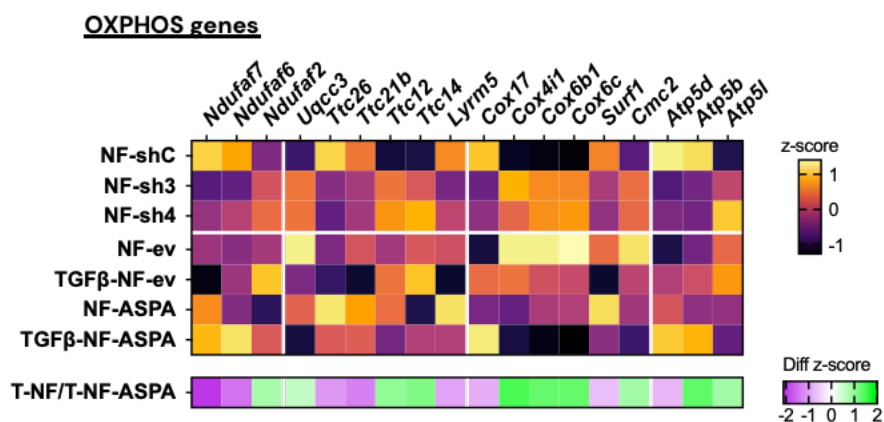
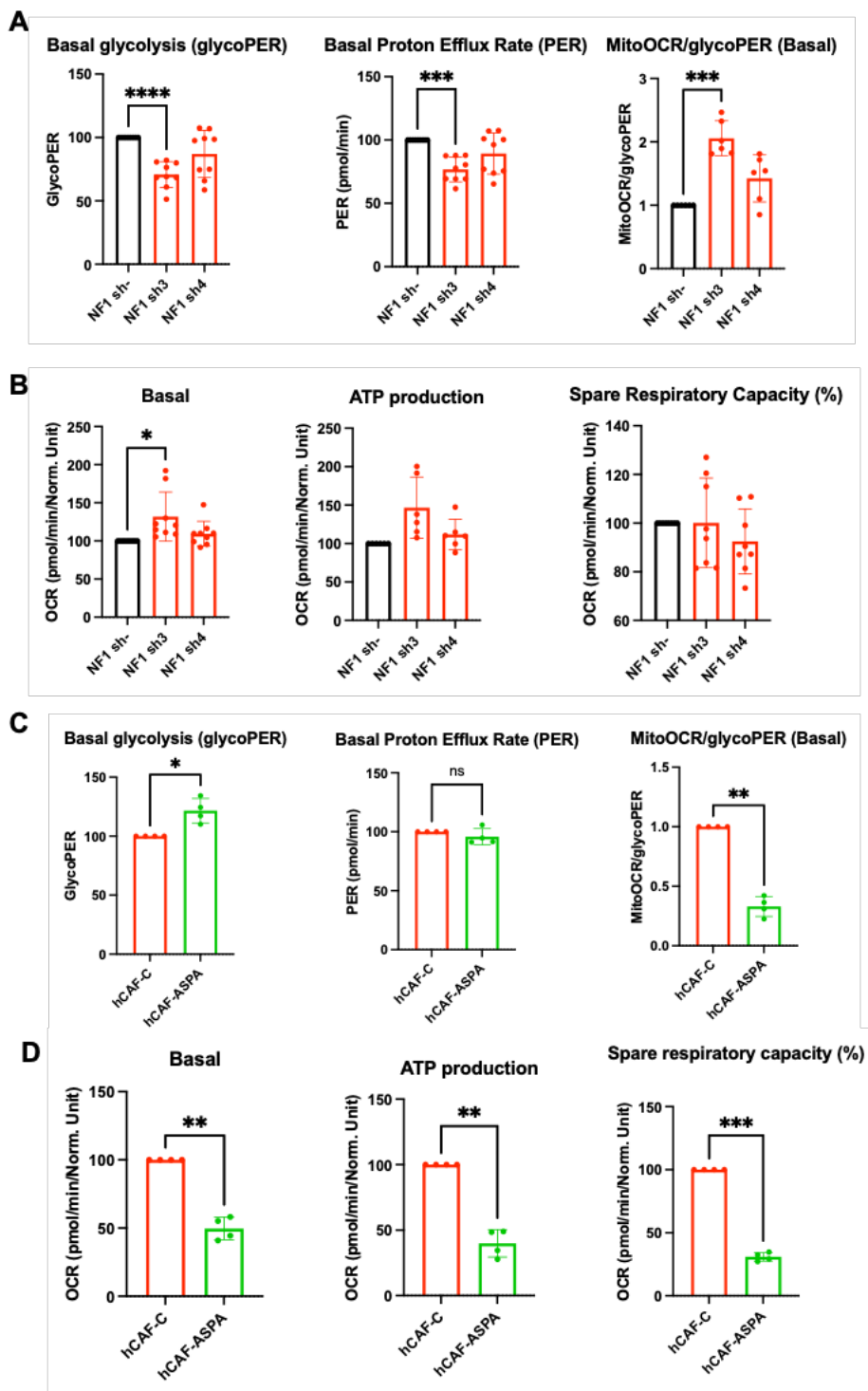


**Figure 5.8. ASPA loss potentially correlates with higher OXPHOS activity.** Heatmap showing average z-score values of OXPHOS-related gene expression in mNF1-shC, mNF1-sh3/4 and mNF1-EV, mNF1-EV + TGF $\beta$ , mNF1-ASPA, and mNF1-ASPA + TGF $\beta$  (triplicates). Difference in mean z-score between mNF1-EV + TGF $\beta$  (T-NF) vs mNF1-ASPA + TGF $\beta$  (T-NF-ASPA) is represented at the bottom. Where indicated, cells were stimulated with 5 ng/mL of TGF $\beta$  for 24 h. In all cases, cells were treated with 2  $\mu$ M of doxycycline for 5 days.

## RESULTS

Given the transcriptomic changes mentioned before, and the previous results which indicated that the loss of *Aspa* is potentially associated with a higher OXPHOS, we aimed to study the generation of ATP through oxidative metabolism. For that, glycolytic and mitochondrial stress analysis were performed using Seahorse methodology in both NF-loss-of-function and hCAF-gain-of-function systems. Results showed that the loss of *Aspa* in mNF1-sh3 and -sh4 triggered a decreased in the basal glycolysis (GlycoPER) and the Basal Proton Efflux Rate (PER). Besides, the ratio between the Oxygen Consumption Rate (OCR) and the GlycoPER was significantly higher, pointing out that the mitochondrial respiration is potentially enhanced over *Aspa* loss (**Figure 5.9.A**). Mitochondrial parameters revealed a significantly increase of the basal respiration, ATP production and the spare respiratory capacity of the cells following *Aspa* silencing (**Figure 5.9.B**), in line with the results suggested by the transcriptomic analysis. Continuing this analysis, same correlations between glycolytic parameters and *ASPA* expression were observed in the hCAF system. For instance, basal glycolysis was significantly higher in hCAFs overexpressing *ASPA*, while no differences were detected in PER. Additionally, a drastic increase of MitoOCR/GlycoPER was observed in hCAF-control, compared to hCAF-*ASPA*, reinforcing that *ASPA* loss triggers an increase of mitochondrial respiration (**Figure 5.9.C**). Finally, all mitochondrial parameters were significantly decreased in hCAF-*ASPA*, compared to control CAFs (**Figure 5.9.D**). Altogether, these results suggest that *Aspa* loss in fibroblasts boost oxidative metabolism by potentiating mitochondrial respiratory chain activity.

# RESULTS



## RESULTS

**Figure 5.9. Study of the energetic status of the cells after *Aspa* perturbation in mNFs and hCAFs. (A and C)** Glycolytic parameters in mNF1-shC, mNF1-sh3 and mNF1-sh4 (A) (n=6-9, each “n” is the average of duplicates); and hCAF-control (hCAF-C) and hCAF-ASPA (C) (n=4, each “n” is the average of duplicates). “Basal glycolysis (glycoPER)” refers to Proton Efflux Rate derived from glycolysis; “Basal Proton Efflux Rate (PER)” refers to the number of protons exported by cells into the assay medium over time; “MitoOCR/GlycoPER” refers to the ratio between mitochondrial oxygen consumption and glycolytic activity. **(B and D)** Mitochondrial parameters in mNF1-shC, mNF1-sh3 and mNF1-sh4 (B) (n=6-9, each “n” is the average of duplicates); and hCAF-control (hCAF-C) and hCAF-ASPA (D) (n=4, each “n” is the average of duplicates). “Basal respiration” refers to the oxygen consumption used to meet cellular ATP demand resulting from mitochondrial proton leak; “ATP production” refers to the decrease in oxygen consumption rate upon injection of the ATP synthase inhibitor oligomycin and represents the portion of basal respiration that was being used to drive ATP production. “Spare respiratory capacity” refers to the capability of the cell to respond to an energetic demand as well as how closely the cell is to respire to its theoretical maximum. In all cases, cells were treated with 2 $\mu$ M doxycycline for 5 days except for hCAF-C. Statistical significance: \*P < 0.05; \*\*P < 0.01; \*\*\*P < 0.001; \*\*\*\*P < 0.0001.

### **4.5.5.3 TCA cycle is reduced in the presence of ASPA.**

To further decipher the metabolic perturbations driven by *Aspa* modulation, TCA cycle related genes were studied in the same systems. Our results revealed a strong downregulation of key genes involved in the TCA cycle in mNF1-shC compared to mNF1-sh3/sh4 (**Figure 5.10.A**). On the other hand, the mNF1-EV vs mNF1-ASPA system presented more variability, since there was an upregulation of some genes with the overexpression of *ASPA*, such as *Idh2*, *Idh3b* and *Sdha*, while other genes, such as *Ogdh*, *Sdhaf1* and *Sdhad* were downregulated. Nevertheless, with these data we could assume that there is a TCA cycle impairment when overexpressing *Aspa*, since a drastic downregulation of several key enzymes would trigger the decrease in the metabolic flow of the cycle. Like *Aspa* silencing, TGF $\beta$  stimulation triggered a drastic downregulation of some genes in mNF1-EV, such as *Idh2*, *Idh3b* and *Sdha*. However, this downregulation was attenuated with the overexpression of *ASPA* (**Figure 5.10.A**). Taking all these results together, data suggest that *Aspa* expression triggers an impairment of TCA cycle, driven by the downregulation of several key genes.

## RESULTS

Additionally, the catabolism of pyruvate in the TCA cycle was studied to unravel how *Aspa* modulation affected this metabolic process. As previously mentioned, transcriptomic data presented an increase of TCA cycle related genes upon *Aspa* silencing in mNF1-sh3/4. For instance, genes that encode for subunits of the enzyme succinate dehydrogenase (SDH), such as *Sdhaf1* or *Sdhb*, which catalyses the conversion of succinate to fumarate, presented an increased expression after *Aspa* silencing (**Figure 5.10.B**). Thus, we examined TCA cycle metabolites generated from glucose- $^{13}\text{C}^6$  (i.e.  $\alpha$ -Ketoglutarate, succinic acid and malate). We found that the levels of these two carbons labelled metabolites generated from the incorporation of the carbons derived from the acetyl-CoA, tended to increase with the silencing of *Aspa* (**Figure 5.10.C and Figure 5.6.A**). Besides, we also checked the labelled metabolites generated from the oxaloacetate- $^{13}\text{C}^3$ , which is a result of the anaplerotic pathway that transforms pyruvate- $^{13}\text{C}^3$  into oxaloacetate- $^{13}\text{C}^3$  (**Figure 5.10.E**). This oxaloacetate- $^{13}\text{C}^3$  can go to the TCA cycle or to generate Aspartate- $^{13}\text{C}^3$ . In our case, results indicated that with the silencing of *Aspa*, oxaloacetate- $^{13}\text{C}^3$  tended to be destined to both pathways, since there is significant increase of three carbon labelled TCA intermediates, and the generation of Aspartate- $^{13}\text{C}^3$  (**Figure 5.10.D**). Of note, no clear differences were observed in the generation of Asparagine- $^{13}\text{C}^3$ .

## RESULTS

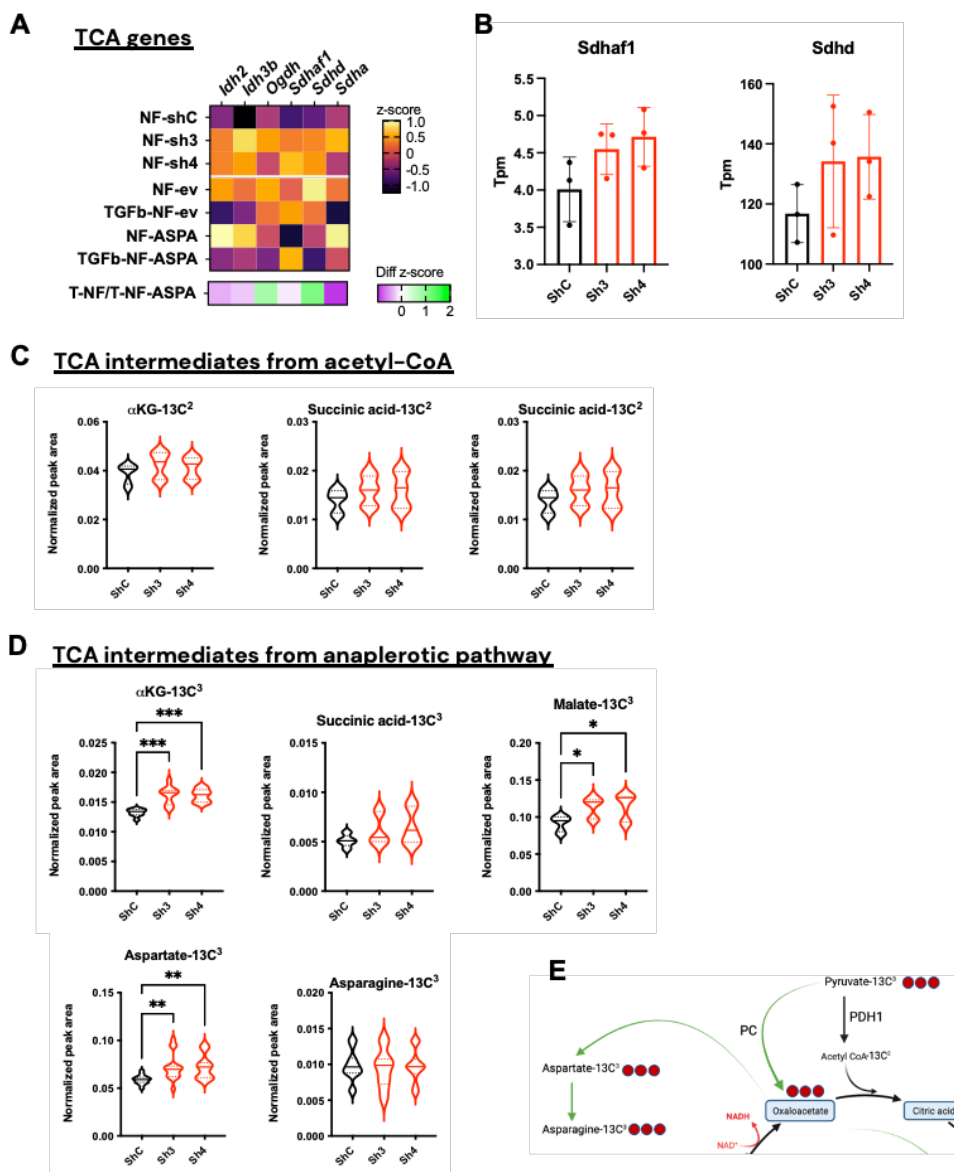


**Figure 5.10. Study of the TCA cycle activity after Aspa silencing.** (A) Heatmap showing average z-score values of glycolytic gene expression in mNF1-shC, mNF1-sh3/4 and mNF1-EV, mNF1-EV + TGF $\beta$ , mNF1-ASPAs, and mNF1-ASPAs + TGF $\beta$  (triplicates). Difference in mean z-score between mNF1-EV + TGF $\beta$  (T-NF) vs mNF-ASPAs + TGF $\beta$  (T-NF-ASPAs) is represented at the bottom. Where indicated, cells were stimulated with 5 ng/mL of TGF $\beta$  for 24 h. (B) Graphs showing gene expression (in TPMs) *Sdhaf1* and *Sdhb* in mNF1-shC, and mNF1-sh3/4 (n=3). (C) Metabolite level of intracellular  $\alpha$ -Ketoglutarate-13C<sup>2</sup>, succinic acid-13C<sup>2</sup> and malate-13C<sup>2</sup> generated from glucose-13C<sup>6</sup> in mNF1-shC (shC), mNF1-sh3 (sh3) and mNF1-sh4 (sh4) (n=9, from 3 biological replicates). (D) Metabolite level of intracellular  $\alpha$ -Ketoglutarate-13C<sup>3</sup>, succinic acid-13C<sup>3</sup>, malate-13C<sup>3</sup>, Aspartate-13C<sup>3</sup> and Asparagine-13C<sup>3</sup>, generated from glucose-13C<sup>6</sup> in mNF1-shC

## RESULTS

(shC), mNF1-sh3 (sh3) and mNF1-sh4 (sh4) (n=9, from 3 biological replicates). In all cases, cells were treated with 2  $\mu$ M doxycycline for 5 days except for hCAF-C. All metabolites are expressed by peak area and normalized by total metabolites. **(E)** Anaplerotic pathway catalysed by Pyruvate Carboxylase (PC), forming Oxaloacetate- $^{13}\text{C}^3$  from pyruvate- $^{13}\text{C}^3$ , using Glucose- $^{13}\text{C}^6$ . Statistical significance: \*P < 0.05; \*\*P < 0.01; \*\*\*P < 0.001; \*\*\*\*P < 0.0001.

Additionally, we investigated the same parameters in our human system with *ASPA* overexpression. Glucose- $^{13}\text{C}^6$  tracing experiments revealed that two carbon labelled intermediates of TCA cycle presented a strong trend to decrease with the overexpression of *ASPA* (**Figure 5.11.A and Figure 5.6.A**). Moreover, three labelled metabolites generated from oxaloacetate- $^{13}\text{C}^3$  showed a similar trend (**Figure 5.11.B and Figure 5.10.E**). Thus, these data suggest that *ASPA* overexpression in hCAFs reduce the incorporation of glucose carbons into the TCA cycle. Since one of the key steps to ensure TCA cycle flow is the generation of Acetyl-CoA from pyruvate, the expression of Pyruvate Dehydrogenase 1 (PDHA1) was investigated in our cell lines. WB analysis showed that both hCAF-C and hCAF-*ASPA* presented similar levels of the inactive form of the enzyme (pPDHA1). Nevertheless, the total expression of the enzyme was decreased in hCAF-*ASPA* compared to hCAF-C (**Figure 5.11.C**). Thus, this result indicates a potential impairment of PDHA1, limiting the incorporation of glucose carbons into the TCA cycle.

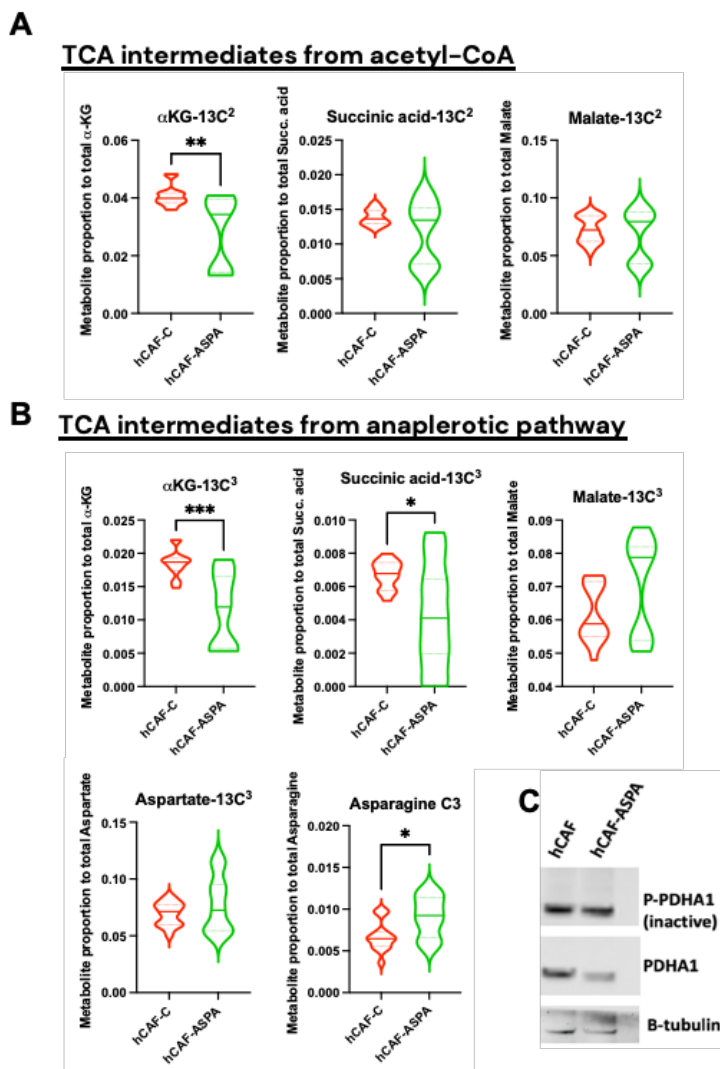


**Figure 5.11. Study of the TCA cycle activity after *Aspa* overexpression. (A)** Metabolite level of intracellular  $\alpha$ -Ketoglutarate- $^{13}C^2$ , succinic acid- $^{13}C^2$  and malate- $^{13}C^2$  generated from glucose- $^{13}C^6$  in hCAF-C and hCAF-ASPA (n=9, from 3 biological replicates). **(B)** Metabolite level of intracellular  $\alpha$ -Ketoglutarate- $^{13}C^3$ , succinic acid- $^{13}C^3$ , malate- $^{13}C^3$ , Aspartate- $^{13}C^3$  and Asparagine- $^{13}C^3$ , generated from glucose- $^{13}C^6$  in hCAF-C and hCAF-ASPA (n=9, from 3 biological replicates). **(C)** Representative WB showing protein expression of phospho (inactive) PDHA1 (S293) (P-PDHA1), total PDHA1, and Tubulin in hCAF and hCAF-ASPA. In all cases, cells were treated with 2  $\mu$ M doxycycline for 5 days except for hCAF-C. All metabolites are expressed by peak area and normalized by total metabolites. Statistical significance: \*P < 0.05; \*\*P < 0.01; \*\*\*P < 0.001; \*\*\*\*P < 0.0001.

## RESULTS

Of note, the addition of exogenous NAA in the tracing experiments in both systems did not appear to affect the observed differences, as levels were similar to basal conditions (**Figure 5.12**).

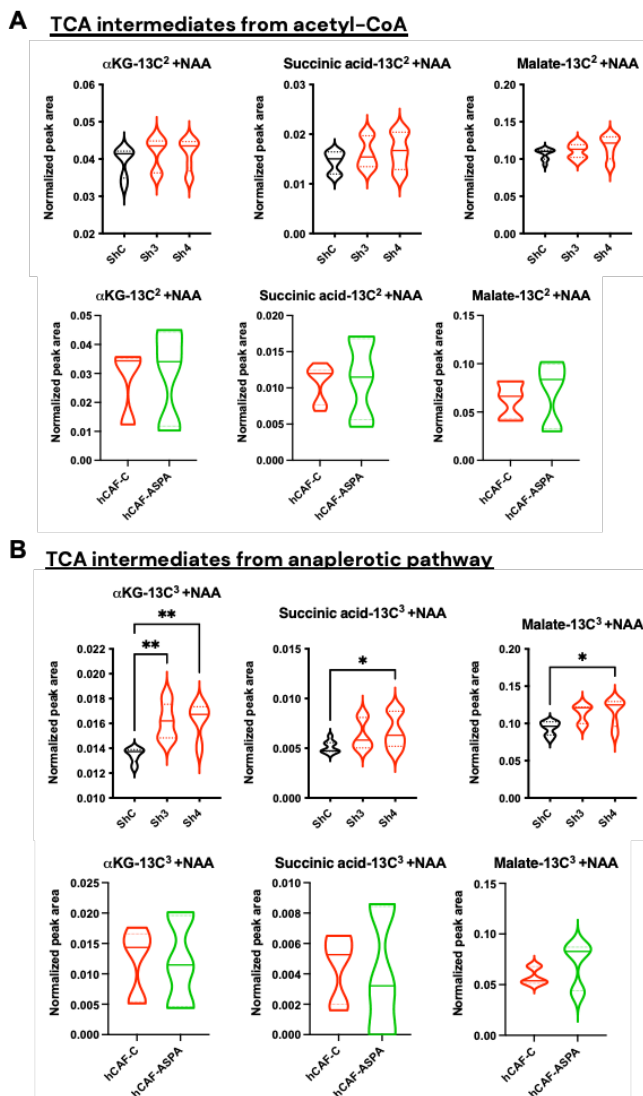


**Figure 5.12. Study of the TCA cycle activity with exogenous NAA after Aspa modulation.** (A) Metabolite levels of intracellular  $\alpha$ -Ketoglutarate- $^{13}C^2$ , succinic acid- $^{13}C^2$  and malate- $^{13}C^2$  generated from glucose- $^{13}C^6$  in mNFI-shC and mNFI-sh3/4, and hCAF-C and hCAF-ASPA ( $n=9$ , from 3 biological replicates). (B) Metabolite levels of intracellular  $\alpha$ -Ketoglutarate- $^{13}C^3$ , succinic acid- $^{13}C^3$  and malate- $^{13}C^3$ , generated from glucose- $^{13}C^6$  in mNFI-shC and mNFI-sh3/4, and hCAF-C and hCAF-ASPA ( $n=9$ , from 3 biological replicates). In all cases, cells were treated with  $100\mu M$  of NAA for 24h, and  $2\mu M$  doxycycline treatment for 5 days except for hCAF-C. All metabolites are expressed by peak area and normalized by total metabolites. Statistical significance: \* $P < 0.05$ ; \*\* $P < 0.01$ ; \*\*\* $P < 0.001$ ; \*\*\*\* $P < 0.0001$ .

## RESULTS

### ***4.5.5.4 Aspa expression correlates with a higher glutamine dependency.***

Since our data indicated a detriment of TCA cycle activity due to the decrease of glucose carbons in systems where ASPA is expressed, we wondered if these cells, that showed poor incorporation of glucose, boosted TCA cycle with glutamine in order to maintain their metabolism.

First, to evaluate Glutamine dependency, control PCa hCAF (hCAF-C) and hCAF-ASPA were cultured in glutamine-deprived media or complete media for 6 days and cell proliferation was assessed by PrestoBlue methodology. This assay presented a proliferative difference at day 6 where hCAF-ASPA were highly affected by the deprivation of glutamine in the media, whereas hCAF-C showed an increased proliferation (**Figure 5.13.A**). Similar to other functional assays, addition of NAA on both cell lines did not affect the outcome, suggesting that the effect may be independent of the catabolic function of ASPA.

To further decipher this metabolic rearrangement, tracing experiments with Glutamine- $^{13}\text{C}^5$  were performed in mNF1-shC and mNF1-sh3/4, and with hCAF-C and hCAF-ASPA. Given the lack of differences in glucose metabolism between basal and NAA-stimulated conditions, for this experiment we focused on basal conditions (no NAA added). Metabolomic data showed a clear increase of intracellular TCA cycle intermediates generated from glutamine- $^{13}\text{C}^5$  in hCAF-ASPA, compared to the control hCAF (**Figure 5.13.B and Figure 5.6.C**). Besides, the use of glutamine to generate other amino acids was investigated. Results showed a trend to increase intracellular glutamate, aspartate, and alanine derived from Glutamine- $^{13}\text{C}^5$  in hCAF-ASPA (**Figure 5.13.C**).

## RESULTS

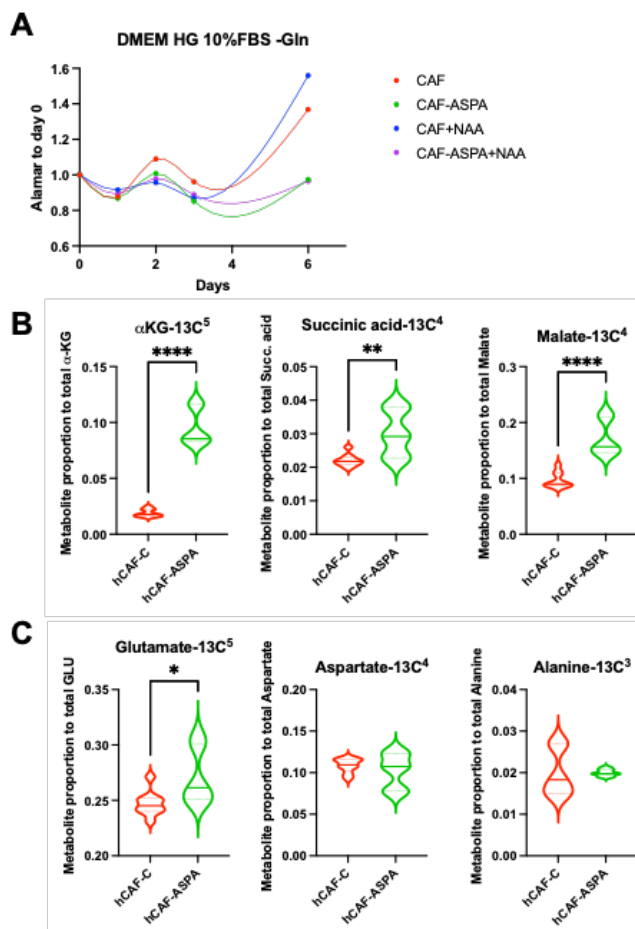


**Figure 5.13. *Aspa* expression triggers a glutamine dependency in hCAFs.** (A) Graph showing the quantification of hCAF and hCAF-ASPA fold proliferation in DMEM with 10% FBS and no L-glutamine by PrestoBlue assay normalized to day 0. Where indicated, 100  $\mu$ M of NAA was added. (B) Metabolite level of  $\alpha$ -Ketoglutarate-13C<sup>5</sup>, succinic acid-13C<sup>4</sup> and malate-13C<sup>4</sup> generated from glutamine-13C<sup>5</sup> in hCAF-C and hCAF-ASPA (n=9, from 3 biological replicates). (C) Metabolite level of glutamate-13C<sup>5</sup>, aspartate-13C<sup>4</sup> and alanine-13C<sup>3</sup> generated from glutamine-13C<sup>5</sup> in hCAF-C and hCAF-ASPA (n=9, from 3 biological replicates). hCAF-ASPA was treated with 2  $\mu$ M doxycycline for 5 days. All metabolites are expressed by peak area and normalized by total protein. Statistical significance: \*P < 0.05; \*\*P < 0.01; \*\*\*P < 0.001; \*\*\*\*P < 0.0001.

## RESULTS

Nevertheless, with mNF1-shASPAsystem, we did not reach any clear differences in the levels of the TCA intermediates neither in the amino acids coming from the Glutamine-13C<sup>5</sup> (**Figure 5.14**). This result suggests that glutamine metabolism and the impact of ASPA modulation may be different between pathologically activated fibroblasts and normal quiescent fibroblasts.

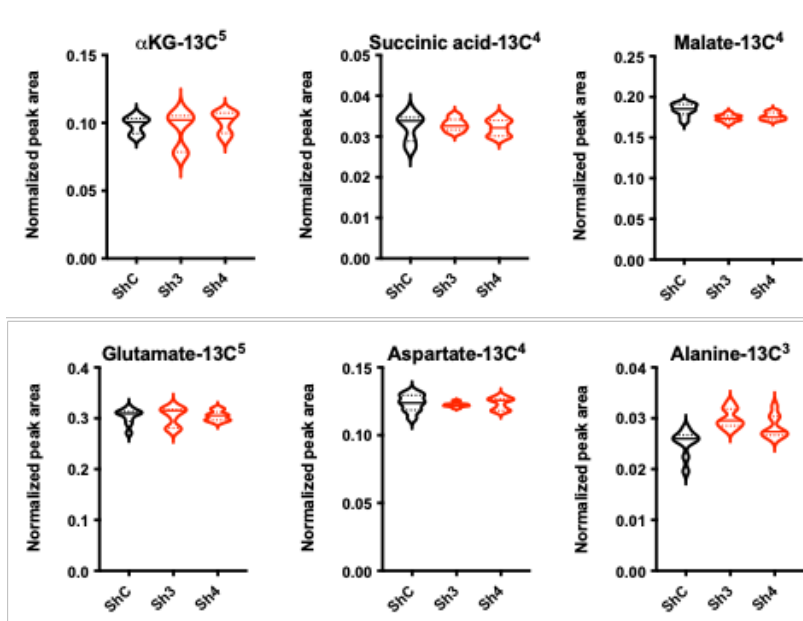


**Figure 5.14. Aspa silencing does not show a clear effect in glutamine dependency in NFs.** Metabolite levels of  $\alpha$ -Ketoglutarate-13C<sup>5</sup>, succinic acid-13C<sup>4</sup> and malate-13C<sup>4</sup>, and glutamate-13C<sup>5</sup>, aspartate-13C<sup>4</sup> and alanine-13C<sup>3</sup> generated from glutamine-13C<sup>5</sup> in mNF1-shC and mNF1-sh3/4. Metabolites expressed by peak area and normalized by total protein (n=9, from 3 biological replicates).

Considering our results, thus far we cannot explain the exact mechanism dictating these metabolic changes. Therefore, these metabolic rearrangements could be a consequence of the signalling adaptations emerging from ASPA modulation in NF/CAFs rather than direct changes in glucose/glutamine metabolism associated to ASPA catabolic function. Further research is required to establish the connection between both observations.



**DISCUSSION**



## 5 DISCUSSION

### 5.1 IDENTIFICATION OF ASPA AS A NEW TUMOUR STROMAL GENE WITH PROGNOSTIC VALUE.

CAFs are considered one of the main contributors to the acquisition of the hallmarks of cancer, representing the major population of the TME<sup>16,49</sup>. These cells are characterized by presenting an aberrant activation which encompass enhanced signalling pathways linked to pro-tumorigenic activities<sup>19,224</sup>; metabolic rearrangements that fuel cancer cell growth<sup>84</sup>; exacerbate collagen deposition and ECM remodelling properties which triggers cancer cell migration, invasions and ultimately, metastasis<sup>29,108</sup>; epigenetic reprogramming which alters their transcriptome landscape to promote the expression of genes related to the aggressive phenotype<sup>34,77</sup>; among other properties that are related to these phenotypes. Therefore, it is increasingly important to decipher the mechanisms whereby CAFs achieve all these processes in order to target them and revert their pro-tumour phenotypes to quiescent fibroblasts.

Previous research from our lab focused on identifying new tumour stroma regulators of tumorigenesis, where DKK3 came out as a significantly upregulated gene in CAFs. Further characterization of DKK3 functions and mechanism of action unravelled its role in potentiating the canonical Wnt signalling pathway in CAFs, that led to enhanced YAP/TAZ activity and to ultimately promote cancer cell proliferation and tumour progression<sup>65</sup>. Leveraging on this approach, we aimed to investigate new potential genes differentially expressed in tumour stroma when compared to normal counterparts using bioinformatic analyses of publicly available datasets. We found Aspartoacylase enzyme (ASPA) as a consistently downregulated gene in the tumour stroma (**Figure 1.4**), specifically in the fibroblast compartment (**Figure 1.7**). Besides, ASPA expression was found to be significantly higher in NFs, while other cell types found in tumours (epithelial, immune, endothelial,

## DISCUSSION

among other cells) showed a low expression or no expression at all (**Figure 1.6 and Figure 1.7.E-G**). These findings were further corroborated by our collaborator Dr. Arkaitz Carracedo (personal communication ahead of publication). Furthermore, *ASPA* downregulation was found to have prognostic value in different types of tumours, suggesting a tumour suppressor role (**Figure 1.5**). This finding is a novelty in the field since *ASPA* has only been fully described in oligodendrocytes<sup>163</sup>, where it catabolizes NAA coming from the neurons. In this context, NAA serves as a reservoir molecule, used for myelin synthesis, among other processes. Besides, *ASPA* implication in cancer has been mainly focused on the role of the substrate, NAA. It has been reported that the accumulation of NAA is implicated in promotion of M2-like phenotype of TAMs<sup>170</sup>, and in promoting cancer cell survival in glucose-deprived scenarios, favouring cancer cell proliferation<sup>177</sup>. Based on our findings, it is reasonable to speculate that in normal tissue stroma, resident fibroblasts could catabolize the NAA coming from epithelial cells, reducing the pro-tumour effect of NAA accumulation. On the contrary, in tumours where CAFs suffer a loss of *ASPA*, NAA is accumulated in the TME, favouring tumorigenesis. However, no potential role of *ASPA* in modulating CAF behaviour has been described.

### 5.2 TO INVESTIGATE THE MECHANISM OF *ASPA* DOWNREGULATION IN CAFs.

First, our aim was to study the mechanism that triggers *ASPA* silencing in fibroblasts. Our studies concluded that TGF $\beta$  is the main responsible factor for *ASPA* downregulation in NFs (**Figure 2.1.A-C**), which is reasonable because of the widely reported implication of TGF $\beta$  to achieve the emergence of CAFs aggressive phenotype. Besides, when blocking TGF $\beta$  receptor, *ASPA* expression was recovered, but no difference was observed using an inhibitor of p38 (SB202190), downstream effector of the non-canonical pathway of TGF $\beta$  (**Figure 2.1.D**). These results suggest that TGF $\beta$ -mediated repression of *ASPA* is potentially driven by its canonical pathway. In addition, our

## DISCUSSION

observations suggested that ASPA loss is primarily associated to myCAF emergence, in line with our scRNAseq-based analyses of clinical datasets (**Figure 1.8**) and multiple NF/CAF pairs of human origin (**Figure 1.9**). To further unravel the mechanism modulating ASPA expression/loss in fibroblasts, we studied the effect on *Aspa* repression of the disruption of pathways associated with TGF $\beta$  signalling and CAF emergence<sup>65,70</sup>. Interestingly, the silencing of TAZ recovered *Aspa* expression in TGF $\beta$ -stimulated murine NFs, while the other factors did not show any differences (**Figure 2.2**). In line with this result, it has been reported that TAZ is able to regulate the nuclear translocation of Smad proteins<sup>53</sup>. Given this tightly interconnection between TAZ and the TGF $\beta$  canonical pathway, it seems logical to hypothesise that in our murine NFs, the repression of *Aspa* could be explained by TAZ/Smad protein complex as downstream effectors of TGF $\beta$  signalling. Still, the relevance of Smad factors in modulating ASPA expression/repression needs to be confirmed by alternative approaches. Additionally, we must consider that this finding could not be extent to other systems, such as murine or human CAFs, suggesting that other regulatory mechanisms must be at play. Thus, we aimed to further investigate potential common mechanism by which TGF $\beta$  is repressing ASPA expression. However, little is known about TGF $\beta$ -mediated gene repression, which has been observed to be context-dependent<sup>225</sup>. Recent reports indicated a novel mechanism by which TGF $\beta$  modulates gene expression through HDAC activity. For instance, it has been described in lung fibrosis that TGF $\beta$ -mediated gene repression of antifibrotic gene *PPARGC1A* (encoding the protein *PGC1 $\alpha$* ) requires HDAC7, which removes the acetyl groups of the gene promoter, driving the downregulation of *PPARGC1A* expression<sup>80</sup>. Moreover, in colorectal cancer, it has been reported that TGF $\beta$  mediates *Prkcz* repression through HDACs activity, leading to an enhanced expression of SOX2 that ultimately will boost cancer cell migration and invasion<sup>202</sup>. In line with these findings, we investigated if by inhibiting HDACs in our systems, ASPA expression could be recovered. In

## DISCUSSION

agreement, we could observe that two different HDAC inhibitors (TSA and PD106) were capable of recovering ASPA expression in TGF $\beta$ -stimulated NFs and in murine/human CAFs (**Figure 2.3**). These findings suggest that the repression of ASPA in activated fibroblasts is driven by a common mechanism defined by HDAC-mediated gene repression downstream of TGF $\beta$  signalling. Given the important functional role of ASPA loss that we described in this study, these observations also underline the previously unappreciated relevance of TGF $\beta$ -mediated gene repression in fibroblast activation/CAF-myCAF emergence.

### 5.3 TO INVESTIGATE ASPA FUNCTIONAL RELEVANCE IN FIBROBLASTS.

ASPA has been described in brain where it is mainly expressed by the oligodendrocytes, catabolizing NAA<sup>163,164</sup>. Thus, since no previous reports ascribed any known function to ASPA in fibroblasts, our aim was to decipher the functional relevance of *Aspa* in our cell lines after genetic silencing in NFs or expression in CAFs. Our transcriptomic data after *Aspa* silencing in mNFs presented a strong negative correlation between *Aspa* and myCAF marker expression, suggesting a conversion of NFs into myCAF phenotypes resulting from *Aspa* loss (**Figure 3.1**). Thus far, the best characterized function of ASPA is to catabolize NAA into acetate and Aspartate. Therefore, ASPA loss may result in the accumulation of NAA. We confirmed that in our system, the loss of ASPA in mNFs triggered an accumulation of NAA (**Figure 3.1.D**), while the overexpression in hCAF<sub>s</sub> diminished intracellular NAA (**Figure 3.8.C**). Since NAA accumulation has been described to boost some pro-tumorigenic properties in cancer cells, we aimed to test if the addition of exogenous NAA had any functional or phenotypic consequence in NFs. However, we did not observe any major difference when compared to the basal conditions, neither in  $\alpha$ Sma expression or their contractile capacity. Thus, it suggests that in fibroblasts, NAA does not trigger any further activation event, and that the phenotype perturbations could be driven by a non-enzymatic activity of

## DISCUSSION

*Aspa*. Alternatively, the effect of ASPA loss in fibroblast activation may result from the lack of its products (acetate and aspartate).

On the other hand, TGF $\beta$  addition presented a higher activation of the fibroblasts after ASPA silencing, boosting their contractile capacity. This result suggested that ASPA loss may be potentiating TGF $\beta$  signalling in fibroblasts or acting over parallel signalling pathways promoting activated phenotypes (**Figure 3.1.G**). To further investigate this, we evaluated whether the constitutive expression of ASPA in NFs could attenuate TGF $\beta$ -mediated activation. Our transcriptomic results showed that ASPA overexpression was impairing the shift to the myCAF transcriptomic programme mediated by TGF $\beta$ . Besides,  $\alpha$ Sma marker and TGF $\beta$ -mediated contraction were significantly impaired with ASPA expression (**Figure 3.2.B-C**). These results suggested that ASPA expression is able to attenuate TGF $\beta$  signalling, therefore impairing the aberrant fibroblast activation program driven by this signalling cascade.

To further understand ASPA function in fibroblasts and its potential implication in cancer progression, we performed cocultures assays of our mNFs after *Aspa* silencing and GFP-labelled cancer cells. Our results show that the silencing of ASPA in fibroblasts in *in vitro* coculture with D2A1 and TS1 cells enhances their proliferation (**Figure 3.3**). Besides, *in vivo* mice studies showed that the silencing of *Aspa* in mNFs accelerated tumour development and boosted tumour growth in early phases (**Figure 3.6**). These results could be explained as NFs with *Aspa* silenced showed a pro-tumorigenic myCAF phenotype, which is linked to enhanced cancer cell growth by secretion of cytokines and growth factors, ECM remodelling, among others<sup>44,88,128</sup>. To corroborate this change of phenotype, a cytokine profile was performed in mNFs after *Aspa* silencing. Results indicated a higher secretion of cytokines related to pro-tumorigenic properties (**Figure 3.5**), validating our findings. myCAFs are also characterized by an increased production of TGF $\beta$  signalling

## DISCUSSION

agonists, and it has been described that the accumulation of TGF $\beta$  in the tumour microenvironment favours cancer cell progression<sup>90,226</sup>. However, our cytokine array did not contain probes for this type of factors. However, our transcriptomic data showed an increase of TGF $\beta$  ligand gene expression after *Aspa* silencing in mNFs, suggesting an additional paracrine effect on cancer cells (**Figure 5.1**). Nevertheless, we could not confirm increased production or secretion of TGF $\beta$  ligands in our system, or its relevance in promoting cancer cell proliferation.

Another fact that can explain the results in the cocultures is that cancer cells have been reported to present higher NAT8L expression and therefore, increased NAA production<sup>175,176,178</sup>. Importantly, NAA accumulation in the TME has been linked to cancer cell survival and growth. For instance, it has been reported in lung carcinoma that NAA promotes cancer cell survival and proliferation in glucose-deprived conditions by maintaining UDP-N-acetylglucosamine levels, therefore ameliorating Endoplasmic Reticulum (ER) stress and enhancing protein synthesis<sup>177</sup>. Besides, in ovarian cancer it has been observed that NAT8L expression exerts anti-apoptotic effects, and the addition of NAA after NAT8L silencing rescued cell survival<sup>175</sup>. Thus, the coculture of cancer cells with fibroblasts lacking *ASPA* expression may trigger the aberrant accumulation of NAA, which could exert its pro-tumorigenic functions. On the other hand, *ASPA* expressing NFs can uptake the NAA secreted by the cancer cells and catabolize it, attenuating its effect. In order to investigate this idea, we added exogenous NAA in our coculture system to push the system (**Figure 3.4.A and C**). However, the results did not show a clear increase in the proliferative capacity compared to the conditions without NAA addition. Of note, this may be dependent on the cellular model and its specific requirements. Thus, further investigation in other conditions, such as glucose-deprived scenario or by activating apoptosis, is required to clarify this point. At the moment, we cannot rule out the possibility that the proliferative advantages that cancer cells present in coculture with mNFs after

## DISCUSSION

*Aspa* silencing are due to the aberrant activation of fibroblasts (and any potential change in pro-tumour factor production), rather than NAA accumulation.

To further investigate the role of ASPA in fibroblasts, we recovered ASPA expression in murine and human CAFs. For the murine CAFs, ASPA overexpression did not trigger any change in  $\alpha$ Sma expression or in their contractile capacity. Besides, cocultures experiments did not present any clear consistent differences between conditions (**Figure 3.7**). One reason could be that the plasmid contains human ASPA sequence, which shares an 84.56% of homology with *Aspa* gene of *Mus musculus*<sup>227</sup>. Therefore, to express human ASPA in a murine CAF might not trigger a clear phenotypic change. However, this cDNA did induce relevant changes when constitutively expressed in murine NFs (**Figure 3.2**). Moreover, mCAF1 present a strong myCAF phenotype, with very aggressive properties and a high expression of markers. Thus, in this system, ASPA recovery may not be sufficient to observe clear changes in the phenotype. Therefore, it is possible that the main signalling cascade/transcriptional program modulated by ASPA in NFs is dysregulated or not relevant in mCAF1. Thus, ASPA may modulate TGF $\beta$  ligands expression in NFs (**Figure 5.1.A**) and not in mCAF1, which could sustain Smad activity by alternative ways. Of note, it has been observed by our collaborator Dr. Arkaitz Carracedo, that ASPA modulation in mCAF1 appears to only affect NAA levels (without any changes in their activation state), and that the NAA accumulation due to *Aspa* loss in mCAF1 drive the conversion from M1 to M2 macrophage phenotype (data not published). Therefore, these two models (mNF/NF-ASPA and mCAF1) represent useful tools to identify NAA-dependent and NAA-independent functions of ASPA in fibroblasts and in tumours. To shed further light into this issue, we are currently investigating the functional implications of a catalytic dead mutant of ASPA (i.e. that cannot catabolize NAA), and study if we observe the same results in cancer cell proliferation, and in cell autonomous functions.

## DISCUSSION

On the other hand, human CAFs, which do not show such a strong aggressive phenotype, presented a clear negative correlation between  $\alpha$ Sma marker and *ASPA* expression. Besides, pro-tumorigenic properties such as their contractile and migratory capacity, and the promotion of cancer cell proliferation were attenuated with the overexpression of *ASPA* (**Figure 3.8**). Similar to mNF systems, no clear differences were observed when comparing basal conditions and NAA addition (**Figure 3.9.A-C**). To understand to a greater extent *ASPA* involvement in tumour progression, the chick embryo *in vivo* experiment was performed, which revealed that *ASPA* rescue in hCAF<sub>s</sub> impaired tumour growth and brain metastasis (**Figure 3.10**). These results could be linked to the attenuated myCAF phenotype that hCAF-*ASPA* presents, which implies a decrease on cancer cell proliferation, ECM remodelling and migration. Therefore, taking all these results together, it suggests that *ASPA* recovery in hCAF<sub>s</sub> impairs key pro-tumorigenic properties of CAFs to boost tumour growth and invasion.

To sum up the functional relevance of *ASPA*, our results suggest that *ASPA* loss in fibroblasts is linked to the myofibroblastic conversion from NFs to CAFs, triggering an enhanced ECM remodelling capacity, an increase of pro-tumoral cytokine secretion and the promotion of cancer cell growth. Conversely, these same events seem to be impaired by the rescue of *ASPA* expression in hCAF<sub>s</sub>. Therefore, we propose *ASPA* as a novel regulator of fibroblasts phenotype which can modulate their pro-tumoral properties.

## 5.4 INVESTIGATING THE MECHANISM OF ACTION OF ASPA IN MODULATING CAF BEHAVIOUR.

### 5.4.1 Studying signalling pathways perturbations after *Aspa* modulation.

To elucidate the mechanism employed by *Aspa* to modulate fibroblast behaviour, we performed a thorough transcriptomics analysis (RNAseq) of mNF1 control and after *Aspa* silencing. In agreement with our functional and phenotypic analyses, transcriptomic results indicated a marked shift on the gene expression profile in *Aspa*-depleted fibroblasts (**Figure 4.1**), which showed an enrichment on CAF-related signatures such as ECM organization, collagen synthesis, Wnt and TGF $\beta$  signalling, HDACs, among others (**Figure 4.2–4.4**). Besides, the overexpression of *ASPA* in TGF $\beta$ -stimulated mNFs resulted in an attenuation in the enrichment of signatures related to CAF phenotypes, and Wnt and TGF $\beta$  signalling (**Figure 4.5**). Together, these results corroborate that *ASPA* modulation triggers profound changes at transcriptomic levels in fibroblasts.

As mentioned in the introduction, TGF $\beta$  is a key activator of fibroblasts. Through its canonical pathway, Smad2/3 complex binds to Smad4, promoting CAF-related gene expression, higher levels of contractility, ECM deposition and promotion of cancer cell growth<sup>50,51</sup>. Moreover, another relevant pathway in the emergence of CAFs is the canonical Wnt signalling. Upon Wnt ligand stimulation,  $\beta$ -catenin gets internalized in the nucleus, activating gene expression programs that will ultimately trigger cell proliferation and ECM remodelling capacity, promoting tumour progression<sup>47,58,63</sup>. Besides, it has also been described a key role of HDACs in the activation of pro-tumorigenic programs in CAFs by transcriptomic rearrangements which involve changes chromatin architecture<sup>77,80,220</sup>. Therefore, and considering our findings in the transcriptomic analysis, our aim was to study these pathway perturbations in a greater extend in our models after *ASPA* modulation.

## DISCUSSION

To validate our findings, we performed *in vitro* assays with our stable cell lines to perturb these signalling pathways and assess their relevance in the activated phenotype emerging from *ASPA* loss. Since our RNAseq revealed a drastic increase of TGF $\beta$  ligands upon *Aspa* silencing in mNFs (**Figure 5.1.A**), indicating a potential upregulation of autocrine TGF $\beta$  signalling in these cells, we decided to perform an ECM remodelling assay with the inhibitor of TGF $\beta$  receptor (SB431542). Results showed a reduction in the contractile capacity elicited by *Aspa* silencing when cells were cultured with SB431542 (**Figure 5.1.D**). This suggested that the loss of *Aspa* in fibroblast triggers the increase of TGF $\beta$  ligands genes, that would drive fibroblasts' activation in an autocrine manner, and the impairment of TGF $\beta$  receptor transduction upon ligand binding decreases the promotion of contractility. Moreover, the addition of exogenous TGF $\beta$  further increased the contraction capacity triggered by *Aspa* silencing (**Figure 3.1**). Therefore, our data indicates that autocrine TGF $\beta$  signalling upon *Aspa* loss in fibroblasts is one potential mechanism which explains the increase of myCAF phenotypes and the ECM remodelling in these cells.

Moreover, considering that RNAseq showed an enrichment in Wnt signalling signatures upon *Aspa* silencing in NFs, we studied Wnt ligands and related factors in our RNAseq data. Interestingly, several Wnt-related genes presented an increase upon *Aspa* silencing (**Figure 5.2.A**), suggesting an activation of Wnt signalling in NF1-sh3/4. This result was corroborated by the increase of  $\beta$ -catenin activation by WB (**Figure 5.2.B**). Due to the relevance of Wnt signalling on the ECM remodelling capacity<sup>58,228,229</sup>, we studied if the inhibition of this pathway would decrease the acquired contractility of NF1-sh*Aspa* cells. Results indicated that the contractility of NF1-sh4 was reduced after inhibiting Wnt signalling (**Figure 5.2.E**). Thus, these results suggest that the activation of Wnt pathway upon *Aspa* silencing could be a potential mechanism to explain the aberrant activation of these cells.

## DISCUSSION

Similarly, transcriptomic data indicated an upregulation of HDAC signatures upon *Aspa* silencing in mNFs. Our aim was to study perturbation on histone acetylation levels after *Aspa* modulation. Several HDACs were upregulated after silencing *Aspa* in NFs (**Figure 5.3.A**). Moreover, TGF $\beta$ -stimulated NFs presented a decrease of Ac-H3 levels, which could indicate an enhanced HDAC activity upon fibroblasts activation. Besides, the overexpression of *ASPA* in TGF $\beta$ -stimulated NFs attenuated TGF $\beta$  effects on Ac-H3 (**Figure 5.3.C**). This could be explained by the decrease of TGF $\beta$  signalling upon *Aspa* overexpression, leading to a diminish of HDAC activity. Interestingly, the addition of NAA increased AcH3 levels in mNF-EV compared to TGF $\beta$ -stimulated mNF-EV, suggesting that the effect of *ASPA* over AcH3 levels may be dependent on its NAA catalytic activity. These results suggest that *ASPA* expression contribute to the acetylation levels of the histones, which can be explained as *ASPA* activity generates acetate, which can be converted to acetyl-CoA, which in the nucleus could be used to acetylate histones, as it has been reported in oligodendrocytes or brown adipocytes<sup>162,163,168</sup>. Furthermore, some reports indicated that *ASPA* can present a nuclear localization. However, *ASPA* functions in nucleus have not been determined<sup>165</sup>. Some hypothesis pointed out that nuclear *ASPA* could be more efficient to generate acetyl-CoA for histone acetylation process. Of note, in our immunostaining experiments, we could observe an overlapping of DAPI and *ASPA* expression (**Figure 1.10.E and Figure 3.8.B**). Thus, we cannot rule out the possibility that *ASPA* presents activity within the nucleus in fibroblasts. Nevertheless, more studies are needed to unravel the role of nuclear *ASPA* to a greater extend.

Considering all these signalling perturbations occurring in fibroblasts upon *Aspa* modulation, we aimed to study the potential interconnection between these pathways. Several studies pointed out a clear connection between TGF $\beta$  signalling and Wnt pathway. For instance, it has been reported that TGF $\beta$  enhances Wnt signalling by decreasing an antagonist of this

## DISCUSSION

pathway<sup>58</sup>. Besides, it has been shown that  $\beta$ -catenin inhibition impairs the activation of TGF $\beta$  effectors, Smad2/3<sup>230</sup>. Our results suggested that TGF $\beta$  exert an effect on Wnt signalling pathway, since the inhibition of TGF $\beta$  receptor triggered the reduction of  $\beta$ -Catenin active form in both TGF $\beta$ -stimulated mNF1-shC and in basal mNF1-sh4. Conversely, the inhibition of Wnt pathway did not show any downregulation in TGF $\beta$  effectors Smad proteins, or target genes such as  $\alpha$ Sma (**Figure 5.4**). Thus, these findings indicate that TGF $\beta$  pathway is modulating Wnt signalling upon ASPA modulation in our fibroblast, but not the other way around.

Furthermore, this increase of HDAC expression upon *Aspa* silencing (**Figure 5.3.A**) can be linked to TGF $\beta$  signalling, as previously mentioned. For instance, TGF $\beta$ -mediated EMT requires HDAC6 activity<sup>231</sup>, and interestingly, the inhibition of HDAC6 triggered the impairment of Smad2/3 complexes by the accumulation of acetylated Smad3 in the cytoplasm<sup>232</sup>. Thus, TGF $\beta$  signalling presents a tight connection to HDAC activity to exert its effects. Therefore, we hypothesise that in our system, the upregulation of TGF $\beta$  pathway upon *Aspa* silencing could act through HDAC proteins, decreasing the levels of histone acetylation levels and repressing key genes to achieve a pro-tumorigenic phenotype. To confirm our hypothesis, HDAC inhibitor PD106 was tested in TGF $\beta$ -stimulated mNF1-shC and in mNF1-sh4. Our findings revealed that the impairment of HDAC activity drives a drastic downregulation of TGF $\beta$  effectors Smad2/3, Wnt signalling and  $\alpha$ Sma expression, while there was a strong upregulation of *Aspa* (**Figure 5.4**). Thus, these observations suggested that TGF $\beta$  could exerts its effects through HDAC activity in our fibroblasts upon *Aspa* loss.

In addition, we are currently assessing the activity and relevance of LYN kinase in our fibroblasts cell lines after ASPA modulation. As previously mentioned, it has been observed in prostate cancer cells that ASPA impairs cancer progression through the blockade of LYN activity by physical

## DISCUSSION

interaction. Therefore, this blockade is independent of ASPA enzymatic activity<sup>167</sup>. Furthermore, LYN has been described as a key modulator of fibroblasts in leukaemia, enhancing their inflammatory and ECM remodelling features, ultimately boosting cancer cell progression<sup>233</sup>. Of note, in leukemic cell lines, it has been reported a link between TGF $\beta$  pathway and LYN signalling, as TGF $\beta$  enhances LYN activity<sup>234</sup>. Considering all these evidences, we hypothesised that upon ASPA loss in CAFs, LYN may be activated promoting CAF-related gene expression programmes. This could promote TGF $\beta$  signalling, that in turn may maintain LYN activity. Thus, we are currently studying LYN expression and its relation to *Aspa* in our systems. Preliminary data from our transcriptomic data showed an upregulation of LYN gene expression levels after *Aspa* silencing in mNFs, suggesting that the modulation of *Aspa* potentially perturbs the expression of LYN. Besides, in our human system, a drastic downregulation of LYN protein was observed by WB in hCAF-ASPA when compared to the control (data not shown). Considering these data, it indicates that ASPA may modulate LYN expression and potentially its activity in fibroblast, in an enzymatic-independent manner. To further address these hypotheses, we have just generated a catalytic inactive mutant of ASPA that will be assessed for its ability to influence all the different signalling cascades affected by ASPA silencing or overexpression. In this way, we would be able to understand in a greater extend the potential non-enzymatic roles of ASPA in fibroblasts and their influence over fibroblast activation/CAF emergence. However, further studies need to be done in order to elucidate if ASPA is binding LYN kinase in fibroblasts and if this event has any implication on fibroblasts pro-tumour features.

#### 5.4.2 Studying metabolic rearrangements after *Aspa* modulation.

RNAseq analyses revealed several perturbations in metabolic processes, which consisted on a significant downregulation of glycolytic-related genes upon *Aspa* silencing in mNFs, such as *Pfkl* or *Pfkp*, which are key regulators of the glycolytic flux<sup>223</sup> (**Figure 5.7.A-B**). Since we observed changes at transcriptomic level, this may be related to signalling and fibroblast activation process, which triggers a metabolic rearrangement, rather than a direct effect of *ASPA* on metabolism. We also found a significant increase in OXPHOS activity in systems lacking *ASPA* expression (mNF1-sh*Aspa* and hCAF-C), while cells expressing *ASPA* (mNF1-shC and hCAF-*ASPA*), showed a reduction in mitochondrial respiration (**Figure 5.9**). Tracing experiments indicated an increase of glucose carbon incorporation to the TCA in the absence of *ASPA*, while the systems that expressed *ASPA* presented lower glucose-derived TCA metabolites (**Figure 5.10 and Figure 5.11**), which was already reported by Alkan, H. F. et. al, where *ASPA* overexpression in lung carcinoma cells (LLC1) presented a decreased in Citrate-<sup>13</sup>C<sup>2</sup> coming from Glucose-<sup>13</sup>C<sup>6</sup>, suggesting an impairment in the incorporation of the glucose in TCA. Besides, the addition of exogenous NAA did not trigger any further change in both systems, suggesting that these metabolic perturbations are not NAA-dependent (**Figure 5.12**). Finally, tracing experiments with Glutamine-<sup>13</sup>C<sup>5</sup> indicated an increase of metabolic intermediates in hCAF overexpressing *ASPA*, while no clear changes were observed in mNF1-sh*Aspa* system (**Figure 5.13 and 5.14**). All together, these results indicate that the expression of *ASPA* enhances glycolysis. Nevertheless, as we observed a decrease in PDHA1 enzyme in hCAF-*ASPA* (**Figure 5.11.C**), which catalyses a key step that connects glycolysis to TCA cycle, our results also suggest an impairment in this process by blocking the incorporation of carbons from glucose to the TCA cycle, therefore, enhancing the anaplerotic pathway to produce oxaloacetate-<sup>13</sup>C<sup>3</sup> (**Figure 5.11.B and Figure 5.10.E**). Furthermore,

## DISCUSSION

hCAFs-*ASPA* showed a clear glutamine dependence in the proliferation assays, and by metabolic tracing, results evidenced that these cells uptake and incorporate glutamine to the TCA cycle in order to restore the TCA cycle intermediates (**Figure 5.13**).

In sum, at metabolic levels it appears that *ASPA* loss in CAFs elicits specific adaptations that enable them to resist nutrient-deprived condition, reducing their dependency on glutamine and anaplerotic pathways and increasing TCA and OXPHOS. Considering that we have observed a pro-tumorigenic behaviour in cells lacking *ASPA* (mNF1-sh3/4 and hCAF-C) in cell autonomous functions and in coculture with cancer cells, we hypothesise that the metabolic rearrangements upon *ASPA* loss in fibroblasts favours cancer cell progression. Besides, it has been described that CAFs presenting higher OXPHOS promote tumour progression in oral squamous carcinoma<sup>152</sup>. Moreover, and considering the exacerbate ECM remodelling process presented by CAFs, which is a highly energetic demanding process, it is reasonable that CAFs present an increase of OXPHOS and ATP production<sup>235</sup>, as observed in the mitochondrial stress assay (**Figure 5.9**). Thus, even though we have not completely elucidated the metabolic advantage of these rearrangements in CAFs and the potential crosstalk to cancer cells by fuelling their metabolism, it is clear that the modulation of *ASPA* triggers a metabolic reprogramming.

To sum up, in this project we have elucidated *ASPA* as a new regulator of CAFs phenotype. The loss of *ASPA* triggers the activation of key pathways in fibroblasts, such as TGF $\beta$  and Wnt signalling, which are interconnected and boost the pro-tumoral features of CAFs. Besides, we have demonstrated that TGF $\beta$  potentially acts through HDAC activity, to achieve an epigenetic reprogramming that, ultimately, will generate the aberrant activated state of CAFs. Due to this signalling perturbations, there is a transcriptomic shift in fibroblasts, as we observed changes in CAFs' markers. Moreover, these cells

## DISCUSSION

present an enhanced capacity to remodel the matrix, a pro-tumoral crosstalk to cancer cells which leads to a higher cancer cell proliferation and metastasis. Altogether, it appears that *ASPA* loss is potentiating TGF $\beta$  signalling possibly by the upregulation of TGF $\beta$  ligands, and that this effect is then propagated to other TGF $\beta$ -dependent pathways such as Wnt, HSF1 and HDACs. Besides, upon *ASPA* loss, metabolic adaptations are taking place, which may be a result of the transcriptomic rearrangements.

Furthermore, we have presented TGF $\beta$  as a key suppressor of *ASPA* expression, and that the inhibition of TGF $\beta$  receptor or HDAC activity triggers the rescue of *ASPA*. In cancer scenarios, where cancer cells are secreting TGF $\beta$ , normal fibroblasts surrounding the tumour will be activated and transformed into CAFs, therefore losing *ASPA* expression and exerting all the effects previously mentioned. In turn, CAFs will also secrete TGF $\beta$  and Wnt ligands, among others, which will act in autocrine and paracrine manner, in order to recruit and maintain CAFs population, but also promoting cancer cell progression. Nevertheless, we have not fully elucidated the mechanism whereby *ASPA* loss triggers all these effects. As previously mentioned, our data points out the possibility of an enzymatic independent mechanism, which will imply the interaction of *ASPA* with key factors to exert its effects.

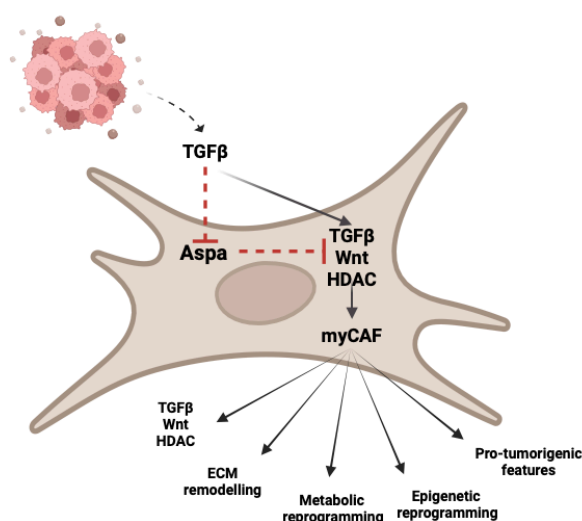


Figure 1. Discussion section. Representative scheme of the findings in this project.

**CONCLUSIONS**



## 6 CONCLUSIONS

In this project, we identified the metabolic enzyme ASPA as a key regulator of fibroblast behaviour and a potential target to normalise or revert the aberrant activation of CAFs to impair tumour progression. Thus, conclusions are the following:

1. *ASPA* gene expression is significantly downregulated in human cancer stroma and has prognostic value in several tumour types.
2. *ASPA* loss affects primarily stromal fibroblasts in tumours, and its expression is significantly downregulated in murine and human CAF models when compared to normal counterparts.
3. *ASPA* loss correlates with a myCAF phenotype, while there is no clear correlation with iCAFs.
4. Transforming growth factor  $\beta$  (TGF $\beta$ ) is a potential repressor of *ASPA* expression in CAFs/myCAFs. TGF $\beta$ -dependant *ASPA* repression is mediated by HDAC1-3, by potentially modifying the acetylation state of *ASPA* regulatory domains.
5. *ASPA* loss in NFs enhances myCAF features such as marker expression, matrix remodelling capacity and tumour cell growth *in vitro* and *in vivo*.
6. Blocking *ASPA* downregulation reduces the effects induced by TGF $\beta$  stimulation in NFs, suggesting that *ASPA* is a repressor of fibroblast activation towards myCAF phenotypes.
7. *ASPA* overexpression in CAFs impairs the pro-tumoral features of these cells, attenuating activated fibroblast marker expression, matrix remodelling capacity and tumour cell growth *in vitro* and *in vivo*.
8. *ASPA* loss in NFs drives a transcriptomic rearrangement that implies an enrichment of CAF-related signatures such as "ECM organization", "collagen biosynthesis", and "myofibroblasts", among others.

9. *ASPA* loss triggers an enhanced TGF $\beta$ , Wnt and HDAC activity, which have been observed to be interconnected and could be linked to the pro-tumoral features of CAFs.
10. *ASPA* modulation is associated with metabolic rearrangements: *ASPA* loss in CAFs induces enhanced TCA and OXPHOS employing glucose as a source of carbons; *ASPA* expression was associated with a higher glutamine dependency.
11. *ASPA* effects on CAFs functional properties are independent of NAA catabolism.

## REFERENCES



## REFERENCES

1. Sung, H. *et al.* Global Cancer Statistics 2020: GLOBOCAN Estimates of Incidence and Mortality Worldwide for 36 Cancers in 185 Countries. *CA. Cancer J. Clin.* **71**, 209–249 (2021).
2. Arnold, M. *et al.* Current and future burden of breast cancer: Global statistics for 2020 and 2040. *Breast Edinb. Scotl.* **66**, 15–23 (2022).
3. Weeden, C. E., Hill, W., Lim, E. L., Grönroos, E. & Swanton, C. Impact of risk factors on early cancer evolution. *Cell* **186**, 1541–1563 (2023).
4. Wu, S., Zhu, W., Thompson, P. & Hannun, Y. A. Evaluating intrinsic and non-intrinsic cancer risk factors. *Nat. Commun.* **9**, 3490 (2018).
5. Gerstberger, S., Jiang, Q. & Ganesh, K. Metastasis. *Cell* **186**, 1564–1579 (2023).
6. Quail, D. F. & Joyce, J. A. Microenvironmental regulation of tumor progression and metastasis. *Nat. Med.* **19**, 1423–1437 (2013).
7. Cancer Metastasis: Building a Framework - ScienceDirect. <https://www.sciencedirect.com/science/article/pii/S0092867406014140?via%3Dihub>.
8. Hanahan, D. & Coussens, L. M. Accessories to the Crime: Functions of Cells Recruited to the Tumor Microenvironment. *Cancer Cell* **21**, 309–322 (2012).
9. Hynes, R. O. Extracellular matrix: not just pretty fibrils. *Science* **326**, 1216–1219 (2009).
10. Balkwill, F. R., Capasso, M. & Hagemann, T. The tumor microenvironment at a glance. *J. Cell Sci.* **125**, 5591–5596 (2012).
11. Whiteside, T. L. The tumor microenvironment and its role in promoting tumor growth. *Oncogene* **27**, 5904–5912 (2008).
12. Prajapati, P. & Lambert, D. W. Cancer-associated fibroblasts – Not-so-innocent bystanders in metastasis to bone? *J. Bone Oncol.* **5**, 128–131 (2016).
13. Albini, A. *et al.* Cancer stem cells and the tumor microenvironment: interplay in tumor heterogeneity. *Connect. Tissue Res.* **56**, 414–425 (2015).
14. Lane, A. N., Higashi, R. M. & Fan, T. W.-M. Metabolic reprogramming in tumors: Contributions of the tumor microenvironment. *Genes Dis.* **7**, 185–198 (2020).

## REFERENCES

15. Kalluri, R. & Zeisberg, M. Fibroblasts in cancer. *Nat. Rev. Cancer* **6**, 392–401 (2006).
16. Gieniec, K. A., Butler, L. M., Worthley, D. L. & Woods, S. L. Cancer-associated fibroblasts—heroes or villains? *Br. J. Cancer* **121**, 293–302 (2019).
17. Midwood, K. S., Williams, L. V. & Schwarzbauer, J. E. Tissue repair and the dynamics of the extracellular matrix. *Int. J. Biochem. Cell Biol.* **36**, 1031–1037 (2004).
18. Attieh, Y. & Vignjevic, D. M. The hallmarks of CAFs in cancer invasion. *Eur. J. Cell Biol.* **95**, 493–502 (2016).
19. Fang, Z. *et al.* Signaling pathways in cancer-associated fibroblasts: recent advances and future perspectives. *Cancer Commun.* **43**, 3–41 (2023).
20. Kalluri, R. The biology and function of fibroblasts in cancer. *Nat. Rev. Cancer* **16**, 582–598 (2016).
21. Arina, A. *et al.* Tumor-associated fibroblasts predominantly come from local and not circulating precursors. *Proc. Natl. Acad. Sci. U. S. A.* **113**, 7551–7556 (2016).
22. Karnoub, A. E. *et al.* Mesenchymal stem cells within tumour stroma promote breast cancer metastasis. *Nature* **449**, 557–563 (2007).
23. Kidd, S. *et al.* Origins of the tumor microenvironment: quantitative assessment of adipose-derived and bone marrow-derived stroma. *PLoS One* **7**, e30563 (2012).
24. Iwano, M. *et al.* Evidence that fibroblasts derive from epithelium during tissue fibrosis. *J. Clin. Invest.* **110**, 341–350 (2002).
25. Zeisberg, E. M., Potenta, S., Xie, L., Zeisberg, M. & Kalluri, R. Discovery of endothelial to mesenchymal transition as a source for carcinoma-associated fibroblasts. *Cancer Res.* **67**, 10123–10128 (2007).
26. Kim, D. J. *et al.* Suppression of TGF $\beta$ -mediated conversion of endothelial cells and fibroblasts into cancer associated (myo)fibroblasts via HDAC inhibition. *Br. J. Cancer* **118**, 1359–1368 (2018).
27. Augsten, M. Cancer-Associated Fibroblasts as Another Polarized Cell Type of the Tumor Microenvironment. *Front. Oncol.* **4**, 62 (2014).
28. Lee, H.-O. *et al.* FAP-overexpressing fibroblasts produce an extracellular matrix that enhances invasive velocity and directionality of

## REFERENCES

- pancreatic cancer cells. *BMC Cancer* **11**, 245 (2011).
29. Kay, E. J. *et al.* *PYCR1-Dependent Proline Synthesis in Cancer-Associated Fibroblasts Is Required for the Deposition of pro-Tumorigenic Extracellular Matrix*. <http://biorxiv.org/lookup/doi/10.1101/2020.05.30.125237> (2020) doi:10.1101/2020.05.30.125237.
30. Rattigan, Y. I. *et al.* Lactate is a mediator of metabolic cooperation between stromal carcinoma associated fibroblasts and glycolytic tumor cells in the tumor microenvironment. *Exp. Cell Res.* **318**, 326–335 (2012).
31. Zhang, D. *et al.* Metabolic reprogramming of cancer-associated fibroblasts by IDH3 $\alpha$  downregulation. *Cell Rep.* **10**, 1335–1348 (2015).
32. Valencia, T. *et al.* Metabolic reprogramming of stromal fibroblasts through p62-mTORC1 signaling promotes inflammation and tumorigenesis. *Cancer Cell* **26**, 121–135 (2014).
33. Hembruff, S. L., Jokar, I., Yang, L. & Cheng, N. Loss of Transforming Growth Factor- $\beta$  Signaling in Mammary Fibroblasts Enhances CCL2 Secretion to Promote Mammary Tumor Progression through Macrophage-Dependent and -Independent Mechanisms. *Neoplasia* **12**, 425–433 (2010).
34. Becker, L. M. *et al.* Epigenetic Reprogramming of Cancer-Associated Fibroblasts Deregulates Glucose Metabolism and Facilitates Progression of Breast Cancer. *Cell Rep.* **31**, 107701 (2020).
35. Goicoechea, S. M. *et al.* Palladin promotes invasion of pancreatic cancer cells by enhancing invadopodia formation in cancer-associated fibroblasts. *Oncogene* **33**, 1265–1273 (2014).
36. Dumont, N. *et al.* Breast Fibroblasts Modulate Early Dissemination, Tumorigenesis, and Metastasis through Alteration of Extracellular Matrix Characteristics. *Neoplasia N. Y. N* **15**, 249–262 (2013).
37. Raz, Y. & Erez, N. An inflammatory vicious cycle: Fibroblasts and immune cell recruitment in cancer. *Exp. Cell Res.* **319**, 1596–1603 (2013).
38. Coussens, L. M. & Werb, Z. Inflammation and cancer. *Nature* **420**, 860–867 (2002).
39. Powell, D. W., Adegboyega, P. A., Di Mari, J. F. & Mifflin, R. C. Epithelial cells and their neighbors I. Role of intestinal myofibroblasts in development, repair, and cancer. *Am. J. Physiol. Gastrointest. Liver Physiol.* **289**, G2–7 (2005).

## REFERENCES

40. Rodemann, H. P. Characterization of human renal fibroblasts in health and disease: II. In vitro growth, differentiation, and collagen synthesis of fibroblasts from kidneys with interstitial fibrosis. *Am. J. Kidney Dis. Off. J. Natl. Kidney Found.* **17**, 684–686 (1991).
41. Sharon, Y. *et al.* Tumor-Derived Osteopontin Reprograms Normal Mammary Fibroblasts to Promote Inflammation and Tumor Growth in Breast Cancer. *Cancer Res.* **75**, 963–973 (2015).
42. Kuzet, S.-E. & Gaggioli, C. Fibroblast activation in cancer: when seed fertilizes soil. *Cell Tissue Res.* **365**, 607–619 (2016).
43. Hawinkels, L. J. a. C. *et al.* Interaction with colon cancer cells hyperactivates TGF- $\beta$  signaling in cancer-associated fibroblasts. *Oncogene* **33**, 97–107 (2014).
44. Kellermann, M. G. *et al.* Mutual paracrine effects of oral squamous cell carcinoma cells and normal oral fibroblasts: Induction of fibroblast to myofibroblast transdifferentiation and modulation of tumor cell proliferation. *Oral Oncol.* **44**, 509–517 (2008).
45. Alvarez, R. H., Kantarjian, H. M. & Cortes, J. E. Biology of platelet-derived growth factor and its involvement in disease. *Mayo Clin. Proc.* **81**, 1241–1257 (2006).
46. Cadamuro, M. *et al.* Platelet-Derived Growth Factor-D and Rho GTPases Regulate Recruitment of Cancer-Associated Fibroblasts In Cholangiocarcinoma. *Hepatol. Baltim. Md* **58**, 1042–1053 (2013).
47. Avgustinova, A. *et al.* Tumour cell-derived Wnt7a recruits and activates fibroblasts to promote tumour aggressiveness. *Nat. Commun.* **7**, 10305 (2016).
48. Barker, H. E., Bird, D., Lang, G. & Ertler, J. T. Tumor-secreted LOXL2 Activates Fibroblasts Through FAK Signaling. *Mol. Cancer Res. MCR* **11**, 10.1158/1541-7786.MCR-13-0033-T (2013).
49. Sahai, E. *et al.* A framework for advancing our understanding of cancer-associated fibroblasts. *Nat. Rev. Cancer* **20**, 174–186 (2020).
50. Shi, X., Young, C. D., Zhou, H. & Wang, X.-J. Transforming Growth Factor- $\beta$  Signaling in Fibrotic Diseases and Cancer-Associated Fibroblasts. *Biomolecules* **10**, 1666 (2020).
51. Desmoulière, A., Geinoz, A., Gabbiani, F. & Gabbiani, G. Transforming growth factor-beta 1 induces alpha-smooth muscle actin expression in granulation tissue myofibroblasts and in quiescent and growing cultured

## REFERENCES

- fibroblasts. *J. Cell Biol.* **122**, 103–111 (1993).
52. Kojima, Y. *et al.* Autocrine TGF- $\beta$  and stromal cell-derived factor-1 (SDF-1) signaling drives the evolution of tumor-promoting mammary stromal myofibroblasts. *Proc. Natl. Acad. Sci. U. S. A.* **107**, 20009–20014 (2010).
53. Varelas, X. *et al.* TAZ controls Smad nucleocytoplasmic shuttling and regulates human embryonic stem-cell self-renewal. *Nat. Cell Biol.* **10**, 837–848 (2008).
54. Narimatsu, M., Samavarchi-Tehrani, P., Varelas, X. & Wrana, J. L. Distinct polarity cues direct Taz/Yap and TGF $\beta$  receptor localization to differentially control TGF $\beta$ -induced Smad signaling. *Dev. Cell* **32**, 652–656 (2015).
55. Wu, F. *et al.* Signaling pathways in cancer-associated fibroblasts and targeted therapy for cancer. *Signal Transduct. Target. Ther.* **6**, 1–35 (2021).
56. Reich, N. *et al.* The transcription factor Fra-2 regulates the production of extracellular matrix in systemic sclerosis. *Arthritis Rheum.* **62**, 280–290 (2010).
57. Wilkes, M. C. *et al.* Transforming growth factor- $\beta$  activation of phosphatidylinositol 3-kinase is independent of Smad2 and Smad3 and regulates fibroblast responses via p21-activated kinase-2. *Cancer Res.* **65**, 10431–10440 (2005).
58. Akhmetshina, A. *et al.* Activation of canonical Wnt signalling is required for TGF- $\beta$ -mediated fibrosis. *Nat. Commun.* **3**, 735 (2012).
59. Ringuette Goulet, C. *et al.* Exosomes Induce Fibroblast Differentiation into Cancer-Associated Fibroblasts through TGF $\beta$  Signaling. *Mol. Cancer Res.* **16**, 1196–1204 (2018).
60. Rosenthal, E. *et al.* Elevated expression of TGF- $\beta$ 1 in head and neck cancer-associated fibroblasts. *Mol. Carcinog.* **40**, 116–121 (2004).
61. Yegodayev, K. M. *et al.* TGF- $\beta$ -Activated Cancer-Associated Fibroblasts Limit Cetuximab Efficacy in Preclinical Models of Head and Neck Cancer. *Cancers* **12**, 339 (2020).
62. Dauer, P. *et al.* Inactivation of cancer-associated-fibroblasts (CAF) disrupts oncogenic signaling in pancreatic cancer cells and promotes its regression. *Cancer Res.* **78**, 1321–1333 (2018).
63. Zhou, L., Yang, K., Wickett, R. R., Kadekaro, A. L. & Zhang, Y. Targeted deactivation of cancer-associated fibroblasts by  $\beta$ -catenin ablation

## REFERENCES

- suppresses melanoma growth. *Tumor Biol.* **37**, 14235–14248 (2016).
64. Bochet, L. *et al.* Adipocyte-Derived Fibroblasts Promote Tumor Progression and Contribute to the Desmoplastic Reaction in Breast Cancer. *Cancer Res.* **73**, 5657–5668 (2013).
65. Ferrari, N. *et al.* Dickkopf-3 links HSF1 and YAP/TAZ signalling to control aggressive behaviours in cancer-associated fibroblasts. *Nat. Commun.* **10**, 130 (2019).
66. Azzolin, L. *et al.* YAP/TAZ Incorporation in the  $\beta$ -Catenin Destruction Complex Orchestrates the Wnt Response. *Cell* **158**, 157–170 (2014).
67. Azzolin, L. *et al.* Role of TAZ as mediator of Wnt signaling. *Cell* **151**, 1443–1456 (2012).
68. Yu, F.-X., Zhao, B. & Guan, K.-L. Hippo Pathway in Organ Size Control, Tissue Homeostasis, and Cancer. *Cell* **163**, 811–828 (2015).
69. Dupont, S. *et al.* Role of YAP/TAZ in mechanotransduction. *Nature* **474**, 179–183 (2011).
70. Calvo, F. *et al.* Mechanotransduction and YAP-dependent matrix remodelling is required for the generation and maintenance of cancer-associated fibroblasts. *Nat. Cell Biol.* **15**, 637–646 (2013).
71. Wang, S. *et al.* CCM3 is a gatekeeper in focal adhesions regulating mechanotransduction and YAP/TAZ signalling. *Nat. Cell Biol.* **23**, 758–770 (2021).
72. Olson, E. N. & Nordheim, A. Linking actin dynamics and gene transcription to drive cellular motile functions. *Nat. Rev. Mol. Cell Biol.* **11**, 353–365 (2010).
73. Curtis, M. *et al.* Fibroblasts Mobilize Tumor Cell Glycogen to Promote Proliferation and Metastasis. *Cell Metab.* **29**, 141–155.e9 (2019).
74. Dai, C. & Sampson, S. B. HSF1: Guardian of proteostasis in cancer. *Trends Cell Biol.* **26**, 17–28 (2016).
75. Scherz-Shouval, R. *et al.* The reprogramming of tumor stroma by HSF1 is a potent enabler of malignancy. *Cell* **158**, 564–578 (2014).
76. Levi-Galibov, O. *et al.* Heat Shock Factor 1-dependent extracellular matrix remodeling mediates the transition from chronic intestinal inflammation to colon cancer. *Nat. Commun.* **11**, 6245 (2020).

## REFERENCES

77. Albrengues, J. *et al.* Epigenetic switch drives the conversion of fibroblasts into proinvasive cancer-associated fibroblasts. *Nat. Commun.* **6**, 10204 (2015).
78. Mishra, R., Haldar, S., Suchanti, S. & Bhowmick, N. A. Epigenetic changes in fibroblasts drive cancer metabolism and differentiation. *Endocr. Relat. Cancer* **26**, R673–R688 (2019).
79. Ramaiah, M. J., Tangutur, A. D. & Manyam, R. R. Epigenetic modulation and understanding of HDAC inhibitors in cancer therapy. *Life Sci.* **277**, 119504 (2021).
80. Jones, D. L. *et al.* TGF $\beta$ -induced fibroblast activation requires persistent and targeted HDAC-mediated gene repression. *J. Cell Sci.* **132**, jcs233486 (2019).
81. Li, X. *et al.* Single-cell RNA sequencing reveals a pro-invasive cancer-associated fibroblast subgroup associated with poor clinical outcomes in patients with gastric cancer. *Theranostics* **12**, 620–638 (2022).
82. Galbo, P. M., Zang, X. & Zheng, D. Implication of cancer associated fibroblast subtypes on cancer pathogenesis, prognosis, and immunotherapy resistance. *Clin. Cancer Res. Off. J. Am. Assoc. Cancer Res.* **27**, 2636–2647 (2021).
83. Li, H. *et al.* Interleukin-22 secreted by cancer-associated fibroblasts regulates the proliferation and metastasis of lung cancer cells via the PI3K-Akt-mTOR signaling pathway. *Am. J. Transl. Res.* **11**, 4077–4088 (2019).
84. Sakamoto, A. *et al.* Pyruvate secreted from patient-derived cancer-associated fibroblasts supports survival of primary lymphoma cells. *Cancer Sci.* **110**, 269–278 (2019).
85. Kugeratski, F. G. *et al.* Hypoxic cancer-associated fibroblasts increase NCBP2-AS2/HIAR to promote endothelial sprouting through enhanced VEGF signaling. *Sci. Signal.* **12**, ean8247 (2019).
86. Raz, Y. & Erez, N. An inflammatory vicious cycle: Fibroblasts and immune cell recruitment in cancer. *Exp. Cell Res.* **319**, 1596–1603 (2013).
87. Kuperwasser, C. *et al.* Reconstruction of functionally normal and malignant human breast tissues in mice. *Proc. Natl. Acad. Sci. U. S. A.* **101**, 4966–4971 (2004).
88. Lewis, M. P. *et al.* Tumour-derived TGF- $\beta$ 1 modulates myofibroblast differentiation and promotes HGF/SF-dependent invasion of squamous

## REFERENCES

- carcinoma cells. *Br. J. Cancer* **90**, 822–832 (2004).
89. Castellana, D. *et al.* Membrane Microvesicles as Actors in the Establishment of a Favorable Prostatic Tumoral Niche: A Role for Activated Fibroblasts and CX3CL1–CX3CR1 Axis. *Cancer Res.* **69**, 785–793 (2009).
90. Hao, Y., Baker, D. & ten Dijke, P. TGF- $\beta$ -Mediated Epithelial–Mesenchymal Transition and Cancer Metastasis. *Int. J. Mol. Sci.* **20**, 2767 (2019).
91. Gkretsi, V. & Stylianopoulos, T. Cell Adhesion and Matrix Stiffness: Coordinating Cancer Cell Invasion and Metastasis. *Front. Oncol.* **8**, 145 (2018).
92. Kauppila, S., Stenbäck, F., Risteli, J., Jukkola, A. & Risteli, L. Aberrant type I and type III collagen gene expression in human breast cancer in vivo. *J. Pathol.* **186**, 262–268 (1998).
93. Sanz–Moreno, V. *et al.* ROCK and JAK1 Signaling Cooperate to Control Actomyosin Contractility in Tumor Cells and Stroma. *Cancer Cell* **20**, 229–245 (2011).
94. Plotnikov, S. V., Pasapera, A. M., Sabass, B. & Waterman, C. M. Force Fluctuations within Focal Adhesions Mediate ECM–Rigidity Sensing to Guide Directed Cell Migration. *Cell* **151**, 10.1016/j.cell.2012.11.034 (2012).
95. Oudin, M. J. *et al.* Tumor cell–driven extracellular matrix remodeling drives haptotaxis during metastatic progression. *Cancer Discov.* **6**, 516–531 (2016).
96. Cox, T. R. *et al.* LOX–mediated collagen crosslinking is responsible for fibrosis–enhanced metastasis. *Cancer Res.* **73**, 1721–1732 (2013).
97. Pankova, D. *et al.* Cancer–Associated Fibroblasts Induce a Collagen Cross–link Switch in Tumor Stroma. *Mol. Cancer Res.* **14**, 287–295 (2016).
98. Barker, H. E., Cox, T. R. & Ertler, J. T. The rationale for targeting the LOX family in cancer. *Nat. Rev. Cancer* **12**, 540–552 (2012).
99. Koontongkaew, S., Amornphimoltham, P. & Yapong, B. Tumor–stroma interactions influence cytokine expression and matrix metalloproteinase activities in paired primary and metastatic head and neck cancer cells. *Cell Biol. Int.* **33**, 165–173 (2009).
100. DeClerck, Y. A. Interactions between tumour cells and stromal cells and proteolytic modification of the extracellular matrix by metalloproteinases in cancer. *Eur. J. Cancer* **36**, 1258–1268 (2000).

## REFERENCES

101. Dayer, C. & Stamenkovic, I. Recruitment of Matrix Metalloproteinase-9 (MMP-9) to the Fibroblast Cell Surface by Lysyl Hydroxylase 3 (LH3) Triggers Transforming Growth Factor- $\beta$  (TGF- $\beta$ ) Activation and Fibroblast Differentiation. *J. Biol. Chem.* **290**, 13763–13778 (2015).
102. Taniwaki, K. *et al.* Stroma-Derived Matrix Metalloproteinase (MMP)-2 Promotes Membrane Type 1-MMP-Dependent Tumor Growth in Mice. *Cancer Res.* **67**, 4311–4319 (2007).
103. Dallas, S. L., Rosser, J. L., Mundy, G. R. & Bonewald, L. F. Proteolysis of Latent Transforming Growth Factor- $\beta$  (TGF- $\beta$ )-binding Protein-1 by Osteoclasts: A CELLULAR MECHANISM FOR RELEASE OF TGF- $\beta$  FROM BONE MATRIX \*. *J. Biol. Chem.* **277**, 21352–21360 (2002).
104. Tatti, O., Vehviläinen, P., Lehti, K. & Keski-Oja, J. MT1-MMP releases latent TGF- $\beta$ 1 from endothelial cell extracellular matrix via proteolytic processing of LTBP-1. *Exp. Cell Res.* **314**, 2501–2514 (2008).
105. Talele, N. P., Fradette, J., Davies, J. E., Kapus, A. & Hinz, B. Expression of  $\alpha$ -Smooth Muscle Actin Determines the Fate of Mesenchymal Stromal Cells. *Stem Cell Rep.* **4**, 1016–1030 (2015).
106. Hinz, B., Mastrangelo, D., Iselin, C. E., Chaponnier, C. & Gabbiani, G. Mechanical tension controls granulation tissue contractile activity and myofibroblast differentiation. *Am. J. Pathol.* **159**, 1009–1020 (2001).
107. Hinz, B., Celetta, G., Tomasek, J. J., Gabbiani, G. & Chaponnier, C. Alpha-smooth muscle actin expression upregulates fibroblast contractile activity. *Mol. Biol. Cell* **12**, 2730–2741 (2001).
108. Najafi, M., Farhood, B. & Mortezaee, K. Extracellular matrix (ECM) stiffness and degradation as cancer drivers. *J. Cell. Biochem.* **120**, 2782–2790 (2019).
109. Rahbari, N. N. *et al.* Anti-VEGF therapy induces ECM remodeling and mechanical barriers to therapy in colorectal cancer liver metastases. *Sci. Transl. Med.* **8**, 360ra135 (2016).
110. Mantovani, A., Allavena, P., Sica, A. & Balkwill, F. Cancer-related inflammation. *Nature* **454**, 436–444 (2008).
111. Mace, T. A. *et al.* Pancreatic Cancer-Associated Stellate Cells Promote Differentiation of Myeloid-Derived Suppressor Cells in a STAT3-Dependent Manner. *Cancer Res.* **73**, 3007–3018 (2013).
112. Ksiazkiewicz, M. *et al.* Importance of CCL2-CCR2A/2B signaling for

## REFERENCES

monocyte migration into spheroids of breast cancer-derived fibroblasts. *Immunobiology* **215**, 737–747 (2010).

113. Barnas, J. L., Simpson-Abelson, M. R., Yokota, S. J., Kelleher, R. J. & Bankert, R. B. T Cells and Stromal Fibroblasts in Human Tumor Microenvironments Represent Potential Therapeutic Targets. *Cancer Microenviron.* **3**, 29–47 (2010).

114. Kobayashi, N. *et al.* Hyaluronan Deficiency in Tumor Stroma Impairs Macrophage Trafficking and Tumor Neovascularization. *Cancer Res.* **70**, 7073–7083 (2010).

115. Johnson, D. E., O’Keefe, R. A. & Grandis, J. R. Targeting the IL-6/JAK/STAT3 signalling axis in cancer. *Nat. Rev. Clin. Oncol.* **15**, 234–248 (2018).

116. Mariathasan, S. *et al.* TGF $\beta$  attenuates tumour response to PD-L1 blockade by contributing to exclusion of T cells. *Nature* **554**, 544–548 (2018).

117. Krishnamurty, A. T. *et al.* LRRC15+ myofibroblasts dictate the stromal setpoint to suppress tumour immunity. *Nature* **611**, 148–154 (2022).

118. Orimo, A. *et al.* Stromal Fibroblasts Present in Invasive Human Breast Carcinomas Promote Tumor Growth and Angiogenesis through Elevated SDF-1/CXCL12 Secretion. *Cell* **121**, 335–348 (2005).

119. Unterleuthner, D. *et al.* Cancer-associated fibroblast-derived WNT2 increases tumor angiogenesis in colon cancer. *Angiogenesis* **23**, 159–177 (2020).

120. Xu, J. *et al.* Proteolytic exposure of a cryptic site within collagen type IV is required for angiogenesis and tumor growth in vivo. *J. Cell Biol.* **154**, 1069–1080 (2001).

121. Zanotelli, M. R. & Reinhart-King, C. A. Mechanical Forces in Tumor Angiogenesis. *Adv. Exp. Med. Biol.* **1092**, 91–112 (2018).

122. Vaish, U., Jain, T., Are, A. C. & Dudeja, V. Cancer-Associated Fibroblasts in Pancreatic Ductal Adenocarcinoma: An Update on Heterogeneity and Therapeutic Targeting. *Int. J. Mol. Sci.* **22**, 13408 (2021).

123. Bartoschek, M. *et al.* Spatially and functionally distinct subclasses of breast cancer-associated fibroblasts revealed by single cell RNA sequencing. *Nat. Commun.* **9**, 5150 (2018).

124. Hsu, W.-H. *et al.* Oncogenic KRAS Drives Lipofibrogenesis to Promote Angiogenesis and Colon Cancer Progression. *Cancer Discov.* **13**, 2652–2673

## REFERENCES

(2023).

125. Biffi, G. *et al.* IL1-Induced JAK/STAT Signaling Is Antagonized by TGF $\beta$  to Shape CAF Heterogeneity in Pancreatic Ductal Adenocarcinoma. *Cancer Discov.* **9**, 282–301 (2019).
126. Elyada, E. *et al.* Cross-Species Single-Cell Analysis of Pancreatic Ductal Adenocarcinoma Reveals Antigen-Presenting Cancer-Associated Fibroblasts. *Cancer Discov.* **9**, 1102–1123 (2019).
127. Öhlund, D. *et al.* Distinct populations of inflammatory fibroblasts and myofibroblasts in pancreatic cancer. *J. Exp. Med.* **214**, 579–596 (2017).
128. De Wever, O., Demetter, P., Mareel, M. & Bracke, M. Stromal myofibroblasts are drivers of invasive cancer growth. *Int. J. Cancer* **123**, 2229–2238 (2008).
129. Karta, J., Bossicard, Y., Kotzamanis, K., Dolznig, H. & Letellier, E. Mapping the Metabolic Networks of Tumor Cells and Cancer-Associated Fibroblasts. *Cells* **10**, 304 (2021).
130. Molina, J. R. *et al.* An inhibitor of oxidative phosphorylation exploits cancer vulnerability. *Nat. Med.* **24**, 1036–1046 (2018).
131. Hopkins, B. D. *et al.* Suppression of insulin feedback enhances the efficacy of PI3K inhibitors. *Nature* **560**, 499–503 (2018).
132. McBrayer, S. K. *et al.* Transaminase Inhibition by 2-Hydroxyglutarate Impairs Glutamate Biosynthesis and Redox Homeostasis in Glioma. *Cell* **175**, 101–116.e25 (2018).
133. Faubert, B., Solmonson, A. & DeBerardinis, R. J. Metabolic reprogramming and cancer progression. *Science* **368**, eaaw5473 (2020).
134. Warburg, O. The Metabolism of Carcinoma Cells1. *J. Cancer Res.* **9**, 148–163 (1925).
135. Warburg, O., Wind, F. & Negelein, E. THE METABOLISM OF TUMORS IN THE BODY. *J. Gen. Physiol.* **8**, 519–530 (1927).
136. Vander Heiden, M. G., Cantley, L. C. & Thompson, C. B. Understanding the Warburg Effect: The Metabolic Requirements of Cell Proliferation. *Science* **324**, 1029–1033 (2009).
137. Hu, J. *et al.* Heterogeneity of tumor-induced gene expression changes in the human metabolic network. *Nat. Biotechnol.* **31**, 522–529 (2013).

## REFERENCES

138. Zhang, X. *et al.* The role of YAP/TAZ activity in cancer metabolic reprogramming. *Mol. Cancer* **17**, 134 (2018).
139. Yuneva, M. O. *et al.* The Metabolic Profile of Tumors Depends on both the Responsible Genetic Lesion and Tissue Type. *Cell Metab.* **15**, 157–170 (2012).
140. Valvezan, A. J. *et al.* mTORC1 couples nucleotide synthesis to nucleotide demand resulting in a targetable metabolic vulnerability. *Cancer Cell* **32**, 624–638.e5 (2017).
141. Yun, J. *et al.* Glucose Deprivation Contributes to the Development of KRAS Pathway Mutations in Tumor Cells. *Science* **325**, 1555 (2009).
142. Selak, M. A. *et al.* Succinate links TCA cycle dysfunction to oncogenesis by inhibiting HIF- $\alpha$  prolyl hydroxylase. *Cancer Cell* **7**, 77–85 (2005).
143. Knott, S. R. V. *et al.* Asparagine bioavailability governs metastasis in a model of breast cancer. *Nature* **554**, 378–381 (2018).
144. Hu, S. *et al.* <sup>13</sup>C-Pyruvate Imaging Reveals Alterations in Glycolysis that Precede c-MYC Induced Tumor Formation and Regression. *Cell Metab.* **14**, 10.1016/j.cmet.2011.04.012 (2011).
145. Bertero, T. *et al.* Tumor–stroma mechanics coordinate amino acid availability to sustain tumor growth and malignancy. *Cell Metab.* **29**, 124–140.e10 (2019).
146. Hinow, P. Modeling the bidirectional glutamine/ammonium conversion between cancer cells and cancer-associated fibroblasts. *20* (2021).
147. He, X. *et al.* Tumor-initiating stem cell shapes its microenvironment into an immunosuppressive barrier and pro-tumorigenic niche. *Cell Rep.* **36**, 109674 (2021).
148. Pavlides, S. *et al.* The reverse Warburg effect: Aerobic glycolysis in cancer associated fibroblasts and the tumor stroma. *Cell Cycle* **8**, 3984–4001 (2009).
149. Whitaker-Menezes, D. *et al.* Evidence for a stromal–epithelial “lactate shuttle” in human tumors. *Cell Cycle* **10**, 1772–1783 (2011).
150. Koukourakis, M. I., Giatromanolaki, A., Harris, A. L. & Sivridis, E. Comparison of Metabolic Pathways between Cancer Cells and Stromal Cells in Colorectal Carcinomas: a Metabolic Survival Role for Tumor-Associated Stroma. *Cancer Res.* **66**, 632–637 (2006).

## REFERENCES

151. Kumar, D. *et al.* Cancer-Associated Fibroblasts Drive Glycolysis in a Targetable Signaling Loop Implicated in Head and Neck Squamous Cell Carcinoma Progression. *Cancer Res.* **78**, 3769–3782 (2018).
152. Xiao, L. *et al.* TRAP1 suppresses oral squamous cell carcinoma progression by reducing oxidative phosphorylation metabolism of Cancer-associated fibroblasts. *BMC Cancer* **21**, 1329 (2021).
153. Sousa, C. M. *et al.* Pancreatic stellate cells support tumour metabolism through autophagic alanine secretion. *Nature* **536**, 479–483 (2016).
154. Wang, W. *et al.* Effector T Cells Abrogate Stroma-Mediated Chemoresistance in Ovarian Cancer. *Cell* **165**, 1092–1105 (2016).
155. Linares, J. F. *et al.* ATF4-induced metabolic reprogramming is a synthetic vulnerability of the p62-deficient tumor stroma. *Cell Metab.* **26**, 817–829.e6 (2017).
156. Wang, Y.-P., Li, J.-T., Qu, J., Yin, M. & Lei, Q.-Y. Metabolite sensing and signaling in cancer. *J. Biol. Chem.* **295**, 11938–11946 (2020).
157. Waitkus, M. S., Diplas, B. H. & Yan, H. Biological Role and Therapeutic Potential of IDH Mutations in Cancer. *Cancer Cell* **34**, 186–195 (2018).
158. Lee, D. C. *et al.* A Lactate-Induced Response to Hypoxia. *Cell* **161**, 595–609 (2015).
159. Liu, Y. *et al.* Nuclear lactate dehydrogenase A senses ROS to produce  $\alpha$ -hydroxybutyrate for HPV-induced cervical tumor growth. *Nat. Commun.* **9**, 4429 (2018).
160. Moffett, J. R., Puthillathu, N., Vengilote, R., Jaworski, D. M. & Namboodiri, A. M. Acetate Revisited: A Key Biomolecule at the Nexus of Metabolism, Epigenetics and Oncogenesis—Part 1: Acetyl-CoA, Acetogenesis and Acyl-CoA Short-Chain Synthetases. *Front. Physiol.* **11**, 580167 (2020).
161. Moffett, J. R., Puthillathu, N., Vengilote, R., Jaworski, D. M. & Namboodiri, A. M. Acetate Revisited: A Key Biomolecule at the Nexus of Metabolism, Epigenetics, and Oncogenesis – Part 2: Acetate and ACS2 in Health and Disease. *Front. Physiol.* **11**, 580171 (2020).
162. Bogner-Strauss, J. G. N-Acetylaspartate Metabolism Outside the Brain: Lipogenesis, Histone Acetylation, and Cancer. *Front. Endocrinol.* **8**, 240 (2017).
163. Moffett, J. R., Ross, B., Arun, P., Madhavarao, C. N. & Namboodiri, M. A. A.

## REFERENCES

N-Acetylaspartate in the CNS: From Neurodiagnostics to Neurobiology. *Prog. Neurobiol.* **81**, 89–131 (2007).

164. Baslow, M. H. Functions of N-Acetyl-L-Aspartate and N-Acetyl-L-Aspartylglutamate in the Vertebrate Brain. *J. Neurochem.* **75**, 453–459 (2000).

165. Hershfield, J. R. *et al.* Aspartoacylase is a regulated nuclear-cytoplasmic enzyme. *FASEB J.* **20**, 2139–2141 (2006).

166. Long, P. M. *et al.* N-Acetylaspartate (NAA) and N-Acetylaspartylglutamate (NAAG) Promote Growth and Inhibit Differentiation of Glioma Stem-like Cells. *J. Biol. Chem.* **288**, 26188–26200 (2013).

167. Weng, H. *et al.* Aspartoacylase suppresses prostate cancer progression by blocking LYN activation. *Mil. Med. Res.* **10**, 25 (2023).

168. Prokesch, A. *et al.* N-acetylaspartate catabolism determines cytosolic acetyl-CoA levels and histone acetylation in brown adipocytes. *Sci. Rep.* **6**, 23723 (2016).

169. Singhal, N. K. *et al.* The neuronal metabolite NAA regulates histone H3 methylation in oligodendrocytes and myelin lipid composition. *Exp. Brain Res.* **235**, 279–292 (2017).

170. Menga, A. *et al.* N-acetylaspartate release by glutaminolytic ovarian cancer cells sustains protumoral macrophages. *EMBO Rep.* **22**, e51981 (2021).

171. von Jonquieres, G. *et al.* Uncoupling N-acetylaspartate from brain pathology: implications for Canavan disease gene therapy. *Acta Neuropathol. (Berl.)* **135**, 95–113 (2018).

172. Herga, S., Berrin, J.-G., Perrier, J., Puigserver, A. & Giardina, T. Identification of the zinc binding ligands and the catalytic residue in human aspartoacylase, an enzyme involved in Canavan disease. *FEBS Lett.* **580**, 5899–5904 (2006).

173. Pessentheiner, A. R. *et al.* NAT8L (N-Acetyltransferase 8-Like) Accelerates Lipid Turnover and Increases Energy Expenditure in Brown Adipocytes \*. *J. Biol. Chem.* **288**, 36040–36051 (2013).

174. Huber, K. *et al.* N-acetylaspartate pathway is nutrient responsive and coordinates lipid and energy metabolism in brown adipocytes. *Biochim. Biophys. Acta Mol. Cell Res.* **1866**, 337–348 (2019).

175. Zand, B. *et al.* Role of Increased n-acetylaspartate Levels in Cancer. *J. Natl. Cancer Inst.* **108**, djv426 (2016).

## REFERENCES

176. Kolwijck, E. *et al.* Ovarian Cyst Fluid of Serous Ovarian Tumors Contains Large Quantities of the Brain Amino Acid N-acetylaspartate. *PLOS ONE* **5**, e10293 (2010).
177. Alkan, H. F. *et al.* N-Acetylaspartate Improves Cell Survival When Glucose Is Limiting. <https://papers.ssrn.com/abstract=3631470> (2020) doi:10.2139/ssrn.3631470.
178. Lou, T.-F. *et al.* Cancer-Specific Production of N-Acetylaspartate via NAT8L Overexpression in Non-Small Cell Lung Cancer and Its Potential as a Circulating Biomarker. *Cancer Prev. Res. Phila. Pa* **9**, 43–52 (2016).
179. Wang, J., Akter, R., Shahriar, Md. F. & Uddin, Md. N. Cancer-Associated Stromal Fibroblast-Derived Transcriptomes Predict Poor Clinical Outcomes and Immunosuppression in Colon Cancer. *Pathol. Oncol. Res.* **28**, 1610350 (2022).
180. Crespo, P. & Casar, B. The Chick Embryo Chorioallantoic Membrane as an in vivo Model to Study Metastasis. *Bio-Protoc.* **6**, e1962–e1962 (2016).
181. Subauste, M. C. *et al.* Evaluation of metastatic and angiogenic potentials of human colon carcinoma cells in chick embryo model systems. *Clin. Exp. Metastasis* **26**, 1033–1047 (2009).
182. Di Guida, R. *et al.* Non-targeted UHPLC-MS metabolomic data processing methods: a comparative investigation of normalisation, missing value imputation, transformation and scaling. *Metabolomics* **12**, 93 (2016).
183. Cortazar, A. R. *et al.* CANCEERTOOL: A Visualization and Representation Interface to Exploit Cancer Datasets. *Cancer Res.* **78**, 6320–6328 (2018).
184. Kovács, S. A., Fekete, J. T. & Györffy, B. Predictive biomarkers of immunotherapy response with pharmacological applications in solid tumors. *Acta Pharmacol. Sin.* **44**, 1879–1889 (2023).
185. Györffy, B. Discovery and ranking of the most robust prognostic biomarkers in serous ovarian cancer. *GeroScience* **45**, 1889–1898 (2023).
186. Györffy, B. Survival analysis across the entire transcriptome identifies biomarkers with the highest prognostic power in breast cancer. *Comput. Struct. Biotechnol. J.* **19**, 4101–4109 (2021).
187. Smith, J. J. *et al.* Experimentally derived metastasis gene expression profile predicts recurrence and death in patients with colon cancer. *Gastroenterology* **138**, 958–968 (2010).

## REFERENCES

188. Finak, G. *et al.* Stromal gene expression predicts clinical outcome in breast cancer. *Nat. Med.* **14**, 518–527 (2008).
189. The human cell types - The Human Protein Atlas. <https://www.proteinatlas.org/humanproteome/single+cell+type>.
190. BioStudies. BioStudies < The European Bioinformatics Institute < EMBL–EBI. <https://www.ebi.ac.uk/biostudies/arrayexpress/studies/E-MTAB-10607>.
191. NGDC - GSA for Human. <https://ngdc.cncb.ac.cn/gsa-human/browse/HRA000212>.
192. Jiang, W. *et al.* KIF14 promotes proliferation, lymphatic metastasis and chemoresistance through G3BP1/YBX1 mediated NF- $\kappa$ B pathway in cholangiocarcinoma. *Oncogene* **42**, 1392–1404 (2023).
193. Luo, Q. *et al.* COL11A1 serves as a biomarker for poor prognosis and correlates with immune infiltration in breast cancer. *Front. Genet.* **13**, 935860 (2022).
194. Xu, X. *et al.* Aberrant SOX11 promoter methylation is associated with poor prognosis in gastric cancer. *Cell. Oncol.* **38**, 183–194 (2015).
195. Liu, Q., Ge, H., Liu, P. & Li, Y. High Hepatic leukemia factor expression indicates a favorable survival in glioma patients. *Medicine (Baltimore)* **100**, e23980 (2021).
196. Tissue-based map of the human proteome | Science. <https://www.science.org/doi/10.1126/science.1260419>.
197. Inoue, J. *et al.* Identification of PDHX as a metabolic target for esophageal squamous cell carcinoma. *Cancer Sci.* **112**, 2792–2802 (2021).
198. Chen, Z. *et al.* Single-cell RNA sequencing highlights the role of inflammatory cancer-associated fibroblasts in bladder urothelial carcinoma. *Nat. Commun.* **11**, 5077 (2020).
199. Yang, D. *et al.* WNT4 secreted by tumor tissues promotes tumor progression in colorectal cancer by activation of the Wnt/ $\beta$ -catenin signalling pathway. *J. Exp. Clin. Cancer Res.* **39**, 251 (2020).
200. Foster, C. T., Gualdrini, F. & Treisman, R. Mutual dependence of the MRTF–SRF and YAP–TEAD pathways in cancer-associated fibroblasts is indirect and mediated by cytoskeletal dynamics. *Genes Dev.* **31**, 2361–2375 (2017).

## REFERENCES

201. Miralles, F., Posern, G., Zaromytidou, A.-I. & Treisman, R. Actin Dynamics Control SRF Activity by Regulation of Its Coactivator MAL. *Cell* **113**, 329–342 (2003).
202. Kasashima, H. et al. Stromal SOX2 Upregulation Promotes Tumorigenesis through the Generation of a SFRP1/2-Expressing Cancer-Associated Fibroblast Population. *Dev. Cell* **56**, 95–110.e10 (2021).
203. Tardáguila, M. et al. CX3CL1 promotes breast cancer via transactivation of the EGF pathway. *Cancer Res.* **73**, 4461–4473 (2013).
204. Tang, J. et al. Upregulation of fractalkine contributes to the proliferative response of prostate cancer cells to hypoxia via promoting the G1/S phase transition. *Mol. Med. Rep.* **12**, 7907–7914 (2015).
205. Ong, V. H. et al. Cross-talk between MCP-3 and TGF $\beta$  promotes fibroblast collagen biosynthesis. *Exp. Cell Res.* **315**, 151–161 (2009).
206. Son, D.-S., Parl, A. K., Montgomery Rice, V. & Khabele, D. Keratinocyte chemoattractant (KC)/human growth-regulated oncogene (GRO) chemokines and pro-inflammatory chemokine networks in mouse and human ovarian epithelial cancer cells. *Cancer Biol. Ther.* **6**, 1308–1318 (2007).
207. Wang, L., Lan, J., Tang, J. & Luo, N. MCP-1 targeting: Shutting off an engine for tumor development. *Oncol. Lett.* **23**, 26 (2022).
208. Yan, H. H. et al. CCL9 induced by TGF- $\beta$  signaling in myeloid cells enhances tumor cell survival in the premetastatic organ. *Cancer Res.* **75**, 5283–5298 (2015).
209. Rao, V. S. et al. Extravesicular TIMP-1 is a non-invasive independent prognostic marker and potential therapeutic target in colorectal liver metastases. *Oncogene* **41**, 1809–1820 (2022).
210. Gong, Y. et al. TIMP-1 Promotes Accumulation of Cancer Associated Fibroblasts and Cancer Progression. *PLoS ONE* **8**, e77366 (2013).
211. Chang, X., Li, D., Liu, C., Zhang, Z. & Wang, T. Pentraxin 3 is a diagnostic and prognostic marker for ovarian epithelial cancer patients based on comprehensive bioinformatics and experiments. *Cancer Cell Int.* **21**, 193 (2021).
212. Lecker, L. S. M. et al. TGFBI Production by Macrophages Contributes to an Immunosuppressive Microenvironment in Ovarian Cancer. *Cancer Res.* **81**, 5706–5719 (2021).
213. Wang, M.-Y. et al. The Research Progress in Transforming Growth

## REFERENCES

Factor- $\beta$ 2. *Cells* **12**, 2739 (2023).

214. Gandrillon, O., Schmidt, U., Beug, H. & Samarut, J. TGF- $\beta$  cooperates with TGF- $\alpha$  to induce the self-renewal of normal erythrocytic progenitors: evidence for an autocrine mechanism. *EMBO J.* **18**, 2764–2781 (1999).

215. Chen, Y. *et al.* Pan-Cancer Analysis of the Associations of TGFBI Expression With Prognosis and Immune Characteristics. *Front. Mol. Biosci.* **8**, 745649 (2021).

216. Fan, J. *et al.* Noncanonical Wnt signaling plays an important role in modulating canonical Wnt-regulated stemness, proliferation and terminal differentiation of hepatic progenitors. *Oncotarget* **8**, 27105–27119 (2017).

217. Wei, H. *et al.* Wnt-11 overexpression promoting the invasion of cervical cancer cells. *Tumour Biol. J. Int. Soc. Oncodevelopmental Biol. Med.* **37**, 11789–11798 (2016).

218. Jung, Y.-S., Jun, S., Lee, S. H., Sharma, A. & Park, J.-I. Wnt2 complements Wnt/ $\beta$ -catenin signaling in colorectal cancer. *Oncotarget* **6**, 37257–37268 (2015).

219. Nie, X. *et al.* LRP5 promotes cancer stem cell traits and chemoresistance in colorectal cancer. *J. Cell. Mol. Med.* **26**, 1095–1112 (2022).

220. Liang, G. *et al.* Inhibiting Stromal Class I HDACs Curbs Pancreatic Cancer Progression. *bioRxiv* 2023.09.12.557260 (2023) doi:10.1101/2023.09.12.557260.

221. Glenisson, W., Castronovo, V. & Waltregny, D. Histone deacetylase 4 is required for TGF $\beta$ 1-induced myofibroblastic differentiation. *Biochim. Biophys. Acta BBA - Mol. Cell Res.* **1773**, 1572–1582 (2007).

222. Li, Y. & Seto, E. HDACs and HDAC Inhibitors in Cancer Development and Therapy. *Cold Spring Harb. Perspect. Med.* **6**, a026831 (2016).

223. KANAI, S., SHIMADA, T., NARITA, T. & OKABAYASHI, K. Phosphofructokinase-1 subunit composition and activity in the skeletal muscle, liver, and brain of dogs. *J. Vet. Med. Sci.* **81**, 712–716 (2019).

224. Wu, F. *et al.* Signaling pathways in cancer-associated fibroblasts and targeted therapy for cancer. *Signal Transduct. Target. Ther.* **6**, 1–35 (2021).

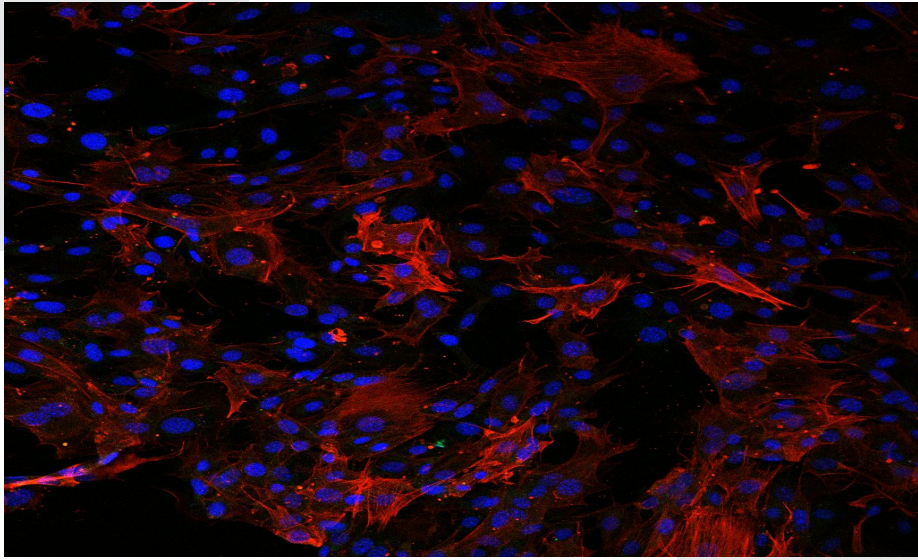
225. Massagué, J. TGF $\beta$  signalling in context. *Nat. Rev. Mol. Cell Biol.* **13**, 616–630 (2012).

## REFERENCES

226. Futakuchi, M. *et al.* The Effects of TGF- $\beta$  Signaling on Cancer Cells and Cancer Stem Cells in the Bone Microenvironment. *Int. J. Mol. Sci.* **20**, 5117 (2019).
227. Gene: ASPA (ENSG00000108381) – Orthologues – Homo\_sapiens – Ensembl genome browser 111. [https://www.ensembl.org/Homo\\_sapiens/Gene/Comparative\\_Ortholog?db=core;g=ENSG00000108381;r=17:3472374-3503405](https://www.ensembl.org/Homo_sapiens/Gene/Comparative_Ortholog?db=core;g=ENSG00000108381;r=17:3472374-3503405).
228. Wu, B., Crompton, S. P. & Hughes, C. C. W. Wnt Signaling Induces Matrix Metalloproteinase Expression and Regulates T Cell Transmigration. *Immunity* **26**, 227–239 (2007).
229. Lin, H. *et al.* sFRP2 activates Wnt/ $\beta$ -catenin signaling in cardiac fibroblasts: differential roles in cell growth, energy metabolism, and extracellular matrix remodeling. *Am. J. Physiol. Cell Physiol.* **311**, C710–C719 (2016).
230. Xu, L. *et al.* Activation of Wnt/ $\beta$ -catenin signalling is required for TGF- $\beta$ /Smad2/3 signalling during myofibroblast proliferation. *J. Cell. Mol. Med.* **21**, 1545–1554 (2017).
231. Shan, B. *et al.* Requirement of HDAC6 for Transforming Growth Factor- $\beta$ 1-induced Epithelial–Mesenchymal Transition. *J. Biol. Chem.* **283**, 21065–21073 (2008).
232. Osseni, A. *et al.* Pharmacological inhibition of HDAC6 improves muscle phenotypes in dystrophin-deficient mice by downregulating TGF- $\beta$  via Smad3 acetylation. *Nat. Commun.* **13**, 7108 (2022).
233. vom Stein, A. F. *et al.* LYN kinase programs stromal fibroblasts to facilitate leukemic survival via regulation of c-JUN and THBS1. *Nat. Commun.* **14**, 1330 (2023).
234. Smith, P. G., Tanaka, H. & Chantry, A. A novel co-operative mechanism linking TGF $\beta$  and Lyn kinase activation to imatinib resistance in chronic myeloid leukaemia cells. *Oncotarget* **3**, 518–524 (2012).
235. Kay, E. J., Koulouras, G. & Zanivan, S. Regulation of Extracellular Matrix Production in Activated Fibroblasts: Roles of Amino Acid Metabolism in Collagen Synthesis. *Front. Oncol.* **11**, (2021).







Los Fibroblastos Asociados al Cáncer (CAFs) constituyen la principal población del microambiente tumoral, y presentan un fenotipo patológicamente activado que promueve la remodelación de la matriz extracelular (ECM) y la señalización pro-tumoral a las células cancerosas. Los CAFs también pueden presentar adaptaciones metabólicas para generar metabolitos que promuevan el crecimiento de las células cancerosas. En este trabajo, se identificó la enzima metabólica Aspartoacilasa (ASPA) como un nuevo gen regulador del estroma tumoral. Su expresión está consistentemente disminuida en CAFs de diferentes tipos de tumores, y está correlacionada con un peor pronóstico. La modulación de la expresión de ASPA en CAFs afecta los niveles de expresión de marcadores asociados a CAFs, su capacidad de remodelación de la ECM y la interacción con las células cancerosas, así como el metabolismo intracelular de los fibroblastos. Por lo tanto, el estudio del papel de ASPA en los CAFs puede ayudarnos a comprender la comunicación entre el tumor y el estroma, y cómo la modulación de ASPA afecta la aparición de un fenotipo completamente pro-tumoral en los CAFs. Esperamos que estos avances informen estrategias para frenar los comportamientos promotores del tumor en los CAFs y comprometer la progresión tumoral.

Cancer Associated Fibroblasts (CAFs) are the major population of the TME, and they present a pathologically activated phenotype that promotes extracellular matrix (ECM) remodelling and pro-tumorigenic signalling to cancer cells. CAFs may also present metabolic adaptations to generate metabolites to fuel cancer cell growth. We identified the metabolic enzyme Aspartoacylase (ASPA) as a new tumour stromal regulator gene. Its expression is consistently downregulated in CAFs of different tumour types, and it is correlated with a poorer prognosis. Modulation of ASPA expression in CAFs affect their levels of CAF marker expression, ECM remodelling capacity and the crosstalk to cancer cells, as well as fibroblasts intracellular metabolism. Therefore, understanding ASPA role in CAFs may illuminate the intricate crosstalk between tumour and stroma, and how ASPA modulation affects the emergence of a fully protumour CAF phenotype. We expect these advances to inform strategies to restrain tumour-promoting behaviours in CAFs and compromise tumour progression.